DOCTOR OF PHILOSOPHY

Digital Orthogonal Filtering-enabled Flexible Transmission Systems and Network Architectures for Fixed and Wireless Network Convergence

Sankoh, Abdulai

Award date:
2022

Awarding institution:
Bangor University

Digital Orthogonal Filtering-enabled Flexible Transmission Systems and Network Architectures for Fixed and Wireless Network Convergence

Abdulai Sankoh

A thesis submitted for the degree of

Doctor of Philosophy

School of Computer Science and Electronic Engineering

Bangor University

June 2022

Declaration and Consent

Details of the Work

I hereby agree to deposit the following item in the digital repository maintained by Bangor University and/or in any other repository authorized for use by Bangor University.

Author Name: Abdulai Sankoh

Title: Digital Orthogonal Filtering-enabled Flexible Transmission Systems and Network Architectures for Fixed and Wireless Network Convergence.

Supervisor/Department: Prof. Jianming Tang / School of Computer Science and Electronic Engineering

Funding body (if any): Commonwealth Scholarship Commission (CSC), Fourah Bay College University of Sierra Leone (FBC-USL), and Government of Sierra Leone (GOVSL).

Qualification/Degree obtained: PhD

This item is a product of my own research endeavours and is covered by the agreement below in which the item is referred to as "the Work". It is identical in content to that deposited in the Library, subject to point 4 below.

Non-exclusive Rights

Rights granted to the digital repository through this agreement are entirely non-exclusive. I am free to publish the Work in its present version or future versions elsewhere.

I agree that Bangor University may electronically store, copy or translate the Work to any approved medium or format for the purpose of future preservation and accessibility. Bangor University is not under any obligation to reproduce or display the Work in the same formats or resolutions in which it was originally deposited.

Bangor University Digital Repository

I understand that work deposited in the digital repository will be accessible to a wide variety of people and institutions, including automated agents and search engines via the World Wide Web.

I understand that once the Work is deposited, the item and its metadata may be incorporated into public access catalogues or services, national databases of electronic theses and dissertations such as the British Library's EThOS or any service provided by the National Library of Wales.

I understand that the Work may be made available via the National Library of Wales Online Electronic Theses Service under the declared terms and conditions of use (http://www.llgc.org.uk/index.php?id=4676). I agree that as part of this service the National Library of Wales may electronically store, copy or convert the Work to any approved medium or format for the

purpose of future preservation and accessibility. The National Library of Wales is not under any obligation to reproduce or display the Work in the same formats or resolutions in which it was originally deposited.

Statement 1:

This work has not previously been accepted in substance for any degree and is not being concurrently submitted in candidature for any degree unless as agreed by the University for approved dual awards.

Signed ……..…Abdulai Sankoh...…….. (candidate)

Date ……30/06/2022……

Statement 2:

This thesis is the result of my own investigations, except where otherwise stated. Where correction services have been used, the extent and nature of the correction is clearly marked in a footnote(s).

All other sources are acknowledged by footnotes and/or a bibliography.

Signed …… Abdulai Sankoh ……. (candidate)

Date ……..30/06/2022…….…….

Statement 3 (bar):

I hereby give consent for my thesis, if accepted, to be available for photocopying, for inter-library loans and for electronic repositories after expiry of a bar on access.

Signed ……..… Abdulai Sankoh …… (candidate)

Date ……..30/06/2022……...……

Statement 4:

Choose **one** of the following options

a) I agree to deposit an electronic copy of my thesis (the Work) in the Bangor University (BU) Institutional Digital Repository, the British Library ETHOS system, and/or in any other repository authorized for use by Bangor University and where necessary have gained the required permissions for the use of third party material.	X
b) I agree to deposit an electronic copy of my thesis (the Work) in the Bangor University (BU) Institutional Digital Repository, the British Library ETHOS system, and/or in any other repository authorized for use by Bangor University when the approved **bar on access** has been lifted.	
c) I agree to submit my thesis (the Work) electronically via Bangor University's e-submission system, however I **opt-out** of the electronic deposit to the Bangor University (BU) Institutional Digital Repository, the British Library ETHOS system, and/or in any other repository authorized for use by Bangor University, due to lack of permissions for use of third party material.	

Options B should only be used if a bar on access has been approved by the University.

In addition to the above I also agree to the following:

1. That I am the author or have the authority of the author(s) to make this agreement and do hereby give Bangor University the right to make available the Work in the way described above.
2. That the electronic copy of the Work deposited in the digital repository and covered by this agreement, is identical in content to the paper copy of the Work deposited in the Bangor University Library, subject to point 4 below.
3. That I have exercised reasonable care to ensure that the Work is original and, to the best of my knowledge, does not breach any laws – including those relating to defamation, libel and copyright.
4. That I have, in instances where the intellectual property of other authors or copyright holders is included in the Work, and where appropriate, gained explicit permission for the inclusion of that material in the Work, and in the electronic form of the Work as accessed through the open access digital repository, *or* that I have identified and removed that material for which adequate and appropriate permission has not been obtained and which will be inaccessible via the digital repository.
5. That Bangor University does not hold any obligation to take legal action on behalf of the Depositor, or other rights holders, in the event of a breach of intellectual property rights, or any other right, in the material deposited.
6. That I will indemnify and keep indemnified Bangor University and the National Library of Wales from and against any loss, liability, claim or damage, including without limitation any related legal fees and court costs (on a full indemnity bases), related to any breach by myself of any term of this agreement.

Signature: … Abdulai Sankoh ……...… Date: ……30/06/2022……..……

Abstract

The 5G networks targeting to provide high connection density at ultra-high speed with very low latency is envisioned to meet the growing traffic demand associated with ever-increasing bandwidth-intensive applications and services emerging in the near future. To meet the stringent 5G requirements, passive optical networks (PONs) are considered as one of the most competitive candidates to seamlessly integrate independently developed traditional optical access/metro networks and mobile fronthaul (MFH)/backhaul (MBH) networks into a converged fixed-mobile cloud access network (CAN). To enable the PONs to support such convergence, it is of great advantage if the PONs are equipped with not only flexible, elastic, and dynamically reconfigurable networking features but also inherent transparency to major network design characteristics such as signal modulation formats, different signal detection schemes, flexible wavelength division multiplexing (WDM)-grids, diversified network topologies and various multiple access techniques. Moreover, to enable high spectral efficient MFHs/MBHs capable of supporting the dynamic traffic with variable signal bandwidths, it is crucial if the PONs can also provide elastic bandwidth allocations enabling a flexible and simple redistribution of the available overall transmission bandwidth among different users with improved quality of service (QoS). Furthermore, since the access networks are cost-sensitive, the use of low-cost and low-complexity transmission systems such as intensity-modulation and direct-detection (IMDD) and transceiver components such as 10G-class narrow bandwidth optical devices are preferred in these PONs to improve the access network cost-effectiveness and reduce the overall transceiver complexity.

The study presented in this PhD dissertation research covers a diversified range of physical-layer fundamental technologies required for achieving flexible, adaptable, dynamically reconfigurable and converged fixed-mobile CANs. Extensive explorations are undertaken of the technical feasibility and performance of advanced optical transceiver-embedded digital signal processing (DSP)-enabled digital filtering techniques, which are to be implemented in the future-proof and cost-effective PON-based converged fixed-mobile CANs. These techniques include: i) hybrid orthogonal frequency division multiplexing-digital filter multiple access (OFDM-DFMA) IMDD PONs utilizing spectrally overlapped digital orthogonal filtering, ii) discrete Fourier transform (DFT)-spread spectrally overlapped hybrid OFDM-DFMA IMDD PONs, iii) hybrid single sideband (SSB) OFDM-DFMA PONs, and iv) experimental demonstrations of 30Gb/s/λ digital orthogonal filtering-multiplexed multiple

channel transmissions over IMDD PON systems utilizing 10G-class optical devices. For each individual technique, a technical summary is given below:

The previously reported hybrid OFDM-DFMA PONs offer a promising solution for seamlessly converging optical and mobile networks for 5G. However, these PONs based on IMDD halves the aggregate upstream signal transmission capacity and overall spectral efficiency since each sub-wavelength just conveys a single upstream sub-band signal produced by an optical network unit (ONU). To offer a spectrally efficient PON-based converged CANs, a new hybrid OFDM-DFMA PON utilizing spectrally overlapped digital orthogonal filters (DOF) is proposed and extensively investigated, where the DSP algorithms embedded in both the ONUs and optical line terminal (OLT) are modified to allow two spectrally overlapped sub-bands to occupy the same sub-wavelength. This is achieved by multiplexing multiple independent OFDM channels using both in-phase (I-phase) and Q-phase (Q-phase) ONU-embedded dynamically reconfigurable and adaptive DOFs. In the OLT, similar to the hybrid OFDM-DFMA PONs, the single fast Fourier transform (FFT) operation is applied. For channel demultiplexing/demodulating, independent equalization is performed on the lower sideband (LSB) and upper sideband (USB) subcarriers of a single sub-wavelength, and the two received spectrally overlapped OFDM sub-bands are demultiplexed by summing and subtracting the LSB and USB subcarriers of the same sub-wavelength. As the proposed PONs signal recovery process in the OLT is still free from digital matching filters (MF), thus the new PONs maintain all the unique features associated with the earlier reported hybrid OFDM-DFMA PONs including i) simplified network as its reduce the OLT-DSP hardware/software complexity, thus leading to cost reductions ii) provide flexible, elastic, and dynamically reconfigurable DSP-enabled network, and iii) backward compatibility with existing OFDM-based 4G networks as they are inherently transparent to underlying signal modulation formats and signal bit rates. More importantly, in comparison with the conventional hybrid OFDM-DFMA PONs, the proposed PON doubles the number of supported ONUs and provides >1.7-fold increases in aggregate upstream signal transmission capacity with <1.5dB upstream power budget degradations. On the other hand, for supporting the same ONU count, the aggregate upstream signal transmission capacity increases by >2.2-fold and achieves >0.7dB upstream power budget improvements. The proposed PON's performance improvements vary by <18% for transmission distances of up to 50km, and tolerant to finite digital filter tap length-induced channel interferences.

As the hybrid OFDM-DFMA PONs utilizing spectrally overlapped DOF is OFDM-based, the clipping/quantization noise in analogue-to-digital converters (ADC) and digital-to-analogue converters (DAC) induced by the high peak-to-average power ratios (PAPR) is identified to be an important factor limiting the maximum achievable performance. To overcome this limitation, the DFT-spread spectrally overlapped hybrid OFDM-DFMA IMDD PONs are proposed by employing the DFT-spread technique in each ONU and the OLT. It is shown that the proposed PON maintains all the unique features associated with the previously reported hybrid OFDM-DFMA PONs, whilst improving the upstream transmission performance to its maximum potential. More importantly, it reduces the PAPR by ≥2 dB, thus resulting in a 1 dB reduction in the optimum signal clipping ratio. As a direct consequence, the proposed PON demonstrates excellent tolerance to low DAC/ADC bit resolution and can reduce the minimum required bit resolution by at least 1 bit. In addition, >1.4 dB improvement in upstream power budget and up to 10% increase in aggregate upstream signal transmission capacity can also be achieved without degrading nonlinearity tolerances.

For cost-sensitive application scenarios, a large number of ONUs simultaneously accommodated by the PONs inevitably increase the overall transmission bandwidth and transceiver DSP complexity and cost. To further enhance the spectral efficiency and transceiver cost-effectiveness, the use of SSB as an alternative to double sideband (DSB) in the hybrid OFDM-DFMA PONs is proposed and explored. In this technique, without the use of the Hilbert transform operation in the ONUs, multiple SSB OFDM channels produced are multiplexed using software-reconfigurable DOFs, while in the OLT, a MF-free single FFT operation similar to the PONs mentioned above is used to simultaneously demultiplex and demodulate the signal. Extensive investigations show that, compared to the hybrid DSB OFDM-DFMA PONs, the proposed SSB PONs achieves >2dB reductions in the PAPRs of digitally filtered OFDM signals, giving rise to >2dB decrease in optimum signal clipping ratio and >1 bit reduction in the minimum resolution bit required by the ADC/DAC. Moreover, for fixed spectral bandwidths, the SSB PON increases the maximum upstream transmission capacity by a factor of approximately 2 and increase the upstream system power budget by >1.2dB without degrading its differential ONU optical launch power dynamic range. On the other hand, for fixed upstream signal transmission capacities, the SSB PON halves the overall signal transmission bandwidth and improves the upstream power budget by >2.5dB compared to the hybrid DSB OFDM-DFMA PONs.

To practically implement PONs for the seamless convergence of traditional optical access/metro networks and MFH/MBH networks for cost-sensitive 5G application scenarios, commercially available off-the-shelf and low-cost narrowband 10G-class optical devices are used to experimental demonstrates 30Gb/s/λ DOF-multiplexed six independent frequency gapless channels transmission systems over >25 km standard single mode fibre (SSMF) IMDD PON link. Experimental results show the independence of the channel locations in the digital filter space, all channels have very similar transmission performances when simple adaptive channel power loading is implemented in the digital domain. In addition, under various transmission system configurations, >0.2dB negative power penalties are observed for all the channels mainly due to the interaction between the transmission system-associated negative chromatic dispersion and the intensity modulation-induced frequency chirp. Moreover, the demonstrated systems also exhibit excellent performance robustness over a wide range of transmission distances of up to 45km.

Acknowledgements

First and foremost, I would like to thank God, for giving me strength and courage and for letting me through all the difficulties. I wish to express my sincere and profound gratitude to my supervisor, Prof. Jianming Tang, for his guidance and support throughout my PhD study. I am also deeply thankful to Dr. Roger Giddings for his support and valuable contributions to my research work whenever I needed some additional technical assistance. Without their constructive insights and detailed suggestions on various aspects of my PhD research study, it would not have been possible to accomplish this PhD dissertation work.

Furthermore, I would also like to extend my heartfelt gratitude to Dr. Wei Jin, Dr. Mingliang Deng, Dr Zhuqiang Zhong and Dr. Yanhua Hong for their support and technical assistance. I would particularly like to gratefully acknowledge Dr. Wei Jin for his never-ending commitment and invaluable contributions to my research work, and his willingness to impart his knowledge through technical discussions with cooperation to our co-authored papers. Furthermore, I also wish to thank all my colleagues in the Optical Communications Research Group and the School of Electronic Engineering for making our work environment sociable, exciting and motivating. It is a pleasant journey studying with them at Bangor University.

Moreover, I also would like to thank my sponsors, the Government of the United Kingdom via the CSC, GOVSL and FBC-USL for their financial support, based on which I have been able to achieve this milestone of my educational career.

Finally, it is with great gratitude that I thank my family wholeheartedly for their everlasting love, unequivocal support and encouragement during this research. Thank you, for all their understanding and unconditional love, I can only dedicate this modest work to them.

Abbreviations

ADC	Analogue to Digital Converter
ADSL	Asymmetric Digital Subscriber Line
AMOOFDM	Adaptively Modulated Optical OFDM
APD	Avalanche Photodiode
APON	ATM Passive Optical Network
ARoF	Analogue Radio-Over-Fibre
ATM	Asynchronous Transfer Mode
AR	Augmented Reality
AWG	Arrayed Waveguide Grating
BBU	Baseband Unit
BER	Bit Error Rate
BPON	Broadband Passive Optical Network
BS	Base Station
CAN	Cloud Access Network
CATV	Community Antenna Television
CD	Chromatic Dispersion
CCDF	Complementary Cumulative Density Function
C-OFDM	Coded OFDM
CO	Central Office
CoMP	Coordinated Multipoint Transmission
CN	Core Network
CP	Cyclic Prefix
CPRI	Common Public Radio Interface
CRAN	Centralized Radio Access Network
CU	Central Unit
CW	Continuous Wave
CWDM	Course Wavelength Division Multiplexing
DAC	Digital to Analogue Converter

DBA	Dynamic Bandwidth Allocation
DC	Direct Current
DBPSK	Differential Binary Phase Shift Keying
DFB	Distributed Feedback
DFMA	Digital Filter Multiple Access
DFT	Discrete Fourier Transform
DML	Directly Modulated Laser
DMT	Discrete Multi-Tone
DOF	Digital Orthogonal Filter
DPD	Digital Pre-Distortion
DQPSK	Differential Quadrature Phase Shift Keying
DRAN	Distributed Radio Access Network
DSB	Double Sideband
DSF	Dispersion Shifted Fibre
DSL	Digital Subscriber Loop
DSO	Digital Storage Oscilloscope
DSP	Digital Signal Processing
DU	Digital Unit
DWDM	Dense Wavelength Division Multiplexing
EAM	Electro-Absorption Modulator
eCPRI	Enhanced Common Public Radio Interface
eMBB	Extreme Mobile Broadband
EML	Electro Absorption-Modulated Laser
EDFA	Erbium-Doped Fibre Amplifier
EFM	Ethernet in the First Mile
E-O	Electrical-to-Optical
EPON	Ethernet Passive Optical Network
10G-EPON	10 Gigabit-Ethernet Passive Optical Network
FBMC	Filter Bank Multicarrier
FDM	Frequency Division Multiplexing

FEC	Forward Error Correction
FFT	Fast Fourier Transform
FSAN	Full Services Access Network
FTTH/B/C/P	Fibre-To-The-Home/Building/Curb/Premises
FSO	Free Space Optics
FWM	Four-Wave Mixing
GPON	Gigabit-capable Passive Optical Network
G-EPON	Gigabit-Ethernet Passive Optical Network
GEM	GPON Encapsulation Mode
10G-PON	10 Gigabit-Passive Optical Network
10G-EPON	10 Gigabit-Ethernet Passive Optical Network
3GPP	3rd Generation Partnership Project
HD	High-Definition
HDTV	HD Television
HFC	Hybrid Fibre Coax
HLS	High Layer Split
ICI	Inter-Channel Interference
IDFT	Inverse Discrete Fourier Transform
IFFT	Inverse Fast Fourier Transform
IF	Intermediate Frequency
IMDD	Intensity Modulation and Direct Detection
IP	Internet Protocol
ISI	Inter-Symbol Interference
ITU	International Telecommunication Union
IEEE	Institute of Electrical and Electronics Engineers
LAN	Local Area Network
LD	Laser Diode
LED	Light Emitting Diode
LLS	Low Layer Split
LTE	Long-term Evolution

MAC	Medium Access Control
MAN	Metropolitan Area Network
MBH	Mobile Backhaul
MCM	Multicarrier Modulation
MF	Matching Filter
MFH	Mobile Fronthaul
MIMO	Multiple Input, Multiple Output
MMF	Multi-Mode Fibre
mMTC	Massive Machine-Type Communication
mmWave	Millimeter Wave
MNO	Mobile Network Operator
MPLS	Multiprotocol Label Switching
MZM	Mach-Zehnder Modulator
M2M	Man-to-Machine
NGFI	Next Generation Fronthaul Interface
NG-PON	Next Generation Passive Optical Network
NZDSF	Non-Zero Dispersion Shifted Fibre
OBSAI	Open Base Station Architecture Initiative
ODN	Optical Distribution Network
OCDM	Optical Code Division Multiplexing
O-E	Optical-to-Electrical
OFDM	Orthogonal Frequency Division Multiplexing
OLT	Optical Line Terminal
ONU	Optical Network Unit
OOFDM	Optical Orthogonal Frequency Division Multiplexing
OOFDMA	OOFDM Multiple Access
OSNR	Optical Signal-to-Noise Ratio
ORI	Open Radio Equipment Interface
OTN	Optical Transport Network
PAM	Pulse-Amplitude Modulation

PAPR	Peak-to-Average Power Ratio
PD	Photodiode
PDCP	Packet Data Convergence Protocol
PDH	Plesioynchronous Digital Hierarchy
PON	Passive Optical Network
P/S	Parallel-to-Serial
PSK	Phase Shift Keying
PSTN	Public Switch Telephony Network
QAM	Quadrature Amplitude Modulation
QoE	Quality of Experience
QoS	Quality of Service
QPSK	Quadrature Phase Shift Keying
RAN	Radio Access Network
RAT	Radio Access Technology
RB	Rayleigh backscattering
RF	Radio Frequency
RLC	Radio Link Control
RN	Remote Node
RSOA	Reflective Semiconductor Optical Amplifier
ROADM	Reconfigurable Optical Add-Drop Multiplexer
RRH	Remote Radio Head
RU	Radio Unit
SBS	Stimulated Brillouin scattering
SDN	Software Define Network
SDM	Space Division Multiplexing
SMF	Standard Single Mode Fibre
SF	Shaping Filter
SSMF	Standard SMF
SNR	Signal-to-Noise Ratio
SOA	Semiconductor Optical Amplifier

SONET	Synchronous Optical Networking
S/P	Serial-to-Parallel
SPM	Self-Phase Modulation
SRS	Stimulated Raman Scattering
SSB	Single Sideband
STM	Synchronous Transport Mode
STO	Symbol Timing Offset/Sample Timing Offset
TDM	Time Division Multiplexing
TDMA	Time Division Multiple Access
TWDMA	Time Wavelength Division Multiple Access
URLLC	Ultra-Reliable Low Latency Communications
VOA	Variable-Optical Attenuator
VCSEL	Vertical Cavity Surface Emitting Laser
VDSL	Very High Bit Rate Digital Subscriber Line
VR	Virtual Reality
WDM	Wavelength Division Multiplexing
WDMA	Wavelength Division Multiple Access
WiMAX	Worldwide Interoperability for Microwave Access
WLAN	Wireless Local Area Network
WWAN	Wireless Wide Area Network
XPM	Cross-Phase Modulation

Contents

1. Introduction

Contents

1.1 Cloud Access Networks and Future Network Challenges

Since the advent of 4G wireless networks, the emergence of 4G/long term evolution (LTE) new services and innovative applications of smart mobile devices, 4G end-users have been enjoying a wide diversity of broadband services with their mobile devices on an unprecedented scale [1]. Driven by the proliferation of smart mobile devices, together with the vast adoption of bandwidth-intensive mobile video services such as immersive video conferencing, on-line gaming, and a variety of augmented reality/virtual reality (AR/VR) applications, the mobile data traffic is ever-increasing, as shown in Fig. 1.1, where it is projected to reach 5016 exabyte per month by 2030, an approximately eight-fold increase from 2025 [2]. Such a massive volume of mobile data consumption will put severe strain on current mobile networks to deliver the required capacity. On the other hand, low latency, high flexibility, and QoS inevitably arises as stringent new requirements in addition to the signal transmission capacity. Furthermore, another factor contributing to the network connectivity and usage scenarios is the rapid uptake in the number of smart mobile devices per user pushed by the emerging application of Internet

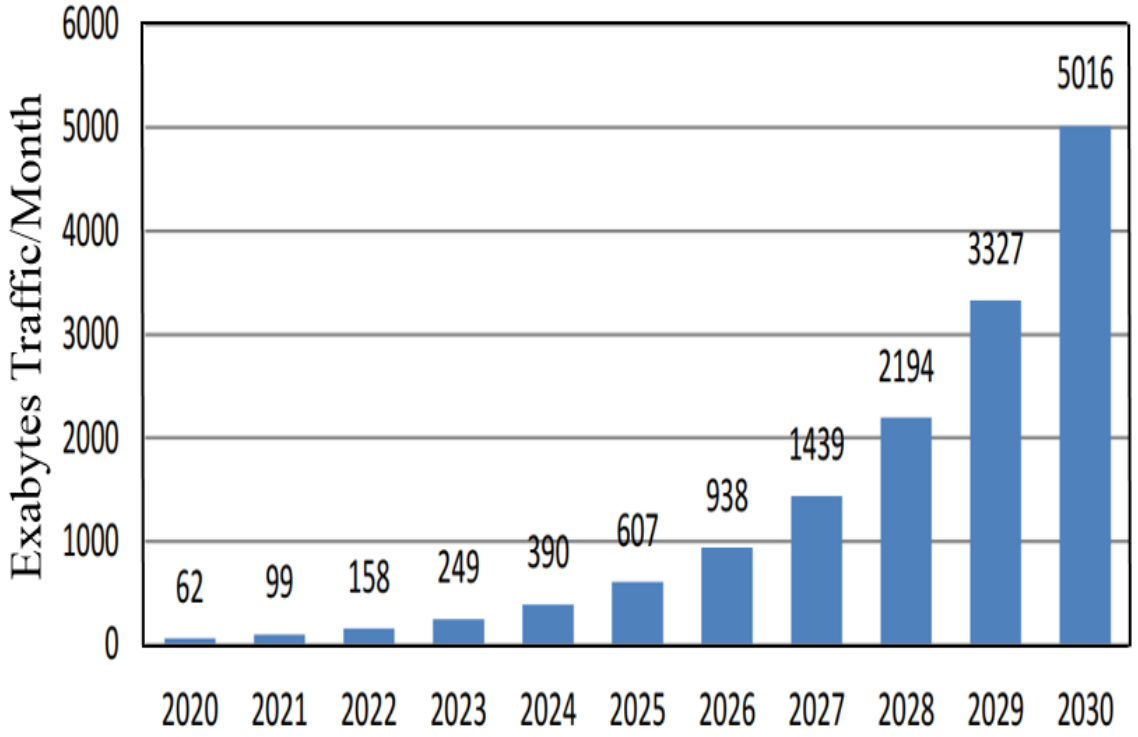

Fig. 1.1. IMT Global Mobile Data Traffic Forecast for the period 2020-2030 [2]

of Things (IoTs) in intelligent demand/supply control and machine-to-machine (M2M) communications utilized in industrial automation. It is envisaged that 30 billion of smart mobile

devices with an average of six to seven devices per user will be connected to the internet by 2023 [3]. This will further impose additional requirements on future mobile networks in terms of cost-effectiveness, reliability, and connectivity density.

To enable the future mobile networks to provide end-users with ubiquitous connectivity and QoS guaranteed for different usage scenarios, the fifth generation (5G) mobile technology has been proposed to meet the stringent requirements that are not adequately addressed by 4G [4,5]. Compared to 4G, 5G is expected to provide up to 1000 times more signal transmission capacities, with target peak data rates of up to 20 Gb/s for downlinks and 10 Gb/s for uplinks [6]. Apart from the significantly improved network transmission capacity, 5G must also provide ultra-reliable low-latency communication (uRLLC) aiming to support an end-to-end (E2E) latency below 1 millisecond compared to 4G's 5ms latency, while the 5G reliability is targeted to be as high as 99.999% [7,8]. Such requirements are highly important for supporting real-time mission-critical services such as sensor-based control nodes for autonomous driving, industrial automation, control of robots, and telesurgery. Furthermore, to meet the requirements of increased connection density, the 5G also aims to deliver massive machine-type communication (mMTC) which allows the networks to scale up to support billions of active devices connected simultaneously, with the connectivity density of as high as 1 million units per square kilometre (km^2), with 10 times extended battery life for low-powered massive MTC devices [9]. In practice, the realization and operational sustainability of such diverse services require significant changes to be made in the underlying network architectures and enabling technologies across all layers.

To practically implement 5G networks, a wide range of key enabling technologies at physical layer have been proposed [10-15]. Firstly, the use of millimetre wave (mmWave) [10,11] in the high frequencies ranging from 30 to 300 GHz has been proposed, leveraging on the abundantly unused available spectral band to provide multi-gigabit transmission data rates to end users. Secondly, the implementation of massive multiple input multiple output (m-MIMO) [12,13] into limited spaces at mmWave with a steerable-beamforming technique has also been widely investigated as an attractive 5G technology strategy to scale up the transmission data rates and improved the spectral efficiency. On the other hand, the deployment of small cell networks [14,15] such as pico-cells, femto-cells, and micro-cells combined with the existing macro-cell infrastructure on a massive scale have also been widely adopted as a viable 5G technology solution to offer a better network coverage and increase the device connectivity

density. Each of the abovementioned technologies can be utilized separately or in combination to address the stringent requirements associated with particular 5G usage scenarios. However, their implementations also impose significant technical challenges in the physical, medium access control (MAC) and network architectures. For instance, the current MFHs adopted in 4G LTE mobile networks based on common public radio interface (CPRI) [16] are not spectrally efficient and require high bitrates which scale in proportion to signal bandwidth, number of antenna port and sampling rate. To address these challenges, a new enhanced CPRI (eCPRI) [17] specification with flexible functional splits at the physical layer has been released where the MFHs transmit digital signals. However, the resulting digital MFHs are still bandwidth inefficient and are also constrained by the massive bandwidth consumption of radio signal digitalization. This together with the low E2E latency required by 5G (less than 250 μs for MFHs alone) [18] unavoidably hinders the radio access network (RAN) from utilizing the highly desired mmWave wideband spectrum and/or multiple antenna techniques with high density small cell networks.

From the signal transmission technique point of view, several technical approaches have been proposed to overcome the limitations of current digitised MFH/MBH networks. The DSP-assisted analogue radio-over-fibre (ARoF) [19,20] technique combine with higher-order signal modulation formats has extensively been studied and is considered as one of the most promising solutions for MFHs. ARoF achieves a high spectral utilization efficiency by multiplexing multiple radio frequency (RF) channels through up-conversion to intermediate frequencies utilizing extra RF components. However, the ARoF spectral efficiency gain comes at an expense of a reduction in performance tolerance against nonlinear distortions and fibre transmission impairments. On the other hand, ARoF requires a high optical signal-to-noise ratio (OSNR), which is much higher than the value determined by the signal modulation formats used to transmit the RF signal over fibre. In addition, advanced signal multiplexing techniques such as WDM [21,22], polarization division multiplexing (PDM) [22] and space division multiplexing (SDM) [22,23] have also been exploited with using ARoF to further increase the signal transmission capacity. Nevertheless, these advanced multiplexing techniques often requires expensive opto-electronic components and/or highly complex transceiver architectures. As well, spectrally efficient signal modulation techniques such as optical subcarrier multiplexing (SCM) [22,24], OFDM [25] and multi-band carrierless amplitude and phase modulation (MB-CAP) [26] in combination with DSPs over ARoF have also been explored as potential candidates to enhance the transmission capacity in mobile

networks. For these techniques, complicated DSPs and high-bandwidth opto-electronic devices are often required for achieving the high spectral utilization efficiency, both of which restrict their applications in cost-sensitive MFH/MBH networks.

Although all the above-mentioned techniques increase the network capacity, however, they are ill-suited to scale on demand, as such they cannot support networks with largely differentiated traffic characteristics. Therefore, flexible MFH/MBH networks capable of transparently supporting various data rates at arbitrary bandwidth granularity are highly preferred to meet the highly dynamic mobile traffic demands. In addition, for achieving the low latency requirement of MFHs, it is of great advantage to use advanced DSPs in transceivers due to their high-performance processing capabilities. As an example, a DSP-based transceiver has been demonstrated to achieve a round-trip processing latency of low microseconds [27]. Moreover, as independently developed and separately operated fixed and mobile networks also contribute to the E2E latency, merging optical access networks and mobile access networks into a seamlessly converged fixed-mobile network is also an effective way to reduce the E2E latency [28,29]. It should be mentioned that converging traditional optical access networks, metropolitan area networks and 4G/5G MFHs/MBHs can also further simplify the overall network architecture, offer a larger bandwidth, provide a dynamic connectivity, and increase the network scalability and flexibility in a cost-effective way.

Moreover, in order to further enhanced the mobile access network capacity and optimize the use of network resources along with increased user demands over the same network infrastructure, a centralized RAN (CRAN) [30,31] approach, where a baseband unit (BBU) is separated from a remote radio unit (RRU), has been widely adopted in 4G for the cost-effective mobile access network and is also expected to play a significant role in future 5G mobile networks. The MFH and MBH are both key network elements in the CRAN architecture, where the MFH connects a centralized pool of BBUs with the RRUs, whereas the BBU pool connect to the mobile core network (CN) through the MBH, which performs traffic aggregation and transport the user data, control and management data, as well as handover data exchanged between them. To improve the spectral efficiency and network traffic/management control, multiple BBUs are co-located in a centralized BBU pool and perform the baseband signal processing functions including sampling, modulation/demodulation, resource block mapping/demapping. While the RRUs are embedded with basic radio front-end functions such as DAC/ADC, frequency up/down-conversion, power amplification and filtering.

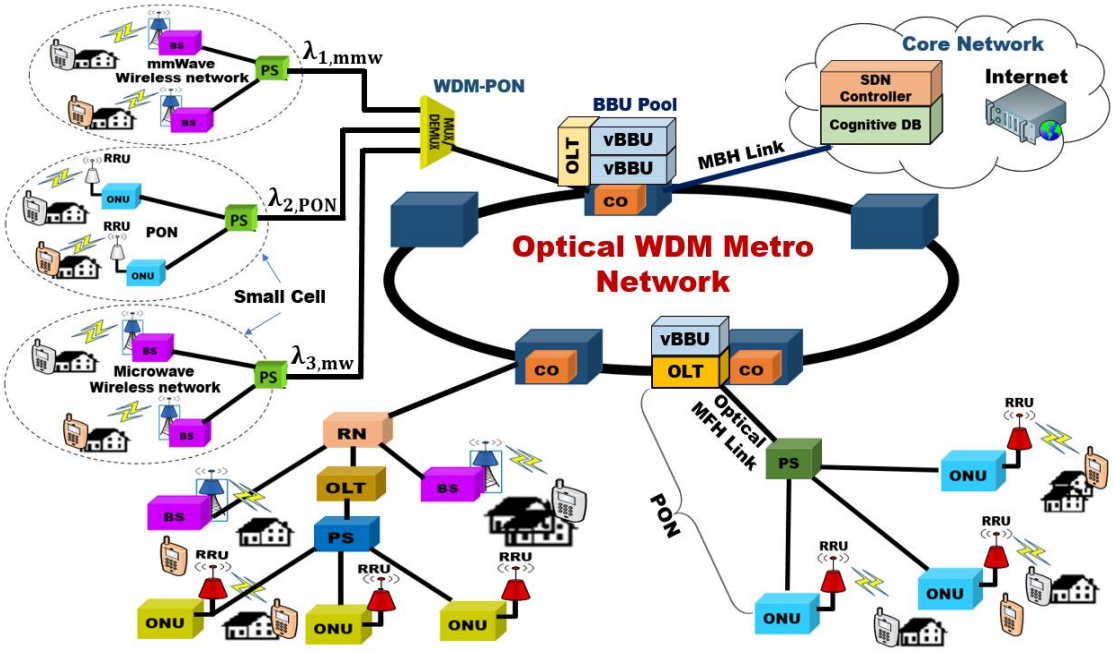

Fig. 1.2. An example of a PON-based converged fixed-mobile cloud CAN architecture for future 5G network.

From the practical implementation point of view, to cost-effectively achieve the fixed-mobile convergence between the traditional optical access networks, metropolitan area networks and 4G/5G MFH/MBH networks to form integrated converged CANs, PONs [32-34] have been considered as an attractive technical strategy to support both mobile and optical access networks over the same network infrastructure. Typically, a PON is a point-to-multipoint (PtMP) optical network consisting of an OLT in the central office (CO) connected to multiple ONUs at remote nodes closer to end-users sharing the same fibre link through a passive optical splitter/coupler. Fig. 1.2 illustrates an example of a PON-based converged fixed-mobile network CAN, where the PON headend is at the CO comprising of the BBUs and OLTs both integrated together and act as a gateway to the optical metropolitan backbone network serving multiple BBUs/OLTs. Such a converged network is highly desirable to reduce the transceiver complexity and cost and may also help to minimise the E2E latency through the joint processing of signals and synchronization of the BBUs and OLTs. Furthermore, the utilization of PONs in the converged networks is of great advantage since it provides a cost-effective and "future-proof" fibre infrastructure enabling end-users to enjoy transmission speeds beyond 10 Gb/s [35,36].

To further enhanced the signal transmission capacity to meet the ever-increasing traffic demand, it is envisaged that the PON-based converged networks may adopt the maturing time WDM

(TWDM)-PON leverage on the existing fibre infrastructure in an approach recommended by the Full Services Access Network (FSAN) group, by using the next-generation-PON stage 2 (NG-PON2) via WDM channels overlay [37,38]. The future PONs may also incorporate advanced signal modulation techniques to further increase the signal transmission capacity. Moreover, to deal with the highly dynamic traffic driven by a unpredictable user behaviour and bandwidth granularity of a wide range of emerging internet applications and services, it is of great advantage if the PON is equipped with the features of flexibility, elasticity and dynamic reconfigurability. Furthermore, since the mobile traffic tends to be highly dynamic nearer to the network edge, to avoid the network over-provisioning and inefficient utilization of the resources, it is greatly beneficial if the future PON can provide elastic bandwidth allocations enabling a flexible and simple redistribution of the available overall transmission bandwidth among different users, without compromising on their quality of user experience (QoE).

Apart from the high signal transmission capacity, to enable a high spectral efficient MFHs/MBHs capable of supporting the dynamic traffic with variable signal bandwidths adopted in various mobile standards, it is also significantly important if the PONs not only offers flexibility for elastic bandwidth allocation, but also has excellent transparency to various traffic characteristics including signal modulation formats and signal bit rates. More especially, it is essential that the converged PON networks should not only have strong adaptability to deal with the dynamic traffic variation at wavelength, sub-wavelength, and sub-band levels, but also simultaneously accommodate various network design features including, signal modulation formats, different signal detection schemes, flexible WDM-grids, diversified network topologies and various multiple access techniques. To further maximise the overall network flexibility and reconfigurability for the effective delivery of the desirable PON features, implementing software defined networking (SDN) down to the physical layer in PONs is also vital [39,40], since SDN makes use of the centralized network resource abstraction and virtualization infrastructure to easily and dynamically reconfigure the networks, which not only deal with traffic uncertainty efficiently but also provide end-users with on-demand broadband connections/services.

Furthermore, since the future PON technologies must be cost efficient and backward compatible to previous standards to reuse the already deployed optical fibre infrastructure, it is therefore critical for the PONs to provide excellent backward compatibility with existing networks such as OFDM-based 4G networks [41,42]. Moreover, since the high cost-

effectiveness is one of the most notable features for an access network, it is also highly preferred for the PON-based converged fixed-mobile network to use low-cost and low-complexity transceiver components in order to keep the access network cost to a minimum. On the one hand, one attractive approach is to reuse off-the-shelf and low-cost 10G-class optical and electrical components in combination with advanced modulation by making full use of DOF implemented with DSP embedded in optical transceivers. This offers a high spectral efficiency and excellent suitability for allowing the usage of low-bandwidth optoelectronics. On the other hand, the utilization of low-cost DACs/ADCs with low resolution bits are also preferred to keep the overall transceiver cost down. In addition, PONs that make use of IMDD systems due to their simplified optical transceiver front-end architectures, low installation cost, minimal maintenance expenditure, and low power consumption are particularly cost effective, and are a preferred choice over coherent systems. Therefore, since the achievement of high transceiver cost-effectiveness is vital for implementing future PONs, advanced transmission techniques with new network architectures are required to improve the spectral efficiency and relax the requirements on the hardware design without using any expensive optoelectronic components and complicated transceiver DSP architectures.

To address the technical challenges outlined above, this dissertation proposes a series of novel techniques with the potential for practically implementing future CANs including: i) hybrid OFDM-DFMA IMDD PONs utilizing spectrally overlapped digital orthogonal filtering, chapter 3, ii) DFT-spread spectrally overlapped hybrid OFDM-DFMA IMDD PONs, chapter 4, iii) Hybrid SSB OFDM-DFMA PONs, chapter 5, and iv) Experimental demonstrations of 30Gb/s/λ digital orthogonal filtering-multiplexed multiple channel transmissions over IMDD PON systems utilizing 10G-class optical devices, chapter 6. The research in this dissertation demonstrates that the abovementioned techniques are promising technical solutions for practical implementation in various 5G scenarios.

1.2 Major Achievements of the Dissertation Research

The objective of this research work is to verify the technical feasibility of the PhD dissertation research-developed techniques for future CANs, by exploring numerically and/or experimentally, optical transceiver-embedded DSP-enable DOF-based multiple channel transmission techniques with independently multiplexing optical channels at the wavelength, sub-wavelength, and orthogonal sub-band levels to implement dynamically reconfigurable,

flexible, and adaptive PON-based converged fixed-mobile CANs in a cost-effective manner. The major achievements of the research work are summarized as follows:

Hybrid OFDM-Digital Filter Multiple Access PONs Utilizing Spectrally Overlapped Digital Orthogonal Filtering, Chapter 3

As low-cost and low-bandwidth optoelectronics devices are essential for realizing cost-effective reconfigurable CANs for 5G application scenarios, DFMA PONs have been proposed [47], where the transceiver-embedded DSP-based software-reconfigurable DOF is employed in each individual ONU and OLT to allow multiple independent channels of arbitrary bandwidth granularities to dynamically share the fibre transmission medium. As the number of required parallel MFs implemented in the OLT is always proportional to the overall ONU count, the IMDD DFMA PONs accommodating large number of ONUs are ill-suited for cost-sensitive application scenarios since the transceiver-DSP implementation complexity and the network operational expenditure may have to increase with ONU count. To resolve this technical issue, hybrid OFDM-DFMA IMDD PONs have been proposed [48], where regardless of the ONU count, a single FFT operation and the relevant DSP processes are implemented in a pipelined way without incorporating parallel MFs. However, the PONs in [48] halve the aggregate upstream signal transmission capacity and overall spectral efficiency because each individual sub-wavelength just conveys a single upstream ONU sub-band signal.

To address this technical challenge, a new hybrid OFDM-DFMA PON utilizing spectrally overlapped DOF is proposed in chapter 3 and extensively investigated to reclaim the spectral efficiency. In the new PON technique, the DSP algorithms embedded in both the OLT and ONUs are slightly modified to allow two spectrally overlapped sub-bands to occupy the same sub-wavelength. For channel demultiplexing/demodulating, the MF-free single FFT operation, the independent equalization of identified LSB and USB subcarriers, and the summation and subtraction operations of LSB and USB subcarriers of the same sub-wavelength are employed in the OLT. It is shown that the proposed PON retains the highly desirable properties associated with the previously reported PONs [48] including i) simplification in the OLT-DSP complexity, giving rise to reductions in the transceiver complexity and overall network cost, ii) provision of a useful framework for developing optical transceiver for cost-sensitive ONUs, iii) excellent transparency to underlying signal modulation/detection techniques, signal bandwidths, multiple access techniques and network topologies. Therefore, this approach not only provides good backward compatibility with existing PONs but also have great potential for supporting

converged fixed-mobile CANs. More importantly, in comparison to the PONs in [48], the proposed PON almost double the aggregate upstream signal transmission capacity and spectral efficiency. As a direct result of the dynamic provision at wavelength, sub-wavelength, and orthogonal sub-band levels, the proposed technique offers improved PON reconfigurability, flexibility and elasticity to support converged optical access/metro networks and MFHs/MBHs networks. As well, this technique possesses inherent transparency to underlying signal modulation formats and signal bit rates. In addition, the proposed technique also provides low transceiver complexity as it allows the utilization of low-cost and low-bandwidth optical and electrical components which are crucial for achieving high transceiver cost-effectiveness.

DFT-Spread Spectrally Overlapped Hybrid OFDM-Digital Filter Multiple Access IMDD PONs, Chapter 4

As the PONs in chapter 3 suffer from the impacts of OFDM-induced high PAPR which essentially increase the clipping/quantization-induced noise in ADCs and DACs, a DFT-spread spectrally overlapped hybrid OFDM-DFMA IMDD PON is proposed in chapter 4 to combat this challenge and relax the requirement on dynamic variation ranges of the transceiver-embedded optical/electrical devices. In the proposed technique, DFT-spread OFDM sub-band signals are produced by each individual ONU. In the OLT, for channel demultiplexing and demodulating, a single FFT operation and the signal recovery processes including summation and subtraction operations of LSB and USB, and inverse-DFT (IDFT) operations are implemented in a pipelined way without requiring parallel MFs. As the DFT-spread OFDM has been widely adopted in 4G-based LTE standards for uplink transmissions, the proposed PON technique provides improved backward compatibility to the existing 4G networks. Moreover, compared to the PONs in chapter 3, as a direct result of PAPR reductions, the proposed PON not only significantly improves the PON upstream transmission performance to its maximum potential, but also provides the low transceiver DSP complexity because of reductions in the minimum required DAC/ADC bit resolution. As such, this technique offers a feasible solution for the cost-effective practical implementation of converged fixed-mobile networks.

Hybrid SSB OFDM-Digital Filter Multiple Access PONs, Chapter 5

For cost-sensitive converged CANs, large number of ONUs simultaneously accommodated by the PON can unavoidably increase the overall transmission bandwidth, thus giving rise to a

high transceiver DSP complexity and cost. To address this technical problem, the hybrid SSB OFDM-DFMA PON is proposed in chapter 5, based on which multiple SSB OFDM channels produced without employing the Hilbert transform operation are multiplexed using software-reconfigurable orthogonal digital filtering in ONUs, and simultaneously demultiplexed and demodulated by a MF-free single FFT operation in the OLT. Compared to the PONs in chapter 3, the proposed SSB PON technique is shown to maintain all the highly desirable unique features associated with the PONs in [48]. More importantly, in comparisons to the PONs in [47], the proposed technique almost doubles the maximum aggregate upstream signal transmission capacity and spectral efficiency. As a direct result of the proposed PON-induced PAPR reduction which also leads to reductions in minimum required DAC/ADC resolution bits, this technique can offer various DSP-enabled SDN solutions of low transceiver complexity to meet the requirements of converged CANs for various 5G scenarios.

Experimental demonstrations of 30Gb/s/λ digital orthogonal filtering-multiplexed multiple channel transmissions over IMDD PON systems utilizing 10G-class optical devices, Chapter 6

As DOF-enabled optical OFDM channel multiplexing for software-reconfigurable elastic PONs [49] are essential elements for implementing CANs, a fully operational DOF-based multiplexing technique exclusively based on IMDD PONs must be experimentally demonstrated and technically verified. To practically realized the feasibility of converged CANs for cost-sensitive 5G application scenarios, experimental demonstrations of 30Gb/s/λ DOF-multiplexed multiple channel transmission systems incorporating 10G-class optical devices over >25 km SSMF IMDD PON link is reported in chapter 6, where six independent frequency gapless channels are multiplexed/demultiplexed utilizing DOFs in the digital domain. The experimental demonstrations achieve excellent robustness and improved transmission performance in terms of reductions in the overall channel bit error rates (BERs) and significant improvement in aggregate signal transmission capacity. Furthermore, the demonstrated DOF-based PONs not only increase the spectral efficiency but also offer inherent transparency to signal modulation formats. Additionally, the fully off-line DOF-based PON is shown to exploit both hardware-based DSP as well as DSP-enabled networking devices, to achieve a dynamically reconfigurable network with fine granularity and elastic bandwidth channels that can be multiplexed at the wavelength, sub-wavelength and orthogonal sub-band levels. This work demonstrates the potential of the DOF-multiplexing technique as a technical strategy for

realizing low-cost CANs for the seamless integration of traditional optical access networks, metro networks and MFH/MBH networks.

The above-mentioned research work has resulted in the publication of 4 papers, of which as the first author, two journal papers have been published, one in Photonics Journal [43]. and the other in Sensors Journal [44]. As a second author, two journal papers have been published, one in Journal of Lightwave Technology [45] and the other in Optics Express [46].

1.3 A Note on Contributions

This section highlights the major contributions of this thesis and describes my role in the joint work.

Hybrid OFDM-DFMA PONs utilizing spectrally overlapped digital orthogonal filtering, **chapter 3**. To solve the problem of spectral inefficiency of the PONs in [48], I have developed the theoretical PON models, ONU and OLT DSP algorithms and performed the numerical simulations. Moreover, I collected the numerical simulation results and analysed the data. I wrote the original draft of the manuscript, as well as revised the whole paper by including the inputs from the co-authors.

DFT-spread spectrally overlapped hybrid OFDM-DFMA IMDD PONs, **chapter 4**. For improving the upstream transmission performance of the PONs in chapter 3, I designed the PON model and carried out the implementation of the proposed PON by modifying the DSP algorithms embedded in both the ONU and OLT to include the DFT-spreading technique. Furthermore, I planned and carried out the simulations, verified the model, optimised the system performance, collected the results, analysed the data, and as well wrote the whole manuscript.

Hybrid SSB OFDM-DFMA PONs, **chapter 5**. We proposed the SSB PON technique to enhance the upstream transmission capacity and spectral efficiency. This work is done in collaboration with another researcher, Dr. Wei Jin. I was responsible for the system optimization of the two cases considered in simulations, i.e., SSB PONs and DSB PONs in terms of identifying their optimum operating parameters. Moreover, I conducted numerical simulations, collected the results, and analysed the data for the DSB PON technique, which is

used as a benchmark for performance comparisons with the SSB PON. As well, I was also involved in reviewing the manuscript.

Experimental demonstrations of the DOF-multiplexed channels over IMDD PONs, chapter 5. We demonstrated the feasibility of utilizing off-the-shelf and low-cost 10G-class optical devices to support 30 Gb/s single wavelength signal transmissions over >25 km SSMF IMDD PON systems. We built the experimental setup configuring an arbitrary waveform generator and a digital sampling oscilloscope (DSO) together, while I was responsible for equipment calibration and fine tuning to the desired operating range of the electrical/optical components, optimize the overall transceiver system as well as performing the measurements and collecting experimental data. The work was done under the supervision of Dr. Mingliang Deng.

1.4 Thesis Structure

This thesis is structured into seven chapters. Chapter 1 describes the motivation behind the research work, presents an extensive introduction to the growing needs of end-user demand and the challenges encountered in converging the fixed-mobile access networks. In chapter 2, the fundamentals of optical communication and the review of PON technologies and RAN architectures are briefly covered, and chapters 3-6 present the results of the research work carried out exclusively as part of this dissertation. These chapters are outlined as follows:

In chapter 2, to aid the understanding of the work presented in this thesis, the fundamental principles of relevant concepts are introduced. The chapter presents the literature review of fibre-optical communication systems. SSMFs together with their linear and nonlinear transmission impairments, followed by discussions on photodetectors. Also presented is an extensive introduction to the converged fixed-mobile CAN, outlining its fundamental concept, advantages, and applications. An overview of the basic operating principle of the PON is introduced with detailed discussions on the various PON architectures, multiple access techniques and PON evolution. Subsequently, the RAN evolution with focus on the MFH/MBH networks, including their challenges and future development directions are also discussed. Furthermore, the next-generation MFH/MBH network and emerging mobile midhaul (MMH) networks for 5G RANs are also presented. The chapter also presents an overview of optical OFDM together with IMDD transmission systems, which forms the basis for the research work presented in Chapters 3-6.

Chapter 3 introduces hybrid OFDM-DFMA IMDD PONs utilizing spectrally overlapped digital orthogonal filtering, obtained by modifying DSP algorithms embedded in both the OLT and ONUs. A theoretical analysis of the proposed PON is developed and its upstream transmission performances over 40 km SSMFs are numerically explored for different application scenarios. Based on the identified optimum transceiver parameters, in comparison with the PONs in [48], the proposed PON doubles the number of supported ONUs and provides >1.7-fold aggregate upstream signal transmission capacity increases with <1.5dB upstream power budget degradations. Alternately, for the same ONU count, >2.2-fold aggregate upstream signal transmission capacity increases and >0.7dB upstream power budget improvements are achievable. The performance improvements vary by <18% for a transmission distance range as large as 50km. In addition, the proposed PON is tolerant to finite digital filter tap length-induced channel interferences.

In chapter 4, the DFT-spread spectrally overlapped hybrid OFDM-DFMA PON based on IMDD is proposed by employing the DFT-spread technique in each ONU and the OLT. Detailed numerical simulations are undertaken to identify optimum transceiver parameters and explore maximum achievable upstream transmission performances over IMDD 25 km SSMFs. It shows that the DFT-spread technique in the proposed PON is effective in enhancing the upstream transmission performance to its maximum potential, whilst maintaining all the salient features associated with previously reported PONs in chapter 3 and those in [47, 48]. Compared with the PONs in chapter 3 excluding DFT-spread, a significant PAPR reduction of over 2 dB is achieved, thus leading to a 1 dB reduction in optimum signal clipping ratio. As a direct consequence of the PAPR reduction, the proposed PON has excellent tolerance to reduced DAC/ADC bit resolution, since it can minimize the clipping/quantization-induced noise to allow the use of a minimum DAC/ADC resolution of only 6 bits at the forward error correction (FEC) limit (1×10^{-3}). In addition, the proposed PON can improve the upstream power budget by >1.4 dB and increase the aggregate upstream signal transmission capacity by up to 10% without degrading nonlinearity tolerances.

Chapter 5 present the proposed hybrid SSB OFDM-DFMA PONs without making use of the Hilbert transform operation. In the chapter, a comprehensive theoretical model of the proposed SSB PONs technique is developed, and detailed numerical simulations are also undertaken over >25 km SSMF IMDD PONs to verify the feasibility of the PONs for seamlessly converging optical and mobile networks for 5G. It is shown that similar to the PONs in [48]

referred to here as DSB PONs, the proposed SSB PON has excellent robustness against digital filter characteristic variations and channel interferences. More importantly, it decreases the PAPRs of digitally filtered OFDM signals by >2dB, thus leading to >2dB reductions in optimum signal clipping ratio and >1 bits reductions in minimum required DAC/ADC resolution bits. For fixed spectral bandwidths, the SSB PON almost doubles the maximum upstream transmission capacity without considerably degrading its differential ONU optical launch power dynamic range compared to the DSB PON. While for fixed upstream signal transmission capacities, compared to the DSB PON, the SSB PON not only halves the overall signal transmission bandwidth, but also leads to >2.5dB (>1.2dB) improvements in power budget (differential optical launch power dynamic range for ONUs locating at high frequency regions).

In chapter 6, by utilizing DOF-multiplexed in the digital domain, >30Gb/s aggregate transmission capacity of multi-channel frequency gapless six independent channels over IMDD PONs have been successfully demonstrated incorporating off-the-shelf low-cost 10G-class optical devices. Experimental result show that variable or adaptive bit loading, and channel power loading implemented in the digital domain to mitigate the impact of the physical channel frequency response-induced cross channel interference (CCI) effects enables very similar transmission performances of individual channels regardless of their spectral locations in the digital filter space. As a direct result of the interplay between the transmission system-associated negative chromatic dispersion and the intensity modulation-induced frequency chirp, negative power penalties of >0.2dB are experimentally observed for all the involved channels under various transmission system configurations. In addition, excellent performance robustness of the demonstrated systems is also obtainable for various transmission distances up to 45km.

Chapter 7 summarises my PhD thesis conclusions and outlines important areas for further investigation and research.

References

[1] IEEE, “IEEE 5G and Beyond Technology Roadmap White Paper,” [Online]. Available: https://futurenetworks.ieee.org/images/files/pdf/ieee-5g-roadmap-white-paper.pdf

[2] ITU-R, M.2370-0 “IMT traffic estimates for the years 2020–2030.” [Online]. Available: https://www.itu.int/dms_pub/itu-r/opb/rep/R-REP-M.2370-2015-PDF-E.pdf

[3] “Cisco Visual Networking Index: Annual Internet Report 2018–2023 White Paper - Cisco.” [Online]. Available: https://www.cisco.com/c/en/us/solutions/collateral/service-provider/visual-networking-index-vni/complete-white-paper-c11-481360.pdf

[4] 5GPPP Architecture Working Group, “5G White Paper,” [Online]. Available: https://5g-ppp.eu/wp-content/uploads/2018/01/5G-PPP-5G-Architecture-White-Paper-Jan-2018-v2.0.pdf

[5] ITU-R, M.2083-0 “IMT Vision – Framework and overall objectives of the future development of IMT for 2020 and beyond” [Online]. Available: https://www.itu.int/dms_pubrec/itu-r/rec/m/R-REC-M.2083-0-201509-I!!PDF-E.pdf

[6] P. Popovski, K. F. Trillingsgaard, O. Simeone and G. Durisi, "5G Wireless Network Slicing for eMBB, URLLC, and mMTC: A Communication-Theoretic View," in IEEE Access, vol. 6, pp. 55765-55779, 2018.

[7] A. Dogra, R. K. Jha and S. Jain, "A Survey on beyond 5G network with the advent of 6G: Architecture and Emerging Technologies," in IEEE Access, 2020.

[8] H. Chen et al., "Ultra-Reliable Low Latency Cellular Networks: Use Cases, Challenges and Approaches," in IEEE Comm. Magazine, vol. 56, no. 12, pp. 119-125, 2018.

[9] A. Gupta and R. K. Jha, "A Survey of 5G Network: Architecture and Emerging Technologies," in IEEE Access, vol. 3, pp. 1206-1232, 2015.

[10] Semiari, W. Saad, M. Bennis and M. Debbah, "Integrated Millimeter Wave and Sub-6 GHz Wireless Networks: A Roadmap for Joint Mobile Broadband and Ultra-Reliable Low-Latency Communications," in IEEE Wirel. Commun., vol. 26, no. 2, pp. 109-115, Apr. 2019.

[11] A. N. Uwaechia and N. M. Mahyuddin, "A Comprehensive Survey on Millimeter Wave Communications for Fifth-Generation Wireless Networks: Feasibility and Challenges," in IEEE Access, vol. 8, pp. 62367-62414, 2020.

[12] 21-S. A. Busari, K. M. S. Huq, S. Mumtaz, L. Dai and J. Rodriguez, "Millimeter-Wave Massive MIMO Communication for Future Wireless Systems: A Survey," in IEEE Commun. Surveys & Tutorials, vol. 20, no. 2, pp. 836-869, Second quarter 2018.

[13] B. Yang, Z. Yu, J. Lan, R. Zhang, J. Zhou and W. Hong, "Digital Beamforming-Based Massive MIMO Transceiver for 5G Millimeter-Wave Communications," in IEEE Transactions on Microwave Theory and Tech., vol. 66, no. 7, pp. 3403-3418, 2018.

[14] B. Chang, S. Liou and Y. Liang, "Cooperative communication in ultra-dense small cells toward 5G cellular communication," 8th IEEE Annual Inf. Technol., Elect. and Mobile Commun. Conf. (IEMCON), pp. 365-371, 2017.

[15] J. F. Valenzuela-Valdés, Á. Palomares, J. C. González-Macías, A. Valenzuela-Valdés, P. Padilla and F. Luna-Valero, "On the Ultra-Dense Small Cell Deployment for 5G Networks," IEEE 5G World Forum (5GWF), pp. 369-372, 2018.

[16] "Common Public Radio Interface (CPRI); Interface Specification V7.0," [Online]. Available: http://www.cpri.info/downloads/CPRI_v_7_0_2015-10-09.pdf

[17] eCPRI Specification V2.0. Interface Specification, Common Public Radio Interface, May 2019 [Online]. Available: http://www.cpri.info/downloads/eCPRI_v_2.0_2019_05_10c.pdf

[18] K. Zeb, X. Zhang and Z. Lu, "High-Capacity Mode Division Multiplexing Based MIMO Enabled All-Optical Analogue Millimeter-Wave Over Fibre Fronthaul Architecture for 5G and Beyond," in IEEE Access, vol. 7, pp. 89522-89533, 2019.

[19] G. Giannoulis et al., "Analogue Radio-over-Fibre Solutions for 5G Communications in the Beyond-CPRI Era," 20th Int. Conf. on Trans. Opt. Netw. (ICTON), 2018, pp. 1-5, 2018.

[20] D. Perez-Galacho, D. Sartiano and S. Sales, "Analogue Radio over Fibre Links for Future 5G Radio Access Networks," 21st Int. Conf. on Trans. Opt. Netw. (ICTON), pp. 1-4, 2019.

[21] G. Pandey, A. Choudhary and A. Dixit, "Wavelength Division Multiplexed Radio Over Fibre Links for 5G Fronthaul Networks," in IEEE J. on Sel. Areas in Commun., vol. 39, no. 9, pp. 2789-2803, 2021.

[22] P. Pesek, J. Bohata, S. Zvanovec and J. Perez, "Analyses of dual polarization WDM and SCM Radio over Fibre and Radio over FSO for CRAN architecture," 25th Wirel. and Opt. Commun. Conf. (WOCC), 2016, pp. 1-4, 2016

[23] S. Rommel, D. Perez-Galacho, J. M. Fabrega, R. Muñoz, S. Sales and I. Tafur Monroy, "High-Capacity 5G Fronthaul Networks Based on Optical Space Division Multiplexing," in IEEE Transactions on Broadcasting, vol. 65, no. 2, pp. 434-443, 2019.

[24] S. Noor, P. Assimakopoulos and N. J. Gomes, "A Flexible Subcarrier Multiplexing System with Analogue Transport and Digital Processing for 5G (and Beyond) Fronthaul," in J. of Lightw. Technol., vol. 37, no. 14, pp. 3689-3700, 2019.

[25] D. Konstantinou, A. Morales, S. Rommel, T. R. Raddo, U. Johannsen and I. T. Monroy, "Analogue Radio Over Fibre Fronthaul for High Bandwidth 5G Millimeter-Wave Carrier Aggregated OFDM," 21st Int. Conf. on Trans. Opt. Netw. (ICTON), 2019, pp. 1-4, 2019.

[26] D. Li et al., "Multi-band carrierless amplitude and phase modulation in RoF system for enhanced reliable mobile fronthaul," 2018 Conference on Lasers and Electro-Optics (CLEO), pp. 1-2, 2018.

[27] H. Zeng, X. Liu, S. Megeed, N. Chand and F. Effenberger, "Demonstration of a Real-Time FPGA-Based CPRI-Compatible Efficient Mobile Fronthaul Transceiver Supporting 53 Gb/s CPRI-Equivalent Data Rate Using," ECOC 2016; 42nd European Conference on Optical Commun., 2016, pp. 1-3.

[28] P. T. Dat, A. Kanno, N. Yamamoto and T. Kawanishi, "Seamless Convergence of Fibre and Wireless Systems for 5G and Beyond Networks," in J. of Lightw. Technol., vol. 37, no. 2, pp. 592-605, 2019.

[29] A. Tzanakaki et al., "Wireless-Optical Network Convergence: Enabling the 5G Architecture to Support Operational and End-User Services," in IEEE Commun. Magazine, vol. 55, no. 10, pp. 184-192, Oct. 2017.

[30] M. A. Habibi, M. Nasimi, B. Han and H. D. Schotten, "A Comprehensive Survey of RAN Architectures Toward 5G Mobile Commun. Sys.," in IEEE Access, vol. 7, pp. 70371-70421, 2019.

[31] I. A. Alimi, A. L. Teixeira and P. P. Monteiro, "Toward an Efficient CRAN Optical Fronthaul for the Future Networks: A Tutorial on Technologies, Requirements, Challenges, and Solutions," in IEEE Commun. Surveys & Tut., vol. 20, no. 1, pp. 708-769, 1st quart. 2018.

[32] D. Nesset, "PON roadmap [invited]," in IEEE-OSA J. of Opt. Commun. and Netw., vol. 9, no. 1, pp. A71-A76, 2017.

[33] J. S. Wey, "The Outlook for PON Standardization: A Tutorial," in J. of Light. Technol., vol. 38, no. 1, pp. 31-42, 2020.

[34] ITU-T G.989 Series Recommendations “40-Gigabit-Capable Passive Optical Networks (NG-PON2)”, [Online]. Available: https://www.itu.int/rec/T-REC-G.989-201510-I/en

[35] J. Wei et al., "Demonstration of the First Real-Time End-to-End 40-Gb/s PAM-4 for Next-Generation Access Applications Using 10-Gb/s Transmitter," in J. of Lightw. Technol., vol. 34, no. 7, pp. 1628-1635, 2016.

[36] X. Tang et al., "Experimental Demonstration of 40-Gb/s I-SC-FDM With 10G-Class Optics and Low-Complexity DSP for Next-Generation PON," in IEEE Photo. J., vol. 10, no. 3, pp. 1-9, Art no. 7202509, 2018.

[37] H. Shin, Y. Shim and S. Cho, "NG-PON2 Development for 10G Internet Service: A Study Case of SK," 2018 23rd Opto-Elect. and Commun. Conf. (OECC), 2018, pp. 1-2, 2018.

[38] H. Roberts, N. Proite, P. Lee and C. Smith, "Lessons Learned from NG-PON2 Systems Developments and Deployment," 2019 Optical Fibre Commun. Conf. and Exh. (OFC), pp. 1-3, 2019.

[39] Ma, X. Wen, L. Wang, Z. Lu and R. Knopp, "An SDN/NFV based framework for management and deployment of service based 5G core network," in China Commun., vol. 15, no. 10, pp. 86-98, 2018.

[40] G. Talli et al., "SDN Enabled Dynamically Reconfigurable High-Capacity Optical Access Architecture for Converged Services," in J. of Lightw. Technol., vol. 35, no. 3, pp. 550-560, 2017.

[41] C. Balint and G. Budura, "OFDM-Based Multi-Carrier Waveforms Performances in 5G," 2018 Int. Symposium on Elect. and Telecom. (ISETC), 2018, pp. 1-4, 2018.

[42] A. Saljoghei et al., "Comparison of OFDMA and GFDMA for next-generation pons," in IEEE-OSA J. of Opt. Commun. and Netw., vol. 9, no. 12, pp. 1064-1073, Dec. 2017.

[43] A. Sankoh, W. Jin, Z.Q. Zhong, J. He, Y. Hong, R.P. Giddings, I. Pierce, M. O'Sullivan, J. Lee, T. Durrant, J.M. Tang, "Hybrid OFDM-Digital Filter Multiple Access PONs Utilizing Spectrally Overlapped Digital Orthogonal Filtering," in IEEE Photo. J., vol. 12, no. 5, pp. 1-11, 2020.

[44] Sankoh, A.; Jin, W.; Zhong, Z.; He, J.; Hong, Y.; Giddings, R.; Tang, J. DFT-Spread Spectrally Overlapped Hybrid OFDM–Digital Filter Multiple Access IMDD PONs. Sensors 5903, 2021.

[45] W. Jin, A. Sankoh, Y. X. Dong, Z. Q. Zhong, R. P. Giddings, M. O'Sullivan, J. Lee, T. Durrant and J. M. Tang., "Hybrid SSB OFDM-Digital filter multiple access PONs," J. Lightw. Technol., early access, Jan. 2020.

[46] M. Deng, A. Sankoh, R. Giddings, and J. Tang, "Experimental demonstrations of 30Gb/s/λ; digital orthogonal filtering-multiplexed multiple channel transmissions over IMDD PON systems utilizing 10G-class optical devices," Opt. Express 25, 24251-24261 (2017).

[47] M. Bolea, R. P. Giddings, M. Bouich, C. Aupetit-Berthelemot, and J. M. Tang, "Digital filter multiple access PONs with DSP-enabled software reconfigurability," J. Opt. Commun. Netw., vol. 7, no. 4, pp. 215–222, 2015.

[48] Y. X. Dong, R. P. Giddings, and J. M. Tang, “Hybrid OFDM-digital filter multiple access PONs,” J. Lightw. Technol., vol. 36, no. 23, pp. 5640–5649, 2018.

[49] M. Bolea, R. P. Giddings and J. M. Tang, "Digital Orthogonal Filter-Enabled Optical OFDM Channel Multiplexing for Software-Reconfigurable Elastic PONs," in J. of Lightw. Technol., vol. 32, no. 6, pp. 1200-1206, 2014.

2. Optical Network Technologies and Fixed and Mobile Access Network Convergence

Contents

This chapter introduces the basic concepts common to optical communication systems, provides an overview on the convergence of optical and mobile access networks, discusses the fundamentals of optical OFDM, and presents the application of optical access networks based on IMDD. The above aspects form the basis of the work undertaken in this thesis.

In the subsequent sections of this chapter, an overview of optical transceivers and basic optical components used in contemporary optical communication systems, and fibre channel characteristics (including both linear and nonlinear effects) are discussed in detail. The descriptions of these optical components and fibre transmission effects not only illustrate their roles in optical transmission systems but also provide an in-depth understanding of their impacts on the system performance. In addition, photodetectors are also discussed since they are common to all IMDD-based PONs. After that, effort is made to describe the essential features of major multiplexing technologies employed in typical PONs. Furthermore, details of current and future PON standards are also presented, added to which an overview is given, of IMDD PON-based MFHs/MBHs to support the evolution of mobile RANs.

In addition, to provide an in-depth understanding of the theoretical foundation of this work, OFDM fundamentals and their applications in optical transmission systems are extensively covered in this chapter as OFDM is the basis modulation technique employed in this thesis. The discussion starts with a brief introduction to OFDM and its operating principle, and then the major DSP components that form an OFDM transceiver are described in detail. Finally, the last section of this chapter covers the fundamental concepts associated with IMDD-based OFDM PONs.

2.1 Optical Transmission System

As shown in Fig. 2.1, an optical fibre communication system can be divided into three main subsystems: an optical transmitter, an optical fibre channel and an optical receiver. The role of an optical transmitter is to perform the electrical-to-optical (E-O) conversion. An optical transmitter consists of a narrow linewidth laser source, a modulator and a channel multiplexer. Semiconductor lasers or light-emitting diodes (LEDs) are used as optical sources. The optical signal generated by a semiconductor laser is modulated by an information signal before being transmitted over the optical fibre. There are mainly two schemes of optical modulation including intensity modulation (IM) and coherent modulation. For cost-effective practical

implementation of optical transmission systems, IM is thus considered since coherent modulation requires expensive and complex optical modulators.

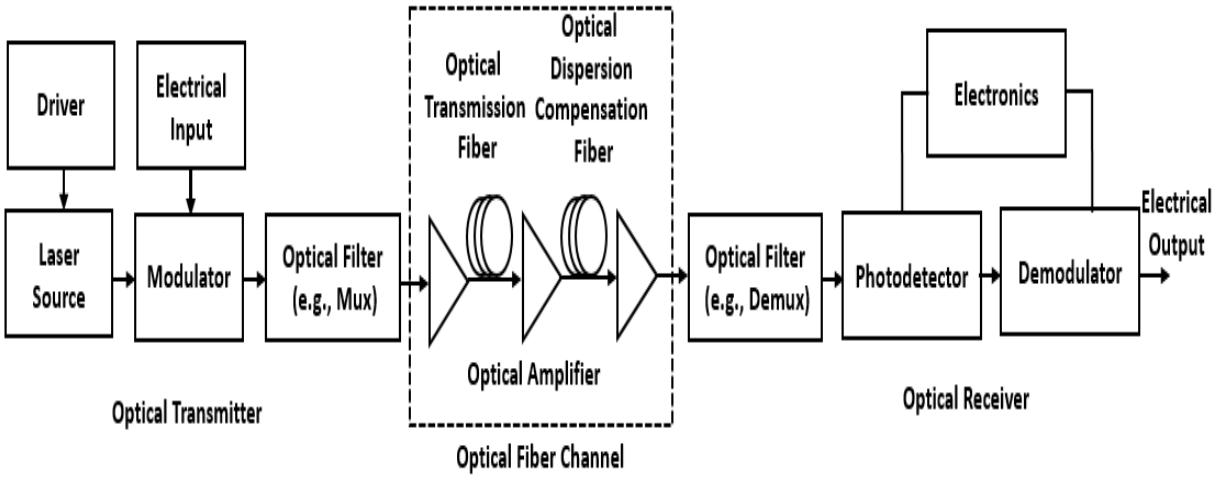

Fig. 2.1. An exemplary optical transmission system identifying key optical components [1].

The second subsystem is the optical fibre channel which is served as a medium to transport the optical signals from the transmitter to the receiver. The optical fibres attenuate the signal during transmission, and optical amplifiers such as erbium-doped fibre amplifiers (EDFAs) or Raman amplifiers, may be included between optical spans to restore the signal quality [1-3]. Fig. 2.1 depicts a typical configuration in which dispersion compensated fibres (DCF) are preceded by two EDFAs. However, the process of amplification is also accompanied by noise addition.

The last key subsystem is the optical receiver, which performs the process of optical-to-electrical (O-E) conversion, and process appropriately the obtained electrical signal to recover the data being transmitted. It consists of a demultiplexer, a photodetector, and a demodulator. The design of the demodulator depends on the modulation scheme used by the optical transmission system.

2.1.1 Optical Transmitter

The basic operating principle of optical intensity modulation is that the intensity or power of the light beam from a laser source is modulated by the amplitude of an electrical signal and no phase information is needed. Assuming that $A_{ele}(t)$ is the electrical signal biased with the direct current, $A_{ele}(t) > 0$, the optical signal produced by an ideal IM can be defined as:

$$E_{opt}(t) = e^{j2\pi f_o t}.\sqrt{A_{ele}(t)} \quad (2.1)$$

where f_o, is the optical carrier frequency. Technically speaking, modulating the electrical signal on an optical carrier can be achieved by two main techniques, namely direct modulation, and external modulation, which are widely used in optical transmission systems [3, 4].

2.1.1.1 Direct Modulation

Direct modulation is the simplest optical modulation technique based on semiconductor lasers. A directly modulated laser (DML) can modulate the optical output power by applying an electrical driving current directly to the laser device to change the intensity of the emitted optical wave. The laser must be biased such that the DML is operating above the threshold current and that there is sufficient scope to ensure the positive and negative swing of the modulating signal is in a highly linear region of operation to minimize unwanted distortions due to saturation or operating too close to the threshold current.

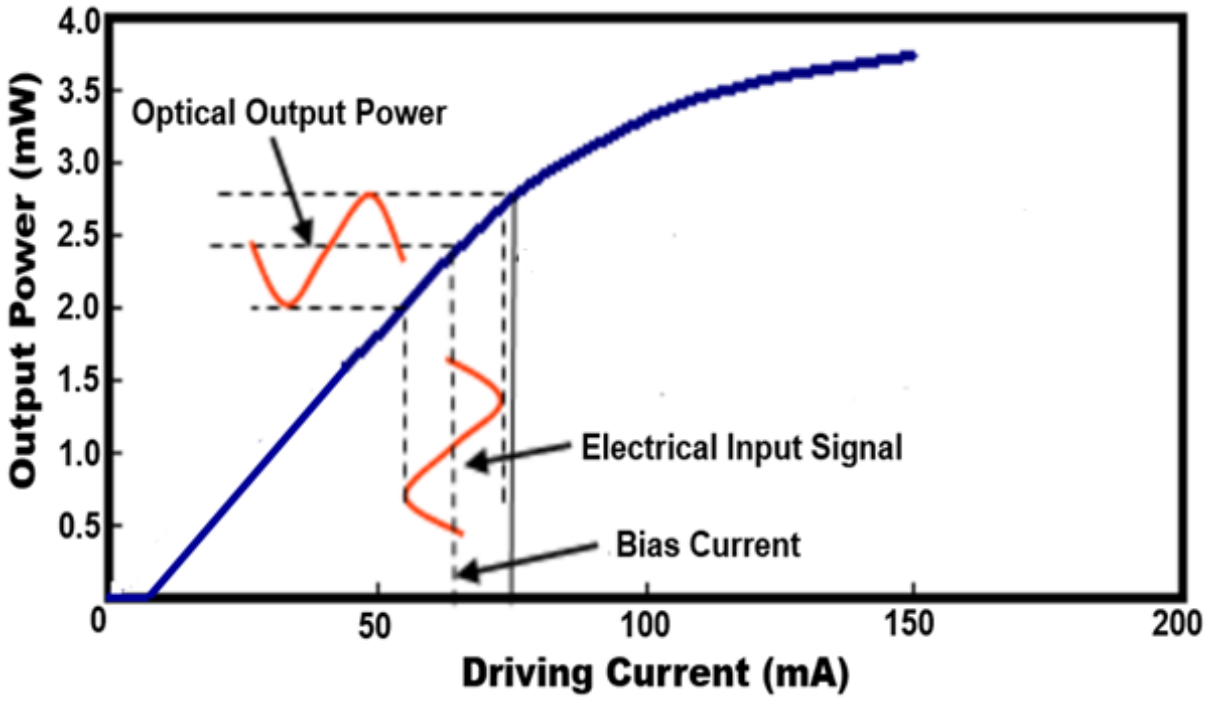

Fig. 2.2. Output power versus the driving current of DML

Fig. 2.2 shows an example of output power versus driving current for a directly modulated distributed feedback (DFB) laser [5]. In the DML, since the optical signal generation and light modulation are functionally integrated within the same device, this technique achieves the simplest and most compact transmitter. Compared to other intensity modulators such as conventional external intensity modulators, DFB-based DMLs are the most widely used devices in optical transmission systems due to their several advantages, which includes low

cost, relatively small driving voltage, low electrical power consumption and high output optical power. The major disadvantage of DMLs, when used over long distances for high bit rates intensity-modulated transmission systems, is their inherent frequency chirp, which is the result of residual unwanted data-dependent phase modulation accompanying the desired intensity modulation [6]. The laser chirp broadens the optical signal spectrum and may result in significant distortions of the optical signal transmitting through the fibre caused by the interaction with chromatic dispersion (CD) and fibre nonlinearity [6-8]. As such, DMLs are limited to systems with low speed-dispersion products. This brings about challenges for high-speed optical fibre communication systems involving DMLs.

2.1.1.2 External Modulation

For high bit rates and long fibre transmission distances, the frequency chirp effect imposed by direct modulation becomes sufficiently large such that DMLs are rarely used. For high-speed transmitters, the laser is biased at a constant current to produce a continuous wave (CW) output, which is converted into a data-coded optical signal by an optical modulator placed next to the laser [3,9]. From the standpoint of device operation, external modulators can be categorised into two types including, the electro-absorption modulator (EAM) where the amount of light absorbed varies with the applied electric field. EAMs are attractive because of their small size and can be easily integrated with driver circuits and/or laser sources to form electro absorption-modulated lasers (EMLs). Like DFB lasers, EAMs produce some residual and component-specific chirp. Through careful designs, the chirp can be used to increase the uncompensated reach of EAM-based transmitters through counteracting with CD [3,6]. In contrast, EAMs are wavelength-dependent and have limited power-handling capabilities. Mach-Zehnder modulator (MZM) on the other hand is another type of external modulation, which uses a two-branch Mach-Zehnder interferometer to modulate the phase of the optical signal passing through each branch experiencing identical phase shifts and interfering constructively [3,6,9]. An MZM is the simplest and most widely used interference structure used for modulation. It can provide good control of the chirp and can produce pure amplitude modulation without residual chirps if its two branches are driven with opposite-sign(“differential”) driving signals, which is commonly referred to as the “push-pull” operation. Compared with the DMLs and EMLs, MZMs offer improved modulation performance with a negligible chirp. However, because MZMs have higher device/system complexity and cost, it is not the preferred choice for cost-sensitive application scenarios.

2.1.2 Basics on Optical Fibres

2.1.2.1 Optical Fibres

In optical transmission systems, the role of optical fibres is to transmit optical signals from a transmitter to a receiver. Typically, an optical fibre consists of a cylindrical core of silica glass surrounded by a cladding with a lower refractive index than the core. The classification of optical fibres is based on their dispersion characteristics and is commonly categorised into two main types, including multi-mode fibres (MMFs), ITU-G.651 and SMFs, ITU-G.652 [10]. An MMF has a large-diameter core typically in the range ~50-62.5μm and allows multiple light modes to propagate through it. In a MMF, different modes propagate at different speeds, this causes mode delay. Such dispersive effect is known as modal dispersion, which narrows the transmission system bandwidth and limits the maximum transmission reach. In contrast to a MMFs, a SMF has a small glass core diameter (4-10μm) and light can propagate in a single mode only, thus eliminating modal dispersion [3]. However, the SMF still suffers from the dispersive effect caused by chromatic dispersion, as discussed in subsection 2.1.2.2. With regards to the bit rate-distance condition, for low bit rates and short transmission reach, a MMF is the preferred choice and is mostly installed in local area networks (LANs). On the other hand, for high bit rates and long transmission reach, a SMF is the ideal choice. In terms of fibre cost, SMFs are relatively cheaper than MMFs. However, the equipment used for communications over MMF-based transmission systems is usually less expensive than those based on SMFs. In this thesis, only a SMF is considered.

2.1.2.2 Chromatic Dispersion

CD is caused by the frequency dependence of the refractive index of an optical fibre. As a result, the different spectral components of an optical pulse travels at slightly different group velocities, leading to optical signal broadening. For a SMF of length L, a specific spectral component at the frequency ω would arrive at the output end of the fibre after a time delay $T = L/v_g$, with $vg = (d\beta/d\omega)^{-1}$ being the group velocity. If Δω is the spectral width of the pulse, the extent of the pulse broadening for a fibre length L is given by:

$$\Delta T = \frac{dT}{d\omega}\Delta\omega = \frac{d}{d\omega}\left(\frac{L}{v_g}\right)\Delta\omega = L\frac{d^2\beta}{d\omega^2}\Delta\omega = L\beta_2\Delta\omega \qquad (2.2)$$

where the parameter β_2 is the group velocity dispersion (GVD) defined as $\beta_2 = d^2\beta/d^2\omega$, and it

determines how wide the pulse will broadening when propagating inside the fibre. Since the frequency spread $\Delta\omega$ is determined by the range of wavelengths $\Delta\lambda$ emitted by the optical source, by using $\omega = 2\pi c/\lambda$ and $\Delta\omega=(-2\pi c/\lambda^2)\,\Delta\lambda$, Eq. (2.2) can be rewritten as:

$$\Delta T = \frac{d}{d\lambda}\left(\frac{L}{v_g}\right)\Delta\lambda = DL\Delta\lambda \tag{2.3}$$

where D is the dispersion parameter defined as $D=d\beta_1/\lambda$, and $\beta_1=1/v_g=c/n_g$ indicating the group velocity, with c being the speed of light in vacuum and n_g the group index. In practice, the CD is characterized by the dispersion parameter D and is also related to the GVD parameter β_2, and can be rewritten as:

$$D = \frac{d\beta_1}{d\lambda} = -\frac{2\pi c}{\lambda^2}\beta_2 = -\frac{2\pi c}{\lambda^2}\frac{d^2\beta}{d\omega^2} \tag{2.4}$$

Thus, the waveguide dispersion factor is directly related to the second-order derivative of the propagation constant with respect to the optical radial frequency. With the demand for reducing the effects of fibre CD, several types of fibres including dispersion-shifted fibres (DSF) and non-zero DSFs (NZDSF) have been developed. Values of D for various types of fibres within the C-band wavelengths of the ITU-Grid standard are shown in Fig.2.3. For SMFs, D is zero near the optical window around 1310 nm and ~17 ps/(km·nm) in the 1550 nm region.

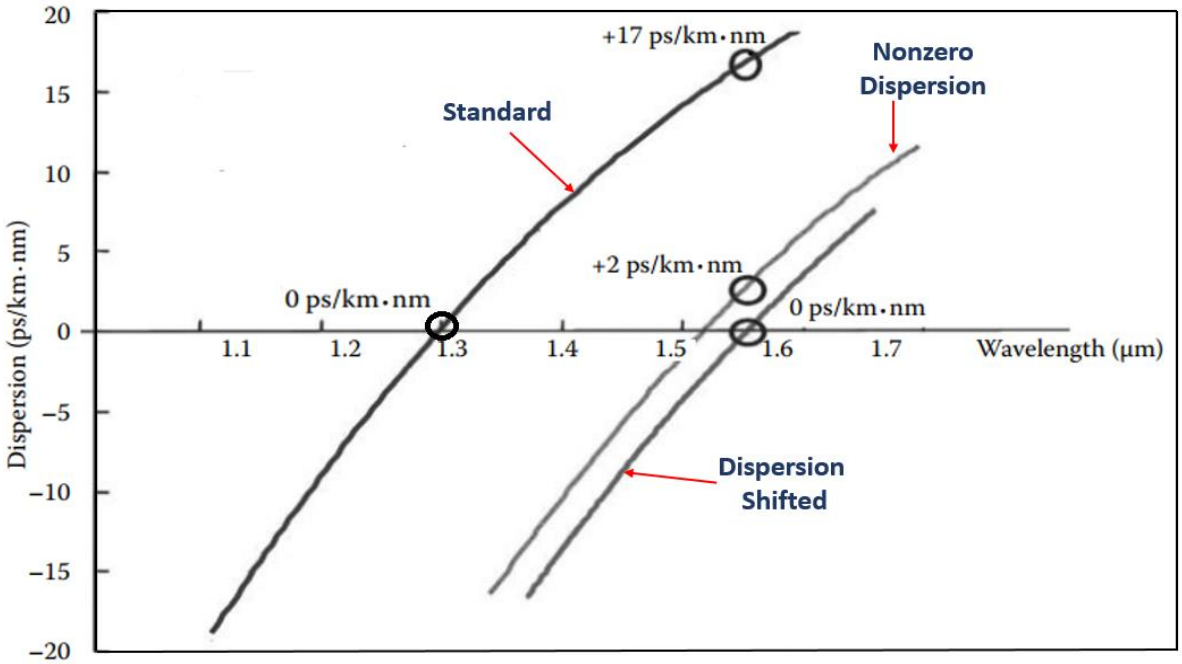

Fig. 2.3. Typical wavelength dependence of the dispersion parameter D for different types of fibre [3]

As signals occupy finite frequency spans, pulse broadening due to CD-induced time delay causes inter-symbol interference (ISI) to occur, thus limiting the maximum achievable signal transmission capacity [9]. In OOFDM transmission systems, the CD-induced ISI can be overcome by adding a cyclic prefix (CP) and by using channel equalization which automatically compensates for the linear effects. CP and channel equalization approaches are discussed in section 2.2.6.2.2 and section 2.2.6.2.4 respectively.

2.1.2.3 Fibre Losses

Fibre losses represent another fundamental limiting factor because it reduces the average optical signal power reaching the receiver. Under general conditions, when transmitting through SMFs, the average optical signal power is attenuated due to fibre loss with the attenuation coefficient of the optical power P governed by Beer's law ($dP/dz = -\alpha L$). If P_{in} is the power launched at the input end of the fibre with length L, the output power P_{out} at end of the fibre is given by [3]:

$$P_{out} = P_{in} 10^{\left(\frac{-\alpha L}{10}\right)} \tag{2.5}$$

where α is the attenuation coefficient and expressed in units of dB/km. This attenuation coefficient includes all effects of power loss when signals are transmitted through the optical fibre. Several factors contribute to the overall losses, however, rayleigh scattering and material absorption are the main physical mechanisms causing fibre attenuation, and such mechanisms are optical wavelength-dependent. These factors have been described in detail and can be found in [3,11].

2.1.2.4 Fibre Nonlinearity

Nonlinear optical effects are a physical phenomenon that occurs in response to optical fibres when subjected to an intense electromagnetic field. Fundamentally, the physical insights into the origins of nonlinearity lie in the anharmonic motion of bound electrons under the influence of an applied field, which can alter the typical properties (absorption, refractive index) of the physical medium. As a direct consequence, fibre nonlinearities affect both the amplitude and phase of optical signals travelling through the SMF.

Nonlinear fibre effects are generally classified into two main categories. The first type exhibits energy transfer from the optical field to the medium via a stimulated inelastic scattering process

in which the frequency (or the photon energy) of the scattered light is downshifted. Such scattering effects include stimulated Brillouin scattering (SBS) and stimulated Raman scattering (SRS) phenomena. A major difference between SBS and SRS is that optical phonons participate in SRS whilst acoustic phonons participate in SBS, both resulting in optical signal power loss at the incident frequency. As a result of the difference in dispersion relations for acoustic and optical phonons, in a SMF, SBS produces a back-scattered propagating light downshifted in a frequency by about 10 GHz, while SRS produces both a forward and backward scattered light with a frequency of up to 13 THz [3]. Furthermore, for both cases, the intensity of the scattered light increases exponentially once the launch power exceeds a certain threshold, which is typically in the order of ~10dBm for SBS and ~30dBm for SRS [3]. In contrast to SBS and SRS, another scattering phenomenon is the Rayleigh back scattering, which is an example of elastic scattering in which the frequency of scattered light remains unchanged. The fibre loss due to Rayleigh scattering arises from local microscopic fluctuations in density leading to random fluctuations of the refractive index on a scale lower than the optical wavelength. As fibre losses depend on the wavelength of a transmitted light, at 1550nm, the fibre loss is dominated by Rayleigh scattering near this wavelength [3].

Besides the above-mentioned nonlinear optical scattering mechanisms, the second type of the nonlinear effect is Kerr nonlinearity, which occurs due to the dependence of the refractive index on the intensity of the propagating signal. The three most important fibre nonlinearities belonging to this category are self-phase modulation (SPM), cross-phase modulation (XPM), and four wave-mixing (FWM) [3,9].

Self-Phase Modulation

SPM is the major nonlinear limitation in a single optical channel and refers to self-induced phase shift experienced by an optical field [3]. A pulse of light, when propagating in optical fibre will induce a varying refractive index of the fibre due to the optical Kerr effect. This variation in refractive index will produce a phase shift in the pulse, resulting in an SPM-induced optical frequency chirp. This effect increases the spectral width of the pulse. Due to the optical intensity dependence of refractive index, the nonlinear phase shift, Φ_{NL}, imposed on the optical field is proportional to the optical intensity which can be expressed as:

$$\Phi_{NL} = n_2 k_0 L |E|^2 \tag{2.6}$$

where n_2 is the second-order nonlinear refractive index coefficient, referred to as Kerr coefficient throughout this thesis, with typical values of 2.2-3.4 x10^{-20} m^2/W. $k_0 = 2\pi/\lambda$ with λ being the central carrier wavelength, and $|E|^2$ is the optical intensity inside the fibre.

In general, for an optical signal propagating through an SSMF fibre link, the interplay between CD and SPM-induced chirp causes optical pulse broadened and may result in signal distortions. This makes SPM undesirable and must be taken into consideration in the dispersion management of optical fibre links. It is also noteworthy that in IMDD transmission systems the CD-induced channel fading effect can be mitigated by SPM when high optical launch power levels are applied. This is mainly attributed to the fact that the co-existence of the phase changes due to CD and SPM with opposite signs will shift the frequency response null towards the high frequency region, as shown in Fig 2.4.

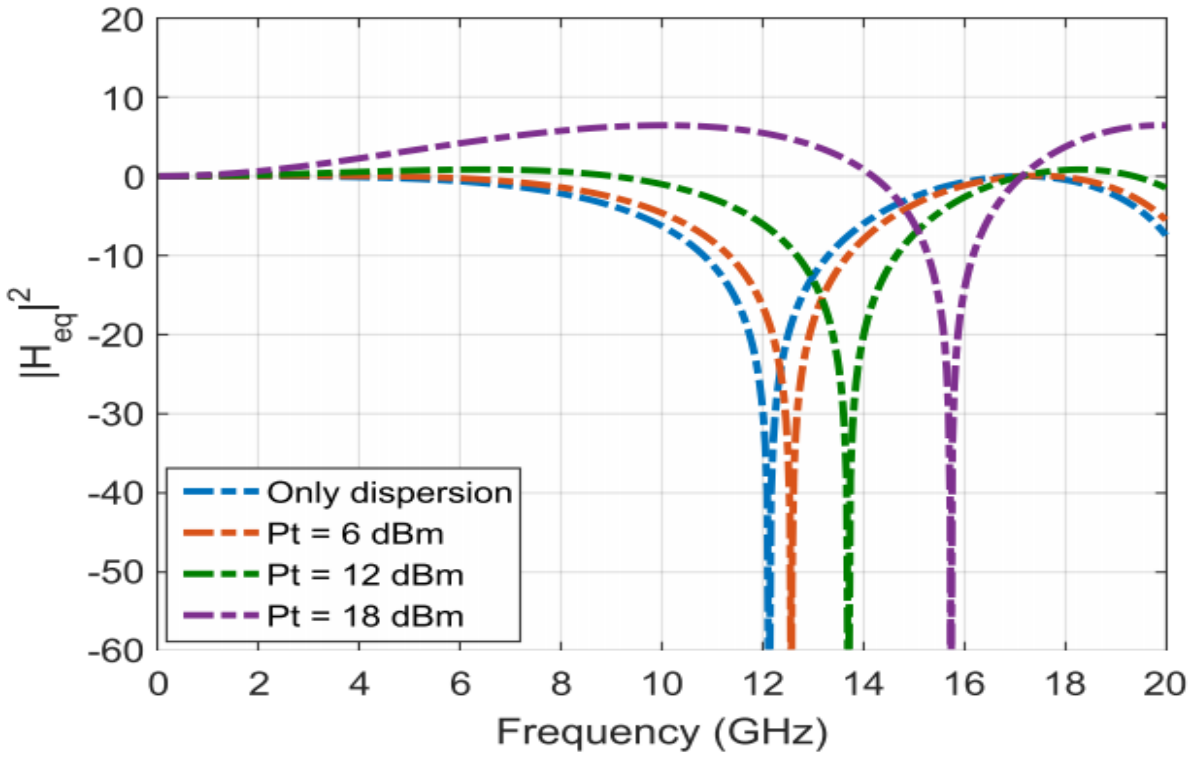

Fig. 2.4. Analysis of channel frequency responses of a 25 km SSMF IMDD PON system for various optical launch powers [12].

Cross-Phase Modulation

Compared to SPM, XPM is another nonlinear optical effect caused by the intensity dependence of the refractive index, but it is related to the multichannel transmission systems such as in WDM or even in dense WDM (DWDM) optical systems where it is often a notorious source

of performance degradation due to the inter-channel crosstalk it introduces. The XPM induced nonlinear phase change of an optical field occurs when two or more optical channels are propagated simultaneously inside an optical fibre at different wavelengths. The nonlinear phase shift of a specific optical channel is affected not only by its power but also by the power of other co-propagating channels. For instance, when two optical fields E_1 *and* E_2 at frequencies ω_1 and ω_2 co-propagate in an optical fibre, the nonlinear phase shift for the field at ω_1 caused by intensity variations in another channel is given by [3,9]:

$$\Phi_{NL} = n_2 k_0 L(|E_1|^2 + 2|E_2|^2) \tag{2.7}$$

From the two terms on the right-hand side of Eq. (2.7), it is easy to understand that the XPM is always accompanied by SPM, which is the first term and that the sum extends over the number of channels. The factor of 2 in the second term has its origin in the form of the nonlinear susceptibility and indicates that for optical fields with the same amount of power (E_1=E_2), XPM is twice as effective as SPM. Like SPM, XPM also causes a greater temporal pulse broadening as the signal propagates along with the fibre due to the CD effect.

Four Wave-Mixing

FWM is an intermodulation phenomenon arising from a third-order optical nonlinearity and occurs when the light of two or more different wavelengths propagates together in an optical fibre such as the WDM signal. Generally, when multiple signals at different wavelengths are simultaneously launched into an optical fibre, the intensity dependence of refractive index not only induces SPM and XPM on each signal but also gives rise to a new wave caused by FWM, the wavelength of which does not coincide with any of the wavelengths. Assuming three optical fields with carrier frequencies ω_1, ω_2 and ω_3 copropagating inside the fibre simultaneously, a refractive index modulation at the difference frequency components occurs, which generates the fourth field components ω_4, whose frequency is related to the others by:

$$\omega_4 = \omega_1 \pm \omega_2 \pm \omega_3 \tag{2.8}$$

When FWM occurs energy transfers efficiently from one frequency to another when phase matching between the copropagating signals is achieved. Thus, FWM is a phase-sensitive process, in that the efficiency of the process is strongly affected by phase matching conditions. FWM mostly manifests itself in WDM transmission systems where the multiple channel

wavelengths are equally spaced, resulting in crosstalk between channels with different wavelengths. The effect of FWM becomes more severe in the DWDM system where the channel spacing is usually small. Its effect can efficiently accumulate over longer fibre distances only if a phase-matching condition is satisfied which is not only influenced by CD but also highly dependent on high signal power levels and/or channel spacing [3,13].

FWM can be suppressed either by reducing the power per channel or by preventing the perfect phase matching by increasing the CD or increasing the channel spacing. To minimize FWM crosstalk in WDM systems, one efficient option is to use an un-equal WDM channel spacing [3,14]. However, for the application scenario of interest of this dissertation research work, the influences of SPM, XPM, and FWM nonlinearities are not significant as only single-channel links are utilized for either upstream or downstream transmission with relatively short transmission distance and low optical launch power levels.

2.1.3 Optical Receiver

2.1.3.1 Photo-Detector

A photo-detector or photodiode (PD) is used to convert the modulated optical signal transmitted by the optical fibre into an electronic signal. Among the many different types of PDs which are commercially available, the semiconductor-based PD is used almost exclusively for high-speed fibre transmission systems due to its compactness, compatibility with optical fibres (being small in size), extremely high bandwidth and relatively low cost. The basic principle behind photodetection using semiconductors is optical absorption. Although the conversion efficiency depends on the complete photoreceiver rather than on the photodetector only, however, to meet the requirements of optical fibre transmission systems, several parameters such as responsivity, the wavelength of interest, bandwidth and noise characteristics are used to characterize the ability of the photodetector.

2.1.3.1.2 PIN and APD

In the receiver, the transmitted optical signal is detected by a photodetector, which converts the optical signal into the electrical domain. The two most common commercially available p-i-n junction photodiodes used in optical transmission systems are the *P* type-intrinsic-*N* type (PIN) photodiode and avalanche photodiode (APD) [3,15,16]. These photodiodes convert the

incident optical power, P_{in}, into an electrical current, I_p, based on square-law detection. The generated photocurrent I_p is proportional to the incident optical power P_{in} and is given by:

$$I_P = RP_{in} = RE_0E_0^* \tag{2.9}$$

where R is the responsivity of the photodetector (in units of A/W) and E_0 is the received optical signal. In the open literature [17,18], such photon detection is often called direct detection due to its square-law operation to the optical field. The responsivity R can be defined in terms of the fundamental quantity, η, called the quantum efficiency, given as [1,3]

$$\eta = \frac{number\ of\ electron\ pairs\ generated}{number\ of\ incident\ photons} = \frac{I_p/q}{P_{in}/h\nu} = \frac{h\nu}{q}R \tag{2.10}$$

where h and q are the plank's constant and electronic charge respectively. All detectors require a minimum current to operate that can be expressed as [1,3]

$$P_{in} = \frac{I_p}{R} \tag{2.11}$$

The relation of Eq. (2.9) assumes a noise free conversion process. In practice, shot noise and thermal noise are the two most significant noise mechanisms associated with an optical detection system. These noises are responsible for current fluctuations in all optical receivers even when the incident optical power is constant.

Shot noises are generated by the random generation of streams of photo-electrons when an optical signal is incident on a photodetector. The noises are specified in noise spectral density which is the square of the noise current per unit frequency (in Hz). The noise variance is proportional to the photocurrent, and can be defined as in [1,3]:

$$\sigma_s^2 = 2qI_p\Delta f \tag{2.12}$$

where Δf is the effective noise bandwidth of the receiver.

Thermal noise is however due to another mechanism detailed as follows: At a finite temperature, electrons move randomly in any conductor. This random thermal motion of electrons manifests as a fluctuating current even in the absence of an applied voltage and adds such fluctuation to the photocurrent. The noise variance is given by [1,3]:

$$\sigma_T^2 = \frac{4TK_B}{R_L}\Delta f \tag{2.13}$$

where K_B is the Boltzmann constant with a value of 1.38×10^{-23} *J/K*, *T* is the absolute temperature (in K) and R_L is the load resistor (in Ω). In practice, the two fundamental noise sources, shot noise and thermal noise cause fluctuations in the generated current I_p even when P_{in} is constant. The total current noise can be obtained by adding the contributions of shot noise and thermal noise, given by:

$$I = I_p + I_s + I_t \tag{2.14}$$

Where I_s and I_t are the current fluctuations induced by shot noise and thermal noise and are independent random processes with approximately Gaussian statistics [1,3]. Eq. (2.14) indicates that the noise lowers the received signal to noise ratio (SNR) and therefore worsens the BERs in the receiver. To enable the receiver to operate reliably at a BER of 10^{-9} referred to as receiver sensitivity, the received optical power should be higher than the minimum optical power. Any powers below the receiver sensitivity will lead to system performance degradation, which is mainly due to thermal noise.

2.2 Optical Network Technologies for Converging Fixed Access and Mobile Fronthaul/Backhaul Networks

With the advent of 5G, to achieve sustainable business models for mobile network operators (MNOs) and service providers offering advanced services such as on-demand dynamic provision, the next generation optical access and mobile access networks are envisioned to evolve into a converged fixed-mobile access network to provide flexible MFHs/MBHs capable of supporting dynamic traffic and user-specific applications. To meet these requirements, converged fixed-mobile CANs capable of transparently supporting various data rates at arbitrary bandwidth granularity are required. Since PONs due to their mature standards and cost-effectiveness account for the vast majority of global deployments of fibre-to-the-home (FTTH) and fibre-to-the-building (FTTB), they are considered as promising candidates to achieve a PON-based "future-proof" converged fixed-mobile CANs for 5G. Among the various optical access networks, next generation (NG)-PONs have attracted extensive research and development interest and are expected to play a significant role in 5G to enable users to enjoy transmission speeds >10 Gb/s [19, 20]. Recent years have seen a paradigm shift in the evolution

of PON standards from the traditional time division multiple access (TDMA) PONs [21, 22] to several other variants of PONs such as wavelength division multiple access (WDMA) PONs [23, 24], hybrid TWDMA PONs [25, 26], OFDMA PONs [27-29], and as well the promising new multiple access techniques termed DFMA [30, 31], which apply to both PONs and their associated CANs.

As discussed in Chapter 1, the PON-based converged fixed-mobile CANs have been proposed for 5G [32-35] as future-proof and cost-effective solutions not only to meet the growing traffic demands but also with strong adaptability to deal with dynamic traffic. Chapter 1 introduces the PON-based converged fixed-mobile CANs, in this section, a more detailed description of PON technologies associated with CANs for 5G and beyond networks is presented.

2.2.1 Converge Fixed Access and Mobile Access Networks

From the practical network operation point of view, traditionally fixed and mobile access networks have evolved and mostly been developed and implemented separately, and the current network deployment scenarios are still reflecting this independent evolution. In recent years, for example, with the deployments of 4G mobile networks and FTTH/FTTB fixed networks, in order to address the significant increases in traffic demands, the fixed access and mobile access network, have been subjected to significant evolutions. All these network evolutions require enormous investments from MNOs in implementing new network infrastructures. As a result of all these factors, MNOs are increasingly motivated to converge the fixed access and mobile access networks to reduce both the capital expenditure (CAPEX) and the operational expenditure (OPEX) [36].

A general view of the topology of currently deployed fixed and mobile networks is depicted in Fig. 2.5, which comprises the access network, the metropolitan/regional aggregation network and the core network. The access network is between the metropolitan network and the subscriber. The CO is the gateway to the aggregation network which connects all COs, usually in a large city or region via an optical fibre ring topology that spans over several kilometers. At the end of the chain, the metropolitan network is terminated at the core network. The mobile network itself comprises of two segments, which are different from the fixed network segments, on one hand is the RAN comprising of the wireless access network and the MFH/MBH networks, while on the other hand is the mobile core network, both of which are connected by dedicated and/or shared aggregation infrastructure.

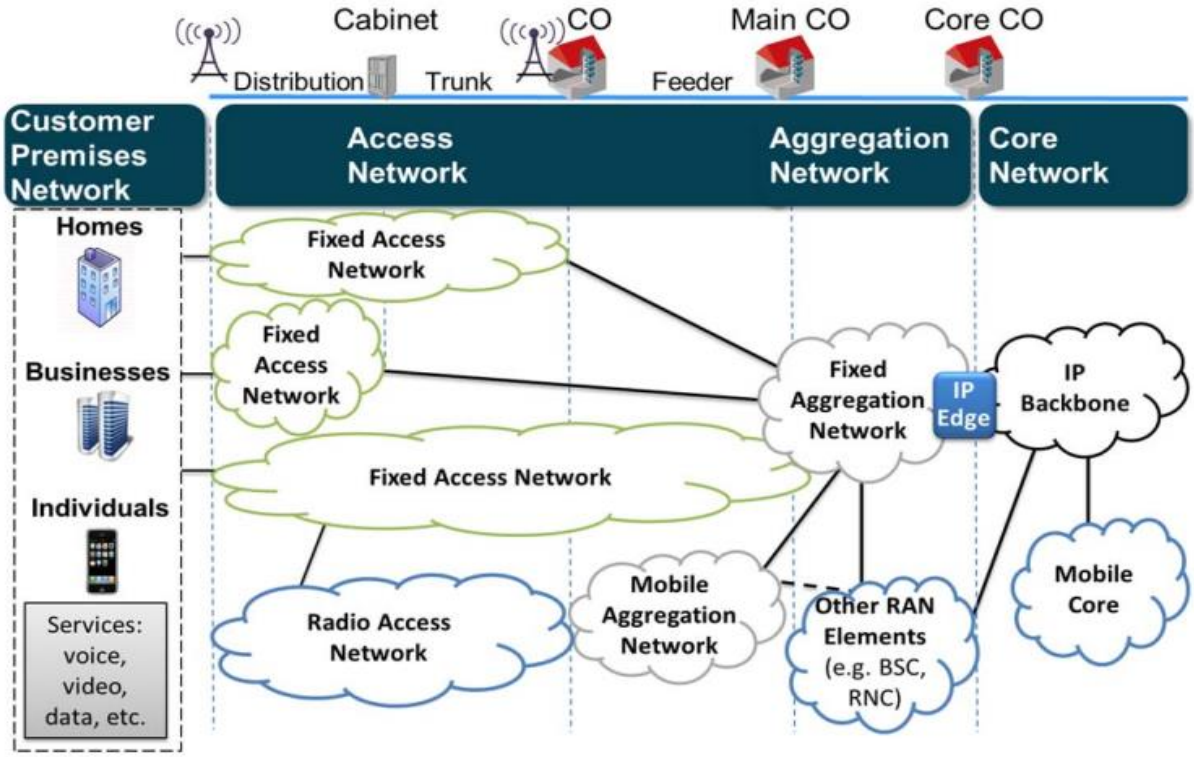

Fig. 2.5. A model fixed-mobile network convergence scenario [37]

As the existing networks are overwhelmed with inherent problems of lower data rates, the convergence of fixed and mobile at the network level is a key requirement of 5G infrastructures, and it has already been considered as a network planning approach for initial 5G architecture to support a wide range of emerging applications/services to realize ubiquitous and elastic connections cost-effectively. Optical fibre networks have been continuously evolving to address the ever-increasing mobile traffic demands, and its role is shifting from FTTH/FTTB to fibre-to-the-x (FTTx) to a universal access platform that supports both fixed and mobile broadband services. As many features of the next generation optical access and mobile access network solutions are complementary to each other, the integrated hybrid infrastructure of fixed-mobile networks can exploit the optical fibre bandwidth and take advantage of the mobility features of the wireless networks to provide continuous broadband access to the fixed and mobile users in a unified networking platform.

As earlier stated, since PONs due to their cost-effectiveness are considered as one of the most promising solutions to realize the convergence between the optical access/metro networks and MFH/MBH networks, aside from SDN to provide on-demand dynamic connections/services, it is highly desirable if the PONs are equipped with features such as dynamic reconfigurability, flexibility, and elasticity with fine bandwidth granularity. Moreover, it is greatly advantageous

if the PONs are backward compatible and inherently transparent to accommodate various major network design features including, for example, signal modulation formats, signal detection schemes, WDM grids, diversified network topologies as well as various multiple access techniques. Apart from the use of advanced signal modulation and multiple access techniques, for cost-sensitive 5G application scenarios, the use of low-cost and low-complexity IMDD-based optical transceivers in combination with DSPs are crucial for cost-effectiveness of the converged fixed-mobile networks. To address the aforementioned technical challenges, this dissertation theoretically, numerically, and experimentally proposes converged fixed-mobile networks based on PONs [32-35], which explore i) innovative technical solutions capable of delivering DSP-enabled digital filtering multiple channel transmissions with independently multiplexed optical channels at the wavelength, sub-wavelength, and orthogonal sub-band levels for elastic bandwidth allocation and ii) the feasibility of introducing advanced solutions into future high-speed PONs for practical implementation of flexible, elastic and reconfigurable converged optical access/metro networks and MFH/MBH networks.

2.2.2 Optical Broadband Access Technologies

The traditional access network infrastructures such as the twisted-pair public switching telephony networks (PSTNs) and the coaxial cable television (CATV) networks cannot meet the new service requirements demand for high-speed broadband access. Until recently, asymmetrical digital subscriber line (ADSL, ADSL2+), very high-bite-rate DSL (VDSL) techniques, and cable modem techniques are the predominant broadband wireline access technologies deployed for residential users and have been evolving into higher speeds, but at the expense of a shorter reach [38]. Optical fibre-based networks due to their wide bandwidth and increased network reach are progressively penetrating the access network domain. Deeper penetration of the fibre in the access feeder links to the subscriber is considered as a potential technology solution to meet the high bandwidth demand. Generally speaking, fibre access networks include hybrid fibre coax (HFC) and the multitenant FTTx system, which is a common architecture of fibre-based access network technologies, as shown in Fig.2.6.

Depending on the fibre termination point, different variations of the FTTx technology include FTTH and FTTB, and the intermediate solutions such as fibre-to-the-curb (FTTC) and fibre-to-the-cabinet (FTTCab). These technologies proffer a viable practical solution to overcome

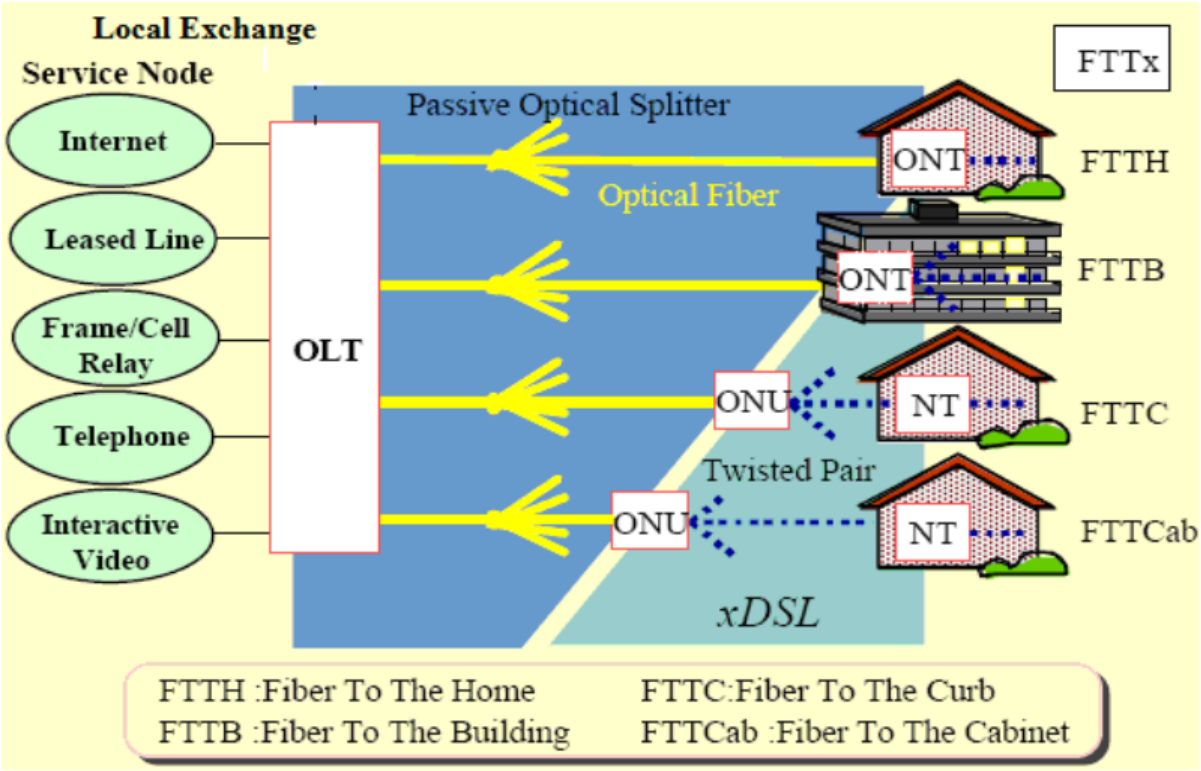

Fig. 2.6. Fibre-to-the-x (FTTx) broadband access network architecture [39]

the network performance bottleneck by increasing capacity and delivering fast fibre connection services close to the various end user's premises. As shown in Fig. 2.6, the FTTC and FTTCab are both hybrid fibre access technologies with decreasing the length of copper lines to the customer premises. In the FTTC and FTTCab architecture, an optical fibre may run from the OLT in the local exchange to an ONU located in a street cabinet or curb, from where a drop to the customer premises is via an ADSL line on twisted copper pairs or VDSL line in shorter links. Alternatively, with the hybrid fibre coax (HFC) access network infrastructure, the fibre runs up to the CATV street cabinet, and from where coaxial cables extend to the customer premises. These approaches can deliver increased bandwidth beyond what traditional legacy copper networks offer. On the other hand, FTTH and FTTB systems push the fibre deeper to the customer premises. Typically, the realization of FTTH and FTTB access networks is primarily based on PONs connecting the OLT in the local exchange with customer premises via passive optical fibre splitters located in the field close to the end user (last mile). PON standards such as GPON, 10G PON (XG-PON), and Ethernet PON (EPON) capable of delivering much higher capacities can be employed to implement the FTTx solutions to offer triple-play services (voice, video and data) to residential and business subscribers in the access network.

2.2.3 Passive Optical Network Architectures

PONs based on power splitting are the most promising network architecture solutions to govern broadband access, due to the unlimited and cost-effective bandwidth potential they can offer.

The general architecture of PON is shown in Fig. 2.7 [40]. The main network entities of a PON are the OLT located at the service provider's CO, multiple ONUs located near the end user, and passive optical splitter/combiner at the remote node (RN) closer to ONUs. The passive network segment between the OLT and the ONUs is referred to as the optical distribution network (ODN). The ODN consists of a feeder fibre between the OLT and RN and distribution fibres between the RN and ONUs. The network between the OLT and ONUs is passive since no active power components are required. The OLT provides ONUs access to the metro/core network. While the ONU provides to user's connection to the metro/core network and obeys the OLT transmission schedule to control and monitor all transmissions.

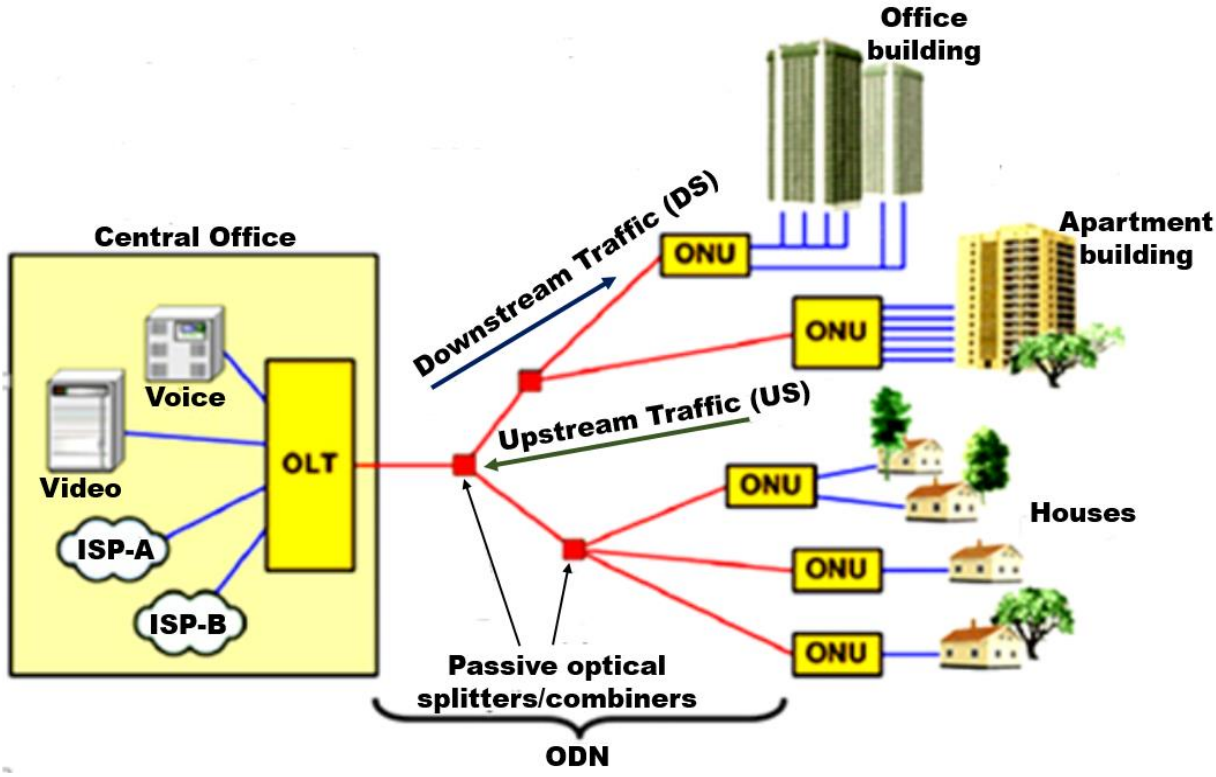

Fig. 2.7. PON network architecture [40]

In the downstream direction, the OLT broadcasts the packets through the ODN, which are received by all ONUs. Each ONU extract the downstream stream packets addressed to it based on its unique identifier (ID) and discards the packet directed to other ONUs. Conversely, in the upstream direction, multiple ONUs shares the upstream wavelength for sending their

subscribers' packets to the OLT. Thus, in the downstream direction, a PtMP architecture is implemented. While in the upstream direction, due to directional properties of passive optical splitter/combiner, the upstream data from any ONU will only reach the OLT, not broadcast to other ONUs. As such, the upstream transmission is a PtP architecture. Generally, the current specification allows the PON architecture to support in the region of 16 to 32 ONUs with a covered transmission distance of typically 10 to 60 kilometers [41]. Moreover, a PON has several advantages which are summarized as followings:

- PON eliminates the need for active optoelectronic components. No power consumption equipment in the field leads to low maintenance costs and high reliability due to the absence of vulnerable electronic components.
- PON is cost-effective (compared to xDSL) due to sharing of OLT devices, fibre installation, and maintenance costs for numerous customers.
- PON offers great scalability and flexibility in the network topology since the power splitter/combiner can be easily located anywhere along the fibre link.

The provision of enormous bandwidth, the efficient use of fibre resources, and CO equipment, space, and power have led PONs to be deployed on a massive scale worldwide. There are several other variants of traditional PONs including time division multiplexing-PON (TDM-PON) and WDM-PON. In addition, OFDM-PON and other multiple access PON techniques have also been widely researched as a future technology for the next generation network.

2.2.3.1 TDM-PONs

The typical architecture of TDM-PON is shown in Fig.2.8 [42], where a single wavelength channel is used in the downstream direction for broadcasting the same transmitted signal from the OLT to ONUs by utilizing a 1:N passive optical power splitter/combiner. While another dedicated channel is used in the upstream direction for multiplexing signals from different ONUs in the time domain toward the OLT. Each ONU is assigned to a specific transmission time slot and starts transmitting only upon the beginning of the time slot dedicated to this ONU.

In the downstream, the OLT broadcasts the signal to all connected ONUs by interleaving frames destined for different ONUs as a continuous stream. Then, only a particular ONU with a specific logical link-identifier (LLID) in the downstream traffic may extract the stream slot allocated to it. As there is only one receiver in the OLT and a single feeder fibre, ONUs take

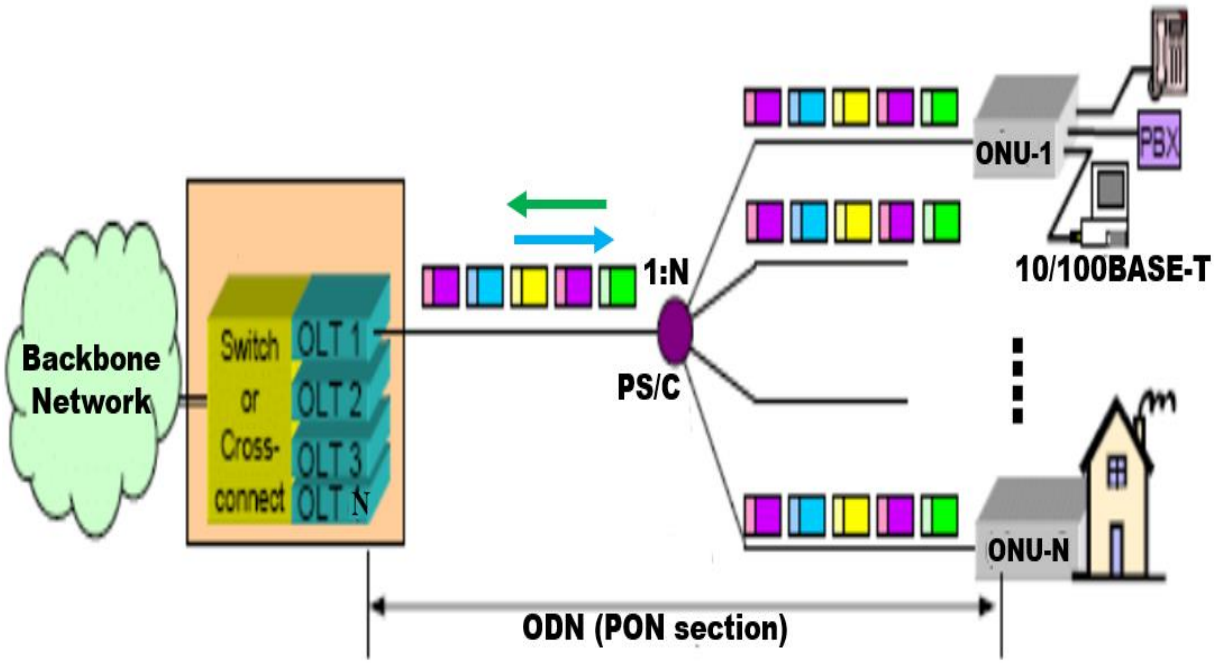

Fig. 2.8. TDM PON network architecture [42]

turns sending their data in a TDM schedule. More importantly, when an ONU is not sending data, it must turn off its laser to avoid interference with another ONUs' upstream transmission. As a direct consequence, the use of burst mode ONU transmitters is essential in TDM-PONs. So far, only two variants of the TDM based solutions corresponding to the Ethernet PON (EPON) and gigabit capable PON (GPON) standards have been utilized for mass rollout [21,22,42,43].

2.2.3.2 WDM-PONs

Although TDM PONs provide higher bandwidth than copper wire-based access technologies, they are having a hard time keeping up with the ever-increasing bandwidth demands. It is widely agreed that the TDM-PON architectures are bandwidth limited since a single wavelength is shared among the PON users, resulting in a reduction of the average bandwidth per user. A promising technical strategy to mitigate this challenge is to adopt WDM-PON technology without drastically changing the fibre infrastructure. The WDM-PON minimizes the complexities needed for TDM and can provide excellent network scalability and flexibility. It offers a potentially high reach and good transparency and security because it can support different wavelengths channels over the same fibre infrastructure as described in detail below [23].

Fig. 2.9 depicts the basic architecture of the WDM-PON supporting multiple wavelengths in

either or both upstream and downstream directions by using a passive arrayed waveguide grating (AWG) router at the CO and RN. A multiwavelength source at the OLT is used for transmitting multiple wavelengths to the various ONUs. The WDM-PON employs a separate wavelength channel from the OLT to each ONU for each of the upstream and downstream directions. This approach creates a PtP link between the OLT and each ONU, which differs from the PtMP topology of the typical TDM-PON.

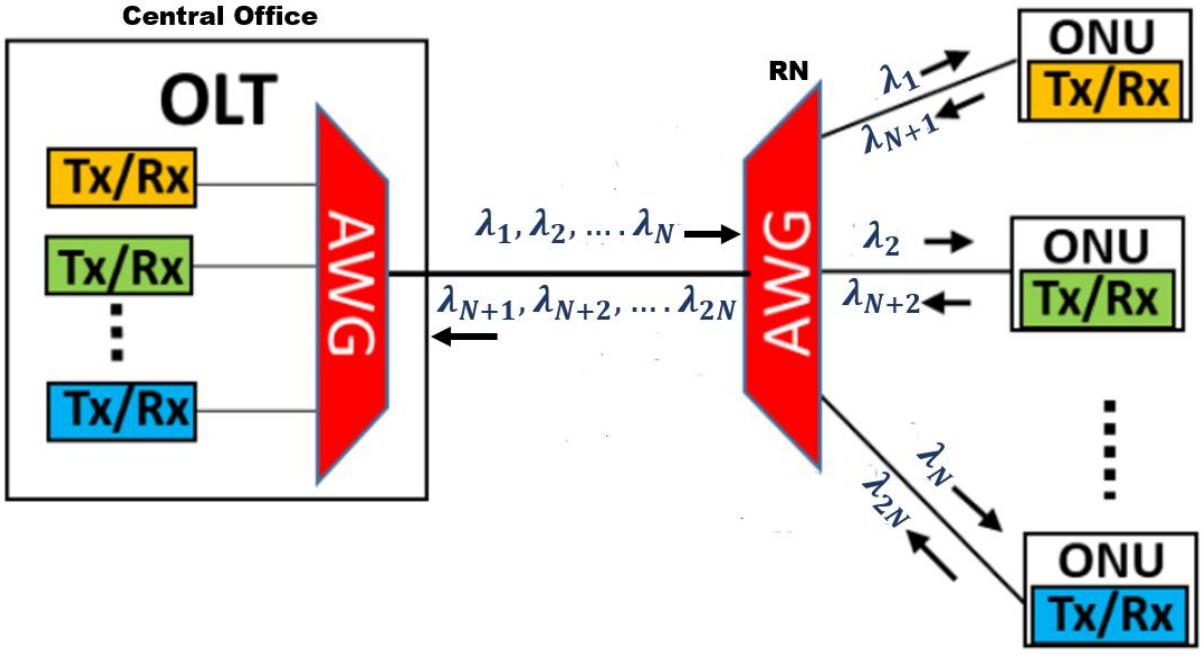

Fig. 2.9. WDM PON network architecture [43]

In the downstream direction, once the wavelength channels ($\lambda_1, \lambda_2, \ldots\ldots, \lambda_N$,) have been multiplexed by the AWG at the CO, they are fed into the fibre and routed to the ONUs. At the RN, another passive AWG router demultiplexes and distributes the downstream wavelength channels to the corresponding ONUs. Each ONU is equipped with a transceiver for receiving and transmitting on its corresponding wavelengths. In the upstream direction, individual ONUs generates different wavelengths channels ($\lambda_{N+1}, \lambda_{N+2}, \ldots\ldots, \lambda_{2N}$) to convey their upstream signal to OLT.The AWG located at the RN multiplexes the uplink wavelength signals from the multiple ONUs to form a combined WDM signal, which is routed to the OLT. The OLT embedded AWG demultiplexes the receive WDM signal along with a receiver photodetector array for receiving the upstream ONU signals. While a WDM-PON assigns a dedicated wavelength to increase the capacity for each user, the high transceiver cost due to each ONU requiring an expensive tunable laser with a wide detuning range makes it prohibitive for large-scale deployment [24,44].

2.2.3.3 Hybrid WDM/ TDM-PONs

For cost-sensitive practical implementation of PONs, combining TDM-PONs and WDM-PONs to form a hybrid WDM/TDM or TWDM in a PON could be a cost-effective approach of introducing both technologies into access networks achieving high resource utilization efficiency. The TWDM PON is a two-way communication system with improved reachability, capacity, power split ratio and system scalability.

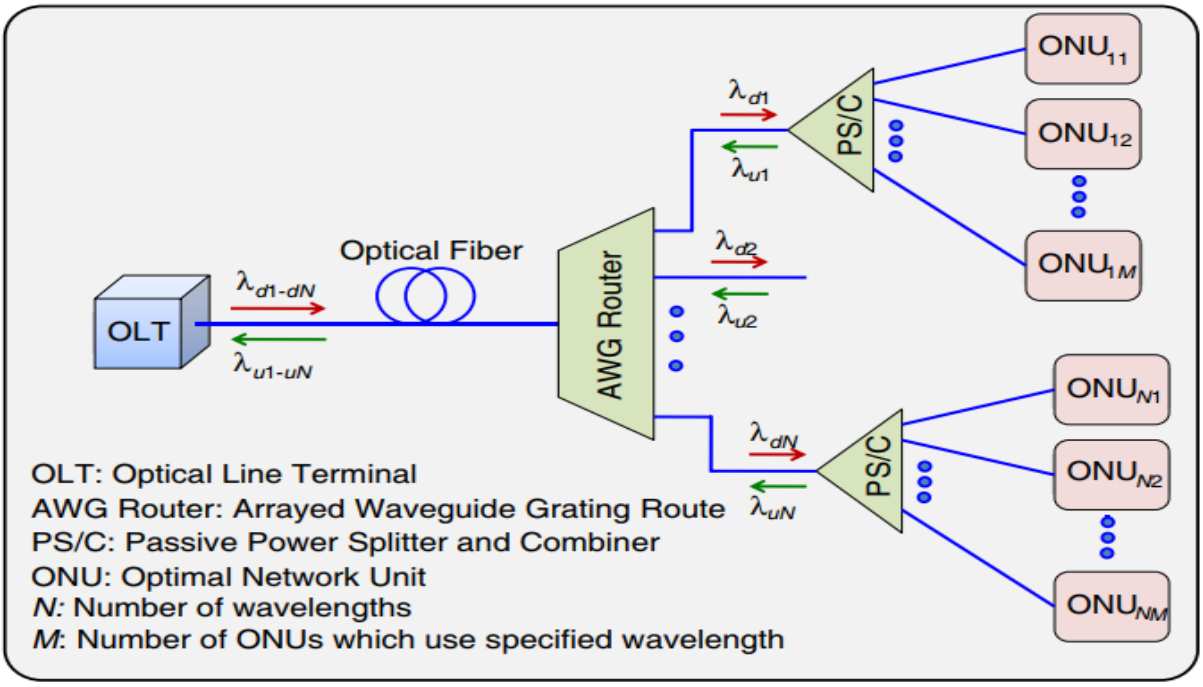

Fig. 2.10. TWDM PON network architecture [45]

Fig 2.10 depicts the TWDM PON architecture [45] in which one individual wavelength is utilized in the upstream and downstream links for communications between the OLT and ONU, and each wavelength can also be shared among multiple ONUs by using the TDM technique. The TWDM PON offers several advantages over both WDM and TDM including the ability to decrease costs by sharing wavelengths between users. As the TWDM PONs exploit the full bandwidth of each wavelength efficiently and provide services to more subscribers, it has been recommended by the FSAN group as a promising solution for NG-PON2 [25,26].

2.2.3.4 OOFDMA-PONs

The OFDMA-PON has been widely used in both wired and wireless broadband access networks and is considered an attractive candidate for next-generation PONs because of its

merits of better spectral efficiency, robust dispersion tolerance, cost-efficient implementation, flexibility in both multiple services provisioning and dynamic bandwidth allocation (DBA) [27,28]. In an OFDMA-PON, the upstream/downstream bandwidth can be divided into orthogonal frequency subcarriers, one or more of which can be allocated in a time slot and assigned statistically to a specific ONU, and each OFDM subcarrier can also be time shared among different applications via TDM. Fig. 2.11 shows an example of a typical network architecture of an optical OFDM-PON that combines OFDM modulation with TDM in a PON, where the OLT can support heterogeneous ONUs using a single OLT and a single optical receiver.

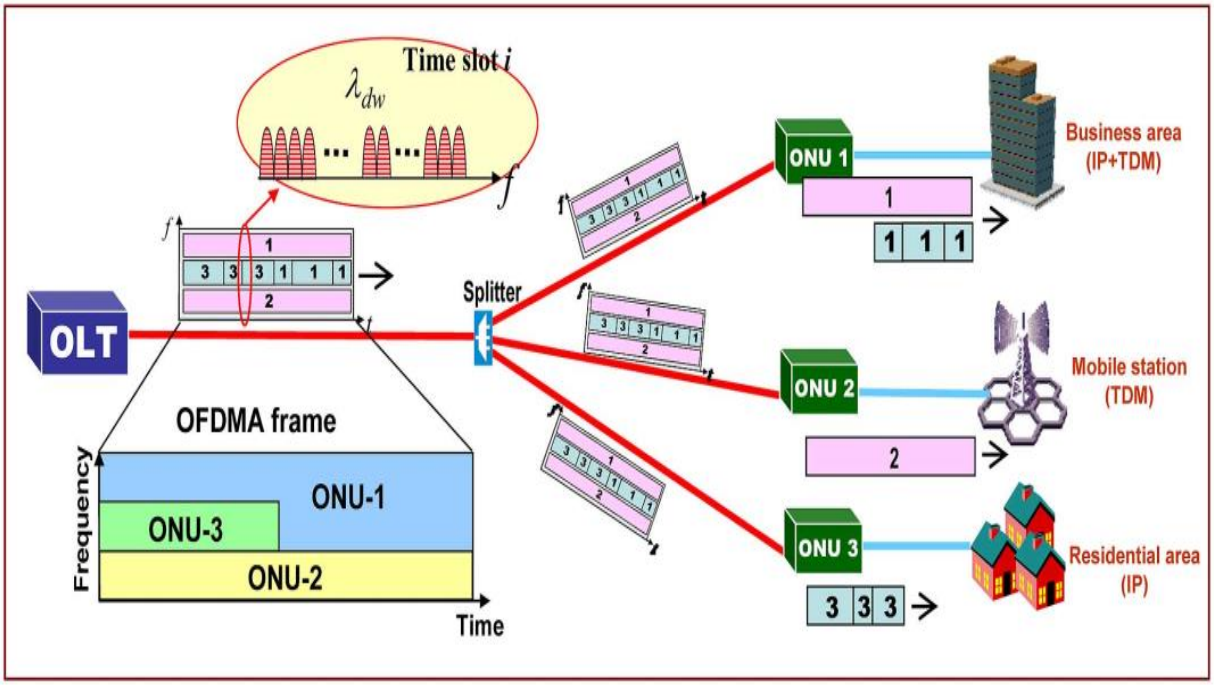

Fig. 2.11. Single wavelength OFDMA PON network architecture [28]

For downstream traffic, according to the frequency/time domain scheduling process at the OLT, the packet-based data for all ONUs will be encapsulated into the subcarriers and timeslots to create the complete OFDM symbol. The OFDM symbols are broadcast to all ONUs over a feeder fibre terminated by a passive optical splitter at the remote node. The bandwidth resources are shared by multiple user-side ONUs, which access the broadcast channel sharing the same laser and the downstream wavelength. At the ONUs, each ONU extracts its data from its allocated subcarriers and/or timeslots using DSP. For upstream traffic, each individual ONU maps its data onto the allocated subcarrier(s), sets all the other subcarriers to zero, and completes the OFDM modulation to generate an electrical OFDM symbol. For optical

modulation, a CW laser and either an IM or optical I/Q modulator can be used to convert the OFDM symbols into the optical domain for transmission over the fibre. As well, DMLs can also be exploited for the E-O conversion [29,46]. The optical OFDM symbols from multiple ONUs will be combined at the optical coupler in the remote node, forming a single OFDM frame. After transmitting through the ODN, the OOFDM signal is detected by a single photodetector at the OLT receiver. It is noteworthy that to enable multiuser access and avoid collisions for both downstream and upstream, timeslots must be synchronized so that the OFDM symbols are aligned accurately at the OLT.

Moreover, OOFDMA PONs offer several benefits including, on the one hand, providing high spectral efficiency and achieving better utilization of network resources due to increasing bandwidth granularity. On the other hand, it enables adaptive modulation formats based on channel characteristics and provides excellent scalability and flexibility to dynamically allocate bandwidth tailored to meet the needs of different end users. In terms of implementing the OFDMA-PON, use can be made of DSP to maximize the transmission capacity and realize cost-effective and flexible OFDM transceivers. Furthermore, the OFDMA PON not only has good compatibility with OFDM-based 4G networks but also facilitates coexistence with legacy systems and migration from existing access technologies to future 5G networks. For example, 1510nm-1540nm downstream and 1340nm-1360nm upstream OFDMA PON operations can enable its coexistence with GPON, XG/10 G-EPON, and legacy RF video overlays [28]. In addition, OFDM can also be used in hybrid operations over TDM/WDM architecture to scale up the aggregate network capacity and flexibility without increasing complexity and cost.

2.2.3.5 DFMA PON

To provide in a cost-effective way the highly desirable dynamic software-reconfigurable networking-based CAN for converging traditional optical access networks, metropolitan optical networks and MFH/MBH networks, a novel PON technique known as DFMA PON has been proposed [30].

In DFMA PONs, adaptive software reconfigurable and transceiver-embedded DSP-enabled digital orthogonal filtering is employed in each ONU and OLT to dynamically manipulate multiple channels with elastic bandwidth granularity and arbitrary signal modulation formats. This enables all ONUs to dynamically share a common fibre transmission medium with aid of the centralized software-defined controllers and the transceiver-embedded DSP controllers.

The use of SDN, which leverages on transparent abstraction and network infrastructure virtualization to improve network reconfigurability and elasticity and operation flexibility in the access network extended down to the physical layer, is crucial for attaining highly efficient utilization of the available dynamic network resources. The block diagram of DFMA PONs based on IMDD is illustrated in Fig. 2.12. As shown in the figure, the DFMA PON employs DOFs for multiplexing or demultiplexing various downstream/upstream encoded signals in the digital domain.

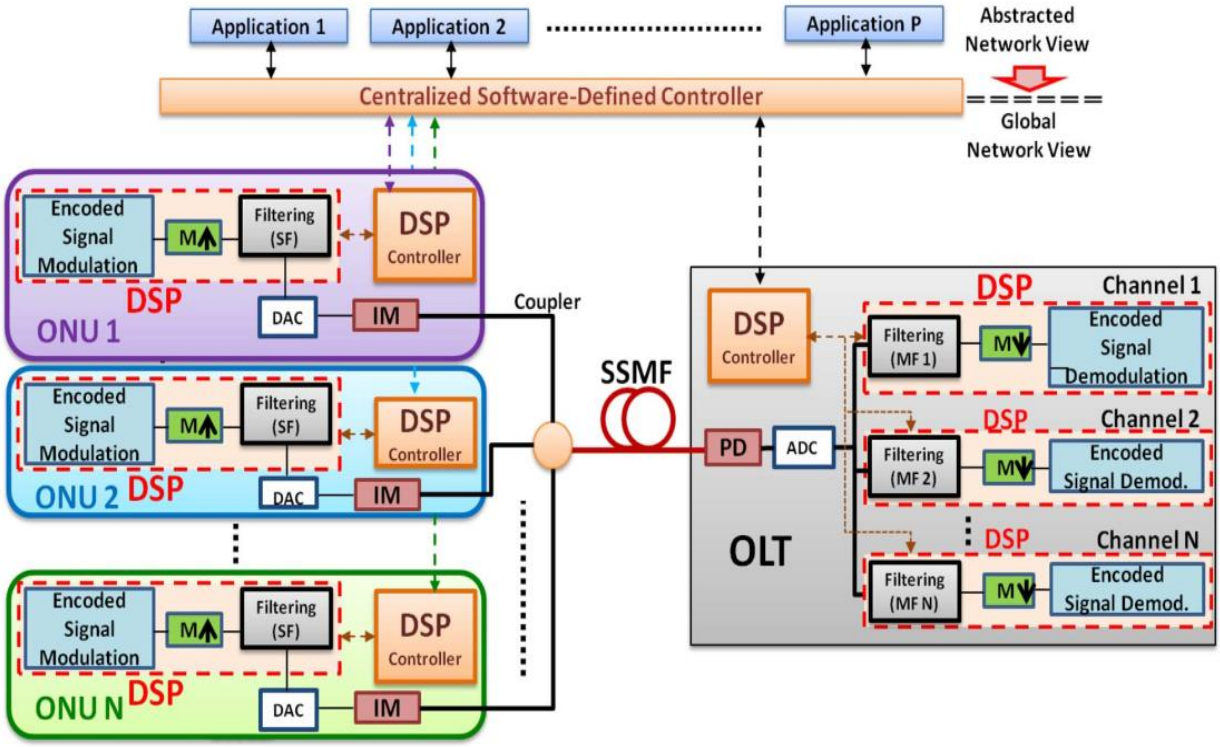

Fig. 2.12. DFMA PON network architecture [30]

For upstream transmission, each independent *i*-th ONU channel is digitally encoded by an arbitrary signal modulation format. The produced digital data is first up-sampled (M↑) by a factor of *M* via inserting *M*-1 zeroes between two consecutive original data samples. Subsequently, the up-sampled data sequence is digitally filtered by passing it through a dynamically reconfigurable digital shaping filter (SF) to generate either an I-phase sub-band signal or a Q-phase sub-band signal. Based on the prevailing services and dynamic network characteristics including the total number of ONUs simultaneously supported, the ONU embedded DSP controller working in conjunction with both the centralized SDN controller and the OLT DSP controller, computes a set of shaping filter coefficients to perform the filtering process required by the ONU. As such, this gives rise to the establishment of online software

reconfigurable connections in the physical layer. After digital shape filtering, the output data sequence is passed through a DAC to generate an analogue electrical signal, which is then fed to an optical IM to perform the E-O conversion. Finally, different optical signals from the various ONUs are passively combined by an optical coupler in the remote node, and the combined optical signal propagates through the shared fibre transmission link to the OLT.

After propagating through the fibre, in the OLT, the optical signal is detected by a photodetector and converted from the optical domain to the electrical domain. The ADC digitalizes the analogue signal which is then forwarded to the DSP-based receivers each dedicated to recover ONU data information. To demultiplex each ONU signal from the aggregated signal, the data stream corresponding to a specific ONU is digitally filtered by the corresponding MF, whose coefficients are computed by the OLT-embedded DSP controller following a procedure similar to its' ONU counterpart. As well, the OLT-embedded DSP controller through periodically communicating with each ONU DSP controller also takes full responsibility for maintaining the orthogonality among all the filters employed in the DFMA PON. After digital filtering, the demultiplexed signal is then down-sampled (M↓) by selecting every *M*-th sample from each sample sequence. Finally, the down-sampled sequence from each ONU is demodulated according to the adopted signal modulation to recover the encoded binary data information. Thus, a DSP-enabled dedicated physical connection between the ONU and the OLT is established, which is online software reconfigurable. Indeed, such a connection can be further extended to link any users inside and/or outside the network if these users are served by the same centralized software-defined controller.

To construct the required DOFs, use can be made of Hilbert-pair-based digital SFs and MFs [31]. The impulse responses of the *i*-th Hilbert-pair, $h_i(t)$ can be given as:

$$\begin{aligned} h_i^I(t) &= p(t)\cos(2\pi f_{ci}t) \\ h_i^Q(t) &= p(t)\cos(2\pi f_{ci}t) \end{aligned} \tag{2.15}$$

where f_{ci} corresponds to the central frequency of the *i*-th Hilbert-pair, and $p(t)$ is the baseband pulse, which has a square-root raised-cosine form expressed as:

$$p(t) = \frac{sin[\pi(1-\alpha)t'] + 4\alpha t' cos[\pi(1+\alpha)t']}{\pi t'[1-(4\alpha t')^2]},\ t' = t/T \tag{2.16}$$

where *T* is the sampling period before up-sampling, and the α parameter controls the excess of bandwidth of the square-root raised-cosine function with respect to the minimum bandwidth determined by the symbol period (1/T). The superscripts "*I*" and "*Q*" indicate the I-phase and Q-phase filter components of the Hilbert-pair, respectively. Each of these components can be independently utilized to convey an individual signal channel. The impulse responses of the OLT filters are written as a matched version of the corresponding ONU Hilbert-pair, $g_i(t)$:

$$\begin{aligned} g_i^I(t) &= h_i^I(-t) \\ g_i^Q(t) &= h_i^Q(-t) \end{aligned} \tag{217}$$

with

$$g_i^A(t) \otimes h_j^B(t) = \begin{cases} \delta(t - t_0) & A = B \text{ and } i = j \\ 0 & A \neq B \text{ and } i \neq j \end{cases} \tag{2.18}$$

where the superscript *A* and *B* each denote *I* or *Q*, and t_0 corresponds to the time delay induced by the digital filtering process. For supporting *N* independent ONU channels, the minimum oversampling factor, *M*, satisfies *M=N*. In addition, assuming the DAC and ADC have identical sampling speeds, the central frequencies, f_{ci}, of the *i*-th Hilbert-pair is given by:

$$f_{ci} = (2i - 1)\frac{f_{DAC/ADC}}{2N}, \quad i = 1,2,3, \ldots . N \tag{2.19}$$

where $f_{DAC/ADC}$ is the sampling speed of the DAC and ADC. Here, the central frequency of the Hilbert-pair is chosen to uniformly distribute the filter frequency responses within the available spectral region determined by the DAC/ADC.

Using the Hilbert-pair approach, each sub-wavelength occupies one whole pair of the DOFs, where individual sub-wavelength occupies two spectrally overlapped orthogonal sub-bands, i.e., I-phase sub-band and Q-phase sub-band. As an example, Fig. 2.13 illustrates how individual ONUs are dynamically assigned to available DOFs, whose frequency responses of both the I-phase and Q-phase components at different central frequencies are plotted. It can be seen in Fig. 2.13 that each ONU can be assigned independently to a filter component in the available spectral region. For instance, ONU 1, ONU 2, and ONU 5 employ Filter 1 (the I component of the first Hilbert-pair), Filters 2 and 4 (the Q components of the first and second Hilbert-pairs), and Filter 5 (the I component of the third Hilbert-pair), respectively. Different filters can also be assigned to the same ONU when the ONU requires a higher transmission

bandwidth, as illustrated in Fig. 2.13 for ONU 2. In addition, it should be mentioned that the aggregation of the independent individual channels can be gapless, thus giving DFMA PONs improved spectral efficiency.

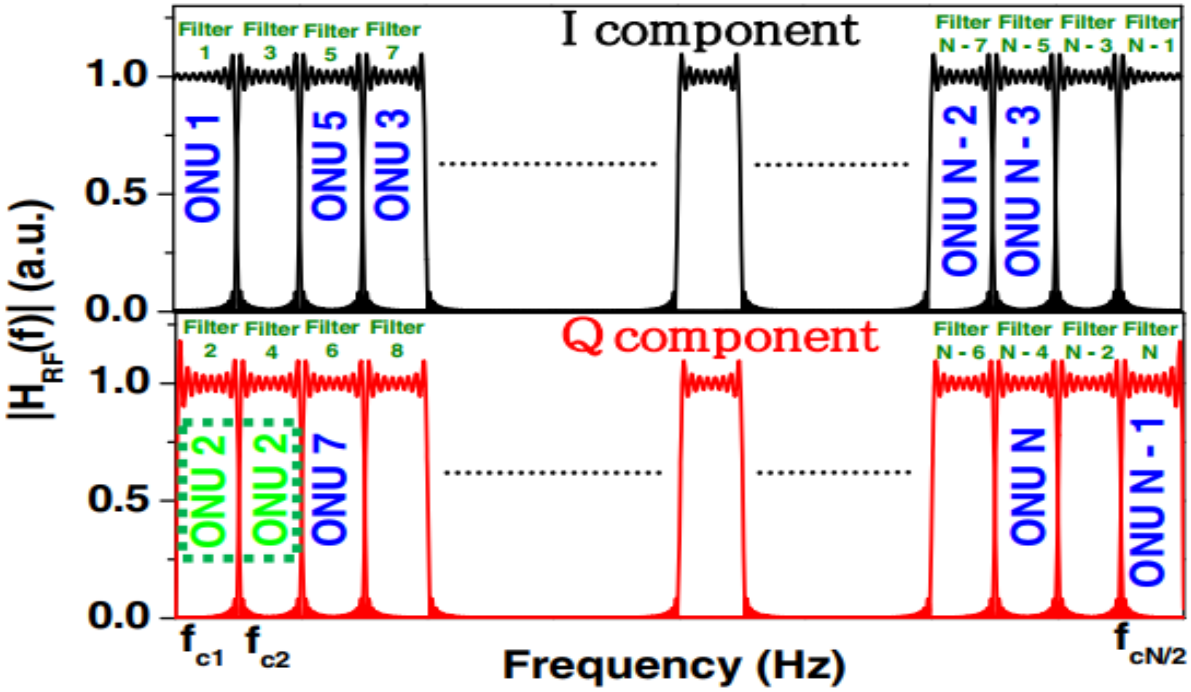

Fig. 2.13. illustration of Hilbert-pair-based frequency responses at different central frequencies of orthogonal filters and corresponding ONU spectral allocations [39].

From the above discussion, it is easy to understand that DFMA PONs are built upon digital filtering and are dependent on reconfigurable DSP controllers embedded in both the ONUs and the OLT. As the filter parameters are software-reconfigurable in the digital domain, the allocation of individual ONUs to DOFs in the available spectral space is fully flexible and dynamic. Furthermore, due to the dynamic reconfigurability, a single high-speed ONU can simultaneously accommodate several channels, and a single channel can also be shared by two or more low-speed ONUs using a multiple access scheme such as TDMA. In addition, as the DSP controllers and the centralized SDN-controller work together to establish a dedicated physical connection between an ONU and the OLT, the digital filter parameters can be adjusted dynamically and adaptively according to transmission system spectral characteristics and network traffic demands. Therefore, flexibility, dynamic reconfigurability and elastic bandwidth provisioning with fine granularity at sub-wavelength and orthogonal sub-bands levels are achievable in the DFMA PON. More importantly, the DFMA PON also offers several unique advantages including.

- Provide full support for the SDN solution with its network functionalities further extended to the physical layer to improve network slicing/virtualization, dynamic reconfigurability, and network bandwidth elasticity.
- Excellent transparency to both underlying transmission technologies and network topologies, such as signal modulation/detection techniques and signal bandwidths.
- Offering a useful framework for developing universal optical transceivers for cost-sensitive ONUs.
- Proffer "future-proof" optical network solutions with excellent backward compatibility with existing installed PON networks.
- Inherent network flexibility and scalability to allow the preferred pay-as-you-grow network operation strategy due to the ability to incrementally add new channels online as required by exploiting a modular DSP solution in the OLT.
- Enhanced data security in the physical layer as received data cannot be decoded without the full knowledge of the digital filter parameters to correctly demultiplex a channel from the aggregated signal.

2.2.5 A Perspective to Radio Access Network Evolution

In 1G/2G/3G cellular networks, traditional RAN architecture has a base station (BS) composed of two basic units i.e., RU, also known as the remote radio head (RRH), and the digital unit (DU), or BBU [47]. These basic elements in early generation cellular systems are physically integrated into an all-in-one BS located at a physical cell site consisting of a tower or mast, on top of which are installed RF antenna linked by heavy electrical coaxial cable, as shown in Fig. 2.17.

The S1/X2 interfaces connect the BS to the CN via the MBH. Depending on the scenario, MBH links used different types of transmission mediums, including copper, microwave, and optical fibre. However, in the traditional RAN architecture, the use of coaxial cable causes significant RF signal propagation losses, which is undesirable since it results in degraded signal transmission/reception, high power consumption, and limited transmission range, thus, necessitating the BS's proximity to the antenna site. Furthermore, each BS is stand-alone, with a defined number of sector antennas that cover a small cell area and solely handle signal transmission/reception inside that coverage area. As a result, the interference limits the system's

capacity, making it more difficult to improve the performance. As well, the BSs are built on proprietary platforms as vertical solutions.

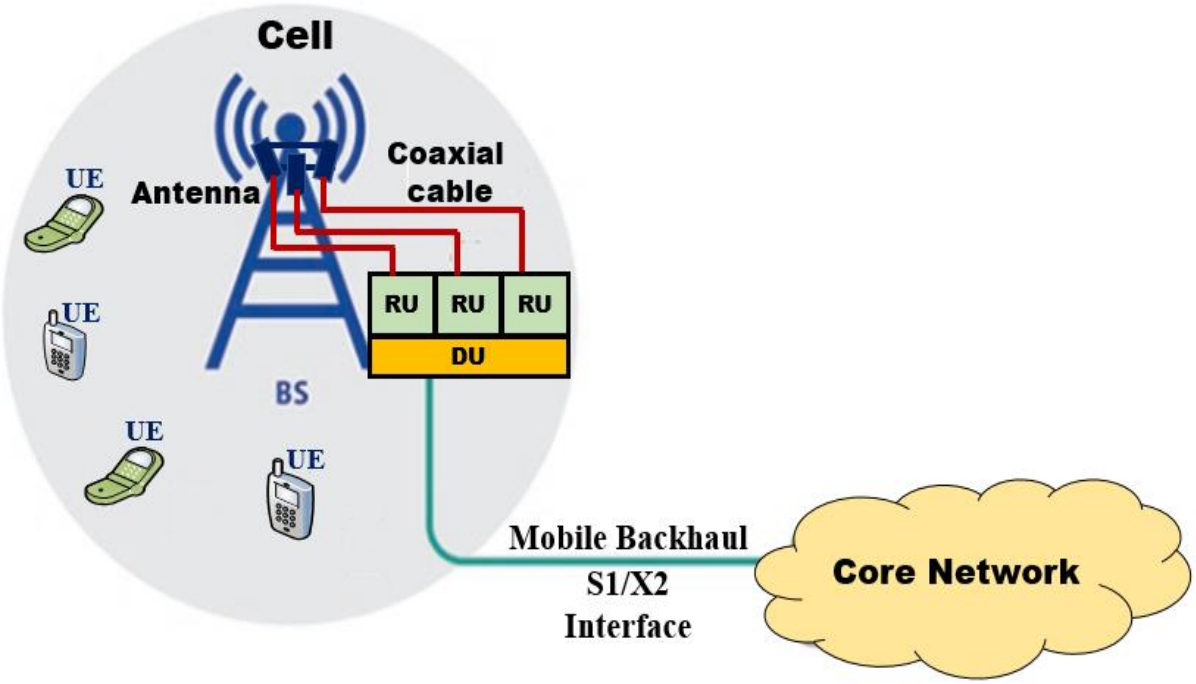

Fig. 2.17. Traditional RAN architecture [47]

As a result of the issues faced by traditional RANs, the telecommunication industry began to adopt a separated BBU and RRH architecture based on distributed RAN (DRAN) [47]. The BBU handles baseband processing, such as calls and traffic forwarding, while the RRH handles digital radio signal processing, such as transmitting/receiving and converting signals. The DRAN architecture is depicted in Fig. 2.18, with each BS consisting of a BBU and RRH, which are both collocated together. The RRH can be placed at the top of the tower closer to the antenna and is connected to the BBU at the bottom of the tower via optical fibre. The BBU connects to the CN via the MBH, which carries user data, control and management data, and handover data that are exchanged between the BBU and the CN. The MFH, which employs the CPRI standard [48], connects the BBU to the RRH. Other standard interfaces that can be utilized include the open base station architecture initiative (OBSAI) [49] and the open radio equipment interface (ORI) [50]. A microwave link can also be employed for the connection between the RRH and the BBU. Because BBU can be located a few hundred meters or kilometers away from the RRH, using optical fibre to support MFH can allow great flexibility in network planning and deployment. When compared to a traditional RAN, where the RF signal is propagated over a lengthy coaxial cable, the DRAN architecture minimizes

transmission loss. However, with traditional DRAN, as the network complexity increases, a new drawback emerges. For instance, to minimise interference and increase throughput, a cell's

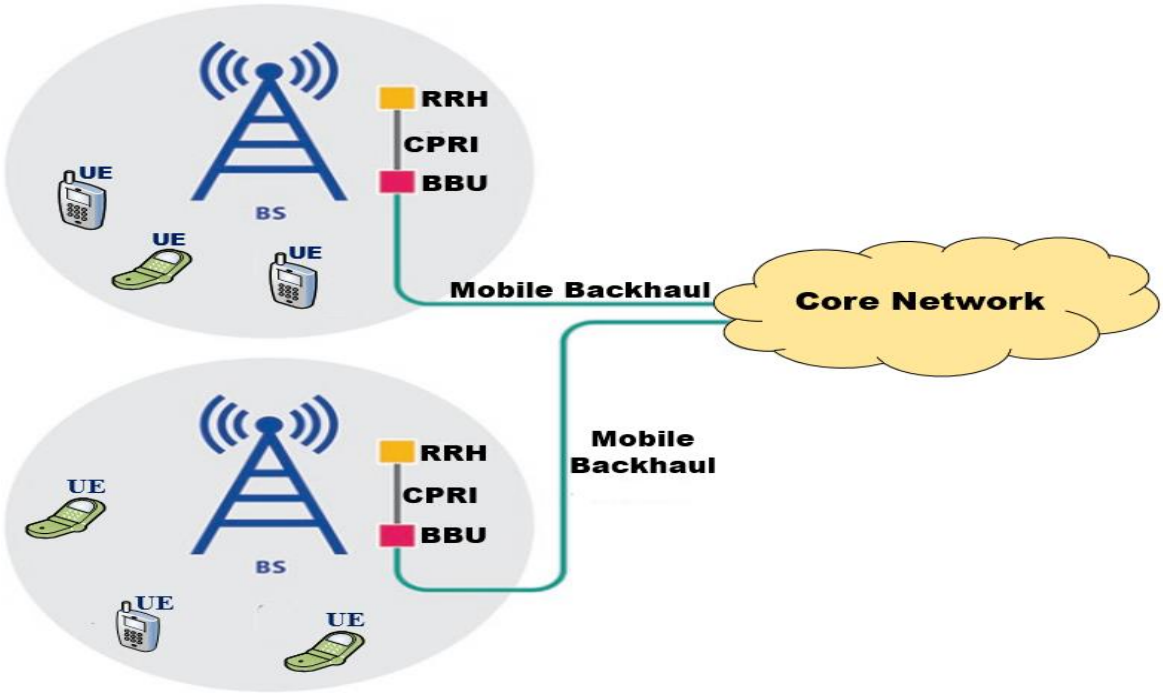

Fig. 2.18. Traditional DRAN architecture [47]

network can be densified by using MIMO technology with coordinated multipoint transmission (CoMP). As a result, costs will rise as more BSs are deployed, and each BS will require a new physical cell site to accommodate both the RRH and the BBU. Furthermore, in this scenario, the processing resources of a BBU cannot be shared among different RRHs. As a result, the first stage of advanced RAN solution has emerged as CRAN that moves BS capabilities to the cloud to optimize resources and enhance operational efficiency [47].

CRAN was initially presented by China Mobile [51] in 2009 and has since been implemented by several mobile operators. Following the deployment of CRAN, several mobile operators indicated that their CAPEX/OPEX costs decreased by more than 50% [52,53]. The core design concept behind the CRAN architecture is to move certain cellular network functionality to the cloud computing infrastructure. In CRAN, the RRH and BBU functions are physically decoupled to address the limitations of conventional DRAN architectures. Fig. 2.19 illustrates the CRAN architecture where the RRH is decoupled from the BBUs clustered as BBU pool in a centralized cloud server. Centralizing the BBUs allows the multiple RRHs to share processing resources, which greatly improves efficiency, reduces the power consumption and, therefore,

operational cost. It was proved in a study on China mobile's commercial networks that the CRAN deployment may reduce power consumption by up to 70% when compared to traditional

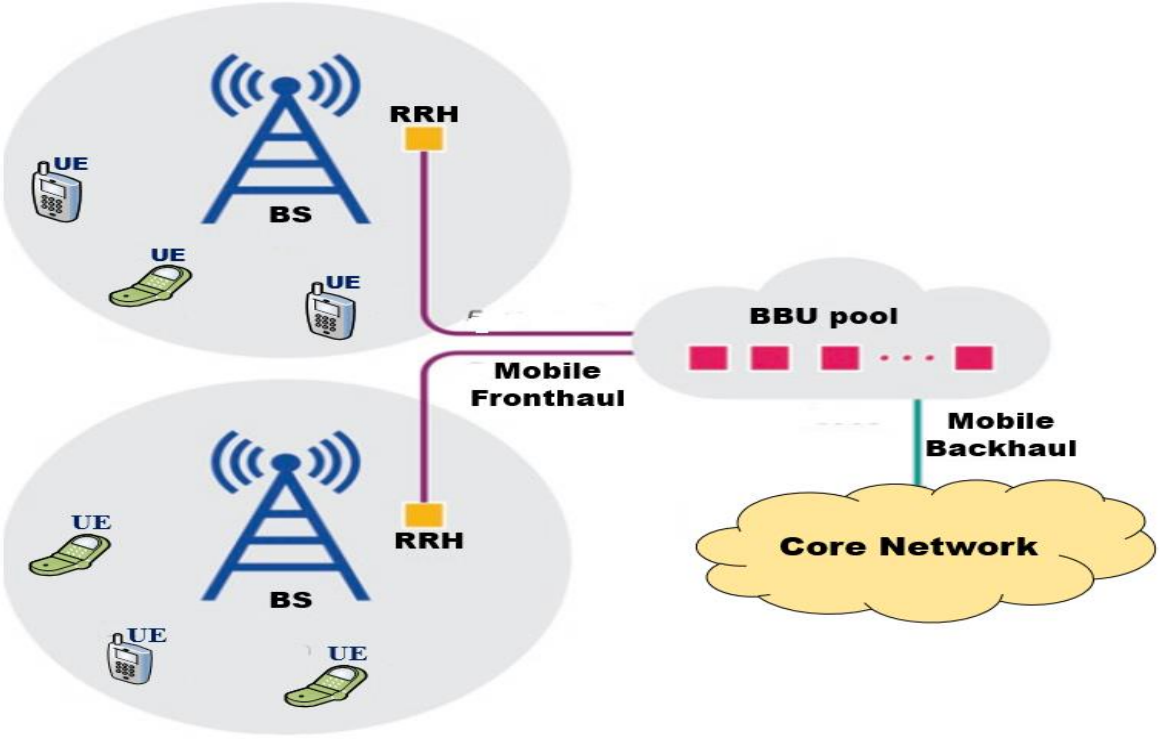

Fig. 2.19. Centralized/Cloud RAN architecture [47]

RAN deployment methods [52]. The centrally located BBU pool is connected to multiple RRHs via the digital MFH network. The above-mentioned CPRI, OBSAI, and ORI interface protocols are still used to transport the digitised baseband signal between the RRH and the centralized BBUs. The bandwidth requirements for these links vary depending on the degree of splitting between the cloud-based BBU pool and the RRHs. In the CRAN architectures, there are three functional splits: fully centralized, partially centralized, and hybrid architectures [47].

In a fully centralized system, the BBU pool in the cloud handles all processing and administrative functions for base stations. This strategy necessitates the transmission of practically all data from RRH to the cloud, which requires a significant amount of bandwidth. In the partially centralized setup, the RRH handles RF-related functions, such as signal processing, while the BBU pool handles other management tasks in the cloud. The bandwidth needs between the RRH and the cloud are reduced with this option. The interplay between the processing and management tasks, on the other hand, can be complicated, making separation impossible. The hybrid split, in this situation, shifts some sorts of processing functions to the cloud and assigns them to a new distinct process. On the cloud side, this solution simplifies

resource management and minimises energy use.

CRAN does not end with centralization, the second stage of CRAN evolution is BBU virtualization, which can have a significant impact on mobile networks as they allow network tasks, such as baseband processing, to be decoupled from network hardware, thus reducing network costs and enabling the flexible deployment of services. The current RAN equipment is built on dedicated hardware, with indivisible RAN components (hardware + software) offered by RAN manufacturers. Virtualization enables the baseband processes to be virtualized in software running on generic servers, allowing the operators to have more control over their networks. Additionally, as 5G is envisioned to offer a wide range of services, including mMTC, URLLC, and extreme mobile broadband (eMBB), virtualization is expected to provide the required flexibility, scalability, and service-oriented management. Moreover, CRAN was shown to be an appropriate framework for supporting 5G technologies as 5G became a research emphasis recently. Because of its inherent centralization and the flexibility and scalability of a cloud-based implementation, CRAN is expected to support and facilitate numerous 5G enabling technologies such as mmWave, MIMO large scale antenna system with ultra-dense small cell networks. Therefore, CRAN can be viewed as an advanced architectural evolution of the traditional RANs and has become a critical component of future 5G and beyond networks.

2.2.5.1 Challenges and Future Development of CRAN

Towards the deployment of m-MIMO and small cell networks, the CRAN architecture is effective, and it is expected to play a vital role in the next generation 5G mobile networks. The future 5G aims to outperform 4G in terms of bandwidth, latency, and reliability while also supporting a wide range of use cases over a single mobile network to meet end user needs with better QoS. To achieve 5G goals, not only must mobile technology be revolutionised, but also changes to the network architecture and design are required. Besides, the ambitious 5G requirements present significant technical challenges for the MFH. In the current CRAN architecture, CPRI is the most prevalent MFH interface and has proven to be effective on standard mobile transport networks designed for 4G LTE networks.

With mobile networks evolving to next generation 5G, there is consensus that CPRI is not viable, and it is becoming impractical to support the evolution. Traditional MFH uses CPRI, which is designed based on a TDM mechanism with constant transmission data rates, regardless of the actual network traffic [48]. Even when there is no traffic on the network, the

data rate on a CPRI link is always constant. Thus, if the same protocol is employed in the future 5G, data rates exceeding the order of 100 Gb/s can be expected. This is understandably not a very efficient mechanism since it wastes the bandwidth and therefore limits the transport efficiency. Another key factor to consider is the latency, which is restricted to 250 µs in 4G for the maximum roundtrip delay between the BBU and RRH. Because the BBU and RRH are directly connected by fibre at the same cell site, the latency requirement is not an issue for 4G, but it does when it comes to future 5G. Further, since mobile data traffic is highly dynamic due to an unpredictable user behaviour and bandwidth granularity of a wide range of emerging mobile applications and services, MFHs are ill-suited to adapt to the varying traffic load condition of the network. It should be noted that a centralized/cloud transport network is becoming increasingly crucial to effectively support a massive scale of connected devices. Ideally, all BBUs would be moved to a single location for centralized processing of all physical, MAC, and radio link control (RLC) layer (L1, L2, L3) functions, leaving only the ADC/DAC function to RRH at the cell site. When numerous BBUs (and hence many cells) are centralized as in the CRAN case, the MFH will be overburdened since a huge amount of bandwidth is required. For instance, for a 5G cell site with 32 antenna ports and 100 MHz radio channel bandwidth, the required CPRI bandwidth will be about 157 Gb/s [54]. It is clear that the CPRI-based MFH operation mode is inefficient and may restrict the centralization scalability of RANs.

Furthermore, supporting a large number of antennas brings with it new challenges since the current MFH bandwidth is largely dependent on the number of antennas. As the number of antennas increases, the MFH data rates increase in proportion. For instance, an LTE sector configured as 2 x 2 MIMO with 20 MHz bandwidth requires approximately 2.5 Gb/s, which gives a 7.5 Gb/s total MFH for a typical 3-sector cell site. In most cases, such data rates do not scale with the varying traffic load condition of the cell, leading to inelastic traffic. Additionally, since the approaches to enhance data rates in 5G are primarily in the direction of adding more cells, and more antennas, due to increasing antenna count in 5G, it is expected that the bandwidth will further increase at an unprecedented scale. Unavoidably, this could become a major hindrance for the RAN from utilizing the highly desired 5G enabling technologies such as m-MIMO with high density small cell networks.

Moreover, each antenna transmission in the CPRI-based MFH requires a dedicated fibre, making it lack networking capability. Even though the optical fibre infrastructures are readily

available in the field, as the number of antenna/MIMO increases, it will become impractical to provide a dedicated fibre for each antenna in 5G. As a result, for the cost sensitive 5G scenarios, it is determined that mobile fronthauling through CPRI will not be cost-effective since it requires a large number of optical fibres. In addition, since the mapping between the BBU and the RRH is a fixed one-to-one correspondence, MFHs are not flexible and can pose significant challenges for CRAN. For instance, as the CRAN deployment of BBUs is virtualized and centralized in a pool, and since each BBU pool is responsible for supporting a large number of end users, reliability becomes increasingly critical. Therefore, it would be preferable if one RRH in CRAN could be dynamically reconfigured to another BBU pool. However, the current MFH does not allow for such dynamic reconfigurability and flexibility. Therefore, to ensure smooth evolution towards 5G mobile networks, CRAN should be re-designed not only in terms of the transport technologies, but also the interface itself, hence the notion of next generation fronthaul interface (NGFI).

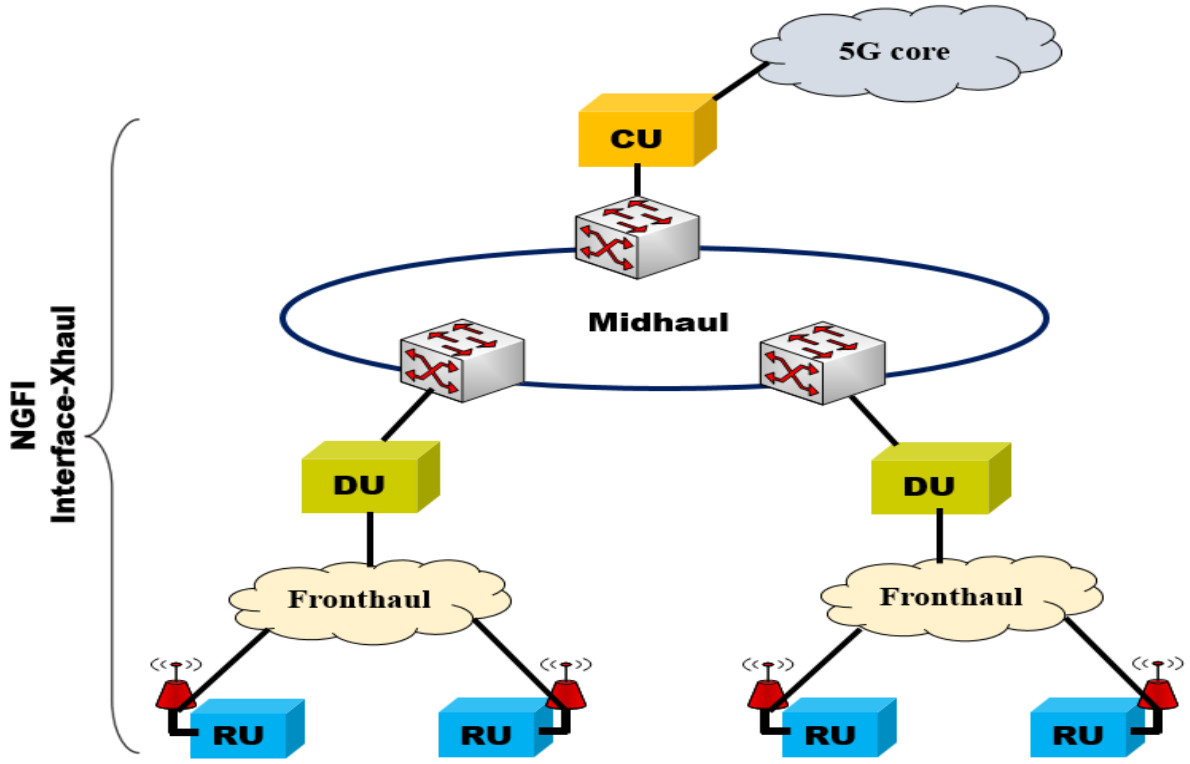

Fig. 2.20. 5G CRAN architecture

2.2.5.2 Next Generation 5G CRAN

To support the bandwidth requirement of 5G and to address the shortcomings of traditional MFHs, the NGFI was proposed for 5G [55]. The goal for developing NGFI is based on re-

designing the fronthaul with key features targeting a packet-based, traffic-dependent, and antenna scale-independent interface that will be central to the 5G RAN evolution. NGFI proposes splitting the different radio functions and implementing them into three logical entities: the central unit (CU), the distributed unit (DU), and the remote radio unit (RU).

Fig. 2.20 depicts the NGFI-based 5G CRAN architecture, which consists of two-level segments logically mapped to the transport network between the DU and RU referred to as the fronthaul network, as well between the CU and DU referred to as the midhaul network. As both the fronthaul and midhaul originate from the principle of NGFI, these combined 5G transport technologies are referred to as NGFI interface-xhaul. The segment of the transport network that connects the CU to the 5G_Core (5GCC) is referred to as the backhaul network. In the fronthaul, the eCPRI standard [56] is used to relax the requirements induced by CPRI, thus allowing for a more flexible BS split. On the other hand, the midhaul supports various baseband functional split options, which enables the use of statistical packet multiplexing while reducing the latency and capacity constraints.

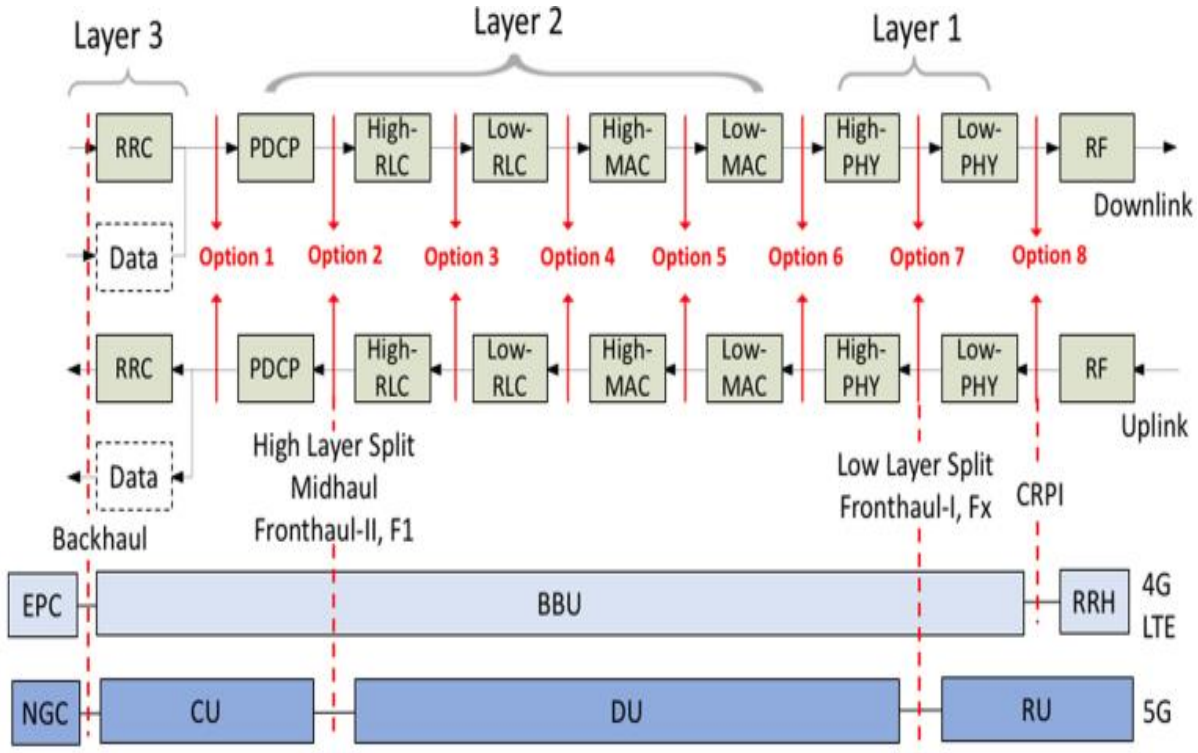

Fig. 2.21. Functional splitting block diagram with different split options [57]

Meanwhile, because the packet data convergence protocol (PDCP), radio link control (RLC), MAC, and physical layers are all part of the 5G mobile radio baseband protocol stack, these

layers have different requirements in terms of latency and bandwidth, which may be leveraged by using functional splits to control the network connectivity. To realized NGFI, the 3rd Generation Partnership Project (3GPP) has identified eight possible functional splits since Release 14 and introduced new functional blocks and interfaces for the 5G radio RAN architecture as shown in Fig. 2.21. The functional composition in BBU and RRH for 4G LTE, as well as an example implementation for 5G, are also presented in Fig. 2.21. The function splitting mechanism involves moving partial baseband functions from the local BBU to the remote RRH. By shifting any split point towards the RRH, a new fronthaul interface, also known as a non-ideal fronthaul solution is created, which significantly reduces fronthaul bandwidth requirements when compared to CPRI in 4G.

There are several approaches to implement functional splits, each with its advantages and drawbacks. For instance, Option 8 (referred to as the splitting between the physical layer and RF) is a traditional 4G fronthaul interface, which allows full centralization of all Layer 1/2/3 processing operations. However, this architecture necessitates an extremely low latency and a constant high bit rate for data transmission. Options 1-7 offer dynamic network architecture features such that the volume of data carried can scale with user traffic. This enables the transport network to adapt to changing traffic conditions and aggregate traffic from various cells efficiently when a shared infrastructure such as PON is utilised. Option 1 is a fully DRAN architecture that enables edge computing and high throughput but at the expense of increased DUs complexity. It is important to mention that the choice to use any specific split options would depend on the end user service needs and the deployment strategy of each operator. For instance, a RU and DU split at the lower layer is challenging in terms of bandwidth, latency, and packet loss, and deploying a DU far from the cell site often necessitates the operator investing in fronthaul fibre infrastructure. On the other hand, a higher-layer RAN split with DUs deployed at the cell site improves performance, but it may be less efficient in terms of coordination and, may result in higher operational cost. To address operators' diverse requirements, the telecommunication industry has defined two general split points including, a high layer split (HLS) point called Fronthaul-II/Midhaul/F1 and a low layer split (LLS) point called Fronthaul-I/Fx. Therefore, in contrast to a single split between the BBU and RRH in 4G/LTE, the 5G RAN presents a disaggregated architecture in which the individual functional blocks CU, DU, and RU can be deployed in the network flexibly according to the operator's requirements and constraints.

2.2.5.2.1 Fronthaul Technologies

With the emergence of 5G-RAN, various approaches have been explored to implement ideal and nonideal fronthaul interfaces over PONs. Among the various optical access networks, PONs based on TDM, WDM, and NG-PON2 technologies are widely deployed and are considered as an attractive candidate for future 5G fronthauls [19-24]. TDM-PON offers several unique advantages that make it ideal for fronthaul applications. The FSAN group recommended TDM-PONs such as G-PON, XG-PON, and XGS-PON for implementing the high-layer functional split option. TDM-PON uses a single wavelength to enable fibre infrastructure sharing and is considered a simple and cost-effective solution. However, TDM-PON static architecture and incurred latency using conventional DBA [57] remain critical for 5G fronthaul. Several techniques such as fixed bandwidth allocation (FBA) [58] and cooperative DBA [59] have been proposed for new latency-improving mechanisms. Furthermore, since the data rate of a single wavelength has been increased, high-speed TDM-PON for fronthaul service is gaining popularity in the networking industry. The use of 25 Gb/s or 50 Gb/s wavelength over TDM-PON for fronthaul split option 7a based on nonreturn-to-zero (NRZ) modulation scheme [59,60], 4-level pulse-amplitude modulation (4-PAM) [61], discrete multi-tone (DMT) assisted with semiconductor optical amplifier (SOA) and DSP techniques [62] are all possible solutions for 5G fronthaul. With a higher modulation scheme, the high-speed TDM-PON increases system sensitivity, which can be avoided by using TDM-PON for split options and short distances of up to 10 km. Therefore, high-speed single wavelength TDM-PON remains a viable option for 5G fronthaul.

On the other hand, WDM-PON is an alternative solution to TDM-PON since it addresses the issues of capacity, adaptive and dynamic resource allocation at low latency. WDM-PON does not require DBA, making it a suitable candidate for low latency services and arguably the most promising technology for 5G fronthaul. In WDM, fronthaul flows are transmitted on dedicated wavelength channels allocated to each CU/DU and RU pair, thus, increasing the overall capacity over a single fibre. As densification through m-MIMO and small cell networks requires more fronthaul connectivity, WDM-PON can save the fibre resources by multiplexing several wavelengths into a few fibres, via a passive WDM multiplexer placed in each cell site. Among the different WDM technologies, coarse WDM (CWDM) [63] is considered the most practical solution due to its suitability for outdoor equipment and cost-efficiency, when compared to DWDM [64]. With CWDM, up to about 18 wavelengths can be multiplexed into

a single fibre, with 20 nm spacing standardized channels from 1270nm to 1610nm. Because the maximum number of RUs in a cell site considering the radio access technology (RAT), the number of sectors and antennas is in most cases less than the channel number, the whole cell site fronthauls can be aggregated into a single fibre. CWDM offers a PtP coloured connectivity with up to 25 Gbit/s per link and it is ideal for fronthauling a macro antenna site with up to 16 RUs. However, in more complex networks with multiple RUs connected to a central DU cluster, the fixed channel assignment available via CWDM may be insufficient, making it less attractive from the standpoint of network operations and migration. In this case, the wavelength tunable DWDM technology can be utilized, provided it can be implemented at access compliant cost figures, without jeopardizing the cost reductions offered by the centralized RAN concept. Compared to CWDM, DWDM offers improve spectral efficiency and can allow up to 80 channels with typical channel spacing of 100 GHz (0.8 nm) or 200 GHz (1.6 nm). As a result of the small channel spacing, this technology is sensitive to temperature variations, which can cause wavelength deviations. The existing wavelength control mechanisms are complicated and unsuitable for use in an outdoor environment. Furthermore, DWDM networks are also known for their high cost, which can be reduced by using identical transmitters in each network termination, regardless of the specified wavelength.

Furthermore, a new NG-PON2 standard has been introduced, providing an upgrade path for 5G transport networks by exploiting the wavelength resources with many options available for different use cases. NG-PON2 supports the implementation of a DWDM technology that is compliant with cost figures and operational requirements of optical access networks. Enabled by wavelength tunability and channel bonding, NGPON2 significantly enhances the transmission capacity. Apart from the wavelength tunability of the end nodes, NG-PON2 allows real-time dynamic control of the channel assignment per node, making it a promising technical strategy for future 5G fronthaul and midhaul networks. NGPON2 supports two different types of DWDM subsystems, including i) multiple unshared PtP connections via DWDM (PtP-WDM), and ii) multiple TDM/TDMA PtMP connections on separate DWDM channels TWDM. Both subsystems are considered for the construction of fronthaul or a split option, and they can both operate simultaneously on the same ODN. By exploiting the wavelength resources, NG-PON2 can deliver 80 Gb/s data rates by aggregating eight wavelengths using the TWDM technique, and up to 160 Gb/s more if sixteen wavelengths are added using the PtP-WDM overlay technique [20,25]. This appears to be sufficient capacity to meet future traffic demand. However, using the optimized NG-PON2 for fronthaul application

requires wavelength tunability, multiple wavelengths bonding, and stringent cross talk control, all of which significantly increases the transceiver complexity and the overall network cost.

Aiming to further maximize the spectral efficiency while minimizing the latency, a more scalable alternative is the introduction of the DSP-assisted ARoF technique [65], where an analogue RF or intermediate frequency (IF) signal is transmitted over the fibre and all processing remains centralized. With ARoF, the overhead inherent in the digitization of the RF signal is eliminated, as a result, reduces bandwidth usage. In addition to the low bandwidth requirement, ARoF also offers the added benefits of lower power consumption and allow the usage of mm-wave frequency bands, making ARoF an attractive candidate for future 5G fronthaul. However, the ARoF's improved spectral efficiency comes at an expense of a reduction in performance tolerance against nonlinear distortions and fibre transmission impairments. Nevertheless, new technologies such as polarization multiplexing [66] using two orthogonal polarizations transmitting different RF signals in the same optical fibre simultaneously, and digital pre-distortion (DPD) [67] technique based on single mode vertical cavity surface emitting laser (VCSEL) and SSMF have been proposed to enhance the linearity of short and limited range fronthauls for the present 4G-LTE and future 5G mobile networks. To further enhance the capacity of the fronthaul networks with added flexibility for multiplexing, slicing, or routing, optical space division multiplexing (SDM) has been proposed, which directly combines with ARoF [68]. This approach offers not only ultra-high capacity networks that can support different classes of fronthaul traffic but also envisioned fronthauls that are ideally suited to support large RF bandwidths and mm-wave.

Moreover, it should be noted that the developments of the abovementioned PON techniques are aimed at increasing network capacity and are not designed to provide a dynamic network architecture. To enable the 5G fronthauls to adapt to emerging highly dynamic traffic, the next generation optical networks must provide features such as dynamic reconfigurability, flexibility, elastic bandwidth provisioning with fine granularity, sliceable network and as well SDN. To realise highly dynamic networks for fronthauls, this dissertation proposes optical transceiver-embedded DSP-enabled DOF-based multiple channel transmission techniques to implement CANs [32-35] with independently multiplexing optical channels at the wavelength, sub-wavelength and orthogonal sub-band levels. The CANs enable the seamless convergence of traditional optical access networks, metropolitan area optical networks, and 4G/5G fronthauls/backhauls to address future requirements such as ubiquitous connectivity, flexibility,

low power consumption and as well the provision of multi-service and multi-tenancy in a cost-effective way. Apart from the cost-effectiveness, the CANs can support massive device connectivity with highly scalable aggregated elastic channels with fine bandwidth granularity, combined with inherent transparency to underlying signal modulation formats, signal bit rates, and multiple access techniques. In addition, using IMDD and off-the-shelf and low-cost 10G-class optical and electrical components in combination with advanced modulation, the CANs provide low transceiver complexity as they allow the utilization of low-cost and low-bandwidth optical and electrical components which are crucial for achieving cost-effective 5G fronthauls. The CANs are introduced in chapter 1 and the results of the research work carried out exclusively on CANs as part of this dissertation are presented in detail in chapters 3-6.

2.2.5.2.2 Backhaul Technologies

For all generations of cellular networks, the backhaul connects BBU to the CN to transport aggregated baseband signals in both uplink and downlink directions. Developing backhaul technologies are becoming increasingly crucial for future 5G mobile networks with strict requirements in terms of capacity, latency, reliability, and cost efficiency. Traditional backhaul technologies include either RF backhauls or optical fibres backhauls and can support different physical configurations depending on the requirements. The telecommunication industry and academia are focussed on developing advanced backhaul technologies which are based on a dedicated optical fibre supporting PtP and PtMP topologies. The PtP topology is the most straightforward backhauling solution to deploy with abundant optical fibre resources, whereas the PtMP approach enables sharing of available but limited optical fibre resources. In the PtP configuration, each RU is directly connected to its managing CUs and can be implemented for example, in single-hop, chain, tree, ring, or mesh topologies, however, the overall latency will increase in proportion with the link length, hop counts, and latency in the multiplexing/demultiplexing points [69]. While in the PtMP architecture, each RU may communicate with the managing CU through a set of intermediate RUs. The PtMP configuration can reduce the dependence of backhaul networks' performance on the number of aggregation nodes while enabling simple node addition, deletion, and modification.

It is well known that PONs outperform other fibre-based network architectures in terms of cost and efficiency. The most popular and widely used PtMP solution for backhauling is G-PON. In addition to legacy G-PON, XGS-PON is also considered for enriched fixed broadband but

also RAN backhaul. Both solutions are based on a wavelength channel pair to achieve upstream and downstream and can coexist on the same ODN. TDM/TDMA is used for sharing the trunk part of the ODN, which is equipped with optical power splitters at the branching nodes and a single optoelectronic interface at the access/aggregated node. Due to the complexity of operating mobile and fixed networks on the same OLT port, TDM-PON is not widely used for backhauls. Recently, multi-wavelength PON solutions, NG-PON2 standard have been introduced leveraging on using both TWDM-PON and PtP WDM PON approaches. To further enhance the capacity, backhaul solutions exclusively based on WDM can be used to support either wavelength-routed topology or wavelength-selected topology. However, WDM PONs require AWGs as a wavelength multiplexer/demultiplexer device, which is prohibitively costly compared to optical splitters. In addition to PtP and PtMP backhaul topologies, to significantly increase capacity, a more advanced approach employs reconfigurable optical add-drop multiplexers (ROADMs) [70,71] in a ring topology with WDM enabling on-demand dynamic allocation and therefore efficient utilization of the available capacity. This is ideal for backhaul networks since the dynamic traffic fluctuations caused by user mobility and unpredictable behaviour can be addressed by its reconfigurability feature.

Currently, optical fibre is the most widely used physical transmission medium for backhaul networks. Other options such as traditional copper cables and microwave links can also be used, especially when optical fibres are not deployed in the ‘‘last mile’’ to reach the BS from the CN. The use of copper cables for backhauling was introduced in the early 2G cellular network carrying mainly voice and IP traffic over circuit switched networks. TDM techniques based on plesiochronous digital hierarchy (PDH) [72] are the prevalent techniques used for multiplexing multiple voice channels. The T-carriers (T1, T2, …, T4) and the E-carriers (E1,….E5) are the two PDH standards, both of which can be deployed as PtP systems or over PDH multiplexing systems. The T-carriers operate at 1.544 Mbit/s and are primarily used in North America and Japan, while the E-carriers operate at 2.048 Mbit/s and are mostly used in Europe and the rest of the world. As cellular networks evolved towards 3G and the backhaul capacity demand increase, synchronous transport mode (STM) technology for optical fibre standard was developed to carry high data rates backhaul traffic. STM establishes a structure of data payload speeds from STM-1 (155.52 Mbit/s), STM-4 (622 Mbit/s), STM-16 (2.4 Gbit/s) to STM-64 (10 Gbit/s) [72]. The STM standards are known as synchronous optical networking (SONET) in North America, and as a synchronous digital hierarchy (SDH) in Europe and the rest of the

world. SDH/SONET over optical fibres can be implemented in a ring topology with add/drop multiplexers.

Moreover, microwave RF links are a viable alternative to wired backhaul connectivity, particularly in remote locations where wired connections are difficult to deploy. Microwave transmission can be carried out in both licensed (6 GHz to 38 GHz) and unlicensed (2.4 GHz and 5.8 GHz) frequency bands. In all cases, microwave links require a line of sight (LOS) between BSs (BBUs) and CN, hence they are limited to short reach when used in metropolitan environments. The digital transmission technique over microwave links can be based on PDH, SDH/SONET, or Ethernet (Gigabit Ethernet protocol), and can be implemented in the PtP, PtMP, or proprietary multi-hop configurations for better coverage. Backhauling traffic from cell sites onto leased copper links utilising PtP microwave links can result in significant savings, however, adopting a PtMP topology can only be cost-effective if each PtMP system support at least 5 cells. Traditional backhaul technologies described so far majorly rely on circuit-switched technologies. With cellular networks evolving to 4G/LTE systems, the pseudowire framework was introduced as a packet-based backhaul using popular technologies such as multiprotocol label switching (MPLS), G.709 optical transport network (OTN), and carrier Ethernet, all of which support the overlay IP network. Given the packetized requirement of data traffic and the unpredictability of users, the packet-switched networks are cost-effective and can achieve high-speed and efficient backhaul networks with dynamic bandwidth provisioning to meet an uncertain set of demands.

For next generation backhaul networks, microwave radio links and optical fibre links have been considered as feasible solutions. While RF backhaul is a cost-effective solution when compared to optical fibre, especially for backhauls in high-density urban areas, however, RF technology also has its challenges such as limited data rates, licensed spectrum, and interference. Unlike microwave links, millimetre-wave which is itself the key technology within the 5G mobile network evolution is a better option for 5G backhauls because of the availability of massive bandwidth in the radio spectrum (30-300GHz). Recently, free-space optics (FSO) [73-75] technology, which combines both high data rates and relatively low-cost technologies has emerged as a promising solution for 5G backhauls. By transmitting a laser beam using a license-free wavelength in the micrometre range, FSO photo-detector transceivers are not only free to use but also support full-duplex, high-speed transmission, and are immune to electromagnetic interference. FSO and optical fibre are compatible since they both operate at

the same wavelength and data rates. On the other hand, millimetre-wave links can cast very narrow beams, allowing for the deployment of multiple independent links in proximity, and as well have the potential to offer bandwidth similar to optical fibre. In terms of capacity, FSO links due to their high bandwidth and interference immunity features are up to 25 times more efficient than RF links. In contrast to optical fibre links which are always reliable, FSO links are less reliable since they are sensitive to weather conditions such as rain, fog, and snow. To benefit from both the low cost and reliability of the RF technology and the high data rates provided by the FSO technology, the hybrid RF/FSO technology is considered a promising solution for future 5G backhauls [73,74]. The hybrid RF/FSO transceivers communicate using both RF and FSO links and switching to either FSO or RF is determined by the electromagnetic interference levels and weather conditions. In addition, FSO can be utilized with multiplexing techniques such as WDM to enhance the capacity and provide adaptability and flexibility to future 5G backhaul networks.

2.2.6 Fundamentals of OFDM and Optical OFDM IMDD PONs

This subsection presents an introduction to the fundamentals of OFDM and OOFDM IMDD-based PON, which serve as the framework for the work described in the rest of this thesis.

For the past several decades, OFDM has emerged as a dominant research and development area in the field of high-speed optical communications. OFDM has been widely used in high-impact applications such as high-end wire-line access systems via ADSL, digital and high-definition television transmission, and wireless broadband applications ranging from wireless local area networks (WLAN) such as IEEE 802.11a/g and IEEE 802.16, to Wireless Wide Area Networks (WWAN), to Worldwide Interoperability for Microwave Access (WiMAX), and the currently widely adopted 4G LTE mobile networks [76,77]. Moreover, OFDM is considered a strong candidate for NG-PONs, and since the initial stage of 5G is envisaged to have sufficient transparency to OFDM-based 4G networks, thus, OFDM is expected to play a significant role in converging 5G mobile networks [78,79] due to a variety of well-documented benefits it can offer, as described in subsection 2.2.3.4.

2.2.6.1 Basic Concept of OFDM

The OFDM concept is essentially identical to coded OFDM (COFDM) and discrete multi-tone modulation (DMT), which is a frequency division multiplexing (FDM) scheme utilized as a

digital multicarrier modulation (MCM) method. As OFDM is a special form of the FDM technique, therefore descriptions of FDM are first provided. The basic principle of FDM is to transmit multiple signals simultaneously over a wideband channel by modulating each signal onto a dedicated subcarrier with different RFs and multiplexing the modulated subcarriers, as shown in Fig. 2.22.

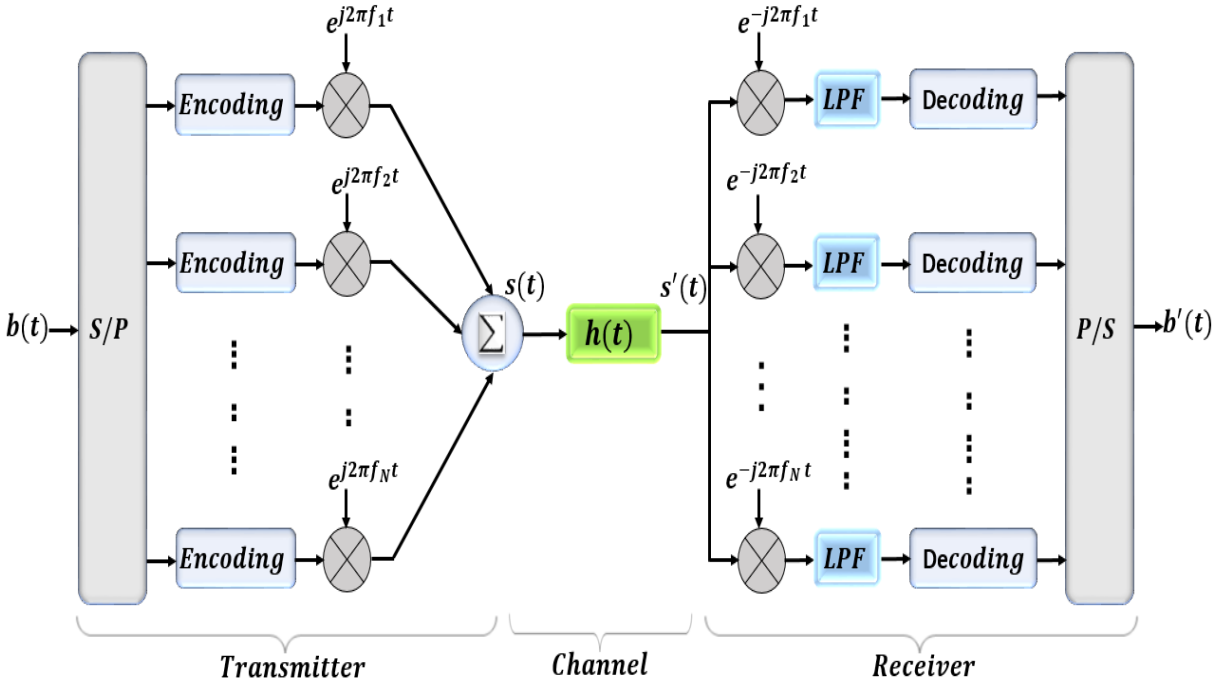

Fig. 2.22. Conceptual block diagram of a generic multicarrier modulation system. S/P: serial-to-parallel, P/S: parallel-to-serial, LPF: Lowpass Filter

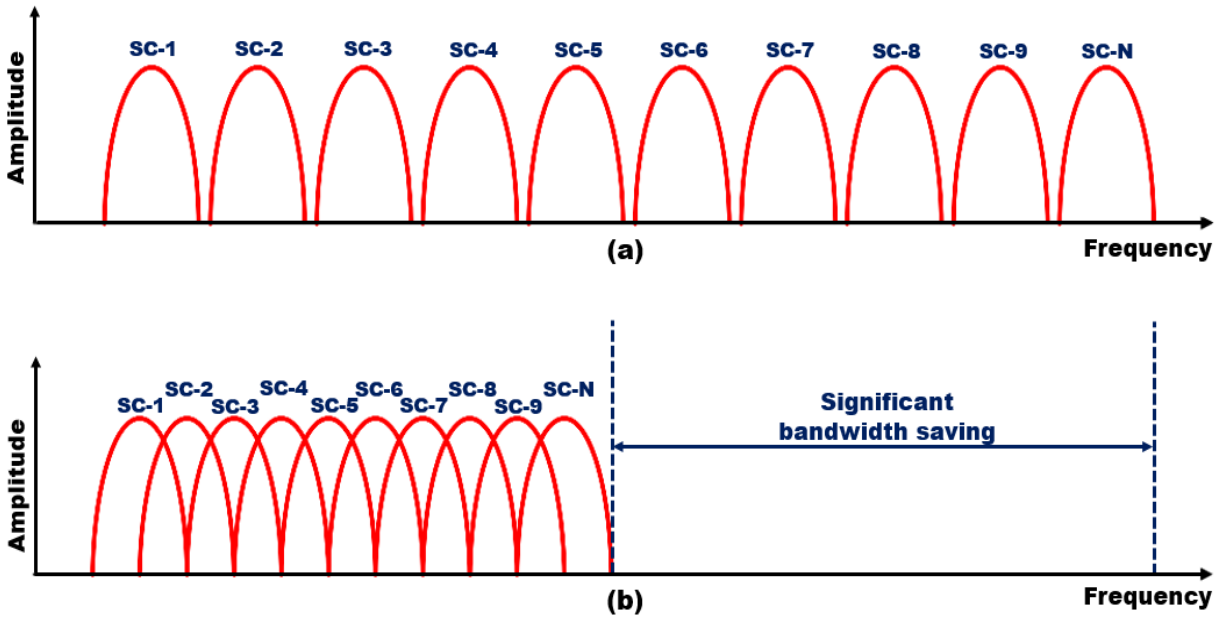

Fig. 2.23. Spectral of (a) FDM, and (b) OFDM. SC: subcarrier

In the transmitter, the serial-to-parallel converter takes the serial stream of input bits and outputs parallel streams, which are encoded using classical modulation formats such as M-ary quadrature amplitude modulation (QAM) or quadrature phase shift keying (QPSK). Once the data bits are converted to the required digital modulation formats, they are simultaneously modulated onto different subcarriers by an oscillator array operating at different RFs with a sufficiently wide guard band frequency between two adjacent subcarrier frequencies, as shown in Fig. 2.23(a). Finally, the resulting outputs from the different modulated subcarriers are multiplexed together before channel transmission. In the receiver, the parallel data streams are recovered by down converting each subcarrier with an identical RF as in the transmitter, followed by the low pass filtering and decoding process.

Compared to FDM, OFDM precisely chooses the inter-subcarrier RF spacing such that all RF frequencies are harmonically related to ensuring orthogonality between subcarriers, as shown in Fig. 2.23(b). OFDM offers significant improvement in spectral efficiency (at least 50%) compared to FDM. In practice, the modulation/multiplexing and demodulation/demultiplexing in the OFDM system can be achieved by using the efficient inverse FFT (IFFT) and FFT operations. As FFT/IFFT can be practically implemented with advanced DSP technology, OFDM systems are relatively simple, as the FDM system requires a significant number of modulators, filters and demodulators, which are not required in the OFDM system. Furthermore, OFDM offers the benefit of mitigating the frequency-selective fading effect caused by wireline or wireless channels.

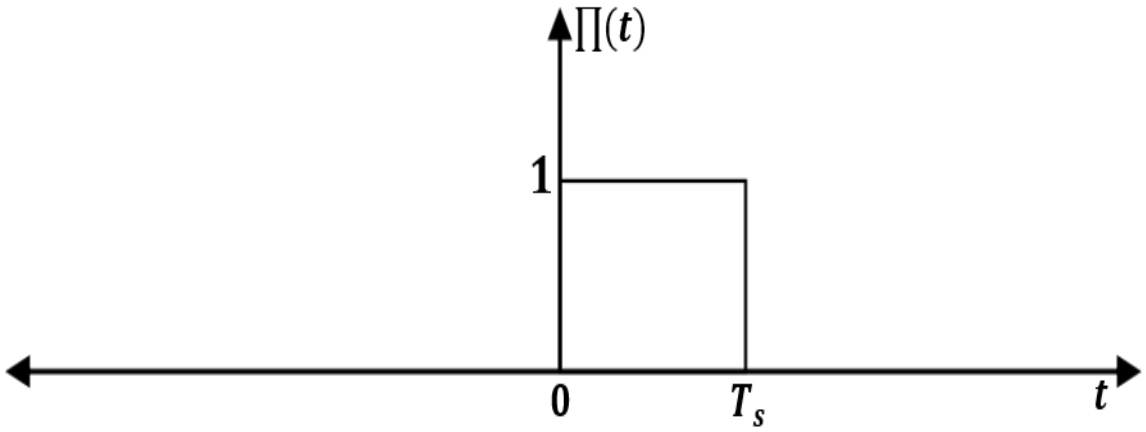

Fig. 2.24. Rectangular pulse shaping function

Consider a generic MCM to describe the concept of orthogonality between OFDM subcarriers, in the time domain, the transmitted signal *k*-th subcarrier in the *n*-th OFDM symbol can be written as [9]:

$$x(t) = \sum_{n=-\infty}^{\infty} \sum_{k=1}^{N_{sc}} X_{k,n} \prod(t) e^{j2\pi f_k (t - nT_s)} \tag{2.20}$$

$$X_{k,n} = A_{k,n} e^{j\theta_{k,n}} \tag{2.21}$$

$$\prod(t) = \begin{cases} 1, & 0 < t \leq T_s \\ 0, & Otherwise \end{cases} \tag{2.22}$$

where $X_{k,n}$ is the k-th subcarrier in the n-th OFDM symbol, N_{sc} is the number of subcarriers, f_k is the RF frequency of the k-th subcarrier. In Eq. (2.21), $A_{k,n}$ and $\theta_{k,n}$ are the amplitude and phase of the encoded data $X_{k,n}$, respectively. In Eq. (2.22), T_s is the OFDM symbol period, and $\Pi(t)$ is the rectangular pulse shaping function of unity magnitude over the time duration of T_s, as shown in Fig (2.24).

Moreover, since OFDM uses signals arranged in an orthogonal set, to examine the orthogonality condition between two subcarriers in more detail, when $X_{k,n}$ is treated as a unit for simplicity, the correlation, $\delta_{k,l}$, between any two subcarriers within the n-th symbol period is given by:

$$\delta_{k,l} = \frac{1}{T_s} \int_0^{T_s} x_{k,n}(t) x_{l,n}^*(t) dt$$

$$= e^{(j2\pi(f_k - f_c)T_s)} \frac{\sin(\pi(f_k - f_l)T_s)}{\pi(f_k - f_l)T_s} = \begin{cases} = 0, & k \neq l \\ \neq 0, & k = l \end{cases} \tag{2.23}$$

Eq. (2.22) demonstrates that two subcarriers are orthogonal to each other if the subcarrier frequency spacing, Δf, satisfy the condition:

$$\Delta f = f_k - f_l = k \frac{1}{T_s} \qquad k = 1,2,3 \ldots \ldots \ldots N_{sc} \tag{2.24}$$

where f_l is the frequency offset common to all subcarriers, which is usually set to zero. In Eq. (2.24), the subcarrier frequencies are spaced at integer multiples (i.e., harmonics) of the inverse of the symbol period T_s, and the number of harmonics between adjacent subcarriers differs exactly by one. This property accounts for the orthogonality between different subcarriers [9,18]. The orthogonality principle indicates that the correlation of an OFDM symbol containing multiple subcarriers with a single complex valued fixed frequency reference subcarrier will result in only the subcarriers with the same frequency contributing to non-zero correlation outputs, while all other subcarriers with different frequencies will result in zero-valued correlation outputs.

Moreover, the orthogonality principle is also illustrated in the frequency domain as shown in Fig. 2.25, where the corresponding subcarriers each have a spectrum with a sinc form with frequency spacing of Δf. It can be seen the spectrum of each subcarrier overlapped with the spectra of other subcarriers such that at the center frequency of any specific subcarrier, all other subcarriers have zero amplitude. As such for ideal cases, no inter-carrier interference (ICI) occurs between different subcarriers even when their spectrums are overlapping, thus, making OFDM highly spectrally efficient compared to the FDM system.

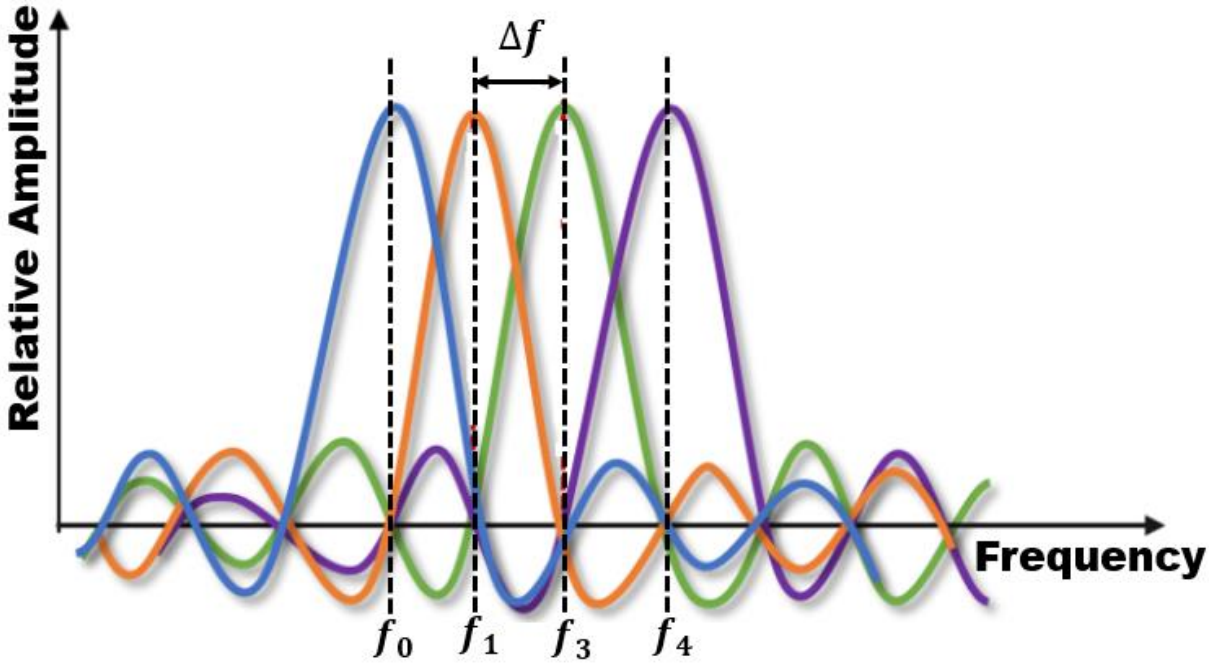

Fig. 2.25. Spectrum of OFDM Modulated signal

Furthermore, even though there is a strong signal spectrum overlap due to the orthogonal property of the subcarriers, the data encoded on individual subcarriers can be recovered. To decode a subcarrier at frequency f_k, multiply the received signal by the complex signal and integrate over the symbol period to obtain the detected symbol $X'_{k,n}$, as described by Eq (2.25). The low-pass filters that match the subcarrier waveform or a correlator matched to the subcarrier as shown in Fig. 2.22 are used to perform the integration function. Any subcarrier that is not at the center frequency, f_k, will integrate to 0 and therefore have no effects on the decoded information symbol, $X'_{k,n}$, given as:

$$X'_{k,n} = \frac{1}{T_s}\int_0^{T_s} s'(t - nT_s)e^{-j2\pi f_k t}dt \qquad (2.25)$$

where $s'(t)$ is the received time domain signal.

2.2.6.2 OFDM Transceiver System

A typical OFDM system consists of a transmitter, a transmission link, and a receiver, as shown in Fig. 2.26. The main DSP functions in the transmitter include bit encoding, IFFT, CP insertion, and parallel-to-serial (P/S) converter. Following the serialization is the DAC, which converts the generated OFDM signal to an analogue signal waveform. Before channel transmission, the electrical analogue OFDM signal is RF up converted. In the receiver, after the analogue signal transmission through the channel, the received OFDM signal is processed by the receiver DSP functions using an inverse procedure of the transmitter, which includes down conversion using an RF carrier with the same frequency as the transmitter, digitalization in an ADC, serial to parallel conversion, cyclic prefix removal, FFT operation, channel estimation, and equalization, and finally decoding to recover the transmitted binary data.

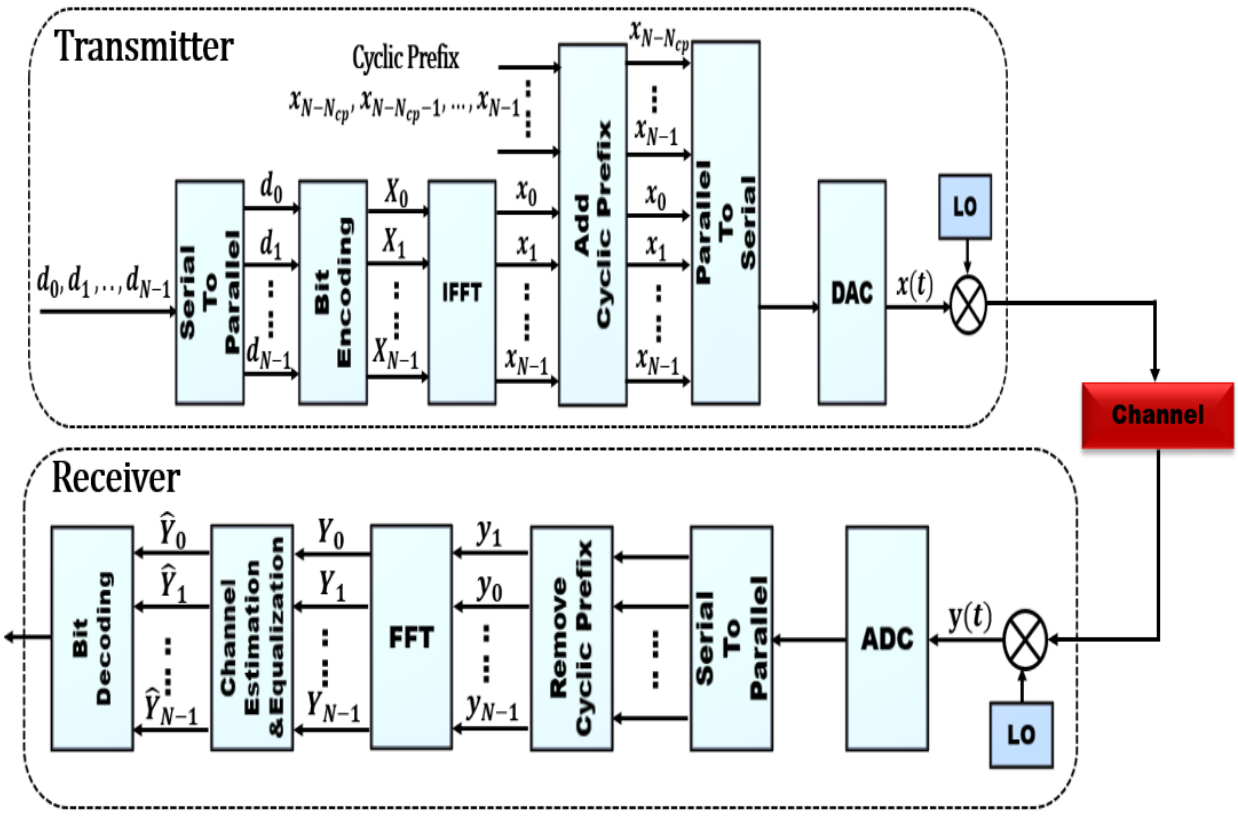

Fig. 2.26. Typical structure of an OFDM transmission system. DAC: digital-to-analogue converter; ADC: analogue-to-digital converter.

2.2.6.2.1 IFFT/FFT

The encoded complex number via bit encoding using a specific modulation format to represent a subcarrier's frequency domain data must be up converted to an RF subcarrier frequency and

then multiplexed with other subcarriers. To maximise OFDM benefits, a large number of subcarriers are required. However, using discrete components to implement OFDM transceivers would result in a complex architecture as each subcarrier requires oscillators and filters in both the transmitter and receiver sides, making this approach impractical. To allow for more practical implementation of OFDM transceivers, signal modulation and multiplexing can be implemented digitally using IFFT in the OFDM transmitter and demodulation and demultiplexing can be performed using FFT in the OFDM receiver [9,18]. In this approach, the OFDM signal is processed in both the frequency and time domain as a discrete signal rather than a continuous signal making OFDM ideal for implementation in DSP. When all the subcarrier waveforms are combined, considering Eqs. (2.20), (2.21), and (2.24), the time-domain *n*-th OFDM symbol within a time duration of [(*n*-1)*Ts*, nT_s] can be expressed as:

$$x_n(t) = \frac{1}{N}\sum_{k=0}^{N_{sc}-1} X_{k,n} e^{j2\pi k f_k t} \tag{2.26}$$

Assuming $x_n(t)$ is sampled at an interval of T_s/N, the *m*-th sampled $x_n(m)$ within of [(*n*-1)T_s, nT_s] can be expressed in discrete form as:

$$x_n(m) = \frac{1}{N}\sum_{k=0}^{N_{sc}-1} X_{k,n} e^{j2\pi \frac{km}{N}} \quad m = 0,1,2 \ldots N-1 \tag{2.27}$$

Eq. (2.27) has a form identical to IFFT indicating that the OFDM signal can be directly produced by the IFFT in the transmitter. Similarly, in the receiver, the FFT can be used to output the discrete frequency domain complex number, $Y_{k,n}$, expressed as:

$$Y_{k,n} = \frac{1}{N}\sum_{m=0}^{N_{sc}-1} y_n(m) e^{-j2\pi \frac{km}{N}} \tag{2.28}$$

where $y_n(m)$ is the received sample time domain signal at the input of the FFT, and all $y_n(m)$ samples are within the same OFDM symbol. $Y_{k,n}$, is the frequency domain sample for the *k*-th subcarrier at the output of the FFT. Therefore, in practice, IFTT/FFT operations are used as they significantly reduce the number of complex computations required.

2.2.6.2.2 Cyclic Prefix

For non-ideal channels, different subcarriers located at different RFs in an OFDM signal will have different delays caused by fibre CD. For simplicity, assuming that T_d is the maximum

differential delay between the fast subcarrier A and slow subcarrier B and that the FFT window containing a full OFDM symbol for subcarrier *A* is selected, as shown in Fig. 2.27.

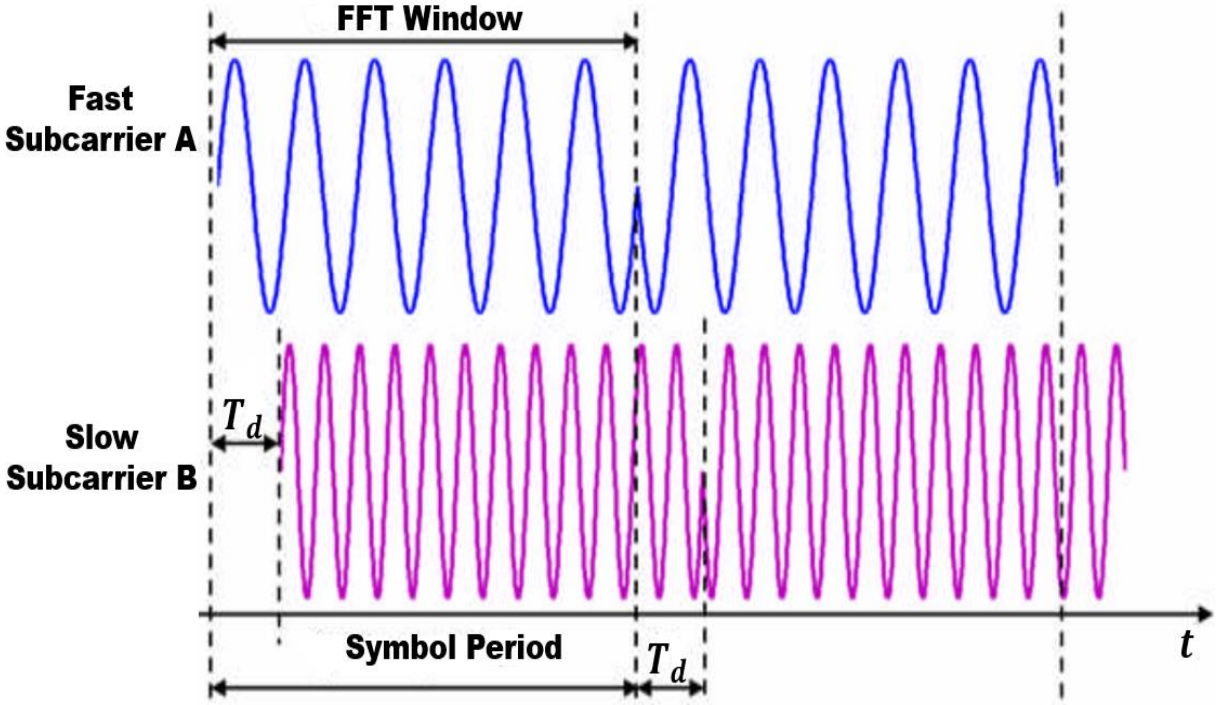

Fig. 2.27. Channel dispersive-induced ISI and ICI.

It is apparent that due to the channel dispersion, subcarrier *B* crosses the symbol boundary, giving rise to ISI between the neighboring OFDM symbols. Furthermore, as the OFDM waveform in the FFT window for subcarrier *B* is incomplete, its dispersive delay will destroy the orthogonality between the subcarriers, causing ICI.

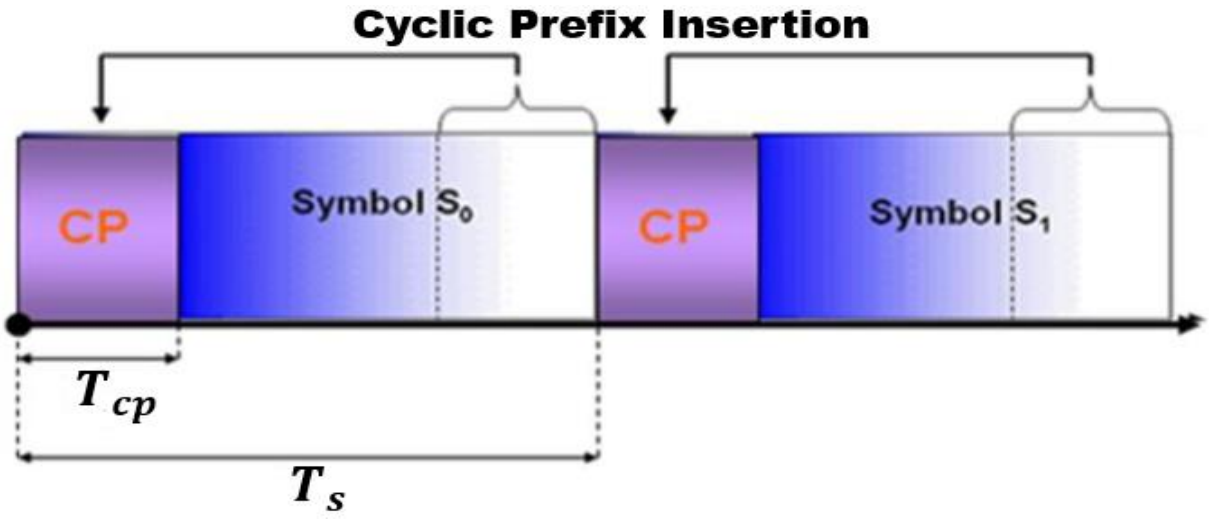

Fig. 2.28. CP insertion in the time domain OFDM signal

To mitigate the problems of channel dispersion-induced ISI and ICI, CP was proposed to improve the performance robustness of the OFDM system [9,28]. A CP is a copy of the tail-end fraction of samples from each OFDM symbol and is added to the front-end of the same symbol, as shown in Fig. 2.28. If N is the number of OFDM samples, due to the addition of CP samples of length N_{CP}, the new OFDM symbol length is $N + N_{CP}$, and the new symbol duration is T_s. Therefore, if the CP duration is T_{CP}, then the duration of the OFDM symbol carrying useful information occupies a time T_s - $T_{CP.}$ Throughout the thesis, the CP parameter used is defined as:

$$\eta = \frac{T_{CP}}{T_s - T_{CP}} \tag{2.29}$$

From the above description, it is apparent that as long as the CP time duration is at least as long as the maximum dispersion-induced time delay spread of the transmission link, the CP, rather than the front-end data symbols, will absorb any residual symbol spreading [9,28]. From this perspective, to ensure an ISI-free OFDM transmission, it is only the CP length that matters.

2.2.6.2.3 DAC/ADC Conversion, Quantization and Clipping

In modern digital transmission systems, the DAC and ADC are critical components, which have limiting factors in their overall system performance due to limitations in their sampling speed, quantization noise, and clipping noise. In the transmitter, after parallel-to-serial conversion, a DAC is utilized to convert the produced digital OFDM signal into an analogue OFDM waveform that can be modulated onto a carrier for transmission. Similarly, in the receiver, an ADC is required to convert the signal back to the digital domain to recover the received signal.

As ADCs/DACs have limited dynamic amplitude ranges, signal clipping occurs when the signal amplitude exceeds their maximum input amplitudes. Moreover, due to the DAC/ADC having limited bit resolution, the OFDM signal samples with a resolution of q bits can only be represented by 2^q-1 discrete levels, resulting in a quantization noise induced by the finite bit resolution, which has greater effect as the signal amplitude reduces. In addition, a characteristic of OFDM signals is the high PAPR. When generating the OFDM signal, the coherent superposition of independently modulated orthogonal subcarriers in the time domain will result in the signal envelope exhibiting high peaks, giving rise to the high PAPR of the OFDM signal. In general, the PAPR [$x(m)$] of the time domain sequence, $x(m)$, with N subcarriers, in Eq.

(2.27), is defined as the ratio of the maximum instantaneous power to the average power, which can be expressed as:

$$PAPR\{x[x(m)]\} = \frac{max\{|x(m)|^2\}}{E\{|x(m)|^2\}}, \qquad m \in [1, N] \tag{2.30}$$

where $E\{.\}$ denotes the mean or expected value of the power of $x(m)$. The theoretical maximum of PAPR is $10log_{10}(N)$ in dB, indicating that the PAPR of an OFDM signal increases as the number of subcarriers increases. In this thesis, the approach used to evaluate the PAPR is the complementary cumulative distribution function (CCDF), which is the probability of OFDM symbols with PAPR exceeding a certain threshold $\curlywedge$, defined as:

$$P_r\{PAPR > \curlywedge\} = 1 - (1 - e^{-\curlywedge})^N \tag{2.31}$$

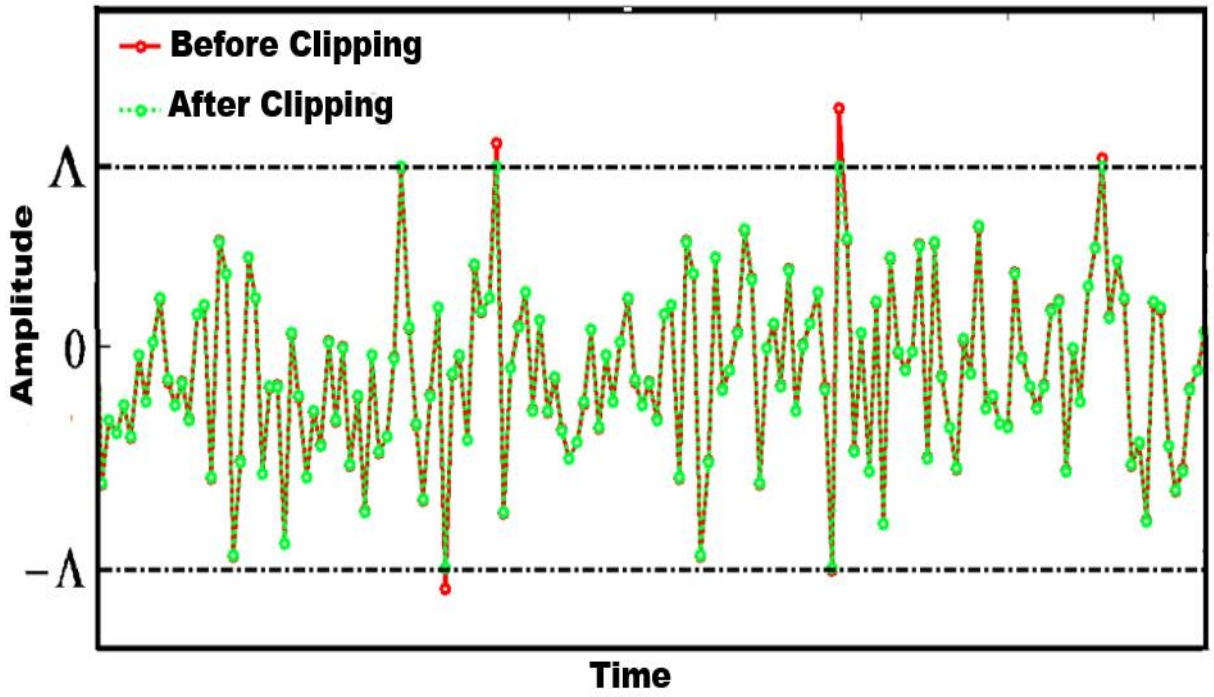

Fig. 2.29. OFDM signal before and after clipping

Technically speaking, OFDM systems with large PAPRs not only require wide dynamic operating ranges for the transceiver-embedded electrical/optical devices but also produce high quantization noise for a fixed number of quantization bits and may force the involved devices to operate in their non-linear regions, thus introducing nonlinear distortions. In addition, the large PAPR may also cause serious nonlinear noise associated with SSMF nonlinearities. Therefore, as one of the simplest PAPR reduction techniques, clipping is applied to the OFDM signal. Assuming an analogue OFDM signal, $A(t)$ is real, for a given clipping ratio (peak power

/ average power) ξ (in dB), the clipped signal has the form:

$$A_{clip}(t) = \begin{cases} A(t), & |A(t)| \leq \wedge \\ \wedge\, e^{jarg[A(t)]} & |A(t)| > \wedge \end{cases} \quad (2.32)$$

where $\wedge$ is the maximal input amplitude of the DAC/ADC, defined as $\wedge = \sqrt{\xi . P_m}$ with ξ being the clipping ratio and P_m being the average signal power. As an example, Fig. 2.29 shows an OFDM signal before and after clipping, where the PAPR is reduced. As clipping is applied to limit the signal power within a predetermined range, in practice, an optimum clipping ratio is chosen since over clipping can cause signal distortion, whereas inadequate clipping can lead to high PAPR which can increase the quantization noise effect.

After clipping, the sampled continuous amplitude, $A(t)$, is linearly quantized into equally distributed quantization levels, which span the entire dynamic range of $[-\Lambda, \Lambda]$. The quantization process can be expressed as follows:

$$Q(A_q) = \sum_{k=-\frac{L}{2}+1}^{\frac{L}{2}} \frac{A_k + A_{k-1}}{2}\, g(A_s, A_k, A_{k-1},) \quad (2.33)$$

where $Q(A_q)$ is the quantized value, A_s is the sampled OFDM values, A_k and A_{k-1} represent the k-th and $(k-1)$-th quantization threshold values. L is the quantization levels specified as $L=2^q$, with a fixed number of quantization bits of q, g is the rectangular function defined as:

$$g(x, x_1, x_2) = \begin{cases} 1, & x_1 \leq x < x_2 \\ 0, & otherwise \end{cases} \quad (2.34)$$

From the above analysis, is it easy to understand that the quantization process introduces the quantization noise since the continuous amplitude waveform of A_s is mapped onto a finite step size of $2\Lambda/L$ discrete values within the dynamic range of $[-\Lambda, \Lambda]$. Therefore, the quantization bit q must be sufficiently large to significantly reduce the quantization noise. However, for specific sampling speeds, a larger quantization bit can increase DAC/ADC complexity and cost. Therefore, in practice, it is crucial to identify the optimum quantization bit by exploring the trade-off between transmission performance and DAC/ADC features.

2.2.6.2.4 Pilot Aided Chanel Estimation and Equalization

When OFDM signals are transmitted in a dispersive channel, the transmission channel frequency response introduces amplitude and phase variations to the subcarrier's time delay between different subcarriers during transmission. Such distortion effect can effectively be compensated for by channel estimation and equalization in the receiver. In the time domain, assuming the *k*-th subcarrier channel impulse response is $h_k(t)$ and the corresponding noise component is $w_k(t)$, after transmitting through a channel, the received OFDM signal for the *k*-th subcarrier can be expressed as:

$$y_k(t) = x_k(t) \otimes h_k(t) + w_k(t) \tag{2.35}$$

where $x_k(t)$ is the transmitted OFDM signal for the *k*-th subcarrier and $\otimes$ denotes the convolution operator. The time domain convolution relationship between $x_k(t)$ and $h_k(t)$ in Eq. (2.35) is equivalent to their multiplication in the frequency domain. Assuming ideal synchronization in the receiver, after FFT, the resulting output corresponding to the *k*-th subcarrier is given by:

$$Y_k = X_k . H_k + W_k \tag{2.36}$$

To perform channel estimation, a number of known sets of pilot signals are interspersed with the user data and transmitted, and following FFT in the receiver, the pilot signals are extracted from the received signals. The frequency response H_k, of the *k*-th subcarrier, can then be estimated by dividing the extracted pilot signals by the transmitted pilot signals, as stated as:

$$H_k = Y_{k,p} / X_{k,p} \tag{2.37}$$

where $X_{k,p}$, and $Y_{k,p}$, are transmitted and received pilot signals of the *k*-th subcarrier before IFFT in the transmitter and after FFT in the receiver, respectively. Following channel estimation, channel equalization can be undertaken to inverts the distortive effect on each *k*-th sub-carrier before signal decoding. The transmitted complex data $X_{k,n}$ for the *k*-th subcarrier in the *n*-th OFDM symbol can be recovered by multiplying the received data $Y_{k,n}$ after FFT with the inverse of the estimated frequency response H_k^{-1}, which is given by:

$$X'_{k,n} = Y_{k,n} H_k^{-1} = X_{k,n} + W_k H_k^{-1} \tag{2.38}$$

where $X'_{k,n}$ is the recovered complex data and W_k is the channel noise for the k-th subcarrier. Eq. (2.38) indicates a simple one-tap equalization as each subcarrier is multiplied by a single complex coefficient. However, this approach has the drawback of not being able to eliminate the channel noise, which can distort the signal significantly when the received OFDM signal has low power. In practice, such a problem can be overcome effectively by averaging the subcarrier channel frequency response estimations over a long-time duration.

2.2.6.3 IMDD-Based Optical OFDM Transceiver

For optical modulation, external modulation of a CW laser source with a modulator such as an MZM or an SOA, and either an IM or optical I/Q modulator can be employed to convert the RF OFDM signal into the optical domain. This can also be achieved by exploiting a DML, where the laser current is generated by combining the OFDM signal with a DC bias current. For a cost-effective IMDD-based PON transmission system of interest in this dissertation, the optical modulator used is the low-cost and low-complexity IM, and in the receiver, the detection is a square-law photodetector.

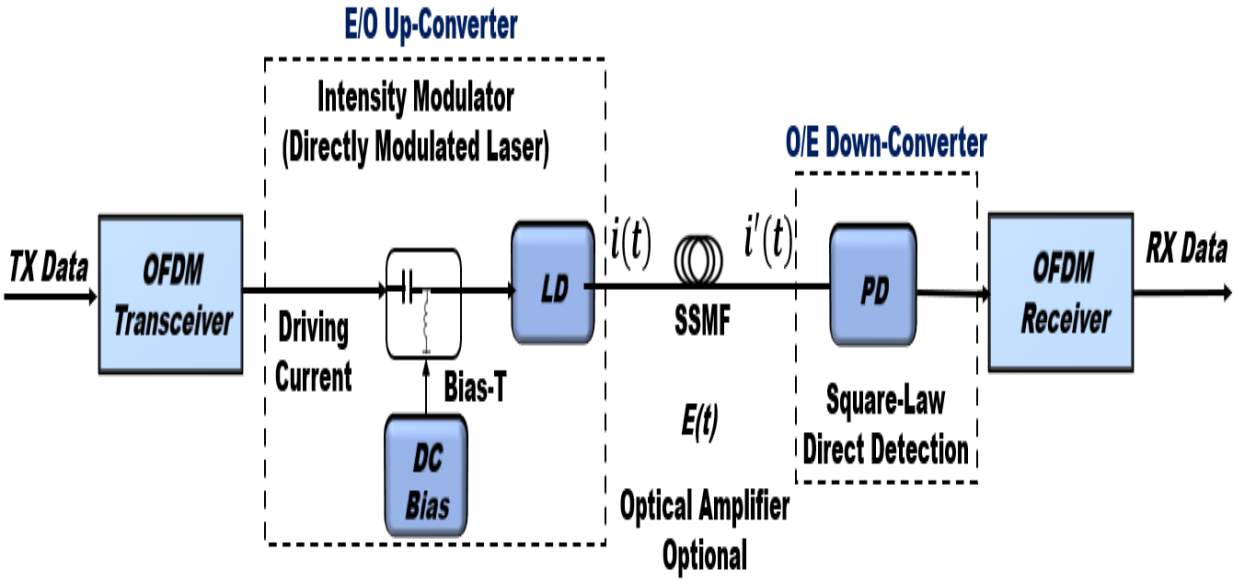

Fig. 2.30. IMDD-base OFDM system

An IMDD OOFDM system is shown in Fig. 2.30. In addition to the OFDM transceiver similar to that shown in Fig.2.26, a number of other key optical components including E-O converters, optical fibres, and O-E converters are also involved in a typical OOFDM transmission system. In the OOFDM transmitter, since an IM is used for E-O up-conversion, the generated electrical OFDM signal must be real-valued to drive a DFB-laser. To generate a real-valued OFDM

signal, the truncated original complex parallel subcarriers in the positive frequency bins and corresponding complex conjugated subcarriers in the negative frequency bins are arranged as the IFFT input to satisfy Hermitian symmetry [18], which is expressed as:

$$\hat{X}_{k,n} = \begin{cases} 0, & k = 0 \\ X_{k,n}, & k = 1,2,\dots N_{sc}/2 - 1 \\ 0, & k = N_{sc}/2 \\ X^*_{N_{sc}-k,n}, & k = N_{sc}/2 + 1, \dots, N_{sc} - 1 \end{cases} \quad (2.39)$$

where $X_{k,n}$ is the encoded complex data expressed in Eq. (2.20) and $X^*_{k,n}$. denotes its conjugate. When $X_{k,n}$ in Eq. (2.27) is replaced with $\hat{X}_{k,n}$, the IFFT outputs have zero imaginary parts. However, in this regard, since half of the spectra do not carry any useful data, the IMDD OOFDM system comes at the expense of halving the spectral efficiency.

In the transmitter, if $i(t)$ is the electrical driving current of the OFDM signal then, the intensity modulated optical signal is defined as:

$$i(t) = I_{DC} + s(t) \quad (2.40)$$

where I_{DC} is the added DC bias to prevent signal distortion. I_{DC} must be sufficiently larger than the peak value of $s(t)$ so that the laser is always positively biased above the lasing threshold and operates in its linear region. As a result, a significant portion of the optical signal power will be contained in the transmitted optical carrier frequency which will limit signal extinction-ratio (ER) [80]. Assuming an ideal intensity modulation, the optical intensity modulator generates an optical power $p(t)=i(t)$. Then, the optical field, $E(t)$ in complex form can be expressed as

$$E(t) = A_I.\sqrt{p(t)} = A_I.\sqrt{I_{DC+s(t).}}e^{j(\omega_{LD}t+\Phi_{LD})} \quad (2.41)$$

where w_{LD} and Φ_{LD} are angular frequency and phase of the diode laser which serves as an optical source, and AI is a proportionality constant. After transmitting through SSMFs, in the receiver, the transmitted optical signal power undergoes direct detection (DD) by a square-law PIN photodetector. If the receive optical signal is $E_R(t)$, the detected photocurrent in the receiver is given by

$$I_R(t) = |E_R(t)|^2 = \left|\left\{\left(A_I.\sqrt{I_{DC+s(t)}}.\, e^{j(\omega_{LD}t+\Phi_{LD})} \otimes h(t)\right)\right\}\right|^2 + w(t) \quad (2.42)$$

where *h(t)* is the channel impulse response and *w(t)* represent the receiver noise. By using the Taylor series expansion on the square root term in Eq. (2.42) and ignoring the noise component for simplicity, the detected signal is expressed as:

$$I_R(t) = A_I^2 \left\{ \left[\left(\sqrt{I_{DC}} + \frac{s(t)}{2\sqrt{I_{DC}}} - \frac{s^2(t)}{8(I_{DC})^{3/2}} + \cdots \right) . e^{j\omega_{LD}t} \otimes h(t) \right] \ldots . \right.$$

$$\left. \times \left[\left(\sqrt{I_{DC}} + \frac{s(t)}{2\sqrt{I_{DC}}} - \frac{s^2(t)}{8(I_{DC})^{3/2}} + \cdots \right) . e^{j\omega_{LD}t} \otimes h(t) \right]^* \right\} \qquad (2.43)$$

$$= A_I^2 \left\{ I_{DC} + \frac{s(t) \otimes [h(t) + h^*(t)]}{2} - \frac{s^2(t) \otimes [h(t) + h^*(t)]}{8I_{DC}} + \cdots \right\}$$

The first term on the right-hand side of Eq. (2.43) denotes the DC bias component, whilst the second term contains the OFDM signal to be recovered. The remaining terms represent the unwanted subcarrier intermixing products due to the square-law detection procedure.

After the O-E down-conversion, the electrical signal is fed into the OFDM receiver, which adjusts the received RF signal gain and low-pass filters the OFDM signal before sampling with a single ADC. The transmitted OFDM signal, *s*(*t*), is then recovered using the receiver functions described in section 2.2.6.2.1.

2.2.7 Alternative Multicarrier Transmission Techniques

For the past two decades, among the many MCM techniques, OFDM dominates the current broadband wired and wireless communication systems. However, OFDM also has its drawbacks such as high spectral leakage, high PAPR, and stringent orthogonality requirements, as such, this makes OFDM less attractive for the next generation networks. For the reasons mentioned above, alternative multicarrier techniques are being investigated as candidates technologies for the physical layer of next-generation optical access and mobile access communication networks [81-83].

2.2.7.1 Discrete Multi-tone Modulation

Derived from the more general OFDM, DMT is a baseband version employed largely in the field of ADSL, VDSL, and powerline communication systems, proving the low-cost implementation of DMT for high-speed data transmission in dispersive channels such as MMF transceivers can be possible [81]. As a result of the large economies of scale and the industry's

extensive research, OFDM and DMT are seen as promising technologies for low-cost, reliable, and robust gigabit transmission over IMDD step-index plastics optical fibre (SI-POF) [81]. Both OFDM and DMT techniques are known to exhibit high spectral efficiency, they are also effective in combating ISI. In both methods, several narrowband subcarriers are superimposed in parallel subchannels implemented digitally by means of a DFT and they both offer the useful trick that a short CP on the transmit signal eliminate ISI by allowing perfect distortionless data recovery at the transmitter, even when transmitting over a dispersive channel. In OFDM, the same number of bits are allocated to each subchannel, while DMT because of the slowly varying nature of the channel allows spectral shaping by using an adaptive approach (bit-loading) to load the subchannels, to take advantage of the measured channel characteristics. The loading algorithm allocates more bits to subchannels with higher SNRs and fewer bits to subchannels with lower SNRs and disabled subchannels with SNRs below a certain threshold. Technically, multitone modulation was originally devised as a way to efficiently allocate power and/or bits in the subchannels, depending on both the channel gain and noise power spectral density in that subchannel. The DMT idea is similar in principle to sub-band coding where a signal to be quantized is first decomposed into sub-bands. The DMT system uses DFT as its modulation basis and can be regarded as a filter bank in trans-multiplexer configuration. Typically, the filter banks used for this purpose are DFT filter banks which can be implemented efficiently with the FFT.

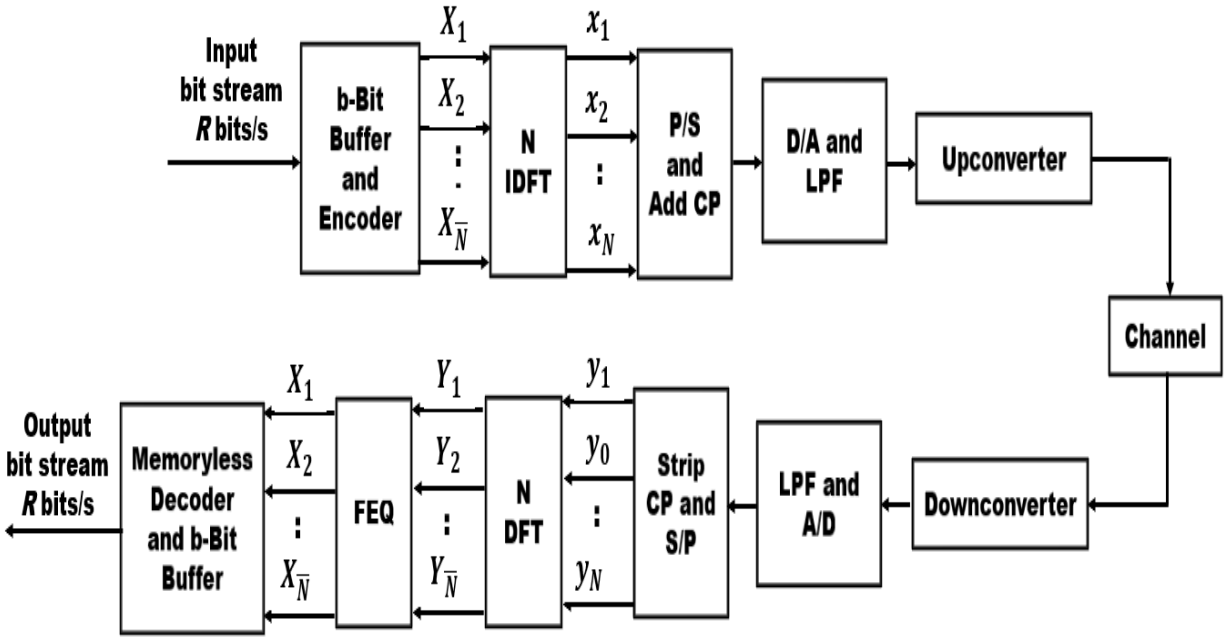

Fig. 2.31. Conventional DFT-based DMT system

A conventional DFT-based DMT transceiver block diagram is shown in Fig. 2.31. Each channel is partitioned into *N* parallel subchannels with an input bit stream of data rate *R* bits/sec buffered into blocks of $b = RT$ bits, where *T* is the DMT symbol period. A loading algorithm, such as waterfill or flat-energy [81] is used to assign bits, b_k, to subchannels, where $\sum_{k=1}^{N} b_k = b$ and *N* is the number of subchannels enabled. Subchannels with higher SNRs receive more bits whereas those with lower SNRs receive fewer bits, and those with SNR below a certain threshold are turned off. The bits in each subchannel, b_k, are mapped to corresponding QAM constellation points, X_k. For the $N - \vec{N}$ subchannels turned off, X_k is set to 0. The resulting output multicarrier DMT time-domain sequence consisting of $2N$ sample points, $\{x_m: m=1, 2,\ldots,N\}$, are obtained by taking the *N*-point IDFT of $X = [X_1, X_2,\ldots..,X_N]^T$ similar to Eq. (2.27).

The resilience of DMT in a dispersive channel is the result of parallel transmission and cyclic prefixes. As a result of the parallel transmission of the data, the symbol period is much longer than in the case of standard serial transmission. Because of this, the ISI affects only a small fraction of the symbol period. Through the use of a cyclic prefix, the ISI effect can easily be eliminated while orthogonality between subcarriers is maintained.

At the receiver, the cyclic prefix samples in each DMT block are discarded. Demodulation of the DMT sequence is then accomplished by using a $2N$-point FFT. With a perfect knowledge of the channel, the transmitted symbols in each subchannel can be recovered independently using a frequency domain equalizer (FEQ), followed by a simple memoryless decoder.

2.2.7.2 Filter-Bank Multicarrier

Filter bank multicarrier communication (FBMC) is another candidate for 5G networks [82]. The advantages of FBMC stem from the fact that, by design, the nonadjacent subcarriers in this modulation scheme are separated almost perfectly by a bank of well-designed filters. OFDM, on the other hand, initial designed placed a strong emphasis on a low-complexity implementation. Much of the OFDM low-complexity is due to the assumption that the subcarrier signals are a collection of perfectly timed orthogonal tones, which are generated at the transmitter using an IFFT block, and are separated at the receiver through an FFT block. Although OFDM is widely adopted in current mobile networks, in many future communication systems, it is not necessarily always the best solution, especially in multiple access and cognitive radio networks where FBMC may be found more appealing.

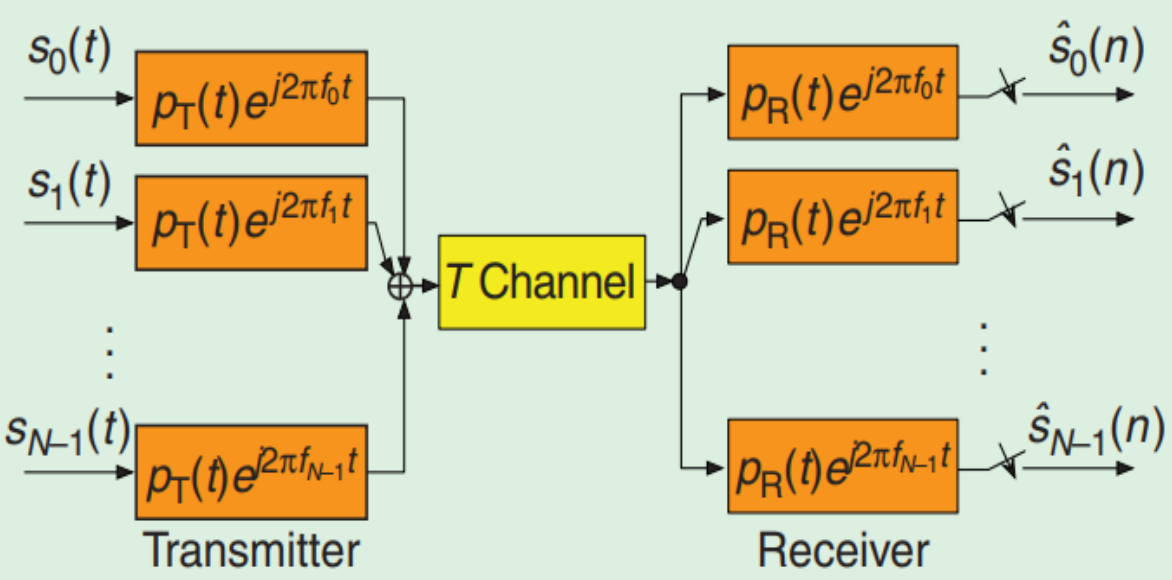

Fig. 2.31. Block diagram of an FBMC transceiver.

Fig. 2.31 depict a block diagram of an FBMC transceiver, which is also applicable to OFDM systems. In FBMC, a set of parallel data symbols $s_k[n]$ is transmitted through a bank of modulated filters, and the transmitted signal can be synthesized according to Eq. (2.44) [83].

$$x(t) = \sum_n \sum_{k \in M} s_k[n] p_T(t - nT) e^{j2\pi(t-nT)f_k} \tag{2.44}$$

where M denotes a set of active symbols. Eq. (2.44) may be viewed as a filtering operation applied to a sequence of impulses, modulated by the data symbols $s_k[n]$. The filter $p_{T,k}(t)$ is obtained by modulating the prototype filter $p_T(t)$. Assuming an ideal channel, the received signal $y(t)$ is the same as the transmit signal $x(t)$. In that case, the data symbols $s_k[n]$, for $k \in M$, and all values of n will be separable if Eq. (2.45) holds.

$$\langle p_{T,k}(t - mT), p_{R,l}(t - nT) \rangle = \int_{-\infty}^{\infty} p_{T,k}(t - mT) p_{R,l}^*(t - nT) dt = \delta_{kl}\delta_{mn} \tag{2.45}$$

To satisfy Eq. (2.45), in FBMC, the receiver uses a prototype filter $p_R(t)$ that is matched to the transmit prototype filter $p_T(t)$, i.e., $p_R(t) = p_T(-t)$, and $p_T(t)$ is designed to satisfy the generalised Nyquist constraints written in terms of ambiguity function, $A_p(nT, 0)$ equal unity for $n = l = 0$ and zero otherwise. Thus, $A_p(t, 0) = p_R(t) \times p_T(-t)$ implies that $p(t)$ is a square root Nyquist pulse [83].

The difference between OFDM and FBMC can be attributed to the choice of T and the prototype filters, $p_T(t)$ and $p_R(t)$ used in the transmitter and receiver respectively. In addition,

the selection of $p_T(t)$ and $p_R(t)$ varies depending on the adopted FBMC modulation technique. FBMC systems are not only limited to the transmission of real-valued (i.e., PAM) data symbols but also can be designed to transmit complex-valued (i.e., QAM) data symbols. In a conventional OFDM/QAM, $p_T(t)$ adopts a rectangular pulse shaping of unit magnitude and width T and is well-located in the time domain. The receiver prototype filter $p_R(t)$ also adopts a rectangular pulse shaping of unit magnitude, but its width is reduced to $T_{FFT} < T$, where $T_{FFT} = 1/B$, and B is the frequency spacing between subcarriers and each subcarrier produces a sinc spectrum in the frequency domain. However, the overlapped spectra among subcarriers have large out-of-band spectral/power leakages. Usually, to avoid ISI, successive blocks of data symbols, $\{s_k[n], k \in M\}$, for different choices of the time index n, are isolated through the use of CP, which constitutes a loss of bandwidth efficiency. Furthermore, OFDM/QAM is also sensitive to timing and sampling/carrier frequency offsets. FBMC addressed these drawbacks by using non-rectangular pulse shapes with better localization in both time and frequency domains. In FBMC systems that are designed for maximum bandwidth efficiency, $T=T_{FFT}=1/B$, however, the duration of $p_T(t)$ and $p_R(t)$ is greater than T. As a result, successive data symbols in FBMC overlap.

Although OFDM/QAM has been extensively studied for both short-reach IMDD and long-haul coherent-detection transmission scenarios due to its high spectral efficiency, robustness against fibre dispersions and simple channel equalization, FBMC has the potential of achieving a higher bandwidth efficiency than OFDM. In particular, FBMC/OQAM can provide higher spectral efficiency and lower out-of-band spectral/power leakages than conventional OFDM/QAM [82,83].

References

[1] L. N. Binh Optical fibre Communication systems theory and practice. Artech House, Boston, MA, CRC press, Taylor & Francis group, London, 2004.

[2] R. Ramaswami, K. N. Sivarajan G. H. Sasaki Optical networks: a practical perspective, 3rd ed. Morgan Kaufman, San Francisco, CA., 2002.

[3] G. P. Agrawal GP Fibre-optic communication systems, 3rd ed. Wiley, New York, 2002 G.

[4] C. Cox III, E. Ackerman, R. Helkey and G. E. Betts, "Techniques and performance of intensity-modulation direct-detection analogue optical links," IEEE Trans. Microwave Theory Tech., vol. 45, no. 8, pp. 1375-1383, 1997.

[5] N. H. Zhu, Q. Q. G. Hasen, H. G. Zhang, J. M. Wen and L. Xie, "Dynamic P-I and P-V Curves for Semiconductor Lasers and Modulators," in Journal of Lightwave Technology, vol. 26, no. 19, pp. 3369-3375, 2008.

[6] A. Chen and E. J. Murphy, Broadband Optical Modulators. Science, Technology, and Application, CRC Press, Taylor & Francis Group, 2012.

[7] X. Zheng, X. Jin, R. Giddings, and J. Wei, "Negative Power Penalties of Optical OFDM Signal Transmissions in Directly Modulated DFB Laser-Based IMDD Systems Incorporating Negative Dispersion Fibres," IEEE Photonics, vol. 2, no. 4, pp. 532–542, 2010.

[8] K. Sato, S. Kuwahara and Y. Miyamoto, "Chirp Characteristics of 40-Gb/s Directly Modulated Distributed-Feedback Laser Diodes," J. Light. Technol., vol. 23, no. 11, pp. 3790-3797, 2005.

[9] W. Shieh, I. Djordjevic, Orthogonal Frequency Division Multiplexing for Optical Communications, Academic Press; 1st ed. 2009.

[10] ITU manual "Optical Fibre, Cable and Systems" [Online]. Available: https://www.itu.int/dms_pub/itu-t/opb/hdb/T-HDB-OUT.10-2009-1-PDF-E.pdf

[11] E. B. Gary and C. C. John, “Fundamentals of Optical communication,” in Broadband Optical Modulators, CRC Press, pp. 93–126, 2011.

[12] X. Gong, L. Guo, Y. Dong, M. Deng, R. P. Giddings and J. M. Tang, "SPM-Improved Transmission Performance of Software-Reconfigurable IMDD PONs Based on Digital Orthogonal Filtering," in Journal of Lightwave Technology, vol. 35, no. 20, pp. 4488-4496, 2017. Bangor

[13] A. R. Chraplyvy, “Limitations on lightwave communications imposed by optical-fibre nonlinearities,”J. Lightwave Technol., vol. 8, pp.1548–1557, 1990.

[14] K.-D Chang, G.-C. Yang, and W. C. Kwong, “Determination of FWM products in unequal-spaced-channel WDM lightwave systems,” J. Lightwave Technol., vol. 18, no. 12, pp. 2113-2122, 2000

[15] J. K. Park and I. Yun, "Modeling of avalanche gain for high-speed InP/InGaAs avalanche photodiodes," 2008 IEEE International Conference on Electron Devices and Solid-State Circuits, pp. 1-4, 2008.

[16] J. C. Campbell, "Recent advances in avalanche photodiodes: Ultraviolet to infrared," IEEE Photonic Society 24th Annual Meeting, Arlington, VA, USA, pp. 202-203, 2011.

[17] J. M. Tang and K. A. Shore, “30Gb/s signal transmission over 40-km directly modulated DFB-laser-based single-mode-fibre links without optical amplification and dispersion compensation,” J. Lightw. Technol., vol. 24, no. 6, pp. 2318-2327, June. 2006. Bangor

[18] J. M. Tang, P. M. Lane and K. A. Shore, “High-speed transmission of adaptively modulated optical OFDM signals over multimode fibres using directly modulated DFBs,” J. Lightw. Technol., vol. 24, no. 1, pp. 429–441, Jan. 2006. Bangor

[19] P. Chanclou, A. Cui, F. Geilhardt, H. Nakamura and D. Nesset, "Network operator requirements for the next generation of optical access networks," in IEEE Network, vol. 26, no. 2, pp. 8-14, 2012.

[20] ITU-T, “40-Gigabit-capable passive optical network 2 (NG-PON2): Physical media dependent (PMD) layer specification” [Online]. Available: https://www.itu.int/rec/T-REC-G.989.2-201902-I/en

[21] K. Grobe and J. Elbers, "PON in adolescence: from TDMA to WDM-PON," in IEEE Comm. Mag., vol. 46, no. 1, pp. 26-34, 2008.

[22] D. Nesset, “Network Operator Perspective on WDM-PON Systems and Applications,” in Proc. Eur. Conf. Exhib. Opt. Commun., 2013.

[23] A. K. Garg and V. Janyani, "Identification of cost and energy efficient multiplexing techniques for LR-PON for different network scenario," 2015 Workshop on Recent Advances in Photonics (WRAP), 2015, pp. 1-4, 2015.

[24] J. Zhang and N. Ansari, "Design of WDM PON With Tunable Lasers: The Upstream Scenario," in Journal of Lightwave Technology, vol. 28, no. 2, pp. 228-236, 2009.

[25] D. Nesset, "PON roadmap [invited]," in J. of Opt. Commun. and Netw., vol. 9, no. 1, pp. A71-A76, 2017.

[26] J. Kani et al., "Next-generation PON-part I: Technology roadmap and general requirements," in IEEE Commun. Mag., vol. 47, no. 11, pp. 43-49, 2009.

[27] X. Q. Jin and J. M. Tang, "First experimental demonstrations of real-time optical OFDMA PONs with adaptive dynamic bandwidth allocation and colorless ONUs," 2012 Future Netw. & Mobile Summit, pp. 1-8, 2012.

[28] N. Cvijetic, "OFDM for next generation optical access networks," 2011 Opt. Fibre Commun. Conf. and Exp. and the Nat. Fibre Opt. Eng. Conf., pp. 1-30. 2011.

[29] R. P. Giddings and J. M. Tang, ‘‘Experimental demonstration and optimisation of a synchronous clock recovery technique for real-time end-to-end optical OFDM transmission at 11.25Gb/s over 25km SSMF,’’ Opt. Exp., vol. 19. No.3, pp. 2831-2845, 2011.

[30] M. Bolea, R. P. Giddings, M. Bouich, C. Aupetit-Berthelemot, and J. M. Tang, “Digital filter multiple access PONs with DSP-enabled software reconfigurability,” J. Opt. Commun. Netw., vol. 7, no. 4, pp. 215–222, 2015.

[31] M. Bolea, R. P. Giddings, and J. M. Tang, “Digital orthogonal filter- enabled optical OFDM channel multiplexing for software-reconfigurable elastic PONs,” J. Lightw. Technol., vol. 32, no. 6, pp. 1200–1206, 2014.

[32] A. Sankoh, W. Jin, Z.Q. Zhong, J. He, Y. Hong, R.P. Giddings, I. Pierce, M. O'Sullivan, J. Lee, T. Durrant, J.M. Tang, "Hybrid OFDM-Digital Filter Multiple Access PONs Utilizing Spectrally Overlapped Digital Orthogonal Filtering," in IEEE Photo. J., vol. 12, no. 5, pp. 1-11, 2020.

[33] Sankoh, A.; Jin, W.; Zhong, Z.; He, J.; Hong, Y.; Giddings, R.; Tang, J. DFT-Spread Spectrally Overlapped Hybrid OFDM–Digital Filter Multiple Access IMDD PONs. Sensors 5903, 2021.

[34] W. Jin, A. Sankoh, Y. X. Dong, Z. Q. Zhong, R. P. Giddings, M. O’Sullivan, J. Lee, T. Durrant and J. M. Tang., "Hybrid SSB OFDM-Digital filter multiple access PONs," J. Lightw. Technol., early access, Jan. 2020.

[35] M. Deng, A. Sankoh, R. Giddings, and J. Tang, "Experimental demonstrations of 30Gb/s/λ; digital orthogonal filtering-multiplexed multiple channel transmissions over IMDD PON systems utilizing 10G-class optical devices," Opt. Express 25, 24251-24261 (2017).

[36] M. Bongard, K. Grunert and S. Aleksic, "Techno-Economic Analysis of Deployment Options for Converged 5G Wireless-Optical Access Networks," 43rd Int. Con. on Inf., Comm. and Elec. Technol. (MIPRO), pp. 401-406, 2020.

[37] S. Gosselin et al., "Fixed and Mobile Convergence: Which role for optical networks?," Opt. Fibre Comm. Conf. and Exhib. (OFC), pp. 1-3, 2015.

[38] ITU-T Recommendation G.992.5, "Asymmetric Digital Subscriber Line (ADSL) transceivers - Extended bandwidth ADSL2 (ADSL2plus)," available online: https://www.itu.int/rec/T-REC-G.992.5-200305-S/en

[39] Y. Maeda, K. Okada, and D. Faulkner, "FSAN OAN-WG and future issues for broadband optical access networks," IEEE Comm. Mag., vol. 39, pp. 126-132, 2001.

[40] S. Ghoniemy, "Enhanced Time and Wavelength Division Multiplexed Passive Optical Network (TWDM-PON) for Triple-Play Broadband Service Delivery in FTTx Networks," 2018 Int. Conf. on Comp. and App. (ICCA), pp. 419-426, 2018.

[41] L. G. Kazovsky, W. Shaw, D. Gutierrez, N. Cheng and S. Wong, "Next-Generation Optical Access Networks," in J. of Lightw. Technol., vol. 25, no. 11, pp. 3428-3442, 2007.

[42] C. F. Lam, Passive Optical Networks: Principles and Practice, Acad. Press, Oct. 2007.

[43] M. Daneshmand, C. Wang and W. Wei, "Advances in passive optical networks [Guest Editorial]," in IEEE Comm. Mag., vol. 49, no. 2, pp. s12-s14, February 2011.

[44] J. L. Wei, X. L. Yang, R. P. Giddings, J. M. Tang and K. A. Shore, "SOA intensity modulator-enabled colourless transmission of adaptively modulated optical OFDM signals for WDM-PONs," 2009 14th OptoElec. and Commun. Conf., 2009, pp. 1-2, 2009.

[45] R. Shaddad, A. Mohammad, and S. Idrus, "Emerging optical broadband access networks from TDM PON to OFDM PON," PIERS Proceedings, pp. 102–106, 2015.

[46] X. Q. Jin and J. M. Tang, "Experimental investigations of wavelength spacing and colorlessness of RSOA-based ONUs in real-time optical OFDMA PONs," J. Lightw. Technol., vol. 30, no. 16, pp. 2603-2609, 2015.

[47] M. A. Habibi, M. Nasimi, B. Han and H. D. Schotten, "A Comprehensive Survey of RAN Architectures Toward 5G Mobile Communication System," in IEEE Access, vol. 7, pp. 70371-70421, 2019.

[48] "Common Public Radio Interface (CPRI); Interface Specification V7.0," [Online]. Available: http://www.cpri.info/downloads/CPRI_v_7_0_2015-10-09.pdf

[49] "Open Base Station Architecture Initiative (OBSAI)," [Online]. Available: https://www.optcore.net/wp-content/uploads/2017/04/OBSAI_System_Spec_V2.0.pdf

[50] Open Radio Equipment Interface (ORI) [Online]. Available: https://www.etsi.org/deliver/etsi_gs/ORI/001_099/00201/04.01.01_60/gs_ori00201v040101p.pdf

[51] China Mobile Research Institute, “CRAN: The Road Towards Green RAN,” White Paper 3.0, 2013. [Online]. Available: http://labs.chinamobile.com/cran/

[52] C. -L. I, J. Huang, R. Duan, C. Cui, J. Jiang and L. Li, "Recent Progress on CRAN Centralization and Cloudification," in IEEE Access, vol. 2, pp. 1030-1039, 2014.

[53] Segel, J., & Weldon, M. “Light radio portfolio-technical overview. Technology White Paper 1, Alcatel-Lucent, 2011. [Online]. Available: https://dokumen.tips/documents/light-radio-alcatel-lucent-bell-labs.html

[54] “Radio access architecture and interfaces,” 3GPP, Sophia Antipolis Cedex, France, 3GPP TR38.801, V2.0.0, R14, 2017. [Online]. Available: https://www.etsi.org/deliver/etsi_ts/136400_136499/136440/16.00.00_60/ts_136440v160000p.pdf

[55] C. -L. I, H. Li, J. Korhonen, J. Huang and L. Han, "RAN Revolution With NGFI (xhaul) for 5G," in Journal of Lightwave Technology, vol. 36, no. 2, pp. 541-550, 2018.

[56] eCPRI Specification V2.0. Interface Specification, Common Public Radio Interface, 2019 [Online]. Available: http://www.cpri.info/downloads/eCPRI_v_2.0_2019_05_10c.pdf

[57] J. S. Wey and J. Zhang, "Passive Optical Networks for 5G Transport: Technology and Standards," in J. of Lightw. Technol., vol. 37, no. 12, pp. 2830-2837, 2019.

[58] Hatta, S., Tanaka, N., & Sakamoto, T. Implementation of ultra-low latency dynamic bandwidth allocation method for TDM-PON. IEICE Commun. Exp., 5(11), 418–423, 2016.

[59] D. Hisano and Y. Nakayama, "Dynamic Bandwidth Allocation and Forwarding Order Control Techniques in TDM-PON for Accommodating Fronthaul Traffic," 2019 IEEE Photo. Conf. (IPC), pp. 1-2, 2019.

[60] E. Harstead, D. van Veen, V. Houtsma and P. Dom, "Technology Roadmap for Time-Division Multiplexed Passive Optical Networks (TDM PONs)," in J. of Lightw. Technol., vol. 37, no. 2, pp. 657-664, 2019.

[61] J. Zhang et al., "Symmetrical 50-Gb/s/λ PAM-4 TDM-PON in O-band with DSP and Semiconductor Optical Amplifier Supporting PR-30 Link Loss Budget," Opt. Fibre Commun. Conf. and Exp. (OFC), pp. 1-3, 2018.

[62] M. Tao, L. Zhou, H. Zeng, S. Li and X. Liu, "50-Gb/s/λ TDM-PON based on 10G DML and 10G APD supporting PR10 link loss budget after 20-km downstream transmission in the O-band," Opt. Fibre Commun. Conf. and Exhib. (OFC), pp. 1-3, 2017.

[63] ITU-T Recommendation G.694.2, “Spectral grids for WDM applications: CWDM wavelength grid” [Online]. Available: https://www.itu.int/rec/T-REC-G.694.2-200312-I/en

[64] ITU-T Recommendation G.694.1, “Spectral grids for WDM applications: DWDM frequency grid” [Online]. Available: https://www.itu.int/rec/T-REC-G.694.1-202010-I/en

[65] N. Shibata et al., "256-QAM 8 wireless signal transmission with DSP-assisted analogue RoF for mobile front-haul in LTE-B," OptoElect. and Commun. Conf. and Aust. Conf. on Opt. Fibre Technol., pp. 129-131, 2014.

[66] N. Badraoui and T. Berceli, "Improvements in Radio over Fibre Links Using Polarization Multiplexing," 21st Int. Conf. on Transp. Opt. Netw. (ICTON), 2019, pp. 1-5, 2019.

[67] M. U. Hadi et al., "Experimental evaluation of digital predistortion for VCSEL-SSMF-based Radio-over-Fibre link," Int. Top. Meet. on Micr. Photo. (MWP), 2018, pp. 1-4, 2018

[68] S. Rommel, D. Perez-Galacho, J. M. Fabrega, R. Muñoz, S. Sales and I. Tafur Monroy, "High-Capacity 5G Fronthaul Networks Based on Optical Space Division Multiplexing," in IEEE Trans. on Broad., vol. 65, no. 2, pp. 434-443, 2019.

[69] J. I. Kani, S. Kuwano, and J. Terada, “Options for future mobile backhaul and fronthaul,” Opt. Fibre Technol., vol. 26, pp. 42–49, 2015.

[70] A. Mathew, T. Das, P. Gokhale and A. Gumaste, "Multi-layer high-speed network design in mobile backhaul using robust optimization," in J. of Opt. Commun. and Netw., vol. 7, no. 4, pp. 352-367, 2015.

[71] M. Fukutoku, "Next generation ROADM technology and applications," 2015 Optical Fibre Communications Conference and Exhibition (OFC), 2015, pp. 1-3, 2015.

[72] O. Tipmongkolsilp, S. Zaghloul and A. Jukan, "The Evolution of Cellular Backhaul Technologies: Current Issues and Future Trends," in IEEE Commun. Surveys & Tut., vol. 13, no. 1, pp. 97-113, 2011.

[73] A. T. Pham, P. V. Trinh, V. V. Mai, N. T. Dang and Cong-Thang Truong, "Hybrid free-space optics/millimeter-wave architecture for 5G cellular backhaul networks," 2015 Opto-Electronics and Communications Conference (OECC), 2015, pp. 1-3, 2015.7340269.

[74] A. Douik, H. Dahrouj, T. Y. Al-Naffouri and M. Alouini, "Resilient backhaul network design using hybrid radio/free-space optical technology," 2016 IEEE Int. Conf. on Commun. (ICC), 2016, pp. 1-7, 2016.

[75] M. M. Ahamed and S. Faruque, "Design a 5G Backhaul Network Based on Free Space Optics and Analyze the Link Performances," 2021 4th Int. Conf. on Inf. and Comp. Technol. (ICICT), 2021, pp. 187-193, 2021.

[76] R. Prasad, ‘‘OFDM for wireless communications systems,’’Artech House, Aug. 2004.

[77] S. Sun, Y. Ju and Y. Yamao, "Overlay cognitive radio OFDM system for 4G cellular networks," in IEEE Wire. Commun., vol. 20, no. 2, pp. 68-73, 2013.

[78] A. Saljoghei et al., "Comparison of OFDMA and GFDMA for next-generation pons," in IEEE-OSA J. of Opt. Commun. and Netw., vol. 9, no. 12, pp. 1064-1073, Dec. 2017.

[79] C. Balint and G. Budura, "OFDM-Based Multi-Carrier Waveforms Performances in 5G," 2018 Int. Symposium on Elect. and Telecom. (ISETC), 2018, pp. 1-4, 2018.

[80] J. L. Wei, C. Sánchez, R. P. Giddings, E. Hugues-Salas, and J. M. Tang, “Significant improvements in optical power budgets of real-time optical OFDM PON systems,” Opt. Express., vol.18, no.20, pp. 20732-20745, 2010.

[81] S. C. J. Lee et al., "Discrete Multitone Modulation for Maximizing Transmission Rate in Step-Index Plastic Optical Fibers," in Journal of Lightwave Technology, vol. 27, no. 11, pp. 1503-1513, 2009.

[82] G. Srikanth, S. L. Nisha and S. G. S. Prasad, "Performance of FBMC for 5G Communication," 2018 3rd IEEE Int. Conf. on Recent Trends in Elec., Inf. & Commun. Technol. (RTEICT), pp. 828-832, 2018.

[83] B. Farhang-Boroujeny, "OFDM Versus Filter Bank Multicarrier," in IEEE Signal Proc. Mag., vol. 28, no. 3, pp. 92-112, 2011.

3. Hybrid OFDM-DFMA IMDD PONs Utilizing Spectrally Overlapped Digital Orthogonal Filtering

Contents

3.1 Introduction

The evolution and accelerating increase in the number of smart mobile devices, stoked by new content-rich services and highly dynamic on-demand bandwidth-hungry video-centric mobile services [1,2], have made CRANs a key enabler for 5G and beyond networks [3]. A 5G CRAN architecture mainly includes three types of network connections, namely, MFH, MMH and MBH. The MFH connects a RRU and a DU, while the MMH connects the DU and a CU, and the MBH connects the CU and a 5GC. Practical, cost effective high-speed 5G CRANs can be based on IMDD PONs [4,5]. However, some modifications to existing IMDD PONs are required to deliver high data rate, low latency, and ubiquitous access [6-8], and address surging dynamic mobile traffic. Furthermore, it is desirable to equip the PONs with SDN and network function virtualization (NFV) across all the network layers for more efficient network operation and resource utilization. Finally, to reduce network cost, the PONs should enable convergence of existing optical metropolitan, optical access, and mobile networks.

A DFMA PON based on IMDD has been proposed to address these requirements [9]. It uses SDN-controllable DOFs in each ONU and OLT to dynamically multiplex/demultiplex many spectrally overlapped sub-bands of arbitrary bandwidth granularity. This does not require extra analogue hardware compared to conventional PON transceivers. Extensive numerical investigations and experimental demonstrations of the IMDD DFMA PONs have been reported in [9-13]. However, as the number of required MFs embedded in the OLT is proportional to the overall channel count, for a large number of ONUs, the OLT DSP complexity grows uncomfortably large for cost-sensitive mobile applications. A comparatively low DSP complexity IMDD PON with inherent transparency to 4G mobile networks, termed hybrid OFDM-DFMA PON, has been proposed and investigated [14]. For upstream transmission, this PON applies an ONU DSP procedure similar to the DFMA-PON, i.e., each ONU uses its embedded digital I-phase shaping filter to locate its OFDM signal at an assigned RF spectral region (referred to as sub-wavelength throughout the chapter). Whilst in the OLT, a single FFT operation and relevant DSP processes are pipelined to simultaneously demultiplex and demodulate the received OFDM signals from different ONUs without using any digital MFs. Compared to the DFMA PON, the hybrid OFDM-DFMA PON reduces the OLT DSP complexity by a factor of >100 when ONU counts are ≥ 32. This can also lower transceiver cost and power consumption. More importantly, the hybrid OFDM-DFMA PON provides upstream performance tolerance to transceiver sample timing offset, channel interferences,

digital filter characteristic variations and transmission system nonlinearity impairments, due to the MF-free receiver DSP design in the OLT [14]. Consequently, >10dB upstream ONU error vector magnitude (EVM) performance improvements provided sufficient received optical powers, and 16dB increases in differential ONU launch power dynamic range are achievable [14]. However, in contrast to the DFMA PON which supports simultaneously two spectrally overlapped sub-bands at each sub-wavelength, the hybrid OFDM-DFMA PON can only transmit a single upstream DSB OFDM signal in any sub-wavelength spectral region. As such, compared to the DFMA PON, the hybrid OFDM-DFMA PON has half of the aggregate signal transmission capacity and overall spectral efficiency.

In this chapter, we show that spectral efficiency can be reclaimed with a new variant of the hybrid OFDM-DFMA PON, in which the DSP algorithms embedded in both the OLT and ONUs are slightly modified to allow two spectrally overlapped sub-bands to occupy each individual sub-wavelength for independent upstream transmission of ONU information. In particular, for the proposed PON, each ONU utilizes a DSP procedure identical to the DFMA PON to produce one or two orthogonal OFDM sub-band(s) occupying the same or different sub-wavelength(s) [9]. In the OLT, similar to the previously reported hybrid OFDM-DFMA PON, a single FFT operation is applied and an operation is conducted to identify the subcarriers in the lower and upper sidebands (LSB and USB, respectively) of each sub-band. After pilot-aided channel estimation and equalization for the LSB and USB, the two received spectrally overlapped OFDM sub-bands of a single sub-wavelength are finally demultiplexed by summing and subtracting the LSB and USB subcarriers of the sub-wavelength. Since the OLT in the proposed PON is still free from digital MFs and uses a pipelined approach in demodulating all received spectrally overlapped OFDM sub-bands, it follows that, compared to earlier reported hybrid OFDM-DFMA PONs, this PON has higher (nearly double) signal transmission capacity and spectral efficiency. It also retains the properties of earlier hybrid OFDM-DFMA PONs, namely, lower OLT DSP complexity, inherent transparency to 4G networks and performance robustness to physical-layer network design factors such as digital filter variations, channel crosstalk and transmission impairments as well as transceiver sample timing offset. In this chapter, we present a model of the proposed PON and numerically explore its upstream transmission performances for various application scenarios. Our results show that compared with previously reported PON, the proposed PON supports twice the number of passively multiplexed ONUs, and a >1.7-fold aggregate upstream signal transmission capacity increase

is obtained with <1.5dB upstream power budget degradations. Alternately, when the proposed PON supports the same number of ONUs each occupying two digitally multiplexed orthogonal sub-bands, a >2.2-fold aggregate upstream signal transmission capacity increase and a >0.7dB upstream power budget improvement can be achieved. For a transmission distance range as large as large as 50km, these performance improvements vary by <18% and are robust to finite digital filter tap-induced channel interferences. The aforementioned performances of the proposed PON are similar to those of a recently published PON termed hybrid SSB OFDM-DFMA PON [15], whose ONU DSP complexity is, however, significantly higher than the proposed PON.

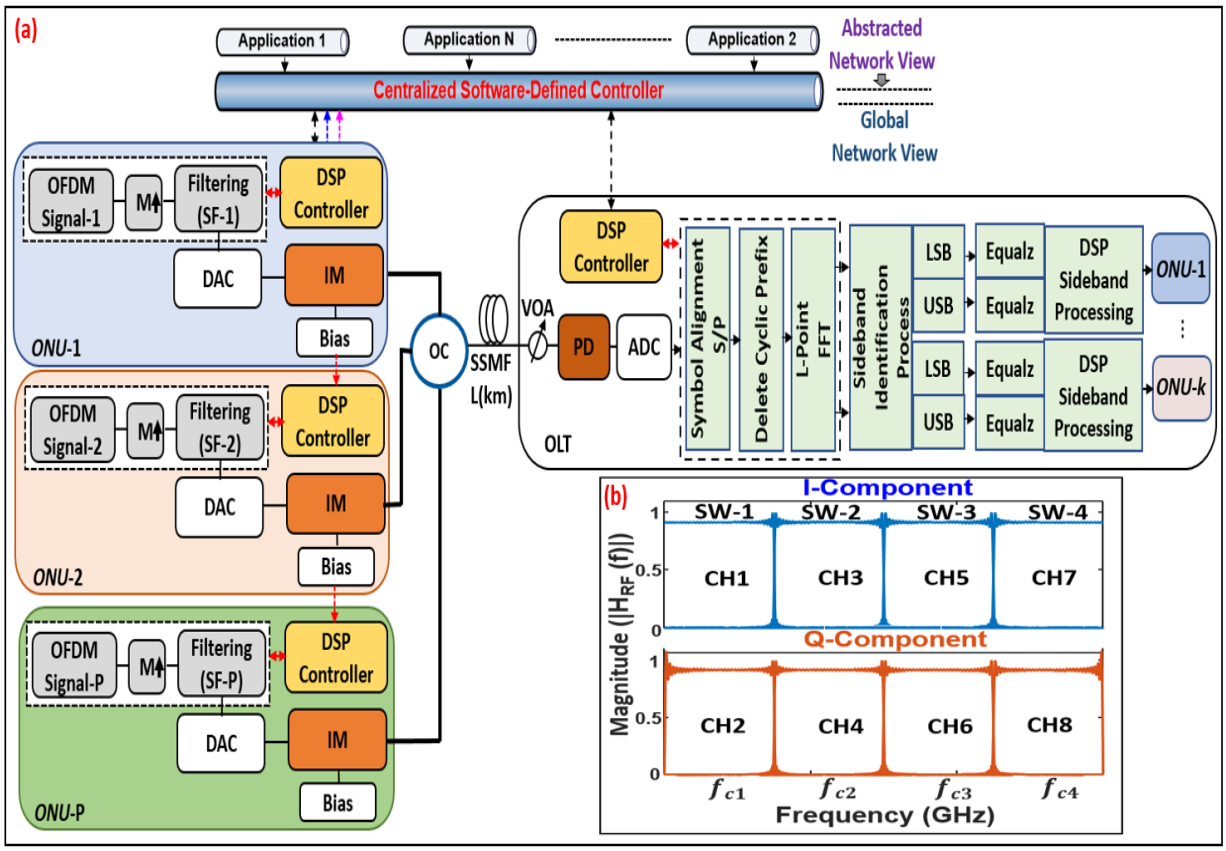

Fig. 3.1. (a) Schematic diagram of orthogonal digital filtering-based hybrid OFDM-DFMA PON based on IMDD (b) frequency responses of the orthogonal digital shaping filters implemented in ONUs. M ↑: digital up-sampling factor, SF: shaping filter, DAC/ADC: digital-to-analogue/analogue-to-digital converter. IM: intensity modulator. OC: optical coupler, PD: photo diode. S/P: serial-to-parallel conversion, LSB: lower sideband, USB: upper sideband, Equalz: equalization, ONU: optical network unit, DSP: digital signal processing, OLT: optical line terminal, SW: sub-wavelength, CH: channel.

3.2 Operating Principle and Theoretical Model

The schematic diagram of the proposed new hybrid OFDM-DFMA PON based on IMDD is shown in Fig. 3.1(a) for upstream transmission only. As shown in Fig. 3.1(a), passively coupled upstream optical signals from *P* ONUs labelled as ONU1, ONU2…, ONU*P* are generated using pairs of different digital orthogonal shaping filters. Signals are processed in each ONU using a DSP procedure similar to that of [14]. This includes DSP algorithms for real-valued OFDM signal generation, *M*× digital domain up-sampling and digital filtering.

To simplify the theoretical analyses, ideal digital filter responses are assumed in this section only. The I-phase sub-band occupies the *i*-th sub-wavelength, as illustrated in Fig. 3.1(b), and can be expressed as:

$$S_i^I(t) = \sum_{k=-N/2}^{N/2-1} \left[a_{k,i} e^{j2\pi k\left(\frac{f_{DAC/ADC}}{MN}\right)t} \right] e^{j2\pi f_{ci} t} + \cdots$$

$$\sum_{k=-N/2}^{N/2-1} \left[a_{k,i}^{*} e^{-j2\pi k\left(\frac{f_{DAC/ADC}}{MN}\right)t} \right] e^{-j2\pi f_{ci} t} \qquad (3.1)$$

where $a_{k,i}$ is the encoded data conveyed on the *k*-th subcarrier of the *i*-th sub-wavelength. $f_{ci}=((2\times i-1)\times f_{DAC/ADC}/2M)$ is the sub-wavelength centre frequency, where $f_{DAC/ADC}$ is the sampling rates of the DAC/ADC. *N* is the IFFT size used in generating the OFDM signal. * is the conjugation operator. In Eq. (3.1), the first term represents the total number of *N* OFDM subcarriers located at the positive frequency bin in the *i*-th sub-wavelength spectral region, while the second term represents their counterpart in the negative frequency bin. Among these *N* OFDM subcarriers in the positive frequency bin, there are *N*/2 LSB subcarriers, which are the conjugation of the remaining *N*/2 USB subcarriers, i.e. $a_{-m,i}=a^{*}_{m,i}$, m=1,2,…(*N*/2-1) and $a_0=a_{-N/2}=0$ [14].

In similarity with Eq. (3.1), when an ONU employs the Q-phase digital shaping filter to locate its OFDM signal which occupies the *i*-th sub-wavelength as illustrated in Fig. 3.1(b), the digitally filtered OFDM signal can be written as:

$$S_i^Q(t) = \sum_{k=-N/2}^{N/2-1} \left(\left[b_{k,i} e^{j2\pi k\left(\frac{f_{DAC/ADC}}{MN}\right)t} \right] e^{j2\pi f_{ci} t} \right) \times (-j) + \cdots$$

$$\sum_{k=-N/2}^{N/2-1}\left(\left[b_{k,i}^{*}e^{-j2\pi k\left(\frac{f_{DAC/ADC}}{MN}\right)t}\right]e^{-j2\pi f_{ci}t}\right)\times(j) \qquad (3.2)$$

where $b_{k,i}$ is the encoded data conveyed on the k-th subcarrier of the i-th sub-wavelength.

Comparing Eq. (3.1) and Eq. (3.2), it can be seen that after digital filtering processing, the Q-phase OFDM subcarriers in the positive frequency bin have a -π/2 phase rotation when compared to the corresponding I-phase OFDM subcarriers. The phase rotation is caused by the Q-phase digital shaping filters.

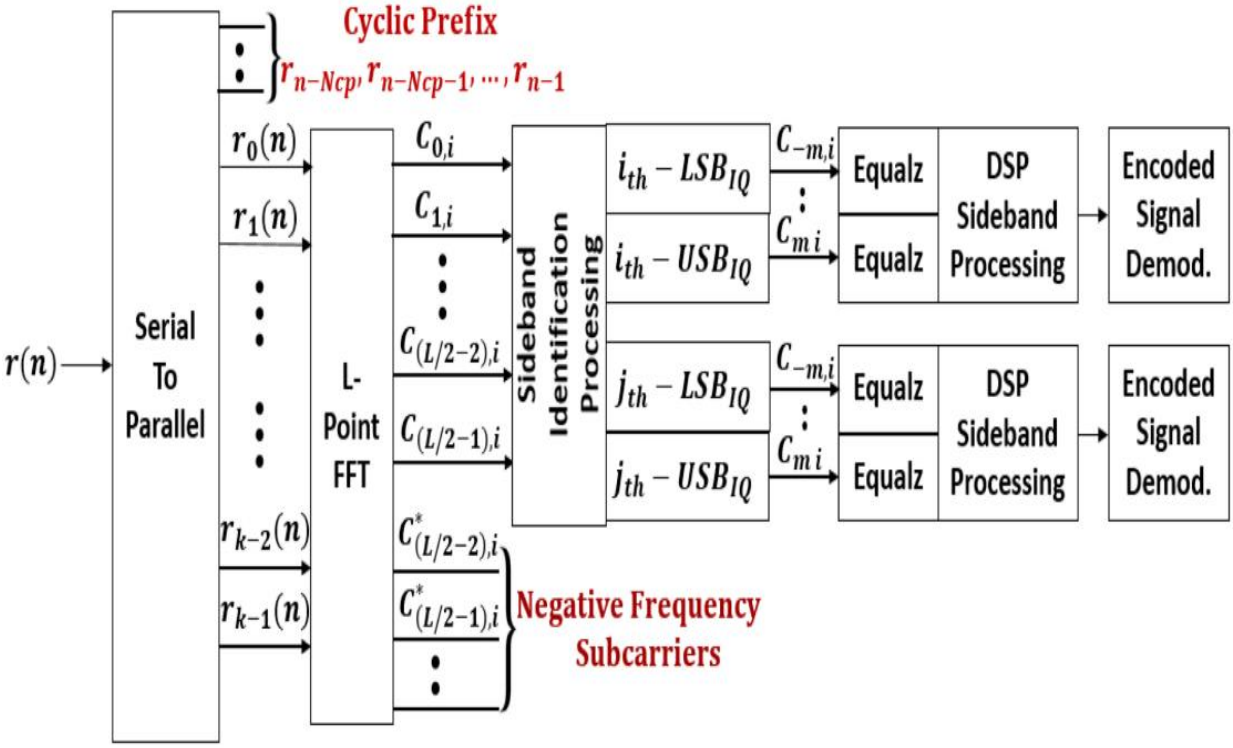

Fig. 3.2. Block diagram of OLT DSP procedure of the proposed PON.

After the DAC, optical intensity modulation converts the electrical signal to an optical signal. For the i-th ONU, the produced optical signal can be given by:

$$S_{opt-i}(t)=\left[\beta_i(t)e^{j\alpha_i(t)}.\sqrt{1+\xi_i*S_i^w(t)}\right]e^{j2\pi f_{opt}t}, w=I\ or\ Q \qquad (3.3)$$

Where f_{opt} is the centre frequency of the optical signal. ζ_i is the intensity modulation index. $B_i(t)$ and $\alpha_i(t)$ stand for the optical intensity modulation-induced optical amplitude and phase of the optical signal $S_{opt\text{-}i}(t)$. When w=I, the optical signal contains an I-phase OFDM sub-band, while for w=Q, it consists of a Q-phase sub-band. Without losing generality, here both the I-phase sub-band and the Q-phase sub-band are assumed to be at a single sub-wavelength.

For upstream transmission, in the remote node, a total number of *P* optical signals from various ONUs are passively combined to produce a signal waveform that can be written as:

$$S_{opt}(t) = \sum_{i=1}^{P}\left[\beta_i(t)e^{j\alpha_i(t)}.\sqrt{1+\xi_i * S_i^W(t)}\right]e^{j2\pi f_{opt}t} \tag{3.4}$$

After upstream transmission, in the OLT, by excluding noise and optical transmission effects and following O-E conversion and an ADC, the received signal S_{IQ}, comprise of multiple pairs of orthogonal sub-bands in different sub-wavelengths. Assuming that the overall sub-wavelength number is *U* and each subwavelength conveys two independent orthogonal OFDM sub-bands, we have *2U=P*, and S_{IQ} can be expressed as:

$$S_{IQ} = \sum_{i=1}^{U}\left\{S_i^I(t) + S_i^Q(t)\right\}$$

$$= \sum_{i=1}^{U}\left\{\left(\sum_{k=-N/2}^{N/2-1} c_{k,i}e^{j2\pi k\left(\frac{f_{DAC/ADC}}{MN}\right)t}\right)e^{j2\pi f_{ci}t} + \cdots\right.$$

$$\left.\left(\sum_{k=-N/2}^{N/2-1} c_{k,i}^{*}e^{-j2\pi k\left(\frac{f_{DAC/ADC}}{MN}\right)t}\right)e^{-j2\pi f_{ci}t}\right\} \tag{3.5}$$

where $c_{k,i}$ is the received data from the *k*-th subcarrier in the *i*-th sub-wavelength. In Eq. (3.5), the first term is all the subcarriers in the positive frequency bin, while the second is their counterparts in the negative frequency bin. As seen in Fig. 3.2, in the OLT, after serial-to-parallel (S/P) conversion and CP removal, an *L*-point FFT operation is applied with *L* satisfying *L=2UN*. After that, the *L*/2 subcarriers in the positive frequency bin are classified into *U* groups each consisting of *N* subcarriers. Here the *N* subcarriers in the *i*-th group occupy the *i*-th sub-wavelength. The group's *N*/2 low frequency subcarriers occupy the LSB of the sub-band, and the remaining *N*/2 high frequency subcarriers occupy the USB of the same sub-band. The received subcarrier matrix of the *i*-th sub-wavelength can then be described as:

$$C_i = \left[\overbrace{c_{-\frac{N}{2},i}, c_{-\frac{N}{2}+1,i}, \ldots\ldots\ldots, c_{-1,i}}^{LSB}, \underbrace{c_{0,i}, c_{1,i}, \ldots\ldots\ldots c_{-1+\frac{N}{2},i}}_{USB}\right] \tag{3.6}$$

In addition, it should also be noted that the subcarrier matrix C_i, is the sum of the received I-phase sub-band subcarriers and Q-phase sub-band subcarriers. Under an assumption of a linear transmission system and considering Eq. (3.1) and Eq. (3.2), Eq. (3.6) can be rewritten as:

$$C_i = \left[\overbrace{\left(a_{-\frac{N}{2},i} - jb_{-\frac{N}{2},i}\right), \ldots, \left(a_{-1,i} - jb_{-1,i}\right)}^{LSB}, \underbrace{\left(a_{0,i} - jb_{0,i}\right), \ldots\ldots, \left(a_{-1+\frac{N}{2},i} - jb_{-1+\frac{N}{2},i}\right)}_{USB}\right] \tag{3.7}$$

Because of $a_{-m,i}=a^*_{m,i}$ and $b_{-m,i}=b^*_{m,i}$, m=1,2,…(N/2-1), we can have;

$$c_{-m,i} = a_{-m,i} - jb_{-m,i} = a^*_{m,i} - jb^*_{m,i} \tag{3.8}$$

$$c_{m,i} = a_{m,i} - jb_{m,i} \tag{3.9}$$

Here $c_{-m,i}$ and $c_{m,i}$ represent the subcarriers in the LSB and USB of the orthogonal sub-bands occupying the i-th sub-wavelength. To demultiplex the spectrally overlapped data $a_{m,i}$ and $b_{m,i}$, Eq. (3.8) and Eq. (3.9) can be rewritten as:

$$a_{m,i} = \frac{1}{2}\left[c^*_{-m,i} + c_{m,i}\right],$$

$$b_{m,i} = \frac{1}{j2}\left[c^*_{-m,i} - c_{m,i}\right] \tag{3.10}$$

Based on Eq. (3.10), it can be seen that in the OLT, orthogonal sub-bands for each sub-wavelength can be demultiplexed. A conjugation operation is applied to the received LSB subcarriers, then sum and subtraction operations are carried out between these subcarriers in the LSB and USB of the same sub-wavelength. In practice, the received LSB and USB subcarriers of the same sub-wavelength may suffer different signal distortions due to transmission system nonlinearities. To minimize this distortion, the LSB and USB subcarriers in each sub-wavelength undergo independent pilot-aided channel estimation and equalization [16] prior to summation and subtraction. For the LSB subcarrier equalization, the received LSB pilot subcarriers are the sum of the I-phase sub-band pilot subcarriers and (+j)-multiplied Q-phase sub-band pilot-subcarriers. On the other hand, for the USB subcarrier equalization, the received USB pilot subcarriers are the sum of the I-phase sub-band pilot subcarriers and (-j)-multiplied conjugate Q-phase sub-band pilot-subcarriers.

3.3 Numerical Simulation Conditions

To verify the model developed in section 3.2 for use in practical nonlinear IMDD PON scenarios, in this section we calculate its upstream transmission performance over 40km SSMF.

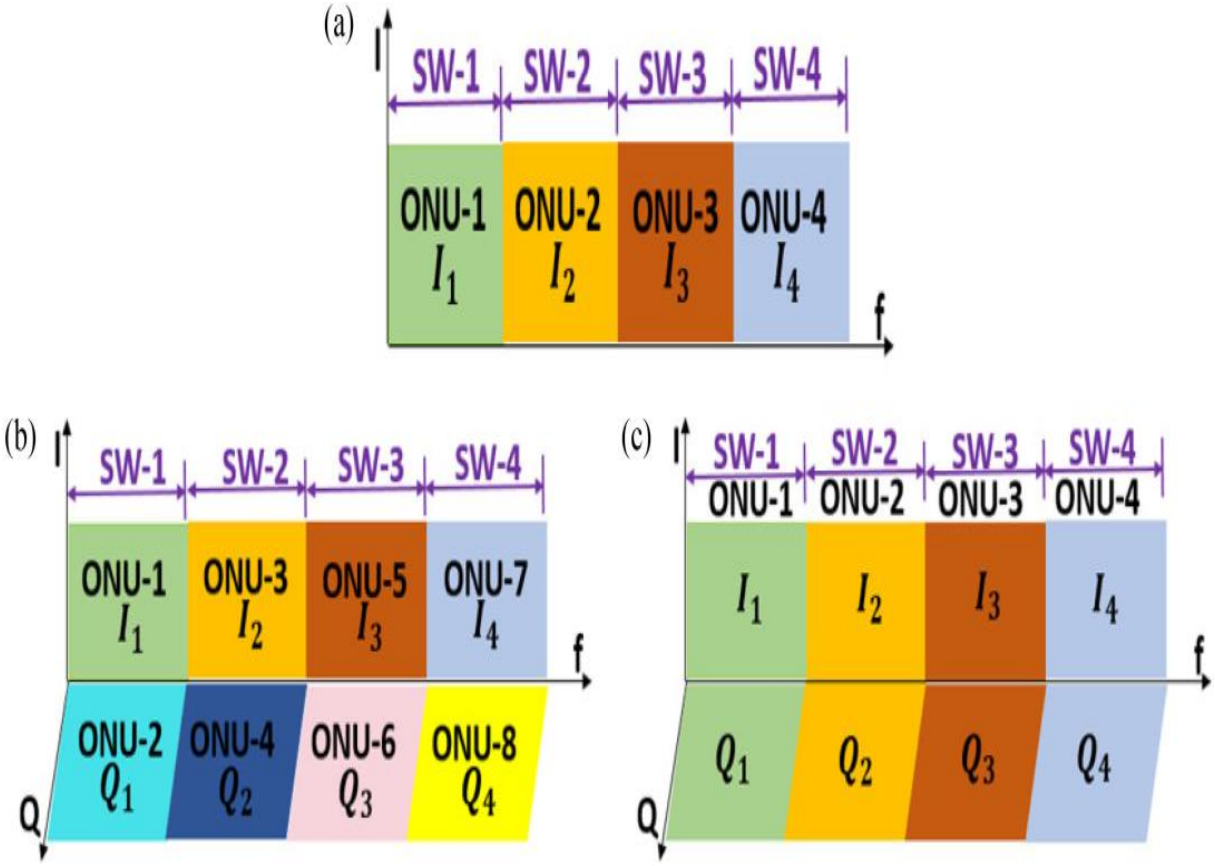

Fig. 3.3. Spectral locations of the digitally filtered signals in different sub-wavelength spectral region. (a) Hybrid Case-I (b) Hybrid Case-IIA and (c) Hybrid Case-IIB. SW: sub-wavelength, ONU: optical network unit, I: in-phase, Q: quadrature-phase.

Optical fibre transmissions are simulated using VPItransmissionMaker. Upstream performance comparisons are also made between the proposed PON and the previously reported PON [14] (used as a reference). Each PON has four identical sub-wavelength regions, as illustrated in Fig. 3.3. The PON of [14], labelled Hybrid Case-I, contains four 4 ONUs each occupying an I-phase OFDM sub-band in a single sub- wavelength. The proposed PON occupies the same bandwidth and has two cases: Hybrid Case-II(A) and Hybrid Case-II(B). Hybrid Case-II(A) contains eight ONUs each occupying a single sub-band and sharing a sub-wavelength with another ONU. Hybrid Case-II(B) involves four ONUs, each of which produces an optical signal comprising two orthogonal sub-bands that share a single sub-wavelength. MATLAB is used to perform signal generations and digital filtering.

Fig. 3.1(a) illustrates the simulation setup for evaluating upstream transmission performances of the two PONs. For the three cases described above, the parameters listed in Table 3.I are used to generate real-valued OFDM signals and required digital filters. In Hybrid Case-I, four

orthogonal digital filter pairs are produced and only the I-phase digital filters are used, while for Hybrid Case-II(A) and Hybrid Case-II(B), both the I-phase and Q-phase digital filters are employed. The spectral locations of the digital filtered OFDM sub-bands for all three cases are shown in Fig. 3.3. The approach reported in [15,17] are used to determine optimum clipping ratios for the three cases as listed in Table 3.1. For the proposed PON, the impacts of quantization bits and signal clipping on the BER performance are very similar to those reported in [15]. For fair transmission performance comparisons with the results presented in [14], in this chapter, DAC/ADC quantization bits of 8 are chosen, which can be further reduced to approximately 5 without considerably degrading the optical back-to-back transmission performance [15]. From the parameters in Table 3.1, an identical upstream net bitrate of 6.25Gb/s can be calculated for each sub-band. As Hybrid Case-II(A) and Hybrid Case-II(B) support eight sub-bands, an aggregate upstream net signal bitrate of 50Gb/s is thus achievable, while for Hybrid Case-I, its supported four sub-bands result in an aggregate upstream net signal bitrate of 25Gb/s. To accommodate eight ONUs in the entire spectral region for the proposed PON, the minimum oversampling factor M is taken to be 8 [10]. In each ONU, an ideal IM is used to convert electrical to optical signal at a fixed optical launch power of 0dBm.

Table 3.1 Transceiver Parameters

Parameter	Value	Parameter	Value
DAC/ADC Sample Rate	30GS/s	DAC/ADC effective number of bits	8-bits
OFDM IFFT/FFT Size	32/256	Clipping Ratio (Hybrid Case-I / Hybrid Case-IIA / Hybrid Case-IIB)	11dB / 10dB / 9dB
Number of Data Carrying Subcarriers	15	Digital Filter Length	64
Modulation Format	16-QAM	Excess of the Bandwidth	0
Number of Transmitted Symbols	6000	PIN Detector Quantum Efficiency	0.8 A/W
Training Symbols	50	PIN Detector Sensitivity	-19 dBm
Cyclic Prefix	12.5%	PIN Detector Bandwidth	Ideal
Channel Bitrate	6.25Gb/s	Fibre Dispersion Slope	0.08 $ps/nm^2/km$
Optical Launch Power	0 dBm	Fibre Loss	0.2 dB/km
Up-sampling Factor(M)	8	Fibre Kerr Coefficient	$2.6x10^{-20}$ m^2/W
FEC overhead	~7%	Transmission distance	40km

*Corresponding to 10 Gb/s non-return-to-zero data at a BER of 1.0×10^{-9}

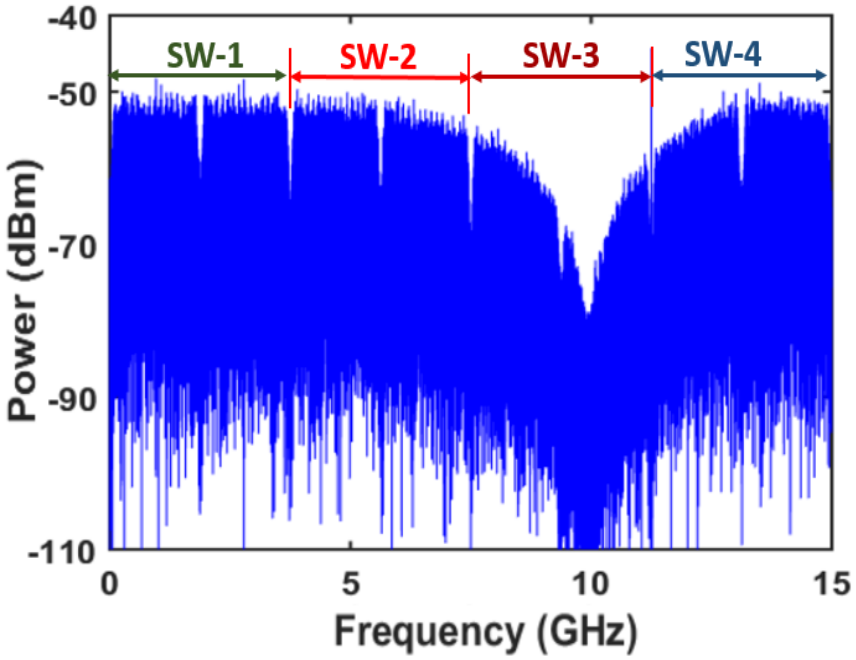

Fig. 3.4. Signal spectrum after 40km fibre transmission over SSMF link. An ideal PIN with an unlimited bandwidth is considered.

In the OLT, a variable optical attenuator (VOA) adjusts the received optical signal power and then a PIN with a quantum efficiency of 0.8 and a receiver sensitivity of -19dBm performs O-E conversion, followed by an ideal 15GHz electrical low pass filter to remove out-of-band noise. After the ADC, the DSP signal demodulation procedure illustrated in Fig. 3.2 is used to demodulate all received OFDM sub-bands for Hybrid Case-II(A) and Hybrid Case-II(B). For Hybrid Case-I, the DSP procedure is similar to that reported in [14], namely S/P conversion, 256-point FFT operation, sub-band identification process, optimum sideband selection process, conventional OFDM subcarrier equalization and decoding. Similar to the sideband identification described in section 3.2, the subcarriers in each sub-band of a specific sub-wavelength are identified. For each identified OFDM signal, the corresponding sideband (LSB or USB) that suffers less channel fading is selected for signal recovery. For a 40km SSMF transmission distance, a system frequency response dip is observed at ~10GHz, as depicted in Fig. 3.4. The LSB in the 1st and 2nd sub-wavelengths and the USB in the 4th sub-wavelength are chosen for signal recovery for Hybrid Case-I. Signals occupying the 3rd sub-wavelength cannot be used to recover any information because of the channel fading effect.

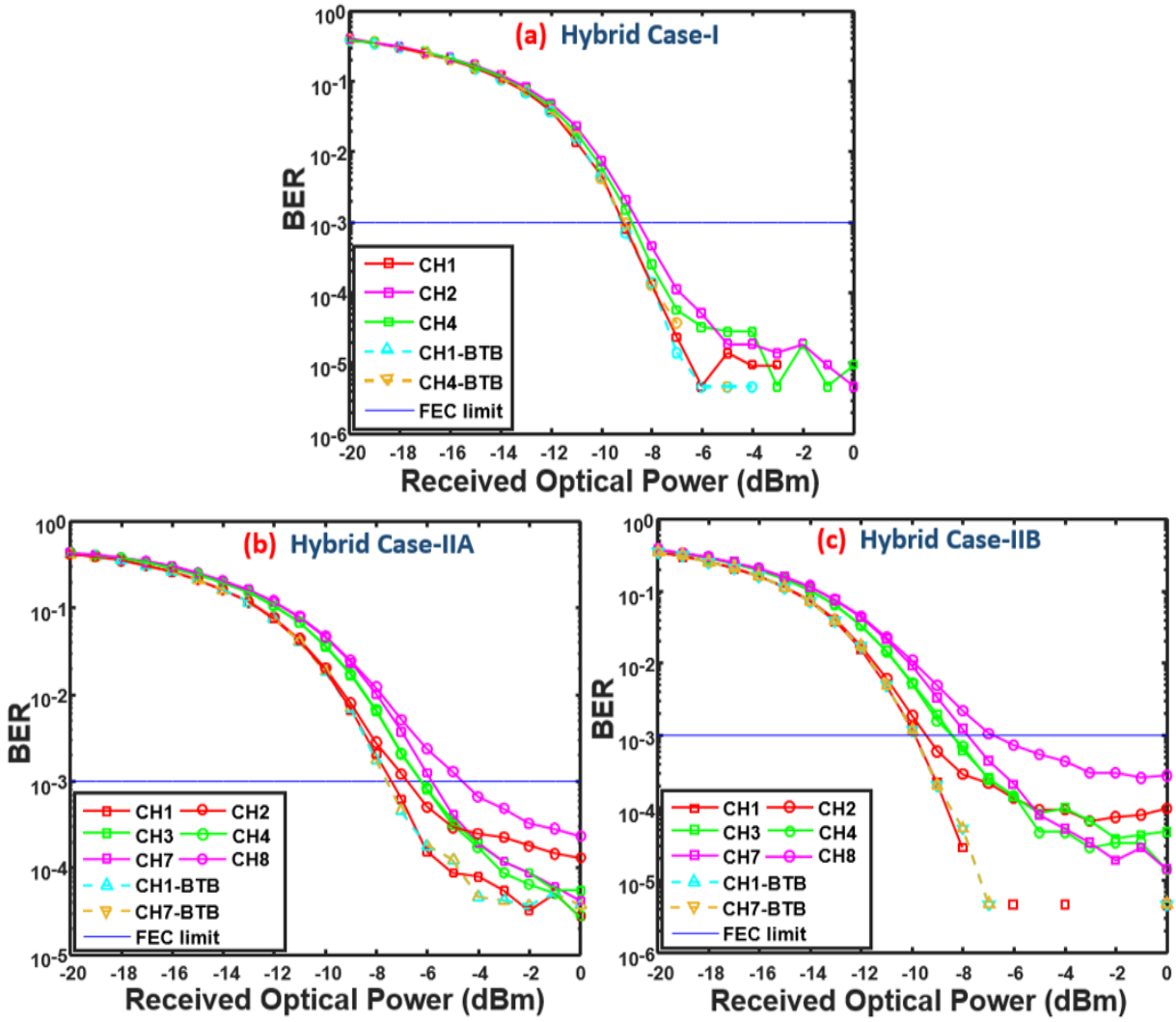

Fig. 3.5. BER performance versus received optical power after 40km SSMF IMDD PON transmission system subject to 0dBm optical launch power with channel bitrate of 6.25Gb/s; (a) Hybrid Case-I (b) Hybrid Case-IIA and (c) Hybrid Case-IIB. SW: sub-wavelength, CH: channel, BTB: back-to-back.

3.4 Simulation Results

3.4.1 Upstream Transmission Performance

Using the parameters mentioned in section 3.3, upstream transmission performances over 40km SSMF IMDD PON systems are modelled for the three cases and results are illustrated in Fig. 3.5. Channel 3 (CH3) for Hybrid Case-I and Channels 5 (CH5) and 6 (CH6) for both Hybrid Case-II(A) and Hybrid Case-II(B) are not operational due to channel fading as shown in Fig. 3.4. Consequently, their BER performances are not depicted in Fig. 3.5. In addition,

back-to-back BER performances of the operational channels at the lowest and highest frequencies for each case are also plotted to investigate nonlinear system impairment-induced upstream performance degradations.

In Fig. 3.5(a), the calculated BER performances show that for Hybrid Case-I, three channels can achieve BERs below the FEC limit. As each channel has a net signal bit rate of 6.25Gb/s, the aggregate upstream net signal transmission capacity is 18.75Gb/s. For Hybrid Case-II(A) and Hybrid Case-II(B), as shown in Fig 3.5(b) and 3.5(c) respectively, six of the channel BERs are below the FEC limit. This results in an aggregate upstream net signal bit rate of 37.5Gb/s. The proposed PON can thus lead to a higher spectral efficiency.

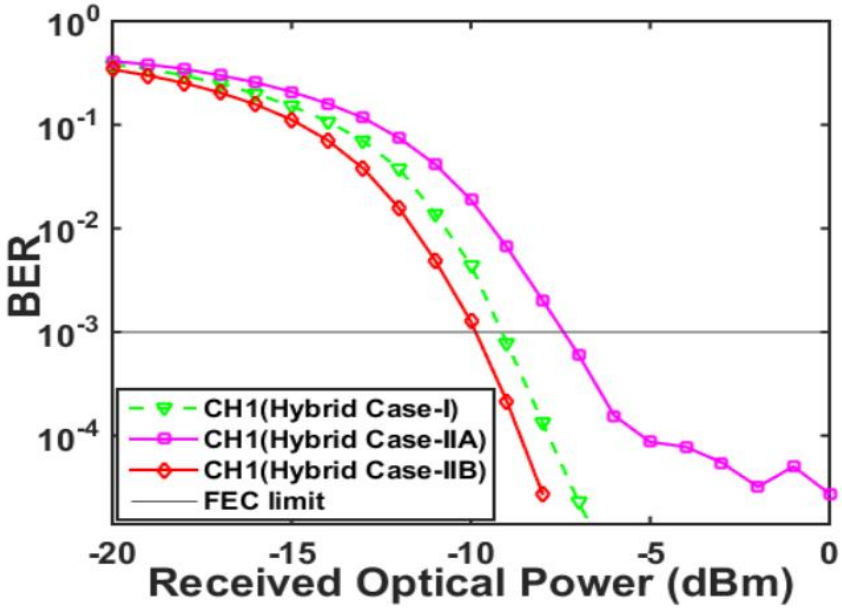

Fig. 3.6. Comparison of BER versus received optical power for all three involved cases after 40km SSMF IMDD PON transmission system for Channel-1.

Fig. 3.5(b) and 3.5(c) also show that in comparison to Hybrid Case-I, relatively large receiver sensitivity variations are observed among different sub-bands for both Hybrid Case-II(A) and Hybrid Case-II(B). This is as a result of channel fading which leads to undesirable power leakage between orthogonal sub-bands sharing a sub-wavelength spectral region [13,18,19]. However, no such power leakage occurs for Hybrid Case-I, as only an I-phase sub-band exists within each individual sub-wavelength spectral region, as shown in Fig.3(a). These receiver sensitivity variations are not observed in the optical back-to-back (BTB) transmission systems where the lowest frequency channel and highest frequency channel have almost identical BER performances for all three cases. It should be noted that the abovementioned imperfect

orthogonality-induced power leakage between different channels can be significantly reduced when the CCI cancellation technique reported in [13,18,19] is used.

CH1 BER curves of the three cases shown in Fig. 3.5 are plotted in Fig. 3.6. It can be seen that Hybrid Case-II(A) has ~1.5dB receiver sensitivity degradations when compared to Hybrid Case-I. This is due to the fact that the overall ONU count in Hybrid Case-II(A) is double that of Hybrid Case-I. The higher ONU count gives rise to effective OSNR reductions in each channel and leads to ~1.5dB receiver sensitivity degradations [20]. Hybrid Case-II(B) has an identical ONU number compared to Hybrid Case-I and a ~0.7dB improvement in receiver sensitivity compared to Hybrid Case-I. This is mainly attributed to an increase in effective OSNR arising from directly combining spectrum-sharing ONU sub-band signals in the digital domain [20].

Fig. 3.6 also shows that for the adopted numerical simulation parameters, for Hybrid Case-II (A) and Hybrid Case-II (B), their receiver sensitivities are -7.3dBm and -9.6dBm respectively, both of which can be further improved when use is made of some well-documented techniques such as wavelength-offset optical filtering [21] and DSP-enabled optical field reconstruction in the receiver [22].

3.4.2 Upstream Transmission Capacity versus Reach Performance

With the simulation parameters used to obtain Fig. 3.6, maximum achievable upstream net signal transmission capacities are explored as a function of fibre transmission distance, and corresponding results are plotted in Fig. 3.7. For these results, adaptive bit-loading is applied to all subcarriers involved in each OFDM signal with signal modulation formats varying from DBPSK, DQPSK, 4/8/16/32/128-QAM to 256-QAM. The received optical powers (ROPs) are fixed at -5dBm. Signal capacity improvement ratios between Hybrid Case-II(A)/Hybrid Case-II(B) and Hybrid Case-I are plotted in the same figure.

In Fig. 3.7, it can be seen that across the transmission distance range of 50km, Hybrid Case-II(A) (Hybrid Case-II(B)) can improve the maximum aggregate upstream net signal transmission capacity by a factor of up to 1.7 (2.2) compared with Hybrid Case-I. Thus, the proposed PON improves the upstream transmission capacity. As expected from Fig.3.5 and Fig.3.6, Hybrid Case-II(B) can further improve the upstream signal transmission capacity with

respect to Hybrid Case-II(A) because of digital-domain sub-band multiplexing-induced effective OSNR improvements, as discussed in section 3.4.1.

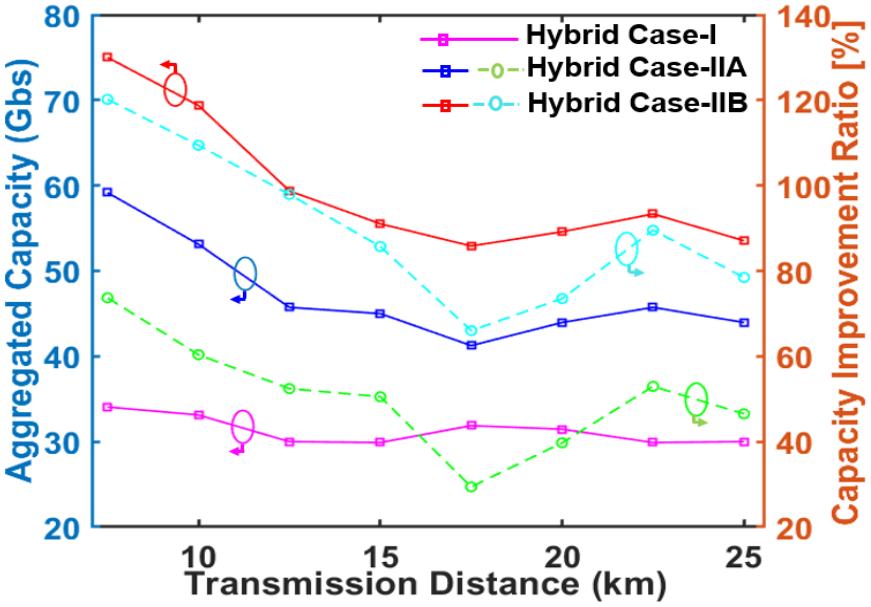

Fig. 3.7. Maximum aggregate upstream transmission capacity versus reach for IMDD PON system.

3.4.3 Channel Interference Effect

As described in section 3.2, digital orthogonal filtering plays a key role in the proposed PON. It is well known [10] that for a specific digital filter, a relatively short filter length can lead to a relatively large power leakage, resulting in undesirable channel interferences. However, a long filter increases the digital filter DSP complexity. Using the simulation parameters identical to those in Fig.3.5, the digital filter length-dependent channel interference-induced power penalties are investigated for all three cases. Results are presented in Fig. 3.8. Here the power penalty is defined as the difference of ROPs at the FEC limit with and without spectral spaces between adjacent channels of different sub-wavelengths. In calculating Fig. 3.8, 16-QAM signal modulation formats are adopted for all subcarriers in each involved OFDM signal, and fibre transmission distances are fixed at 40 km.

As seen in Fig. 3.8, <1.2dB (<0.8) power penalties are observed for Hybrid Case-II(A) (Hybrid Case-II(B)) when the proposed PONs employs digital filter lengths as short as 16. While for a digital filter length of 64 and beyond, <0.3dB power penalties can be observed for all the considered cases. Hybrid Case-II(A) suffers the highest power penalties when compared to

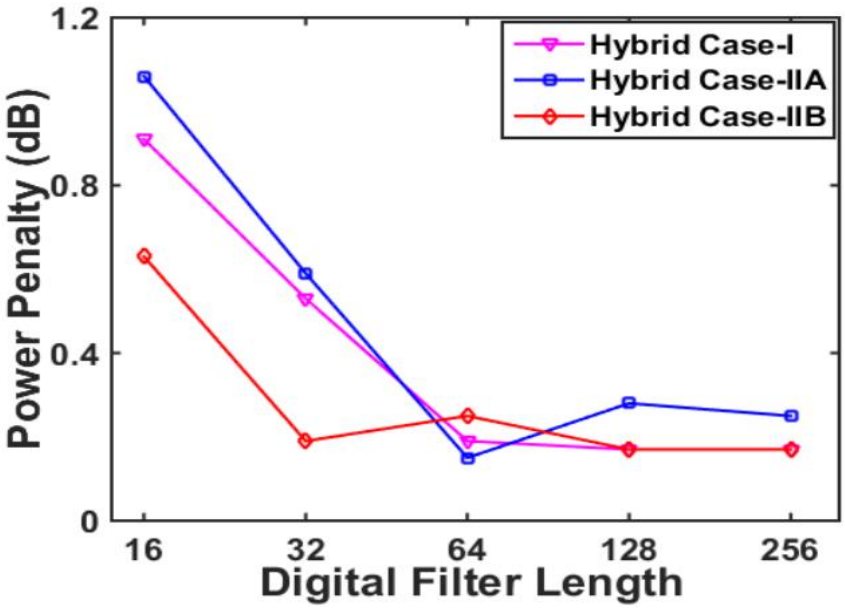

Fig. 3.8. Channel interference-induced power penalties for 40km upstream signal transmission for different IMDD PONs incorporating with various digital filter lengths.

Hybrid Case-I and Hybrid Case-II(B). This is mainly because Hybrid Case-II(A) suffers the strongest unwanted cross talk effect between two spectrally overlapped orthogonal sub-bands [18,19]. It can also be seen from Fig. 3.8 that an optimum digital filter length of 64 results in acceptable channel interferences and has low digital filter DSP complexity.

3.5 Conclusions

By modifying the DSP algorithms implemented in the OLT and ONUs, a new IMDD hybrid OFDM-DFMA PON has been reported for the first time, where digital orthogonal filtering-based two spectrally overlapped sub-bands occupying an individual sub-wavelength spectral region carry independent ONU information for upstream transmission. A model of the proposed PON has been developed, and its upstream transmission performances for various application scenarios have been examined and compared with the previously reported PONs. It has been shown that the proposed PON maintains features associated with the previously reported PONs. Moreover, compared with the previously reported PON, the new PON supports twice as many ONUs passively multiplexed in the optical domain and allows >1.7-fold upstream transmission capacity increases with <1.5dB upstream power budget degradations. Under the condition of the same number of ONUs occupying two digitally multiplexed sub-bands in a single sub-wavelength spectral region, >0.7dB upstream power budget improvements and >2.2-fold upstream transmission capacity enhancements can be achieved.

In addition, the proposed PONs have excellent tolerance to finite digital filter tap length-induced channel interferences.

References

[1] P. Chanclou, A. Cui, F. Geilhardt, H. Nakamura, and D. Nesset, "Network operator requirements for the next generation of optical access networks," IEEE Netw. Mag., vol. 26, Issue 2, pp. 8–14, 2012.

[2] X. Liu and F. Effenberger, "Emerging optical access network technologies for 5G wireless" J. Opt. Commun. Netw., vol. 8, no. 12, pp. B70–B79, 2016.

[3] 3GPP, "3rd generation partnership project; technical specification group radio access network; NG-RAN; architecture description (Release 15)," TS 38.401 V15.3.0, 2018.

[4] Y. Okumura and J. Terada, "Optical network technologies and architectures for backhaul/fronthaul of future radio access supporting big mobile data," Opt. Fibre Commun. Conf. (OFC), 2014.

[5] X. Liu and F. Effenberger, "Emerging optical access network technologies for 5G wireless," J. Opt. Commun. Netw., vol. 8, no. 12, pp. B70–B79, 2016.

[6] M. A. Habibi, M. Nasimi, B. Han and H. D. Schotten, "A Comprehensive Survey of RAN Architectures Toward 5G Mobile Communication System," IEEE Access, vol. 7, pp. 70371–70421, 2019.

[7] S. Chen and J. Zhao, "The requirements, challenges, and technologies for 5G of terrestrial mobile telecommunication," IEEE Commun. Mag, vol. 52, no. 5, pp. 36–43, 2014.

[8] C. I, Y. Yuan, J. Huang, S. Ma, C. Cui and R. Duan, "Rethink fronthaul for soft RAN," IEEE Commun. Mag., vol. 53, no. 9, pp. 82–88, 2015.

[9] M. Bolea, R. P. Giddings, M. Bouich, C. Aupetit-Berthelemot, and J. M. Tang, "Digital filter multiple access PONs with DSP-enabled software reconfigurability," J. Opt. Commun. Netw., vol. 7, no. 4, pp. 215–222, 2015.

[10] M. Bolea, R. P. Giddings, and J. M. Tang, "Digital orthogonal filter- enabled optical OFDM channel multiplexing for software-reconfigurable elastic PONs," J. Lightw. Technol., vol. 32, no. 6, pp. 1200–1206, 2014.

[11] X. Duan, R. P. Giddings, S. Mansoor, and J. M. Tang, "Experimental demonstration of upstream transmission in digital filter multiple access PONs with real-time reconfigurable optical network units," J. Opt. Commun. Netw., vol. 9, no. 1, pp. 45–52, 2017.

[12] M. L. Deng, A. Sankoh, R. P. Giddings, and J. M. Tang, "Experimental demonstrations of 30Gb/s/λ digital orthogonal filtering-multiplexed multiple channel transmissions over IMDD PON systems utilizing 10G- class optical devices," Opt. Express, vol. 25, no. 20, pp. 24251–24261, 2017.

[13] E. Al-Rawachy, R. P. Giddings, and J. M. Tang, "Experimental demonstration of a real-time digital filter multiple access PON with low complexity DSP-based interference cancellation," J. Lightw. Technol., vol. 37, no. 17, pp. 4315–4329, 2019.

[14] Y. X. Dong, R. P. Giddings, and J. M. Tang, "Hybrid OFDM-digital filter multiple access PONs," J. Lightw. Technol., vol. 36, no. 23, pp. 5640–5649, 2018.

[15] W. Jin, A. Sankoh, Y. X. Dong, Z. Q. Zhong, R. P. Giddings, M. O'Sullivan, J. Lee, T. Durrant and J. M. Tang., "Hybrid SSB OFDM-Digital filter multiple access PONs," J. Lightw. Technol., early access, Jan. 2020.

[16] X. Jin, R. P. Giddings, and J. M. Tang, "Real-time transmission of 3Gb/s 16-QAM encoded optical OFDM signals over 75km SMFs with negative power penalties," Opt. Express, vol. 17, pp. 14574-14585, 2009.

[17] Y. X. Dong, W. Jin, R. P. Giddings, M. O'Sullivan, A. Tipper, T. Durrant, and J. M. Tang, "Hybrid DFT-spread OFDM-digital filter multiple access PONs for converged 5G networks," J. Opt. Commun. Netw., vol. 11, no. 7, pp. 347–353, 2019.

[18] Y. X. Dong, E. Al-Rawachy, R. P. Giddings, W. Jin, D. Nesset, and J. M. Tang, "Multiple channel interference cancellation of digital filter multiple access PONs," J. Lightw. Technol., vol. 35, no. 1, pp 34–44, 2017.

[19] E. Al-Rawachy, R. P. Giddings, and J. M. Tang, "Experimental demonstration of a DSP-based cross-channel interference cancellation technique for application in digital filter multiple access PONs," Opt. Express, vol. 25, no. 4, pp. 3850–3862, 2017.

[20] X. Q. Jin, J. Groenewald, E. Hugues-Salas, R. P. Giddings, and J. M. Tang, "Upstream power budgets of IMDD optical OFDMA PONs incorporating RSOA intensity modulator-based colorless ONUs," J. Lightw. Technol., vol.31, no. 12, pp. 1914–1920, 2013.

[21] J. L. Wei, C. Sánchez, E. Hugues-Salas, P. S. Spencer and J. M. Tang, "Wavelength-offset filtering in optical OFDM IMDD systems using directly modulated DFB lasers," J. Lightw. Technol., vol.29, no.18, pp.2861-2870, 2011.

[22] H. Chen, N. K. Fontaine, J. M. Gene, R. Ryf, D. T. Neilson, and G. Raybon, "Dual polarization full-field signal waveform reconstruction using intensity only measurements for coherent communications," J. Lightw. Technol., vol. 38, no. 9, pp. 2587-2597, 2020.

4. DFT-Spread Spectrally Overlapped Hybrid Orthogonal OFDM-Digital Filter Multiple Access IMDD PONs

Contents

4.1 Introduction

To effectively cope with the current avalanche of mobile traffic, driven by the unprecedented increase in users' demands for ultrawide bandwidth multimedia and cloud services that have become ubiquitous, MFHs/MBHs of 5G CRANs capable of converging optical and wireless networks are needed, and require significant changes to network access in order to support the ambitious system requirements [1,2]. Addressing such technical challenges requires multipronged efforts in different network domains across all layers to not only accommodate the explosive expansion in traffic demand, but also efficiently support dynamic bandwidth provisioning, improved cost-effectiveness, and power efficiency [3]. The emergence of SDNs with their extended network-control functionalities leverages the abstraction of different physical resources, and enhances the dynamic reconfigurability, flexibility, scalability, and elasticity of the network [4]. To deliver an SDN-based solution capable of satisfying the abovementioned requirements, a non-incremental solution should be implemented to realize the highly desirable, cost-effective, separately implemented, and independently operated legacy optical and wireless access networks in a converged manner. For cost-sensitive application scenarios such as optical access networks, metropolitan area networks (MANs), and MFH/MBH networks, IMDD PONs are considered to be a competitive technical solution due to their excellent cost-effectiveness and power efficiency [5].

To overcome the abovementioned technical challenges, a novel PON technique termed hybrid OFDM-DFMA PON, utilizing spectrally overlapped digital orthogonal filtering, has recently been proposed and extensively investigated [6] where, regardless of the ONU count, MF-free single FFT operation and the relevant DSP processes are applied in a pipeline approach. In the proposed PON, transceiver-embedded software-reconfigurable digital orthogonal filtering is utilized in each individual ONU, where for upstream transmission two spectrally overlapped digitally filtered orthogonal ONU OFDM sub-band signals occupy the same subwavelength spectral region. In the OLT, for ONU sub-band signal demultiplexing and recovery, a procedure similar to the previously reported hybrid OFDM-DFMA PONs [7] is adopted. Numerical results show that in terms of improving the upstream signal transmission capacity and enhancing the spectral efficiency, the proposed PON outperforms the results previously reported in [7] by a factor of ~2. Moreover, in the context of low OLT-DSP complexity, robustness against practical transceiver impairments, enhanced flexibility, and backward compatibility with existing 4G networks, the proposed PON still maintained all the

aforementioned salient unique features associated with the hybrid OFDM–DFMA PONs [6].

It is important to mention that the PONs reported in [6] are OFDM-based. The OFDM's multi-subcarrier modulation scheme is well known to produce high PAPRs due to the coherent superposition of orthogonal subcarriers in the time domain [8]. Technically speaking, systems with large PAPRs not only require wide dynamic operating ranges for the transceiver-embedded electrical/optical devices, but also produce high quantization noise for a fixed number of quantization bits, and may force the involved devices to operate in their nonlinear regions, thus introducing nonlinear signal distortion. In addition, a large PAPR may also cause serious nonlinear noise associated with SSMF nonlinearities [9]. Therefore, suppressing PAPRs in the PONs reported in [6] is of great importance. Several PAPR reduction techniques have been proposed [10-13]. The most widely adopted and simplest approach is to clip OFDM signals [10,11]; this approach achieves certain levels of PAPR reduction; however, the clipping still causes significant signal distortion. Another solution is to use multiple signalling and probabilistic techniques, such as pilot-assisted partial transmit sequences (PTSs) and selected mapping (SLM) [12,13]. However, due to these approaches requiring redundant information to be transported alongside actual data, they have an intrinsic drawback of reducing the useful data rate and increasing the computational complexity. In contrast to the abovementioned PAPR reduction techniques, DFT-spread OFDM is the ultimate technical solution, because it is free from parallel redundant information and has low complexity, since only deterministic DFT and IDFT operations are required in the transceiver [14]. The DFT-spread OFDM technique has already been reported in SSMF IMDD links, including DFT-spread layered/enhanced asymmetrically clipped OFDM systems [15] and probabilistically shaped OFDM-enabled IMDD systems [16]. In addition, the DFT-spread technique also possesses high compatibility for both long-distance [17] and short-reach IMDD transmission systems [18], and shows superior performance in PAPR reduction. Recently, we have applied the DFT-spread technique in the hybrid OFDM-DFMA PONs to further improve the flexibility of the system transmission performance [19]. However, in these PONs, each individual subwavelength spectral region only conveys either a single I-phase or Q-phase channel upstream of the DSB OFDM signal, which halves the spectral efficiency compared with the spectrally overlapped hybrid OFDM-DFMA PONs [6].

By combining the benefits of the DFT-spread technique and the previously reported PON [6], in this chapter, we propose DFT-spread spectrally overlapped hybrid OFDM-DFMA IMDD

PONs and, via numerical simulations, analyse and optimize their performance characteristics. The simulation results show that when the DFT-spread technique is applied, PAPR reductions of more than 2 dB are attained for a digitally filtered OFDM signal carrying QAM modulated data. More importantly, the proposed PON can achieve a reduction of more than 1 bit in the minimum required DAC/ADC bit resolution, and an improvement of more than 1.4 dB in the upstream power budget. Furthermore, in comparison to the conventional hybrid OFDM–DFMA PON [6], the proposed PON can enhance the aggregate upstream signal transmission rate by factor of up to 10% in a 25 km SSMF IMDD PON transmission system. It is noteworthy that, while the proposed PON still maintains all of the unique advantages associated with the previously reported PONs [6], in the OLT, without utilizing digital MFs, the single FFT operation followed by summing and subtraction operations of the LSB and USB, and the corresponding DSP-enabled data recovery processes applied in a pipelined approach, can directly demultiplex and demodulate ONU sub-band signals within the same subwavelength spectral region, while the same OLT receiver can also be used to demodulate legacy OFDM signals.

The above salient features make the proposed PON a feasible solution for future 5G networks in terms of providing DSP-enabled multichannel aggregation and de-aggregation solutions for fronthaul networks [20] to effectively enhance their bandwidth efficiency in comparison with existing CPRI-based fronthauls [21]. It should also be noted that the proposed PONs are completely different from the multiband OFDM PON reported in [22], since the PONs proposed here have the following unique features: (1) each subwavelength spectral region is shared by two independent orthogonal OFDM sub-band signals [6]; (2) no extra channel spacing is required between adjacent subwavelengths or sub-bands; (3) the side lobes of each OFDM sub-band are considerably reduced by the digital filtering process, which can minimize the ICI effect between sub-bands at adjacent subwavelengths. Furthermore, our results also indicate that for subwavelengths that do not suffer the strong channel fading effect, the ICI effects between different orthogonal OFDM sub-bands in these subwavelengths are negligible; (4) as a direct result of using the digital filtering process, each OFDM sub-band can adaptively and flexibly adjust its signal modulation parameters such as subcarrier count and channel bandwidth without affecting the orthogonality between different sub-bands; (5) the digital-filtering-processing-induced ICI reductions greatly enhance the PON's performance and its robustness against the channel frequency offset. In comparison with the up-conversion-based OFDM multiband PONs, which require multiple tuneable electrical local oscillators [20], the

spectrally overlapped hybrid OFDMDFMA PONs utilize only digital filters to multiplex multiple OFDM sub-bands without requiring extra electrical/optical components compared to conventional transceivers in both the ONUs and the OLT.

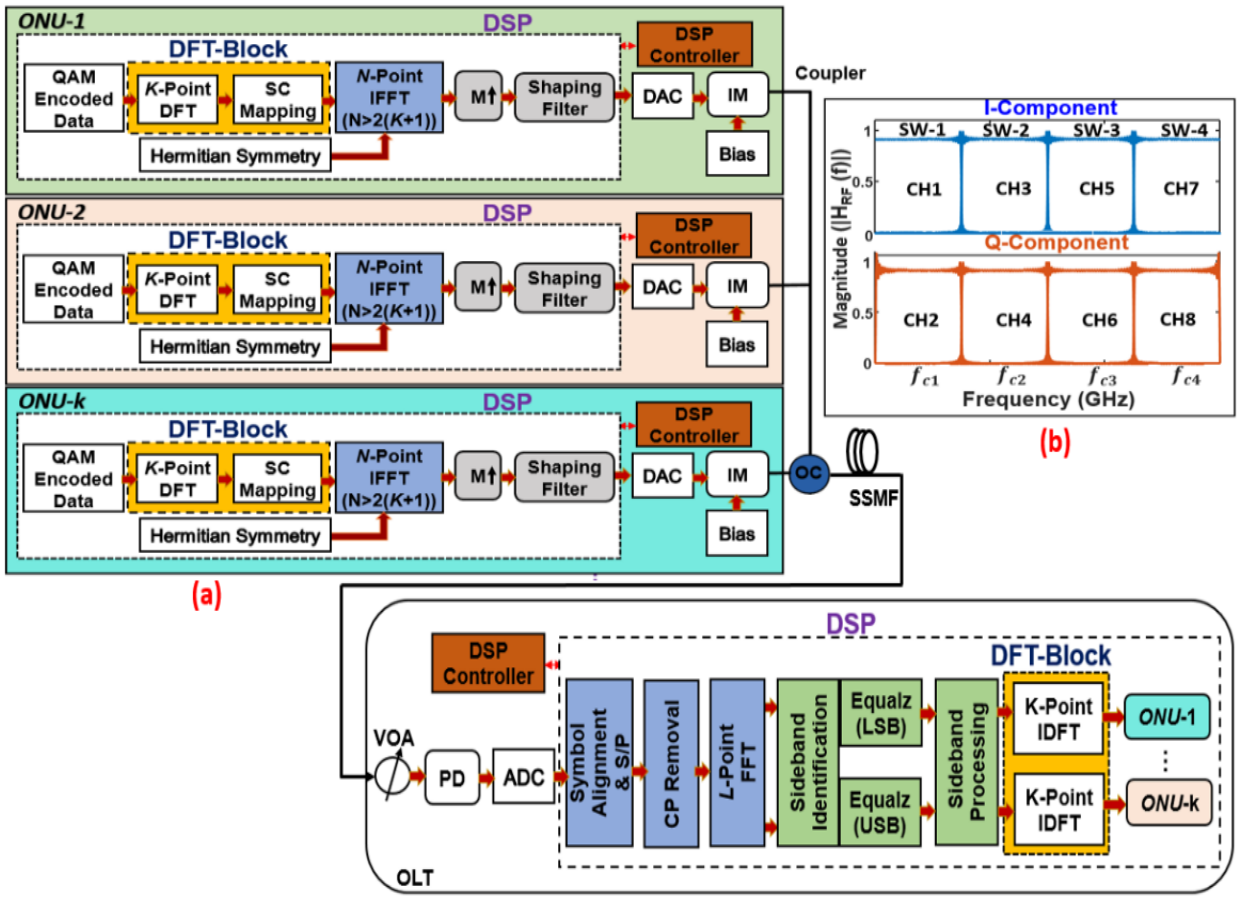

Fig. 4.1. (a) DFT-spread hybrid orthogonal OFDM-DFMA PON (b) Example of Hilbert-pair based frequency responses at different sub-wavelength central frequencies. SC: subcarrier, DFT: discrete Fourier transform, M↑: up-sampling factor, DAC/ADC: digital-to-analogue/analogue-to-digital converter. IM: intensity modulator. OC: optical coupler, SSMF: standard single-mode fibre, VOA: variable optical attenuator, PD: photo-detector. S/P: serial-to-parallel conversion, Equalz: equalization, ONU: optical network unit, OLT: optical line terminal, DSP: digital signal processing, SW: sub-wavelength, CH: channel.

4.2 Principle of DFT-Spread Spectrally Overlapped Hybrid Orthogonal OFDM-DFMA PONs

A representative DFT-spread spectrally overlapped hybrid OFDM-DFMA IMDD PON architecture is depicted in Fig. 4.1, in which only the more challenging multipoint-to-point

upstream operation is considered. The additional *K*-point DFT and IDFT block at each ONU and OLT, combined with a subcarrier mapper and de-mapper module, are shown highlighted in yellow. For upstream transmission, optical signals from *P* ONUs are passively combined, as depicted in Fig. 4.1.

In each ONU, either I-phase or Q-phase M-ary QAM-encoded data symbols are grouped into blocks, each containing *K* symbols. Assuming a complex-valued symbol, $d_m(n)$, chosen from the QAM constellation, $d_m(=n)$: n = 0, 1, 2,…..,*K*-1 is a *K*-size vector. The *K*-point DFT operation is applied to spread the symbols into the frequency domain given by:

$$D_m^I(k') = \sum_{n=0}^{K-1} d_m(n) e^{-j\frac{2\pi nk'}{K}} \tag{4.1}$$

where $D_m(k')$ refers to the DFT spread symbol vector at the *k*-th subcarrier of the *I* sub-band. Localized mapping is then utilized to map, $D_m(k')$, to an *N*-point ($N>2(K+1)$) IFFT with *N*-subcarriers. As the first subcarrier is unused, the *K*-signal carrying subcarriers occupy the first *N*/2 - 1 subcarriers; as such, after zero padding, the signal length is $K \leq N/2 - 1$. The mapped frequency-domain signal, u_k, in the *k*-th subcarrier data is define as:

$$u_m(k) = \begin{cases} D_m^I(k') & 0 \leq k \leq \frac{N}{2} - 1, \ for\ N > 2k \\ 0 & Otherwise \end{cases} \tag{4.2}$$

To produce a real-valued DFT-spread OFDM signal, an *N*-point IFFT operation is applied after enforcing the Hermitian symmetry, which must satisfy $u_{-k,m}=u^*_{k,m}$ *for* k=1,2,…(*N*/2-1), and $u_0=u_{-N/2}=0$ [ref]. The produced real-valued DFT-spread OFDM signal, $s_m(n)$, obtained after the *N*-point IFFT operation can be written as:

$$s_m(n) = \sum_{k=-\frac{N}{2}}^{\frac{N}{2}-1} u_m(k) e^{j\frac{2\pi k(n-mN)}{N}} \tag{4.3}$$

where *N* denotes the IFFT size of a set of *N*-subcarriers for each *m*-th DFT-spread OFDM symbol. Following the addition of the CP, each digitally encoded DFT-spread OFDM sub-band signal sample sequence is up-sampled by a factor of *M*×. Assuming $S_m(n)$ employ an ideal *I*-phase digital shaping filter, after filtering, the *I*-phase sub-band occupying the *i*-th subwavelength can be expressed as:

$$S_i^I(t) = M \uparrow \{s_{i,I}(t)\} \otimes h_i^I(t) \tag{4.4}$$

For the Q-phase sub-band, let $D^{Q}_{m}(k')$ be the *K*-point DFT output spread symbol vector, which is mapped to an *N*-size vector, $v_m(k)$: k = 0, 1, 2, …., *N*-1. The produced *K*-spread spectrum OFDM signal can be obtained based on the same principle described from Eq. (4.1) to Eq. (4.3). Very similar the digitally filtered I-phase sub-band signal generation process describe-above, the generation of the *i*-th digitally filtered *Q*-phase sub-band DFT spread OFDM signal can be given by:

$$S_i^Q(t) = M \uparrow \{s_{i,Q}(t)\} \otimes h_i^Q(t) \tag{4.5}$$

After filtering, the generated digitally filtered sub-band signal is passed through the DAC and then fed into an optical IM to perform E-O conversion. For upstream transmission, in the remote node, a total of *P* ONUs optical field are passively coupled and then launched into a SSMF PON system expressed similar to Eq. (3.4).

Similar to the treatment adopted in [7], the utilization of IM as the preferred light source in the numerical simulations is to completely eliminate the signal-signal beating interference (SSBI) effect [23]. It is noteworthy that, for practical implementation of the proposed PONs, different ONUs can use different wavelengths to transmit their OFDM sub-bands, provided that every two adjacent wavelengths have a minimum wavelength space of ~0.28nm to effectively mitigate the SSBI effects [24].

Without loss of generality, in this section, we assume an ideal channel. In the OLT, without phase noise and fibre nonlinearities in the system, $S_{opt}(t)$ is then converted into the digital signal $S_{i,IQ}$ by being passed through an O-E converter and an ADC. Thus, we obtain:

$$\begin{aligned} S_{i,IQ} = & \sum_{i=1}^{P/2}\left[S_{i,I}(t) + S_{i,Q}(t)\right] \\ = & \sum_{i=1}^{P/2}\Big[\sum_{K=-N/2}^{N/2}\left(Z_{i,I}(k).H_i^I + Z_{i,Q}(k).H_i^Q\right)e^{j2\pi(kf_k+f_{ci})t} + \cdots \\ & \sum_{k=-\frac{N}{2}}^{\frac{N}{2}}\left(Z_{i,I}^*(k).H_i^I + Z_{i,Q}^*(k).H_i^Q\right)e^{-j2\pi(kf_k+f_{ci})t}\Big] \end{aligned} \tag{4.6}$$

$Z_{i,I}(k)$ and $Z_{i,Q}(k)$ are the orthogonal sub-bands data samples at the *k*-th subcarrier in the *i*-th sub-wavelength. $f_k = f_{DAC/ADC}/MN$ is the subcarrier frequency spacing and $f_{ci} = (2\times i\text{-}1)Nf_k/2$ is the subwavelength center frequency. Where $f_{DAC/ADC}$ is the sampling speed of the DAC/ADC converter. H_i^I and H_i^Q are the I-phase and Q-phase filter frequency responses. $S_{i,IQ}$ in Eq. (4.6)

consist of *P*/2-pairs of orthogonal sub-bands in different sub-wavelength. The first term represents the subcarriers in the positive frequency bins, while the second term denotes the subcarriers in the negative bins. Because the channel is assume to be ideal, the filter frequency responses satisfy the condition $H_i^Q = (-j)H_i^I$, where H_i^I has a rectangular pulse-shape of unit magnitude.

As shown in Fig. 4.1, the rest of the subsystems comprising the receiver follow the same procedure adopted in [7]. In the OLT, a single *L*-point FFT transforms each DFT-spread OFDM symbol into the frequency domain and the *L*/2 positive frequency bins subcarriers are extracted. For simplicity, here we assume a single sub-wavelength. After the FFT operation and the subsequent DSP processes, the received subcarrier matrix, Z_i, can be expressed as:

$$Z_i = \left[\overbrace{\begin{matrix} \left(u_i^*\left(-\frac{N}{2}\right) - jv_i^*\left(-\frac{N}{2}\right)\right), \ldots, \left(u_i^*(-1) - jv_i^*(-1)\right), \\ \underbrace{\left(u_i(0) - jv_i(0)\right), \ldots, \left(u_i\left(\frac{N}{2}-1\right) - jv_i\left(\frac{N}{2}-1\right)\right)}_{USB_{LQ}} \end{matrix}}^{LSB_{IQ}} \right] \tag{4.8}$$

In the OLT, based on the pilot subcarriers, channel estimation and channel equalization of the received symbols are performed independently on the LSB and USB. To demultiplex the spectrally overlapped sub-band signals, the spectrum spread subcarrier information $u_i(k)$ and $v_i(k)$ can be obtained based on the same procedure described in detail in the previously reported hybrid OFDM DFMA PONs [7]:

$$u_i(k) = \frac{1}{2}[Z_i^*(-k) + Z_i(k)] = D_{i,I}(k') \tag{4.9}$$

$$v_i(k) = \frac{1}{j2}[Z_i^*(-k) - Z_i(k)] = D_{i,Q}(k') \tag{4.10}$$

Where $Z_i^*(-k)$ and $Z_i(k)$ correspond to the LSB and USB spectrum spread signal. After the above DSP process, the resulting complex output sub-band subcarriers' data of *I*-phase sub-band, $D_{i,I}(k')$, and *Q*-phase sub-band, $D_{i,Q}(k')$, are passed through the subcarrier de-mapper. The output of the de-mapper is then subjected to the *K*-point IDFT and symbol demodulation to obtain data information corresponding to the transmitted I-phase ONU sub-band input data, $d_I(n)$, and Q-phase ONU sub-band input data, $d_Q(n)$, whose output are represented as:

$$d_I(n) = \sum_{k'=0}^{K-1} D_{i,I}(k') e^{j\frac{2\pi nk'}{K}} \quad (4.11)$$

$$d_Q(n) = \sum_{k'=0}^{K-1} D_{i,Q}(k') e^{j\frac{2\pi nk'}{K}} \quad (4.12)$$

4.3 Upstream Optimum ONU Operating Conditions

In performing the numerical simulations over a 25 km SSMF, an IMDD PON theoretical model developed and verified in [6] is adopted, where the procedure detailed in [25] was used to simulate the OOFDM signal generation, nonlinear transmission, and direct detection.

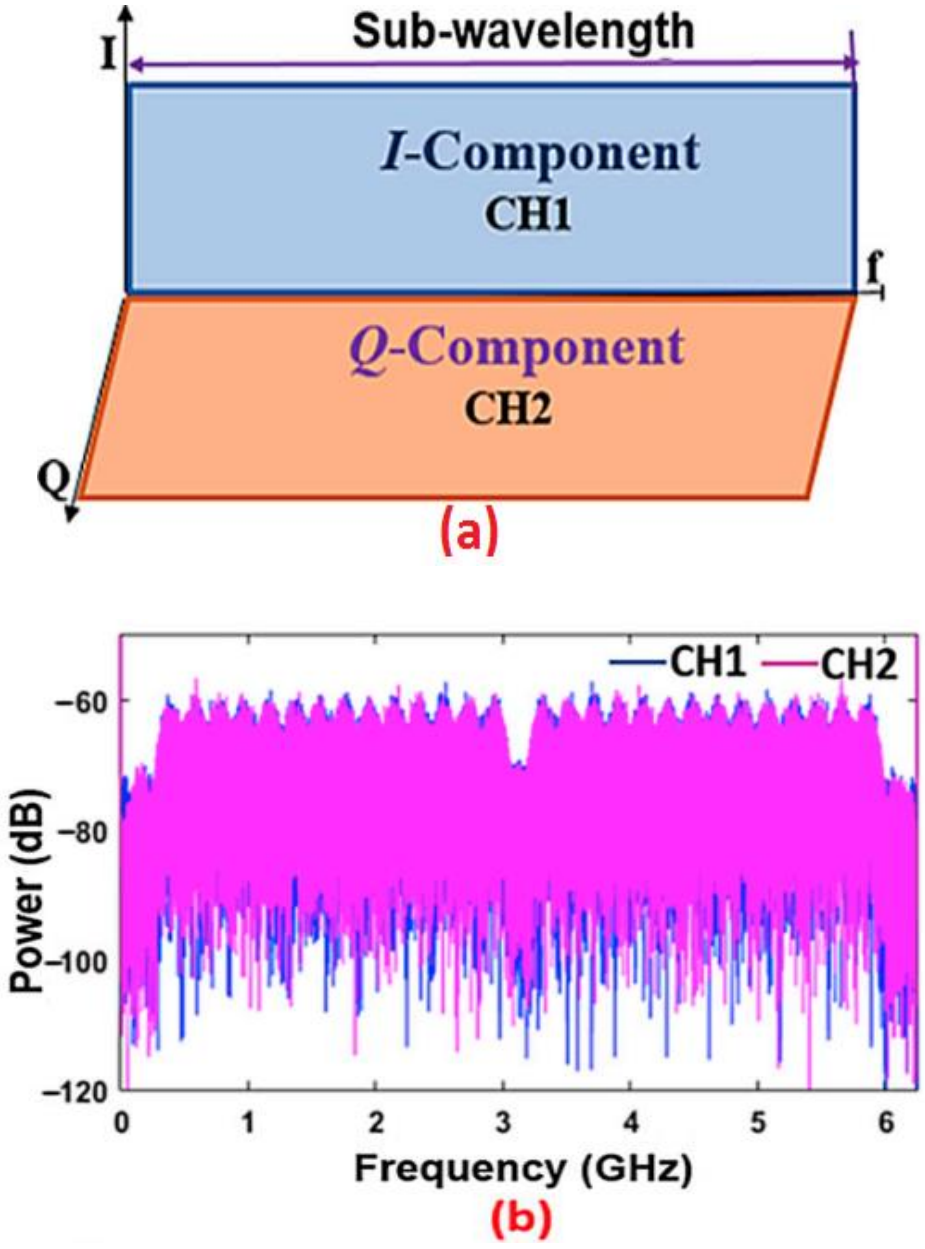

Fig. 4.2. (a) Spectral location of orthogonally digitally filtered sub-band signals (I-phase and Q-phase) and (b) their spectra.

4.3.1 Simulation Models and Key Parameters

In this chapter, 2-ONUs are considered, each producing an optical signal sharing the same sub-sub-wavelength with the other ONU. To conduct the simulation, MATLAB tools were used for signal generation and detection, while the VPITransmissionMaker was used for optical fibre transmission. To implement the shaping filter in each individual ONU, a widely used digital filter construction approach called the Hilbert-pair approach [26,27] was adopted to produce two orthogonal digital shaping filters sharing a subwavelength spectral region. These two orthogonal filters form a Hilbert pair, which have similar amplitude characteristics, but with a $\pi/2$ phase difference in the frequency domain [26-28]. To support two independent ONUs, the up-sampling factor was set at $M = 2$ [26]. Since the DAC/ADC operates at 12.5 GS/s and the two ONUs occupy the same spectral region, the signal bandwidth for each ONU is equal to the Nyquist frequency, fs/M, while the central frequency of the orthogonal digital filter pair is $fs/2M$, where fs is the DAC/ADC sampling speed. For the $M = 2$ case, Figure 4.2(a) and 4.2(b) illustrates the spectral locations of digitally filtered sub-band signals (I-phase and Q-phase) and their spectra. To generate the real-value OFDM signal necessary for intensity modulation, a 32-point IFFT size was considered, in which 15 subcarriers in the positive frequency bins convey real data, one subcarrier contains no power, and the remaining 16 subcarriers in the negative frequency bins are the complex conjugates of data-bearing subcarriers. To reduce the power leakage caused by crosstalk between spectrally overlapped digital orthogonal sub-bands, and maximize the upstream signal transmission capacity, 14 data-bearing subcarriers out of 15 were employed to deliver the acceptable upstream performance for each sub-band. Thus, the DFT block size K was set to be 14. It is, however, expected that all 15 of the subcarriers can be supported if channel interference mitigation techniques are applied [29,30]. In this demonstration, all of the subcarriers were encoded with a 64-QAM signal modulation format; however, any modulation formats are applicable.

Detailed explorations of the impact of quantization and clipping noise on the upstream transmission performance of the digitally filtered spectrum-spread OFDM signals are undertaken in section 4.3.3, in which an optimum 7-bits resolution and optimal clipping ratios of 11 dB and 12 dB are identified for the cases of including and excluding the DFT-spread, respectively. These identified optimal parameters are adopted throughout this chapter. Unless otherwise stated, all other system parameters are summarized in Table 4.1.

Table 4.1: System Parameters

Parameter	Value	Parameter	Value
IFFT/ FFT Size	32/64	Clipping Ratio-Including/Excluding DFT-spread	11 dB / 12 dB
Number of Used Data Subcarriers Per ONU	14	Digital Filter Length/ Excess Bandwidth	64/0
Modulation Format	64-QAM	PIN Detector Quantum Efficiency	0.8 A/W
Cyclic Prefix	25%	PIN Detector Sensitivity	-19 dBm
Channel Bitrate	13.12 Gb/s	PIN Detector Bandwidth	Ideal
Optical Launch Power	0 dBm	Fibre-Dispersion	17 ps/nm/km
DAC/ADC Sample Rate	12.5 GS/s	Fibre-Dispersion Slope	0.08 ps/nm2/km
Number of Bits	7-bits	Fibre Loss	0.2 dB/km
Up-sampling Factor	M=2	Fibre Kerr Coefficient	2.6×10^{-20} m^2/W
FEC Limit	1×10^{-3}	Transmission Distance	25 km

*Corresponding to 10 Gb/s non-return-to-zero data at a BER of 1.0×10^{-9}

In the OLT, an ideal PIN photodetector for direct detection of the optical signal is employed, with a receiver sensitivity of -19 dBm and a quantum efficiency of 0.8 A/W. Both shot noise and thermal noise are considered and are simulated using procedures similar to those presented in [30]. In addition, the OLT-based receiver consists of a VOA to adjust the ROP level, while the ADC incorporates an ideal antialiasing electrical filter with a 6.25 GHz bandwidth to remove out-of-band receiver noise before signal sampling.

Taking into account the transceiver parameters listed in Table 4.1 and the adopted signal modulation formats, the upstream signal transmission rate per ONU is ~13.12 Gb/s, while the aggregate upstream PON transmission rate is ~26.25 Gb/s. It is noteworthy that, due to the high attenuation of the filter near the DC component, only 14 subcarriers (2-15) are activated in each ONU, as the first subcarrier contains no power.

4.3.2 PAPR Performance of DFT-spread Hybrid Orthogonal OFDM-DFMA PON

Having chosen the simulation parameters, identified the optimal conditions, and understood the operating principle of the proposed DFT-spread spectrally overlapped hybrid OFDM-DFMA IMDD PON, in this section, we numerically explore the PAPR reduction efficiency of

the proposed PON consisting of two ONUs. Fig. 4.2(a) and (b) shows the spectral locations of two digitally filtered sub-band signals (I-phase and Q-phase) and their spectra. In addition, the comparative CCDFs of the PAPR, including and excluding DFT-spread, are presented in Fig. 4.3 for various digital filter lengths ranging from 16 to 256 and signal modulation formats varying from 16-QAM to 256-QAM. For the sake of simplicity, only ONU-2 referred to as the channel-2 CCDF curve is plotted for both cases, as the curves of ONU-1 referred to here as channel-1 are similar to those of channel-2.

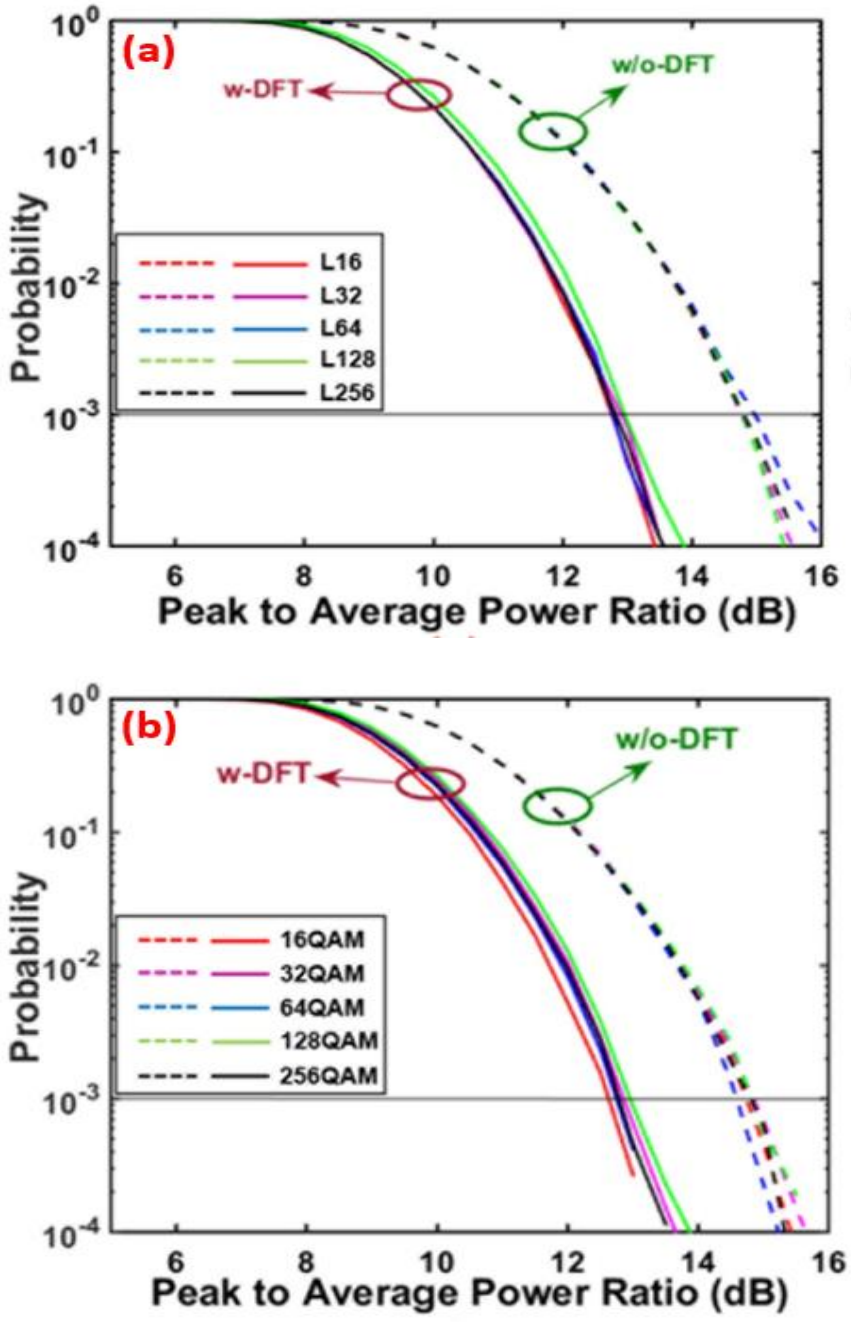

Fig. 4.3. CCDFs of PAPR for (a) varying digital filter lengths and a fixed 64-QAM modulation format, and (b) varying modulation formats and a fixed digital filter length of 64.

It can be seen from Fig. 4.3 that, compared to the case without DFT-spread, the case with DFT-spread can reduce the PAPR ratio by >2 dB at the CCDF value of 1×10^{-3} when the optimal clipping ratio of 11 dB is adopted. The results are similar to those of our previous work, and those observed in WDM-PONs [19,31,32]. It is also very interesting to note in Fig. 4.3 that the proposed PON's upstream transmissions have very similar PAPR performances when varying both digital filter lengths up to 256 and signal modulation formats up to 256-QAM. This indicates that the DFT-spread-induced PAPR reductions are independent of the digital filter length and the signal modulation. Moreover, the obtained results also suggest that, under the same transmission power constraints, the DFT-spread case with a low PAPR can achieve a higher OSNR; this is one of the factors leading to the increased upstream channel rate presented in section 4.4.2. Nevertheless, it is worth noting that the performance of the PONs reported in [6] is largely limited by digital-filter-induced signal distortion. As such, in this chapter, to highlight the unique features of the DFT-spread technique, a digital filter length of 64 as listed in Table 4.1 is utilized to minimize the digital filter impairments.

From the above discussion, it is easy to understand that the proposed PON-induced PAPR reduction gives rise to an excellent improvement in system performance robustness to quantization noise induced by limited DAC/ADC bit resolutions. In addition, it also relaxes the constraints on the linear dynamic operating ranges of the transceiver-embedded optical/electrical devices, reduces the optical nonlinearity impairments, and allows reductions in the DSP complexity and overall cost of the transceivers.

4.3.3 Optimum Clipping Ratio and DAC/ADC Resolution Bits

In order to numerically explore the feasibility of utilizing the proposed technique to improve the upstream transmission performance of the PON, in this section, numerical simulations are first undertaken to identify the optimal operating conditions for achieving the best possible performance. Fig. 4.4 presents the simulated BER contours as a function of quantization bit and clipping ratio for an optical BTB configuration. In obtaining these figures, the ROP at the OLT is fixed at -7 dBm. Since the two ONUs are independent and have the same signal characteristics, without loss of generality, only channel-2 is plotted in Fig. 4.4.

It can be seen in Fig. 4.4 that when the clipping ratio is low, the overall channel BER performance is high because the signal waveform is significantly clipped. In these figures, for a fixed bit resolution within a dynamic range from 7 to 8 bits, to maintain BERs below the FEC

limit, the clipping ratio should be ≥11 dB for the DFT-spread case. On the other hand, for the case without DFT-spread over the same dynamic region, the clipping ratio should be ≥12 dB, which shows an increase in clipping ratio by 1 dB. From the same figures, it can also be observed that the case excluding DFT-spread has a clipping ratio dynamic range of 12 dB ≤ clipping ratio ≤ 14 dB, while the case including DFT-spread achieves a clipping ratio dynamic

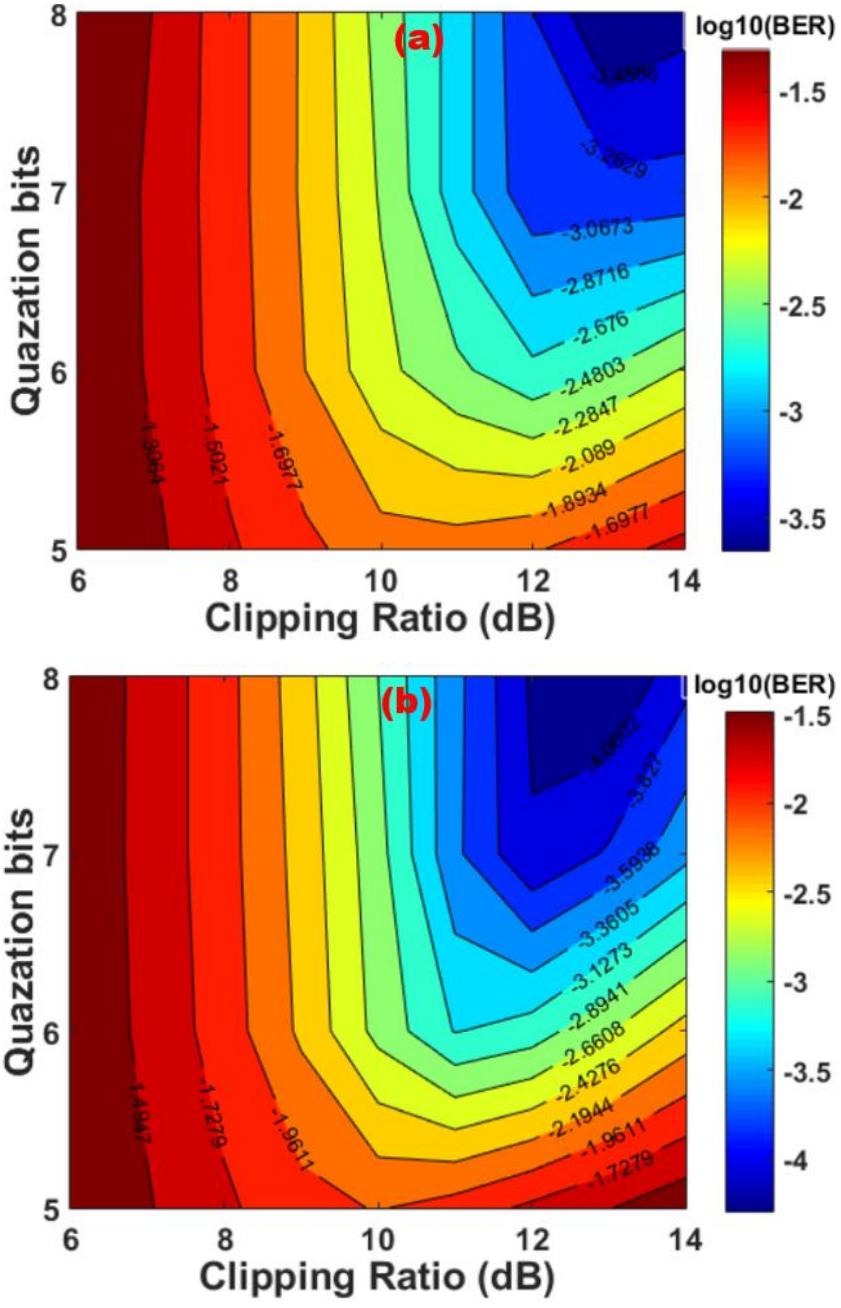

Fig. 4.4. BER contour versus quantization bit resolution and clipping ratio for (a) excluding the DFT-spread, and (b) including the DFT-spread.

range of 11 dB ≤ clipping ratio ≤ 14 dB. Outside these regions, the BER increases with increasing clipping ratio because of the rise in the quantization noise effect, and decreasing the

clipping ratio causes the creation of in-band/out-band noise due to clipping distortion. This result indicates that the proposed PON can reduce the DAC/ADC bit resolution by 1 bit, i.e., from 7 bits to 6 bits and reduce the clipping ratio by ≥1 dB to achieve BERs within the FEC limit. This behaviour clearly demonstrates that the proposed PON with the application of the DFT-spread technique allows the transceiver to adopt low clipping ratios, without greatly compromising the BER performances. The clipping limits the signal power within a predetermined range of amplitude threshold, as such, an optimum clipping ratio which optimizes the OSNR is chosen for optimum system performance. Based on the above, the identified optimal clipping ratio values and a DAC/ADC resolution of 7 bits were chosen to enable the ONUs to operate at their optimal conditions. The obtained results for the optimal parameters are presented in Table 4.1.

4.4 Upstream DFT-spread Hybrid OFDM-DFMA PON Performance

Utilizing the optimal ONU operating conditions identified in section 4.3 and the transceiver parameters listed in Table 4.1, in this section, the investigations of the upstream transmission performance of a spectrally overlapped hybrid OFDM-DFMA PON incorporating the DFT-spread technique are undertaken in terms of upstream performance tolerance to limited DAC/ADC quantization bits, BER performance, maximum aggregate upstream signal transmission rate, and impact of digital filter impairments. To highlight the advantages associated with the proposed technique, the upstream transmission performances of the hybrid OFDM-DFMA PON utilizing spectrally overlapped digital orthogonal filtering are also computed and are treated as benchmarks.

4.4.1 Performance Tolerance to Limited DAC/ADC Quantization Bits

In this subsection, simulations are carried out to demonstrate the performance tolerance of the proposed technique to limited DAC/ADC quantization bits, and to determine the minimum number of required DAC/ADC quantization bits to achieve BERs at or below the FEC limit. The DAC/ADC quantization bits vary from 4 to 8, and the ROP is fixed at -7 dBm. The results are presented in Fig. 4.5 for the 25 km SSMF IMDD PON.

Fig. 4.5 reveals that, while adopting the optimal clipping ratios of 11 dB or 12 dB as determined in section 4.3.3, the case including DFT-spread can reach BERs at the FEC limit when the

DAC/ADC resolution is as low as 6 bits. On the other hand, for the case excluding DFT-spread, the minimum number of required quantization bits to achieve similar performance extends from 6-bit to 7-bit DAC/ADC resolution. This numerical result confirms that the application of DFT-spread in the proposed PON can improve the upstream performance tolerance against quantization noise induced by the limited quantization bits. Most importantly, from a practical PON operation point of view, such an improvement is highly desirable for PON designs, as lower DAC/ADC hardware achieves both lower cost and lower power consumption.

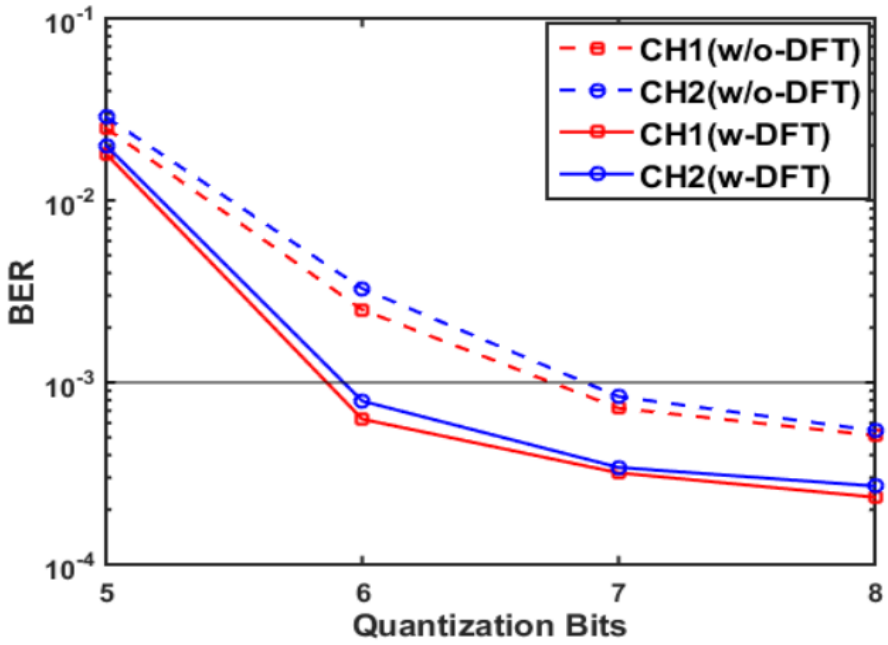

Fig. 4.5. BER versus quantization bits over 25 km SSMF IMDD PON.

From the above discussion, it is easy to understand that the proposed DFT-spread spectrally overlapped hybrid OFDM-DFAM PON confirms the practicability of utilizing the DFT-spread technique in the PONs reported in [6], and that the proposed PON has the ability to reduce the minimum required DAC/ADC bit resolution and, consequently, minimize the transceiver DSP complexity, thus making the proposed PON a promising solution for implementation in future cost-sensitive 5G networks, and beyond.

4.4.2 Upstream Transmission Performance

Fig. 4.6 is the overall channel BER as a function of the received optical power where the total optical launch power into the SSMF transmission system is fixed at 0 dBm. In computing Fig. 4.6, a resolution of 7 bits was used for the ADC/DAC, as shown in Fig. 4.5. All other parameters are specified in Table 4.1.

It can be seen in Fig. 4.6 that, for the case of including/excluding DFT-spread, the calculated channel-1 (CH1) and channel-2 (CH2) BER performances are identical across the entire received optical power range, and these two channels also have very similar signal bit rates. Most importantly, for the same signal bit rates, the case with DFT-spread can achieve an upstream power budget improvement of more than 1.4 dB compared to the case without DFT-spread. Such performance improvement is mainly because of the DFT-spread-induced PAPR reduction, resulting in a considerable decrease in quantization noise, thus giving rise to an increase in the effective OSNRs.

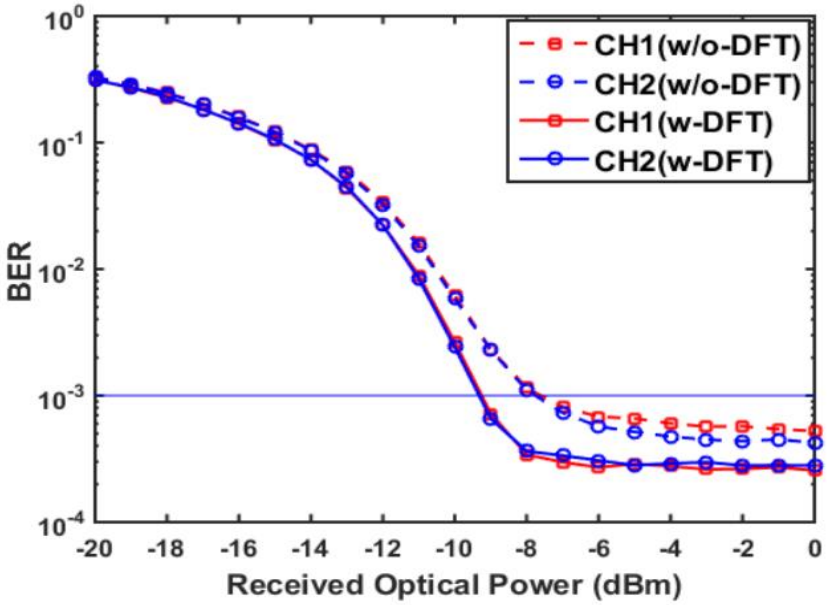

Fig. 4.6. BER versus received optical power after 25 km SSMF IMDD PON transmission system when 7 bits resolution is considered.

4.4.3 Impacts of Digital Filter Parameters on Maximum Aggregated Upstream Transmission Rates

For the proposed PON simultaneously supporting two ONUs, the aggregated upstream signal transmission capacities versus excess of bandwidth parameter, α, are shown in Fig. 4.7. The α parameter governs the bandwidth occupied by each ONU sub-band signal and the rate at which the side lobes of the sub-band signals decay. In obtaining Fig. 4.7, the digital filter length listed in Table 4.1 was adopted. In addition, adaptive bit-loading was applied to all subcarriers involved in each ONU for all the cases of including and excluding DFT-spread. To implementing adaptive bit-loading, the highest possible signal modulation formats within the range from DBPSK to 256-QAM were adaptively selected according to the channels' spectral

characteristics to ensure that the BER across all subcarriers for each sub-band could reach FEC limit of 1×10^{-3}. For each ONU sub-band, the achievable bit rate was $R_b = f_s \sum_{k=1}^{N_s} n_b/2(N_s+1)(1+CP)M$, where n_{bk} is the number of binary bits conveyed by the k-th subcarrier within one OFDM symbol period, N_s denotes the number of data-bearing subcarriers, and C_p indicates the overhead parameter associated with the cyclic prefix and training sequences. The excess of bandwidth, α, was set to vary in the range $0 \leq \alpha \leq 1$. The ROPs are fixed at -6 dBm for both cases.

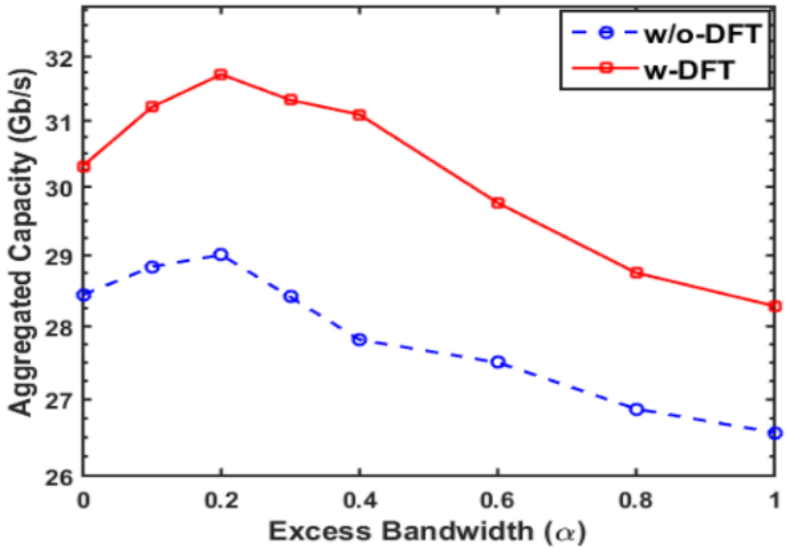

Fig. 4.7. Aggregated rate versus excess bandwidth over a 25 km SSMF IMDD PON transmission system when a 7 bits resolution is considered.

It can be seen in Fig. *4.7* that, for both considered cases, the aggregate upstream signal transmission rate peaks at an α factor value of 0.2, and then reduces steadily as α increases above 0.2. Most importantly, for the case including DFT-spread, the maximum aggregate upstream signal transmission rate increases by up to 10% for α = 0.2, compared to the case without DFT-spread. This performance enhancement is due to the overall improvement in SNRs across the subcarriers, thus allowing higher modulation formats to be used. To understand the physical mechanisms causing an optimum α value of 0.2, the impact of α on the digital filter responses should be observed. For low α values < 0.2, the finite filter-length induced filter magnitude response ripples can impact on performance. For α = 0 and the up-sampling factor M = 2, the I-phase digital filter has a perfectly flat response [26], which is equivalent to a case where the digital filter length (channel-1) is reduced to one, while the Q-phase filter (channel-2) has significant frequency response ripples, as shown in Fig. 4.8(a) and (b), respectively [26]. The length of the filter mainly impacts the sharpness of the filter edge in

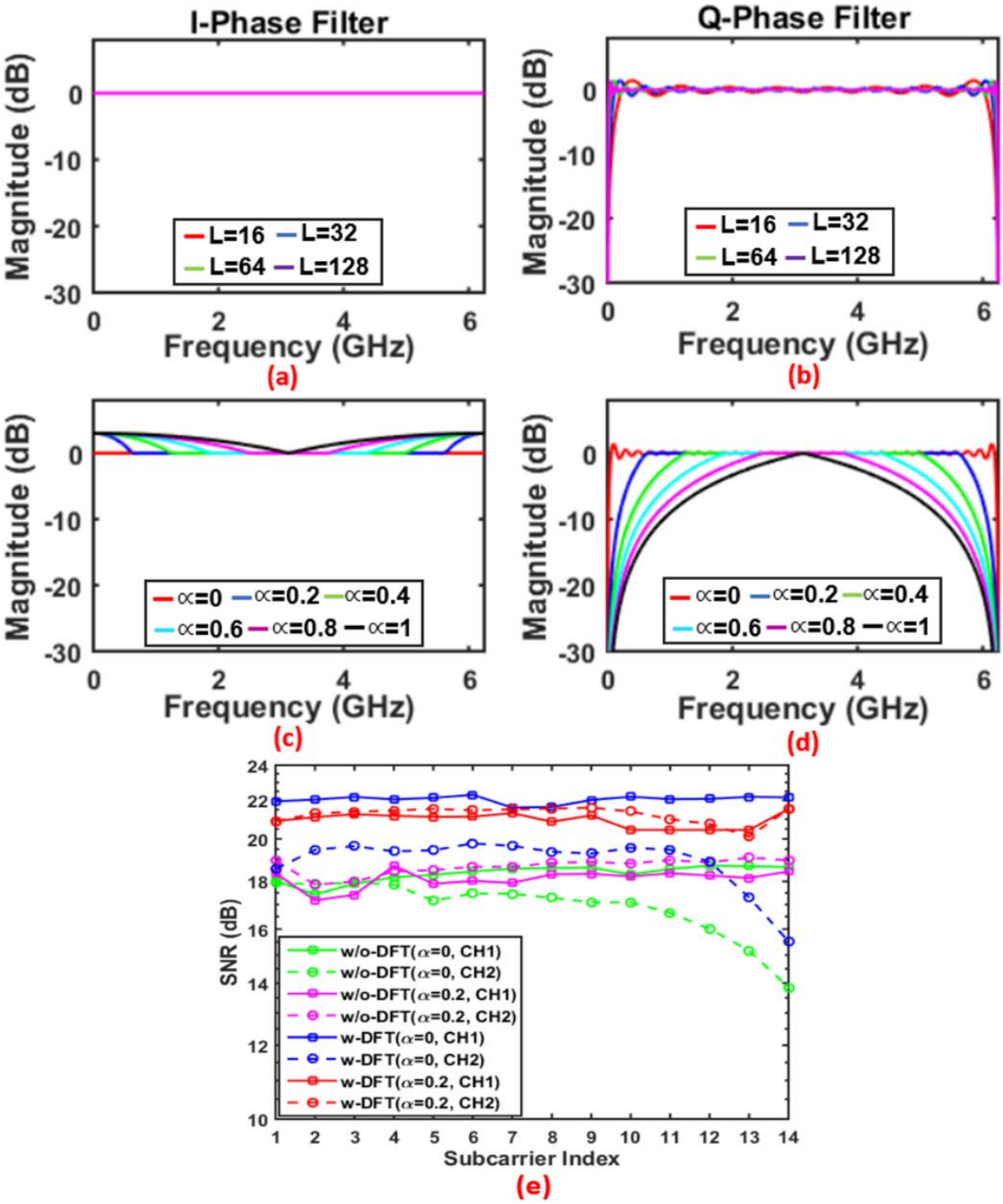

Fig. 4.8. Magnitude response for excess of bandwidth of α=0 for (a) I-phase filter with digital filter lengths 16, 32, 64 and 128 (b) Q-phase filter with digital filter lengths 16, 32, 64 and 128. Magnitude response for filter length 64 for (c) I-phase filter with excess of bandwidth (α) ranging from 0 to 1, and (d) Q-phase filter with excess of bandwidth (α) ranging from 0 to 1. (e) Comparison of SNR distribution across all the subcarriers, using excess bandwidth of α = 0 and optimal value of α = 0.2 for both I-phase (CH1), and Q-phase (CH2).

the case of the Q-phase filter. On the other hand, as shown in Fig. 4.8(c) and (d), as α starts to increase, there is a boost in the magnitude response of the I-phase filter and an attenuation in the magnitude response of the Q-phase filter. In addition, the increasing distortion of the filter responses causes strong unwanted cross-channel-induced interference due to loss of orthogonality. It should be noted that the filter response distortions occur due to the aliasing effect as the employed subwavelength occupies the whole Nyquist band, and a narrower digital filter bandwidth can be observed when $\alpha > 0$ [26]. The increasing α value also reduces the unwanted frequency response ripples in the Q-phase filter. These effects combine to give an overall increase in subcarrier SNR as α increases from 0 to 0.2, beyond which there is an overall reduction in subcarrier SNR.

To observe the effect of α on subcarrier SNRs, with the simultaneous presence of both channels, the SNR performances for all subcarriers for the 25 km SSMF transmission are plotted in Fig. 4.8(e), utilizing the optimum α parameter value of 0.2 and zero excess of bandwidth ($\alpha = 0$) for performance comparisons. In obtaining this figure, the ROP was fixed at -6 dBm. Fig. 4.8(e) shows that the SNRs are similar for CH1 when $\alpha = 0$ and $\alpha = 0.2$; however, there is an obvious improved SNR for subcarrier index 12-14 of CH2 when $\alpha=0.2$. Fig. 4.8e. also shows that the SNR curve for CH1 is almost constant with respect to the subcarrier index for the optimal α value. In comparison with the Q-phase channel for both cases, the high SNR observed for the I-phase channel is mainly a result of the boost in magnitude response, as shown in Fig. 4.8(c). The obtained results indicate that there is an optimum α factor value that minimizes digital filter impairments and subsequently maximizes the upstream transmission rate of both channels.

4.5 Conclusions

The novel DFT-spread spectrally overlapped hybrid OFDM-DFMA PON was proposed and numerically simulated for a 25 km IMDD SSMF transmission system. To the best of our knowledge, this is the first work applying the DFT-spread technique to a hybrid OFDM-DFMA PONs utilizing spectrally overlapped digital orthogonal filtering, in order to simultaneously reduce PAPRs, optimize clipping ratios, and reduce the minimum required DAC/ADC quantization bits, whilst maintaining the upstream transmission performances without increasing the transceiver complexity. The simulation results have showed that, compared to the previously reported PONs, the proposed PON can reduce the PAPR by more than 2 dB, and the optimal clipping ratio is reduced by 1dB. Such a PAPR reduction is independent of the

adopted digital filter characteristic, signal modulation format, and ONU sub-band signal spectral location. As a direct result of the PAPR reduction, the proposed PON can reduce the minimum required DAC/ADC resolution bits by more than 1-bit, whilst achieving BERs below the FEC limit. In addition, the proposed PON can improve the upstream power budget by more than 1.4 dB and increase the aggregate upstream signal transmission rate by up to 10%.

It is well known that the speeds of DACs and ADCs play important roles in limiting the maximum achievable signal transmission capacity for DSP-based signal transmission techniques. However, high-speed DACs and ADCs can be very expensive. To achieve a specific signal transmission capacity, the proposed technique has the potential of allowing low-speed DACs/ADCs to be utilized to produce/receive targeted baseband signals, which can then be up-converted to the targeted sub-bands by low-cost electrical components. This could significantly reduce the overall ONU transceiver cost. In addition, the proposed-technique-induced PAPR reductions also considerably relax the requirements of using expensive electrical/optical devices with large linear operation regions and high-resolution DACs/ADCs. As a direct result, the proposed technique may offer a valuable solution capable of reducing the overall network installation cost for implementation in cost-sensitive application scenarios.

The experimental demonstrations of PtP and PtMP spectrally overlapped hybrid OFDM-DFMA PON transmissions with/without DFT-spreading are currently being undertaken in our research laboratory and corresponding results will be reported elsewhere in due course.

References

[1] Dogra, A.; Jha, R.K.; Jain, S. A survey on beyond 5G network with the advent of 6G: architecture and emerging technologies. IEEE Access 2021, 9, 67512-67547.

[2] Ruffini, M. Multidimensional convergence in future 5G networks. J. Light. Technol. 2017, 35, 535-549.

[3] Gavrilovska, L.; Rakovic, V.; Ichkov, A.; Todorovski, D.; Marinova, S. Flexible CRAN: radio technology for 5G. 13th Int. Conf. on Advanced Technol., Systems and Services in Telecom. (TELSIKS), 2017, 255-264.

[4] Ramantas, K.; Antonopoulos, A.; Kartsakli, E.; Mekikis, P.; Vardakas J.; Verikoukis, C. A CRAN based 5G platform with a fully virtualized, SDN controlled optical/wireless fronthaul. 20th Int. Conf. on Transp. Opt. Netw. (ICTON) 2018, 1-4.

[5] Fu, M.; Zhuge, Q.; Liu, Q.; Fan, Y.; Zhang, K.; Hu, W. Advanced optical transmission technologies for 5G fronthaul. 24th OptoElectronics and Commun. Conf. (OECC) and Int. Conf. on Photo. in Switch. and Comp. (PSC) 2019, 1-3.

[6] Sankoh, A.; Jin, W.; Zhong, Z.Q.; He, J.; Hong, Y.; Giddings, R.P.; Pierce, I.; O'Sullivan, M.; Lee, J.; Durrant, T.; Tang, J.M. Hybrid OFDM-Digital filter multiple access PONs utilizing spectrally overlapped digital orthogonal filtering. IEEE Photo. J. 2020, 12, 1-11.

[7] Dong, Y.X.; Giddings, R.P.; Tang J.M. Hybrid OFDM-digital filter multiple access PONs. J. Light. Technol. 2018, 36, 5640–5649.

[8] Cvijetic, N. OFDM for next generation optical access networks. Opt. Fibre Commun. Conf. and Exposition and the Nat. Fibre Opt. Eng. Conf. 2011, 1-30.

[9] Silva, J.A.L.; Cartaxo, A.V.T.; Segatto, M.E.V. A PAPR reduction technique based on a constant envelope OFDM approach for fibre nonlinearity mitigation in optical direct-detection systems. J. Opt. Commun. Netw. 2012, 4, 296-303.

[10] Vappangi, S.; Mani, V.V. A low PAPR DST-based optical OFDM (OOFDM) for visible light Communication. 21st Int. Symposium on Wireless Personal Multimedia Commun. (WPMC) 2018, 200-205.

[11] Xu, W.; Wu, M.; Zhang, H.; You, X.; Zhao, C. ACO-OFDM-specified recoverable upper clipping with efficient detection for optical wireless communications. IEEE Photo. J. 2014, 6, 1-17.

[12] Popoola, W.O.; Ghassemlooy, Z.; Stewart, B.G. Pilot-Assisted PAPR reduction technique for optical OFDM communication systems. J. Light. Technol. 2014, 32, 1374-1382.

[13] Nadal, L.; Moreolo, M.S.; Fabrega, J.M.; Junyent, G. Comparison of peak power reduction techniques in optical OFDM systems based on FFT and FHT. 13th Int. Conf. on Transparent Opt. Netw. 2011, 1-4.

[14] Shieh, W.; Tang, Y.; Krongold, B.S. DFT-spread OFDM for optical communications. 9th Int. Conf. on Opt. Internet (COIN) 2010, 1-3.

[15] Bai, R.; Wang, Z.; Jiang, R.; Cheng, J. Interleaved DFT-spread layered/enhanced ACO-OFDM for intensity-modulated direct-detection systems. J. Light. Technol. 2018, 36, 4713-4722.

[16] Ma, J.; Chen, M.; Wu, K.; He, J. Performance enhancement of probabilistically shaped OFDM enabled by precoding technique in an IM-DD system. J. Light. Technol. 2019, 37, 6063-6071.

[17] Wang, Y.; Yu, J.; Chi, N. Demonstration of 4×128-Gb/s DFT-S OFDM signal transmission over 320-km SMF with IM/DD. IEEE Photo. J. 2016, 8, 1-9.

[18] Chen, M.; Xiao, X.; Huang, Z.R.; Yu, J.; Li, F.; Chen, Q.; Chen, L. Experimental demonstration of an IFFT/FFT size efficient DFT-spread OFDM for short reach optical transmission systems. J. Light. Technol. 2016, 34, 2100-2105.

[19] Dong, Y.X.; Jin, W.; Giddings, R.P.; O'Sullivan, M.; Tipper, A.; Durrant, T.; Tang, J.M. Hybrid DFT-spread OFDM-digital filter multiple access PONs for converged 5G networks. IEEE J. of Opt. Comm. and Netw. 2019, 11, 347-353.

[20] Wake, D.; Nkansah A.; Gomes, N.J. Radio over fibre link design for next generation wireless systems. J. of Light. Technol. 2010, 28, 2456-2464.

[21] Liu, X.; Zeng, H.; Chand N.; Effenberger, F. Efficient mobile fronthaul via DSP-based channel aggregation. J. of Light. Technol. 2016, 34, 1556-1564.

[22] Chandrasekhar, S.; Liu, X. OFDM based super channel transmission technology. J. Light. Technol. 2012, 30, 3816-3823.

[23] Jung, S.M.; Mun, K.H.; Jung, S.Y.; Han, S.K. Optical-beat-induced multi-user-interference reduction in single wavelength OFDMA PON upstream multiple access systems with self-homodyne coherent detection. J. Light. Technol. 2016, 34, 2804-2811.

[24] Jin, W.; Zhong, Z.Q.; He, J.X.; Sankoh, A.; Giddings, R.P.; Hong, Y.H.; Pierce, I.; O'Sullivan, M.; Laperle, C.; Lee, J.; Mariani, G.; Durrant, T.; Tang, J.M. Experimental demonstrations of hybrid OFDM-digital filter multiple access PONs. IEEE Photon. Technol. Lett. 2020, 32, 751–754.

[25] Tang J.M.; Shore, K.A. 30-gb/s signal transmission over 40-km directly modulated DFB-laser-based single-mode-fibre links without optical amplification and dispersion compensation. J. of Light. Technol. 2006, 24, 2318-2327.

[26] Bolea, M.; Giddings, R.P.; Tang, J.M. Digital orthogonal filter- enabled optical OFDM channel multiplexing for software-reconfigurable elastic PONs. J. Light. Technol. 2014, 32, 1200–1206.

[27] Bolea, M.; Giddings, R.P.; Bouich, M.; Aupetit-Berthelemot, C.; Tang, J.M. Digital filter multiple access PONs with DSP-enabled software reconfigurability. J. Opt. Commun. Netw. 2015, 7, 215–222.

[28] Im, G.H.; Harman, D.D.; Huang, G.; Mandzik, A.V.; Nguyen, M.H.; Werner, J.J. 51.84 Mb/s 16-CAP ATM LAN standard. IEEE J. Sel. Areas Commun. 1995, 13, 620–632.

[29] Dong, Y.X.; Al-Rawachy, E.; Giddings, R.P.; Jin, W.; Nesset, D.; Tang, J.M. Multiple channel interference cancellation of digital filter multiple access PONs. J. Light. Technol. 2017, 35, 34–44.

[30] Al-Rawachy, E.; Giddings, R.P.; Tang, J.M. Experimental demonstration of cross-channel interference cancellation for digital filter multiple access PONs. Opt. Express 2016, 25, Th3C.5.

[31] Agrawal, G.P. Fibre-optic communication systems, 3rd ed. Rochester, NY, USA, 2002, pp. 133–176.

[32] Zeng, Y.; Dong, Z.; Chen, Y.; Wu, X.; He, H.; You, J.; Xiao, Q. A Novel CAP-WDM-PON employing multi-band DFT-spread DMT signals based on optical Hilbert-transformed SSB modulation. IEEE Access 2019, 7, 29397–29404.

5. HYBRID SSB OFDM-Digital Filter Multiple Access PONS

Contents

5.1 Introduction

To meet the high bandwidth, low latency and ultra-dense elastic connection requirements for 5G and beyond networks, CANs have been proposed to seamlessly converge optical access networks, metropolitan area networks and MFH/MBH networks [1]. To practically implement CANs, an IMDD-based PON is widely considered to be a promising candidate due to its excellent cost-effectiveness and power-efficiency [2,3]. On the other hand, to fully accommodate the explosive expansion of various 5G and beyond mobile traffic having a wide diversity of characteristics, SDN with its network control functionalities further extended to physical layer is also highly desirable for dynamically providing elastic network slicing, adaptive multicarrier modulation, simple but efficient network management, optimum network resource utilization as well as dynamic on-demand connections/services.

To address the aforementioned technical challenges, a DFMA PON has been proposed [4], which utilizes SDN-controllable DOFs to dynamically and independently multiplex and demultiplex multiple channels of arbitrary bandwidth granularity without requiring expensive analogue optical/electrical components. Extensive theoretical investigations and experimental demonstrations of the DFMA PON have been conducted in the cost-effective IMDD application scenarios [4-6]. However, the number of required digital filtering process implemented in the OLT-embedded DSP function is proportional to ONU count, therefore a large number of ONUs simultaneously accommodated by the PON can unavoidably result in relatively high OLT DSP complexity and operational expenditure.

To solve this technical issue, very recently, a hybrid OFDM-DFMA PON based on IMDD has been proposed and extensively explored [7,8], where for upstream transmissions, individual ONUs use their embedded digital shaping filters (SFs) to locate the produced OFDM signals at different sub-wavelength spectral regions by following the operating principle similar to the DFMA PONs. While in the OLT, a single FFT operation and the following data recovery DSP processes are implemented in a pipelined way to simultaneously demultiplex and recover the signals from various ONUs without utilizing parallel MFs. In comparison with the DFMA

PONs, the hybrid OFDM-DFMA PONs have the following salient features, including [7]: 1) considerable relaxation of the stringent requirements on high complexity of the ONU transmitter-embedded SFs due to the enhanced system robustness against digital filter characteristic variations; 2) great simplification of the OLT DSP complexity and significant

reductions in OLT expenditure and power consumption due to the elimination of the MFs and the adopted pipelined signal recovery process; 3) considerable improvements in both upstream power budget and upstream performance robustness against practical transceiver/system impairments because of the improved system tolerance to multiple channel interferences and signal distortions, and 4) inherent transparency to the existing OFDM-based 4G networks.

However, in the previously reported hybrid OFDM-DFMA PONs, each individual sub-wavelength just conveys a single digitally filtered DSB OFDM signal. The LSB and the USB of a digitally filtered DSB OFDM signal convey identical data information at different RFs. It therefore leads to an almost halved spectral efficiency and a reduction in signal transmission capacity compared to the DFMA PONs [4].

To effectively address the above disadvantages and still maintain the aforementioned salient features associated with the previously-reported hybrid DSB OFDM-DFMA PONs, in this chapter, for IMDD application scenarios, a novel PON architecture termed hybrid SSB OFDM-DFMA PON is proposed and extensively investigated, for the first time, where in the upstream, without implementing the sophisticated Hilbert transform DSP operation, a complex SSB OFDM signal generation process and software-reconfigurable digital orthogonal filtering, as demonstrated in section 5.2, are utilized in each ONU. Each individual ONU can occupy a single spectral sideband or two independent spectral sidebands within the same sub-wavelength spectral region. In the OLT, for demultiplexing and demodulating the SSB OFDM signals from various ONUs, very similar to the previously reported hybrid DSB OFDM-DFMA PON, a single FFT operation and its following signal recovery processes are performed in a pipelined way without either utilizing digital MFs or implementing the Hilbert transform DSP operation. The elimination of the conventional Hilbert transform DSP operation in both the ONUs and the OLT can considerably decrease the transceiver DSP complexity.

Our results indicate that similar to the hybrid DSB OFDM-DFMA PONs, the proposed hybrid SSB OFDM-DFMA PONs can still offer numerous salient advantages including: 1) excellent robustness against digital filter characteristic variations; 2) ONU count-independent negligible channel interferences when adopting optimum digital filter length and 3) inherent transparency to the 4G networks. In addition to the aforementioned advantages, in comparisons with the DSB cases, the proposed hybrid SSB OFDM-DFMA PON also possesses the unique features listed below:

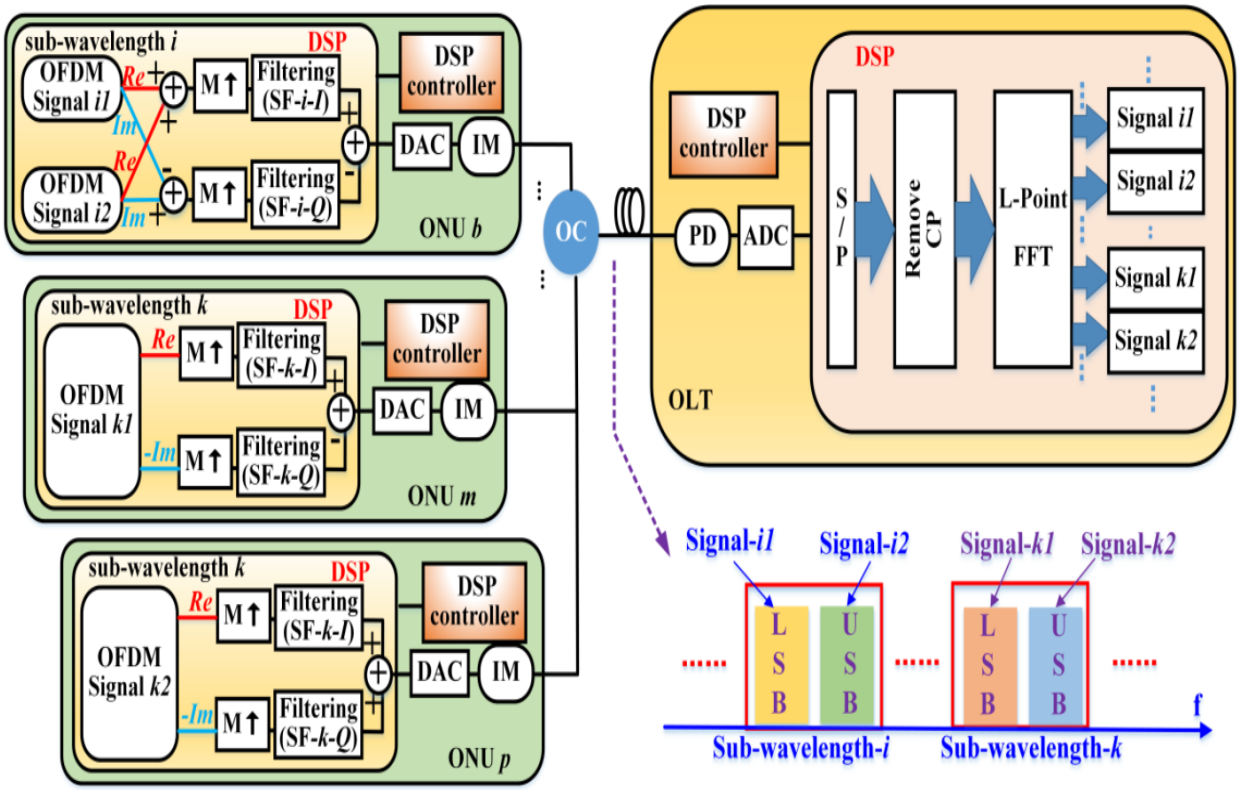

Fig.5.1 Schematic diagram of the proposed IMDD hybrid SSB OFDM-DFMA PON without either performing the Hilbert transform operation or utilizing matching filters. SF: shaping filter. I/Q: I-phase/Q-phase digital filter. M↑: digital-domain up-sampling operation by a factor of M. DAC/ADC: digital-to-analogue/analogue-to-digital conversion. IM: intensity modulation. PD: photodetector. S/P: serial-to-parallel conversion. CP: cyclic prefix. FFT: fast Fourier transform. LSB/USB: lower/upper sideband.

1. >2dB reductions in the PAPRs of the digitally filtered signals. Such PAPR reductions are independent of the digital filter characteristics and modulation formats as well as signal spectral locations. The reduced PAPRs can also lead to >2dB reductions in optimum signal clipping ratio.
2. >1-bit reductions in minimum required DAC/ADC resolution bits for achieving BERs of 1×10-3. Such resolution reductions are mainly because of the SSB technique-induced decreases in PAPRs of the digitally filtered OFDM signals.
3. Almost doubled maximum aggregated upstream signal transmission capacity for fixed overall signal transmission bandwidth for the SSB and DSB cases. In addition, such a significant improvement in upstream signal transmission capacity does not affect the achievable ONU optical launch power dynamic ranges i.e., there exist almost identical

ONU optical launch power dynamic ranges for the above-mentioned two PON architectures.

4. For delivering similar upstream signal transmission capacity between two considered PON architectures, a halved overall signal transmission bandwidth and a >2.5dB upstream system power budget improvement are achievable. Moreover, >1.2dB improvements in differential optical launch power dynamic range are also observed for the ONUs locating at high frequency spectral regions. The halved overall bandwidth requirement allows the utilization of low-cost and low-bandwidth optical/electrical components, thus reducing the overall transceiver costs.

5.2 Theoretical Model of IMDD Hybrid SSB OFDM-DFMA PONs

The proposed hybrid SSB OFDM-DFMA PON is illustrated in Fig. 5.1, in which the more challenging multipoint-to-point upstream operation is considered only. In the hybrid SSB OFDM-DFMA PON, by performing two similar digital filtering processes, each ONU can produce either two different SSB OFDM signals occupying a single sub-wavelength spectral region or a single SSB OFDM signal occupying either a LSB or USB spectral region. In the OLT, a single *L*-point FFT operation is performed to demultiplex and demodulate the multiple SSB OFDM signals from various ONUs without utilizing MFs. Such a MF-free, pipelined OLT DSP procedure is similar to that applied in the previously reported hybrid DSB OFDM-DFMA PONs.

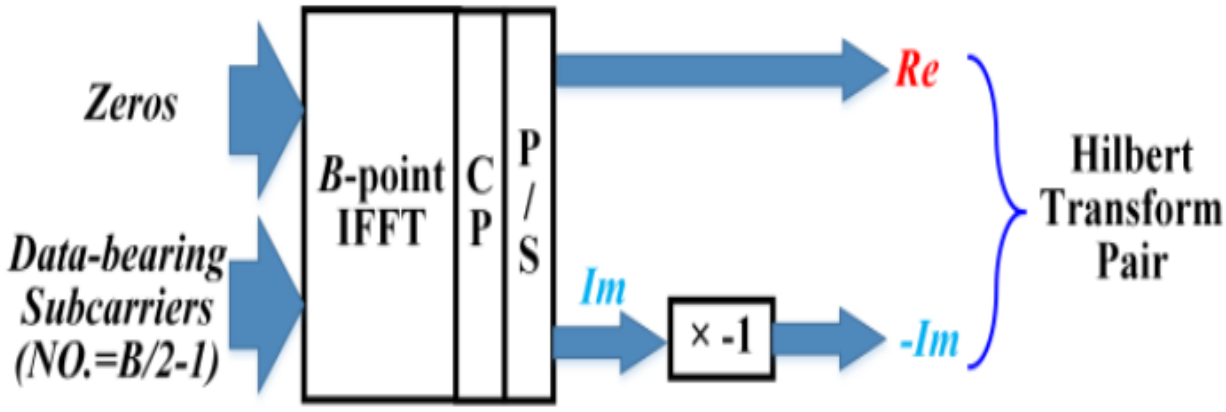

Fig. 5.2 Complex SSB OFDM signal generation process without utilizing the Hilbert transform operation. The real part (Re) and (-1)-multiplied imaginary part (-Im) of the produced OFDM signal form a Hilbert transform pair. CP: cyclic prefix. P/S: parallel-to- serial conversion

In the ONUs, the complex SSB OFDM signal generation process illustrated in Fig. 5.2 is utilized to generate the SSB OFDM signals. As seen in this figure, assuming that the IFFT size is *B*, the *m*-th OFDM symbol at the IFFT output can be expressed as:

$$x_m(n) = \sum_{c=-\frac{B}{2}}^{\frac{B}{2}-1} d_{c,m} e^{j\frac{2\pi c(n-mB)}{B}}, m = 0,1,2 \ldots. \quad (5.1)$$

$$d_{c,m} = \begin{cases} a_{c,m} & -\frac{B}{2}+1 \le c \le -1 \\ 0 & Others \end{cases}$$

where $a_{c,m}$ is the encoded information sample taken by the *c*-th subcarrier of the *m*-th OFDM symbol. The produced complex OFDM signal contains a total of *B*/2-1 data-bearing subcarriers.

After adding the CP and implementing the parallel-to-serial (P/S) conversion, the real part and (-1)-multiplied imaginary part of the produced complex OFDM signal S(t) form a Hilbert transform pair [9], which satisfy the following relationship:

$$Re\big(S(t)\big) = H\big\{-Im\big(S(t)\big)\big\} \quad (5.2)$$

where *Re*(*S*(*t*)) and *Im*(*S*(*t*)) denote the real part and the imaginary part of the signal *S*(*t*) respectively. $H\{\bullet\}$ stands for the Hilbert transform operation [10]. It is also worth mentioning that the real part of the produced complex OFDM signal *Re*(*S*(*t*)) is similar to the corresponding real-valued OFDM signal generated by the Hermitian symmetry in the conventional IMDD hybrid DSB OFDM-DFMA PONs [7]. Therefore, such a signal generation process offers a simple but effective approach of simultaneously producing the required real-valued OFDM signal and its Hilbert transform without performing the Hilbert transform DSP operations.

To generate a LSB OFDM signal occupying the *k*-th sub-wavelength spectral region, as seen in Fig. 5.1, the real part and (-1)-multiplied imaginary part of the produced complex OFDM signal $S_{k1}(t)$ are first up-sampled and then digitally filtered using an orthogonal digital shaping filter pair [4]. The produced LSB OFDM signal at the *k*-th sub-wavelength spectral region can be express as:

$$S_{LSB-k}(t) = M\uparrow\big\{Re\big(S_{k1}(t)\big)\big\} \otimes h_k^I - M\uparrow\big\{-Im\big(S_{k1}(t)\big)\big\} \otimes h_k^Q \quad (5.3)$$

where $M\uparrow$ represents the digital-domain up-sampling operation by a factor of *M*. $\{h^I_k(t), h^Q_k(t)\}$

stand for the *k*-th pair of the orthogonal digital shaping filters with I/Q indicating the I-phase/Q-phase digital filter type [4].

Very similar to the above-described digitally filtered LSB signal generation process, the generation of the *k*-th digitally filtered USB OFDM signal can also be given by:

$$S_{USB-k}(t) = M \uparrow \{Re(S_{k2}(t))\} \otimes h_k^I + M \uparrow \{-Im(S_{k2}(t))\} \otimes h_k^Q \quad (5.4)$$

where $S_{k2}(t)$ is the complex OFDM signal which locates at the USB spectral region of the *k*-th sub-wavelength after digital filtering operation.

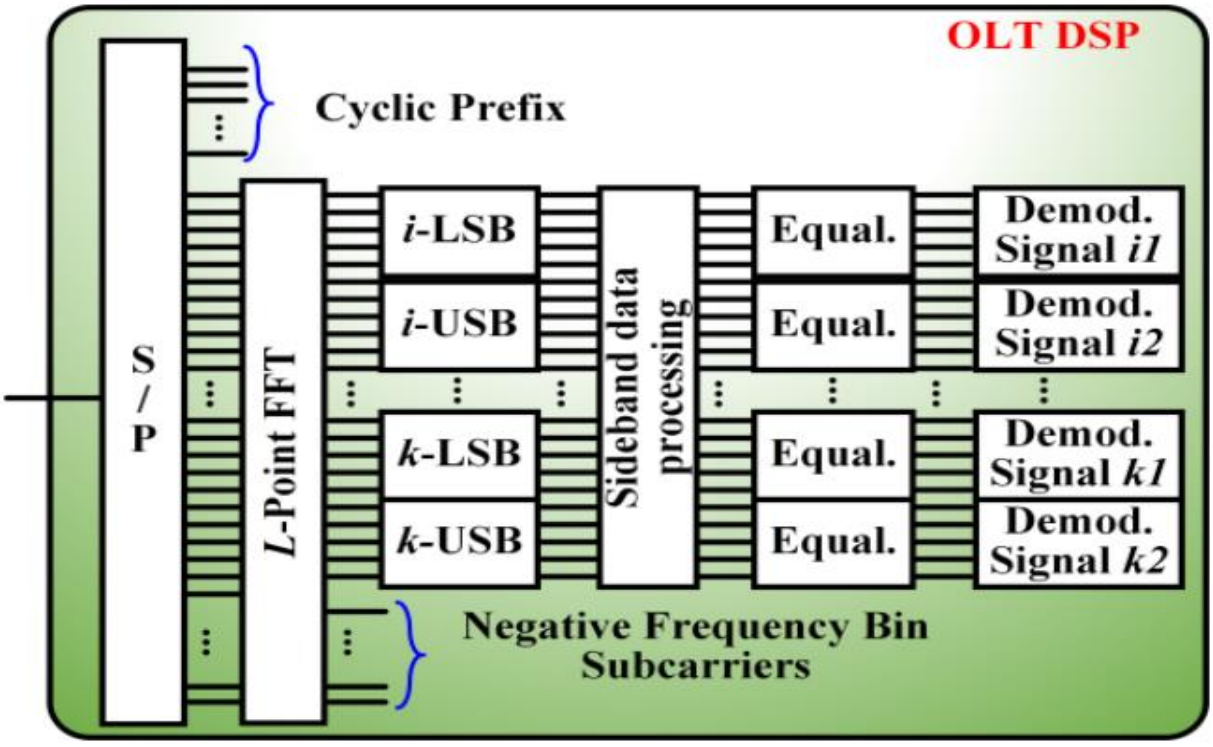

Fig. 5.3. A single FFT operation-enabled signal demultiplexing and recovery process in the OLT DSP. Equal.: equalization. Demod.: demodulation.

After digitally combining the *k*-th LSB signal with the *k*-th USB signal together, the signal occupying the *k*-th sub-wavelength spectral region can be written as:

$$\begin{aligned} S_{subwave-k}(t) &= S_{LSB-k}(t) + S_{USB-k}(t) \\ &= M \uparrow \{Re(S_{k1}(t)) + Re(S_{k2}(t))\} \otimes h_k^I + \cdots \\ &\quad M \uparrow \{-Im(S_{k1}(t)) + Im(S_{k2}(t))\} \otimes h_k^Q \end{aligned} \quad (5.5)$$

Eq. (5.5) implies that the signal generation process of $S_{subwave\text{-}k}(t)$, which contains two different digitally filtered SSB OFDM signals, can be simplified by just performing two similar digital filtering processes only. Such a simplified sub-wavelength signal generation process is also illustrated in Fig. 5.1, in which two SSB OFDM signals at the *i*-th sub-wavelength are simultaneously produced.

After a DAC, the generated analogue electrical signal, $S_r(t)$ is fed to an optical IM to perform the E-O conversion. An optical signal, $S_{opt\text{-}i}(t)$ produced by the *r*-th ONU can be expressed in the form of Eq. (3.3). It is important to mention that the electrical signal, $S_r(t)$, can contain either a single SSB OFDM signal (a LSB OFDM signal or an USB OFDM signal) or two different SSB OFDM signals occupying the *r*-th sub-wavelength spectral region. For the hybrid SSB OFDM-DFMA PON upstream application scenarios, the passively coupled optical signal, $S_{N\text{-}opt}(t)$ from a total number of *N* ONUs can be expressed similar to Eq. (3.4).

To simplify the analytical derivation procedure, linear transmission systems are assumed in this section only. The impacts of nonlinear effects associated with both optical signal modulation/detection and optical signal transmissions over the considered IMDD PON systems are extensively investigated numerically in sections 5.3~5.5 of the chapter. Under the linear transmission system assumption, in the OLT, after O-E conversion and an ADC, the received digital signal consisting of *U* pairs of the LSB and USB OFDM signals is described as:

$$S_{rx}(t) = \sum_{g=1}^{U}\left[S_{LSB-g}(t) + S_{USB-g}(t)\right] \tag{5.6}$$

To recover the received multiple SSB OFDM signals in the OLT, the adopted digital-domain signal demultiplexing and demodulation processes are presented in Fig. 5.3, in which similar to the previously reported hybrid DSB OFDM-DFMA PONs [7], a single *L*-point FFT operation is applied with $L=2B*W$, here *W* stands for the maximum number of digital shaping filter pairs. After the FFT operation, to identify the subcarriers for each SSB OFDM signal, the $L/2$ subcarriers in the positive frequency bin are classified into *W* groups each containing *B* subcarriers. The subcarriers in the different groups locate at different sub-wavelength spectral regions. As such, the first $B/2$ subcarriers in the *i*-th group correspond to the *i*-th LSB signal, while the remaining $B/2$ subcarriers of the same subcarrier group correspond to the *i*-th USB signal. After having identified the LSB signal and the USB signal in each sub-wavelength, the sideband data processing is then applied, in which the subcarriers in all the LSB signals require a conjugation operation and a subcarrier reverse ordering operation, as illustrated in Fig. 5.3.

While for the USB signals, no extra DSP operations are required before the OFDM equalization process. Similar to the reported hybrid DSB OFDM-DFMA PONs [7], the conventional OFDM signal equalization process is still applicable for signal recovery in the proposed PON architecture.

Based on the above theoretical model, it is easy to understand that in the OLT, after the FFT operation, the subcarriers in the negative frequency bin can also be considered for recovering the SSB OFDM signals without compromising the transmission performances. In this chapter, for simplicity, the subcarriers in the positive frequency bin are used in exploring the upstream performances of the proposed PON.

From the practical application point of view, in generating the digitally filtered SSB OFDM signals, the Hilbert-pair approach [4] can be utilized for constructing the required orthogonal digital filter pairs. The impacts of the non-ideal digital shaping filters on the upstream performances are extensively explored in section 5.3~5.5. In the ONUs and the OLT, the digital filtering process and the FFT operation as well as the subcarrier identification process are dynamically controllable by the embedded DSP controllers, as illustrated in Fig. 5.1. Therefore, dynamic and elastic connections can be established between the OLT and the ONUs through the centralized SDN controllers, which work together with their embedded DSP controllers to dynamically set the digital shaping filter pair coefficients and to identify the corresponding subcarriers after the FFT operation.

5.3 Upstream Optimum ONU Operating Conditions

In this chapter, to explore the hybrid SSB OFDM-DFMA PON performances and further demonstrate the advantages associated with the proposed PON, extensive upstream transmission performance comparisons are made between the proposed PON systems and the previously reported hybrid DSB OFDM-DFMA PON systems. To enable these IMDD PONs to operate at their optimum conditions, it is vital to not only explore the PAPRs of the digitally filtered OFDM signals but also identify their corresponding optimum ONU operating conditions. In addition, for maximising the transmission performances of the hybrid DSB OFDM-DFMA PONs, whose performances are regarded as benchmarks for the proposed technique, it is of importance to identify the optimum sideband in each sub-wavelength.

5.3.1 Simulation Models and Key Parameters

A representative IMDD PON with its architecture identical to that illustrated in Fig. 5.1 is considered in upstream numerical simulations. The PON consists of four ONUs each producing an optical signal occupying different DSB/SSB spectral bands. For performance comparisons, here three different cases are considered, including SSB Case-I, SSB Case-II and DSB Case. As shown in Fig. 5.4, in SSB Case-I, by making use of the simplified digital filtering process demonstrated in Fig. 5.1, each ONU produces a sub-wavelength signal simultaneously occupying two different SSB spectral bands. While in SSB Case-II, each ONU only generates a single SSB spectral band. For DSB Case, in each ONU, a single DSB spectral sub-band signal is produced after performing the digital filtering operation.

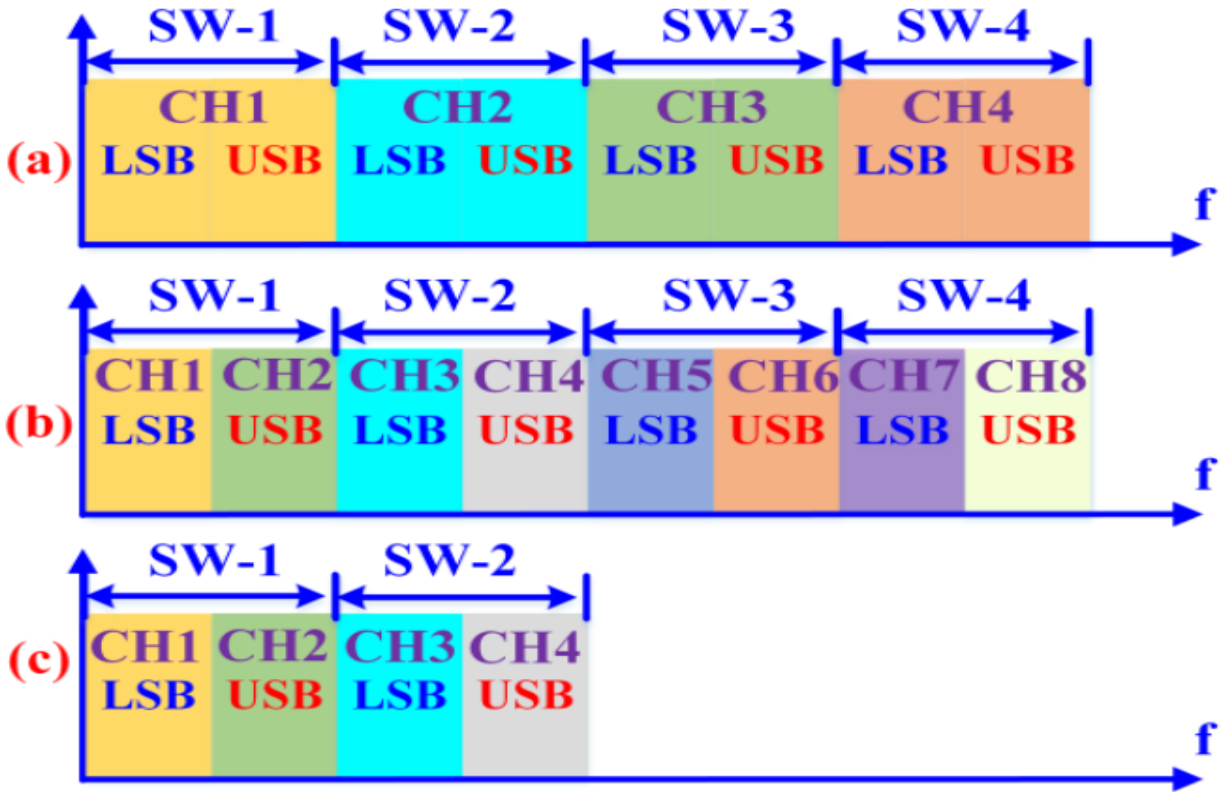

Fig. 5.4. Digitally filtered signal spectral locations for (a) DSB Case, (b) SSB Case-I and (c) SSB Case-II. SW: sub-wavelength. CH: channel

For DSB Case, a real-valued OFDM signal containing 15 data-bearing subcarriers is produced by the Hermitian symmetry in each ONU. While for the two SSB cases, complex OFDM signals each containing 15 data-bearing subcarriers are produced utilizing the complex OFDM signal generation process illustrated in Fig. 5.2. The main parameters for generating the required real-valued and complex OFDM signals are listed in Table 5.I.

Table 5.1 List of Parameters

Parameter	Value	Parameter	Value
DAC/ADC	30GS/s @8-bits	Digital domain Up-sampling Factor	M=8
Digital Filter Length	L=64	Clipping Ratio (DSB case-I / SSB case-I / II)	11dB 9dB 8dB
OFDM IFFT/FFT Size	32/256	Cyclic Prefix	12.5%
OFDM Subcarrier Modulation Format	16-QAM	Data-bearing Subcarriers of Each OFDM Signal	15
Channel Bitrate for SSB Case I/II	6.25 Gb/s	Channel Bitrate for DSB Case I/II	6.25 Gb/s
PIN Detector Sensitivity	-17 dBm	PIN Detector Quantum Efficiencies	0.8
Fibre Dispersion	16 $ps/nm^2/km$	Fibre Dispersion Slope	0.08 $ps/nm^2/km$
Fibre Kerr Coefficient	$2.6e^{-20}$ m^2/W	Fibre Loss	0.2 dB/km

To perform the digital filtering process, four orthogonal digital filter pairs with zero excess of bandwidth are produced by making use of the Hilbert-pair approach [4]. The central frequency of each orthogonal digital filter pair is defined as in Eq. (2.18). For DSB Case, only I-phase digital shaping filters are utilized to digitally filter the up-sampled real-valued OFDM signals. While for SSB Case-I and SSB Case-II, both the I-phase digital filters and the Q-phase digital filters are employed and their corresponding digital filtering processes are explicitly illustrated in Fig. 5.1. After applying the digital filtering process, the signal spectral locations of the considered three cases are shown in Fig. 5.4. SSB Case-I and DSB Case have identical overall signal transmission bandwidths, but the channel number supported by SSB Case-I is doubled. While for SSB Case-II, its corresponding total channel number is identical to DSB Case, but requires a halved overall spectral region.

For performing the E-O conversion in each ONU, similar to the treatment in [7], an ideal optical intensity modulator is utilized, which can completely eliminate the optical beating interference (OBI) effect [11]. For upstream transmissions in practical IMDD PONs, to effectively minimizing the OBI effects, different ONUs can adopt different optical wavelengths and the minimum wavelength spacing between adjacent ONUs can be experimentally identified by

utilizing the approach presented in [12]. For the considered three cases and taking into account the parameters listed in Table 5.I, each DSB/SSB channel has an identical signal bitrate of 6.25Gbit/s. Since DSB Case and SSB Case-II support 4 channels, thus giving rise to an aggregated signal bitrate of 25Gbit/s. While for SSB Case-I, the supported 8 channels result in an aggregated signal bitrate of 50Gbit/s. In addition, in the OLT, an optical attenuator is employed to adjust the optical powers injected into the optical detector.

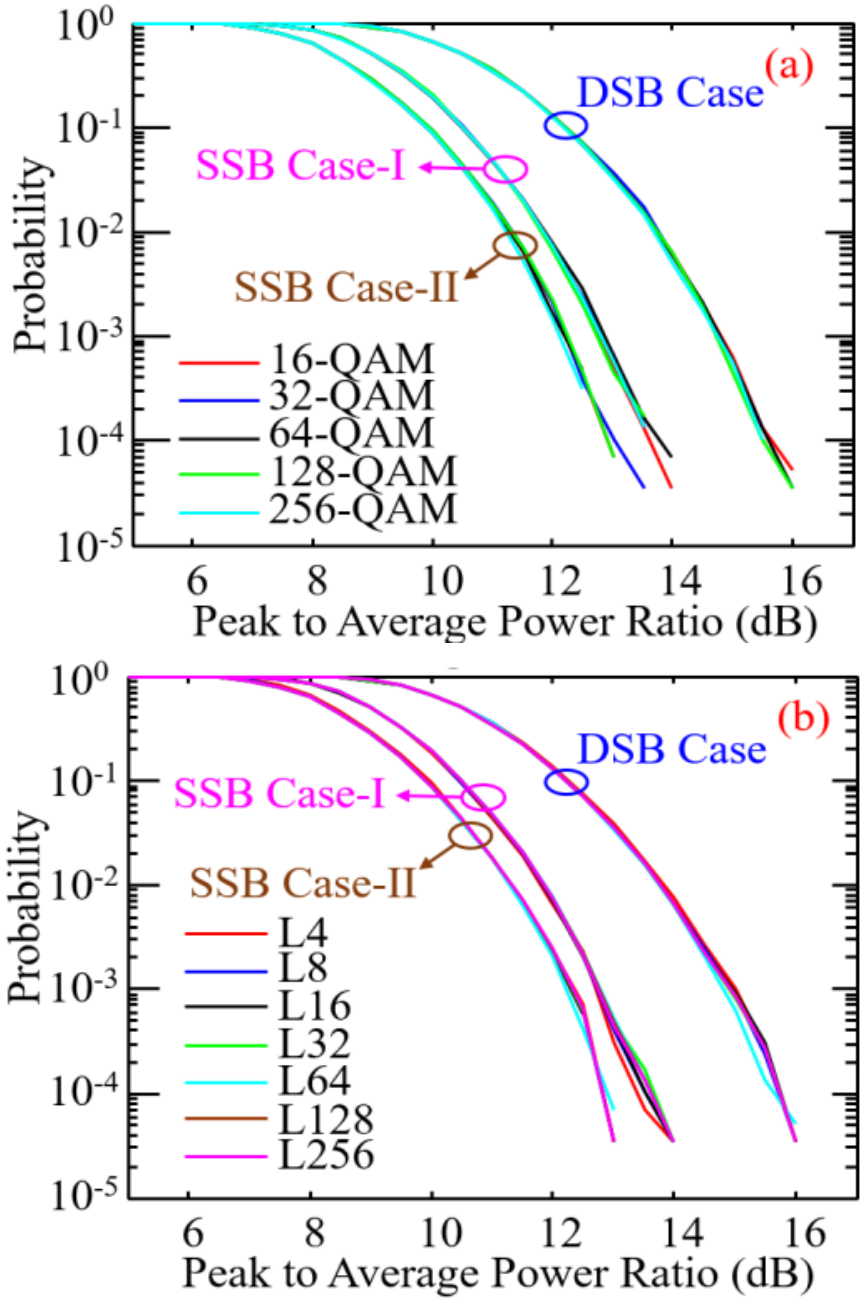

Fig. 5.5. CCDF curves of the digitally filtered signals for (a) various modulation formats and adopting a fixed digital filter length of L=64 and (b) various digital filter lengths and utilizing 16-QAM modulation format.

5.3.2 PAPR of Digitally Filtered OFDM Signals

Utilizing the parameters listed in Table 5.I and the above-stated procedure, the PAPRs of the digitally filtered signals are simulated for the considered three cases. In each case, similar PAPRs can be observed for all the digitally filtered signals. Therefore, for DSB Case and SSB Case-II, the CCDFs of the digitally filtered CH-1 signals are depicted in Fig. 5.5, while for SSB Case-I, the digitally filtered 1st sub- wavelength (SW-1) signal's CCDF curves are plotted in the same figures. It can be seen in Fig. 5.5 that the proposed technique can reduce the PAPRs of the digitally filtered signals by >2dB at the probability of 1×10^{-3}. Such PAPR reductions are independent of the adopted digital filter characteristics and modulation formats as well as the signal spectral locations. In addition, compared with SSB Case-I, SSB Case-II has an extra ~0.5dB PAPR improvement because each digitally filtered signal consists of a single SSB OFDM signal, while SSB Case- I contains two independent SSB OFDM signals. It is easy to understand that the reduced PAPRs can not only improve the system performance robustness to quantization noise induced by the DACs/ADCs with fixed resolution bits, but also relax the stringent requirements on linear dynamic operation ranges of the transceivers-embedded optical/electrical devices.

5.3.3 Optimum Clipping Ratio and DAC/ADC Resolution Bits

To enable the considered SSB/DSB cases to achieve their best performances, the optimum signal clipping ratios and DAC/ADC resolution bits are identified in optical B2B systems for all the considered cases. The CH-3 BER contours versus resolution bits and clipping ratios are illustrated in Fig. 5.6, in obtaining which the ROPs are set to be -11dBm for SSB Case-II and -8dBm for DSB Case and SSB Case-I. These different ROPs for the different cases are selected to not only ensure that BERs of 1×10^{-3} are always achievable when utilizing 8-bit DAC/ADCs, but also clearly illustrate the impact of signal clipping on the BER performances. The results indicate that: 1) the proposed PON can reduce the DAC/ADC resolution bits by at least 1 bit for achieving BERs at FEC limit of 1×10^{-3}; 2) the identified optimum clipping ratios for DSB Case and SSB Case-I/II are 11dB, 9dB and 8dB respectively. For the two SSB cases, their identified optimum clipping ratios are smaller than that identified in DSB Case due to the SSB-induced PAPR reductions. In the following sections, these identified optimum clipping ratios and 8-bit quantization are thus chosen to enable the ONUs to operate at their optimum conditions.

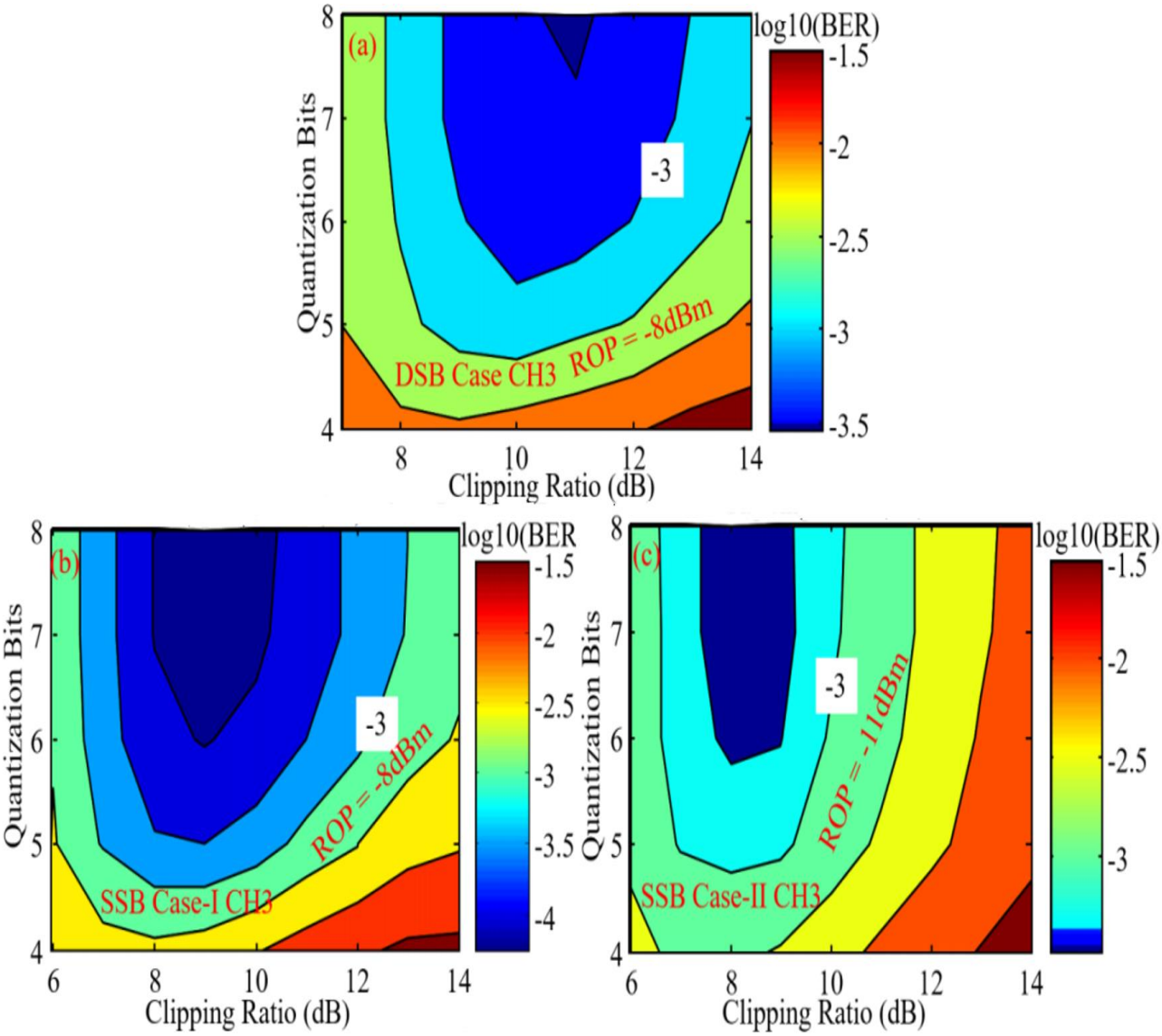

Fig. 5.6. CH-3 BER contour versus quantization bit resolution and clipping ratio. (a) DSB Case, (b) SSB Case-I and (c) SSB Case-II

5.3.4 Optimum Sideband Selection for Hybrid DSB OFDM-DFMA PONs for Various Fibre Transmission Distances

As seen in Fig. 5.7(a), for 30km IMDD hybrid DSB OFDM-DFMA PONs, the signals locating at the 3rd and 4th sub-wavelength spectral regions suffer the severe channel fading effect. For achieving the best transmission performances, the LSB for CH3 and the USB for CH4 suffering the relatively less channel fading effect are thus selected. As a direct result of the transmission distance-dependent channel fading effect, the transmission distance-dependent optimum sideband distribution map is shown in Fig. 5.7(b), in obtaining which the optimum digital filter length of L=64 identified in section 5.4.3 is utilized to minimize channel interferences. As seen

in this figure, the optimum sidebands locate at both sides of the system frequency response dip lines caused by the channel fading effect. In addition, for DSB signals suffering the negligible channel fading effect, the LSB signal always has better transmission performance than the corresponding USB signal of the same sub-wavelength.

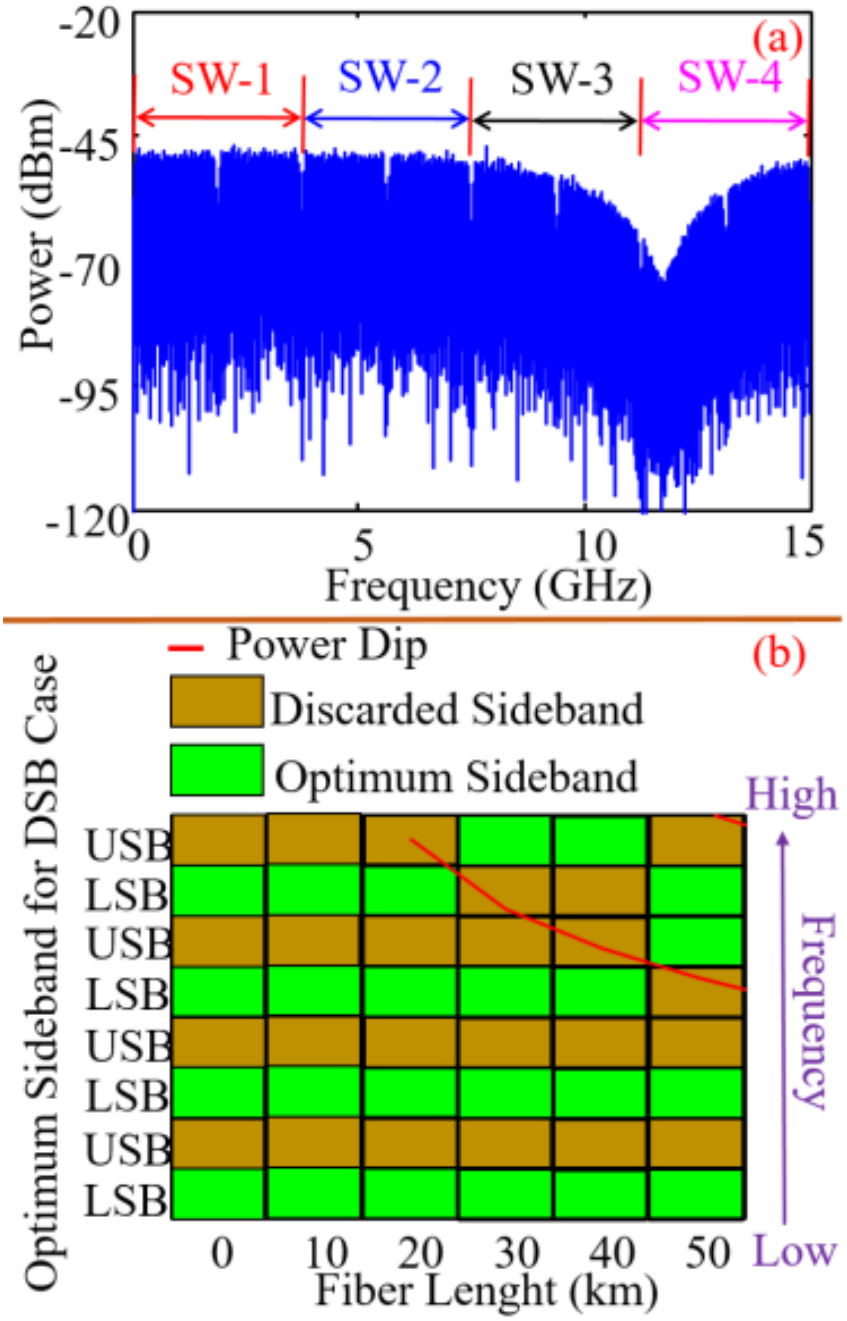

Fig. 5.7. Fibre transmission distance-dependent optimum sideband distributions for the hybrid DSB OFDM-DFMA PONs utilizing digital filtering lengths of L=64. (a) signal spectrum after transmitting over 30km SSMF. (b) optimum sideband distribution map.

5.4 Upstream Transmission Performance of Hybrid SSB OFDM-DFMA PONs

Utilizing the optimum ONU operating conditions identified in section 5.3, the upstream transmission performances of the proposed IMDD hybrid SSB OFDM-DFMA PONs are extensively explored in this section. Spectral attention is focused on the maximum aggregated upstream signal transmission capacity versus reach performances and system robustness against variations in digital filter characteristics. To highlight the advantages associated with the proposed PONs, the upstream transmission performances of the IMDD hybrid DSB OFDM-DFMA PONs are also computed, which are treated as benchmarks.

5.4.1 Upstream Transmission Performances

After 30km SSMF transmission, the BER performances of all the involved channels for the considered three cases are illustrated in Fig. 5.8. The digital filter lengths are set to be L=64 and the data-bearing sub-carriers of each involved OFDM signal are uniformly coded utilizing 16-QAM. In addition, the corresponding optical B2B upstream transmission performances for CH1 are also plotted in the figure for performance comparison.

In Fig. 5.8(a), it can be found that DSB Case supports 4 usable channels with their BERs capable of reaching FEC limit. While for SSB Case-I, since its CH6 and CH7 are not operational due to the channel fading effect, it can thus support total 6 usable channels as seen in Fig. 5.8(b). It implies that the proposed SSB technique can improve the spectral efficiency by a factor of 1.5 when utilizing an identical signal modulation format across all subcarriers. If adaptive bit-loading is adopted for all involved channels, the maximum aggregated upstream capacity can be almost doubled by the proposed technique, as seen in Fig. 5.9.

For SSB Case-II, all the channels suffer the negligible channel fading effect and thus have similar transmission performances. It can be found that DSB Case and SSB Case-II support identical useable channel number. However, SSB Case-II has >2.5dB power budget improvements due to the SSB-induced enhancements in effective OSNR. Our numerical simulation results also show that such power budget improvements are independent of transmission distances and digital filter characteristics. In addition to the above-mentioned power budget improvements, the required signal transmission bandwidth for SSB Case-II is just half of that required by DSB Case, as seen in Fig. 5.4. Such reduced signal transmission

bandwidth requirements allow the transceivers to use low-cost and low-bandwidth optical/electrical devices. It is also worth mentioning the following two aspects: 1) the similar transmission performances of the CH-1 signals between the 30km transmission systems and the optical B2B systems indicate that for all the involved cases, the channels suffering negligible channel fading effect can have negligible performance degradations, and 2) for SSB Case-II, compared to other low frequency channels, CH4 has the better transmission performance, because it suffers less channel interferences as discussed in section 5.4.3.

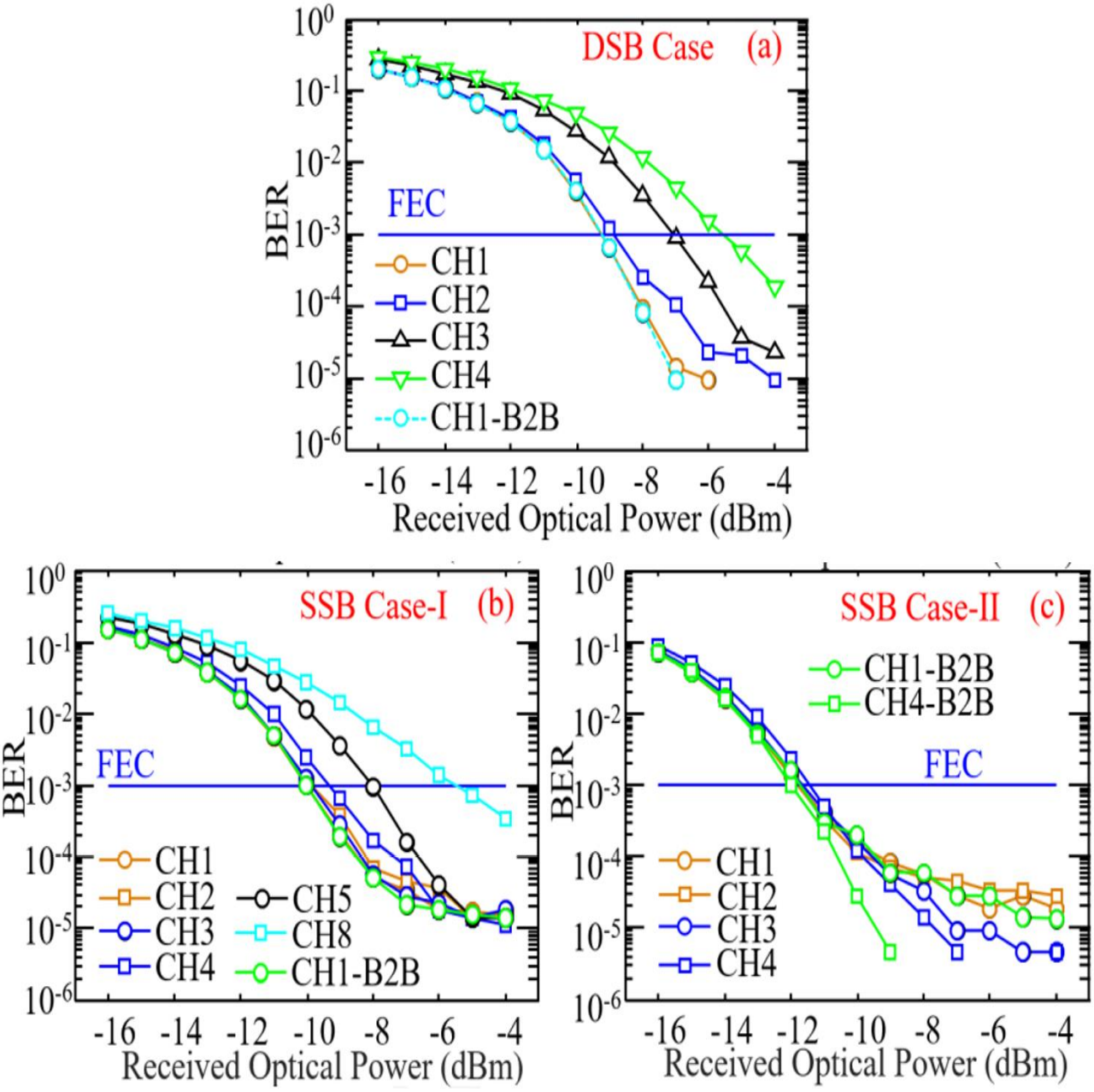

Fig. 5.8. 30km SSMF transmission performances of (a) DSB Case, (b) SSB Case-I and (c) SSB Case-II

5.4.2 Maximum Aggregated Upstream Transmission Capacity versus Reach Performances

As seen in Fig. 5.8(a) and Fig. 5.8(b), the SSB technique considerably improves the spectral efficiency, which can give rise to an improvement in the maximum aggregated upstream transmission capacity. To verify this statement and further examine the performance of the SSB technique in improving upstream signal transmission capacity, adaptive bit-loading is utilized for each involved OFDM signal with signal modulation formats varying from 4/16/32/64-QAM to 128-QAM. The obtained maximum aggregated upstream signal transmission capacity versus reach performance for each considered case is depicted in Fig. 5.9. In addition, the SSB technique-induced capacity improvement ratios are also plotted in the

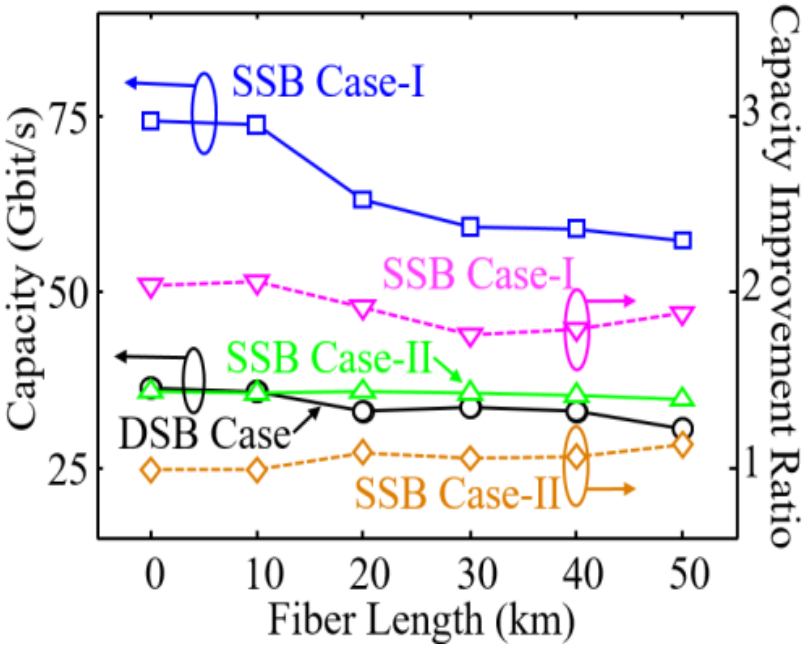

Fig. 5.9. Maximum aggregated upstream transmission capacity versus reach performances and corresponding SSB technique-induced upstream transmission capacity improvement ratio.

figure. The ROPs of -4dBm and the digital filter lengths of L=64 are adopted. Comparing the results between SSB Case-I and DSB Case, it can be found that the upstream signal transmission capacity is almost doubled when the DSB case and the SSB case have similar signal transmission bandwidths. Moreover, the results between SSB Case-II and DSB Case are very similar, as these two cases have identical useable channel numbers. However, compared to DSB Case, the proposed SSB PON can not only halve the required overall signal

transmission bandwidth for delivering the same upstream transmission capacity, but also give rise to >2.5dB power budget improvements as discussed in section 5.4.1.

5.4.3 Impacts of Digital Filter Characteristics on Upstream Transmission Performances

In the hybrid DSB (SSB) OFDM-DFMA PONs, digital filtering is essential in terms of allocating the DSB (SSB) OFDM signals at suitable sub-wavelengths. Generally speaking, a larger digital filter length can result in a better digital filtering performance, but inevitably increases the digital filter DSP complexity [7]. It is therefore vital to explore the impacts of the digital filter characteristics on the upstream transmission performance, based on which the minimum digital filter length can be identified for achieving the targeted performances in a specific application scenario.

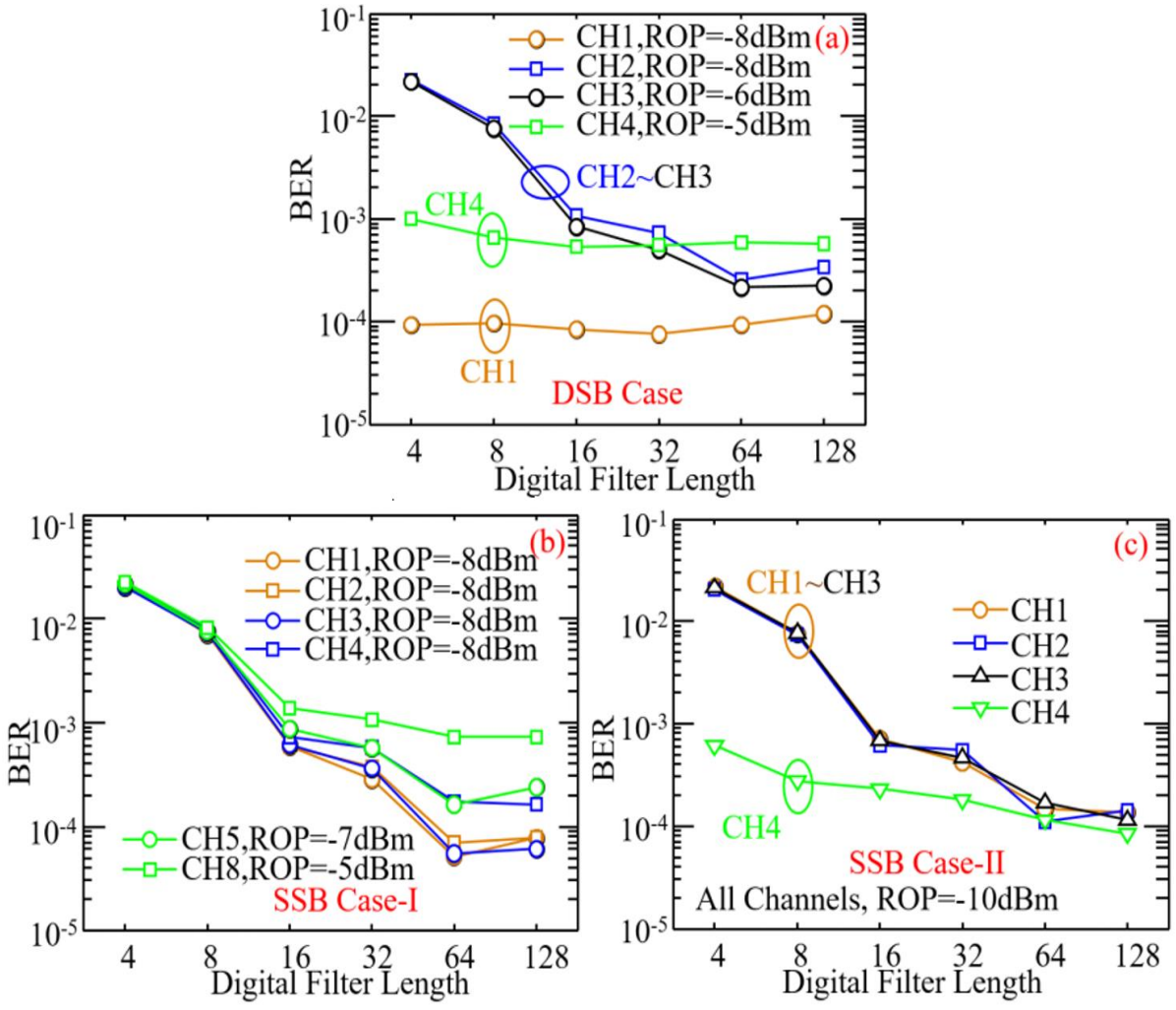

Fig. 5.10. Impacts of digital filter characteristics on upstream transmission performances. (a) DSB Case, (b) SSB Case-I and (c) SSB Case-II.

Fig. 5.10 presents the digital filter characteristic-induced impacts on the upstream BER performances for the considered three PON cases. The fibre transmission distance is 30km. For each involved OFDM channel, the 16-QAM subcarrier modulation format is employed and the ROPs are chosen in the vicinity of their corresponding receiver sensitivities. It can be found that for all the considered cases, the minimum digital filter lengths are L=64, corresponding to which digital filtering-induced performance degradations are negligible.

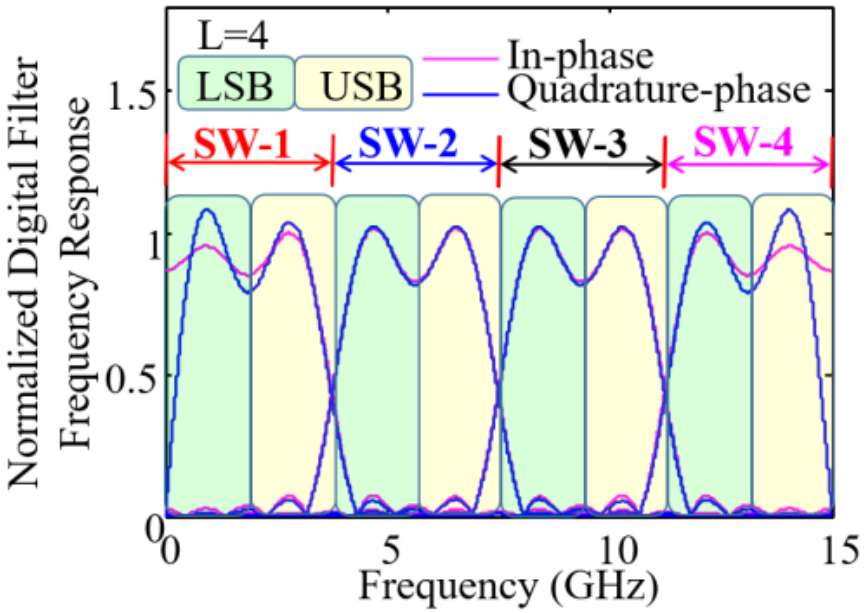

Fig. 5.11. Normalized in-phase and quadrature-phase digital filter frequency responses for the digital filter length of L=4.

In addition, it is also shown in Fig. 5.10 that the BER performances of both CH1/CH4 for DSB Case and CH4 for SSB Case-II are almost independent of digital filter length, this is because these channels suffer negligible power leakages arising from digital filter frequency response overlapping. This can be understood by considering Fig. 5.11, where normalized I-phase and Q-phase digital filter frequency responses for fixed digital filter lengths of L=4 are plotted for different sub-wavelengths. It is easy to find in Fig. 5.11 that, for DSB Case, the digital filter frequency response overlapping-induced power leakage mainly occurs at the CH1's USB spectral region and CH4's LSB spectral region, both of which are, however, not chosen to convey any information. As such, the digital filter length-independent performances are thus observed for these two channels. While for the SSB case, both the I-phase digital filters and the Q-phase digital filters are utilized to generate the SSB OFDM signals at different sub-wavelengths. Therefore, in addition to aforementioned digital filter frequency response overlapping, the digital filter frequency response ripples can also contribute to the power

leakages between the two channels of the same sub-wavelength. As such, for SSB Case-I, all the involved OFDM channels have similar BER developing trends as shown in Fig. 5.10(b). However, for SSB Case-II, due to its location in the highest spectral region, the 4th channel suffers negligible digital filter frequency response overlapping-induced power leakages, thus leading to a different BER developing trend compared to other channels.

To further examine the abovementioned physical mechanisms behind the digital filter length associated signal distortions, and more importantly, to verify the identified minimum digital filter length value from a different angle, the digital filter length-dependent channel interference-induced power penalties for all the considered three cases are plotted in Fig. 5.12, where the power penalty is defined as the difference of ROPs corresponding to the FEC limit with and without a sub-wavelength-wide spectral space between two adjacent ONUs. In numerically simulating Fig. 5.12, the 16-QAM modulation format is used for each involved OFDM signal. The 30km SSMF transmission distance is considered.

It is shown in Fig. 5.12 that for digital filter lengths of $>L$=64, the power penalty curves become flattened, indicating that L=64 is indeed the minimum digital filter lengths for all the considered cases. Since the minimum digital filter length is independent of ONU count [13], it is therefore easy to understand that the digital filter length-dependent power penalty behaviours presented in Fig. 5.12 are applicable regardless of ONU counts.

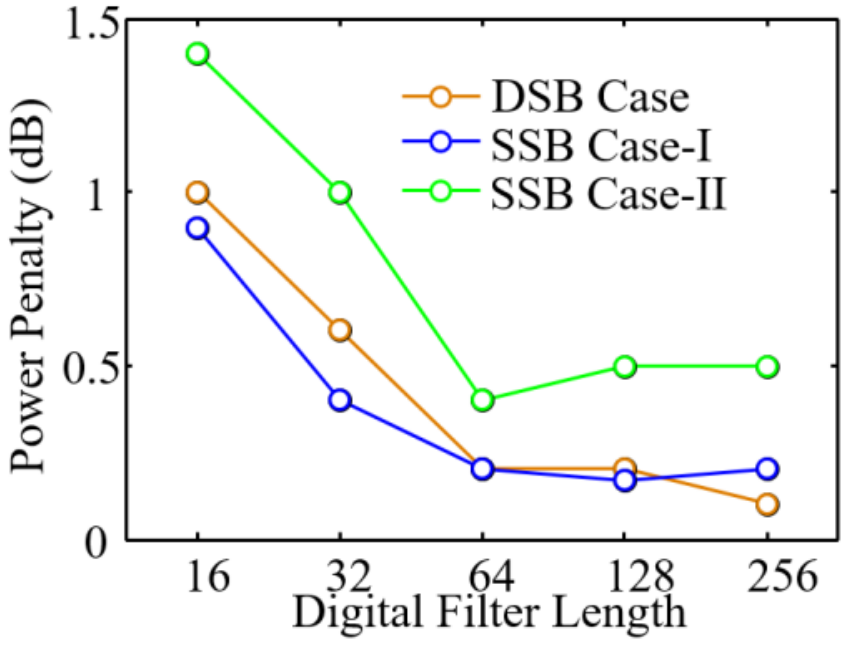

Fig. 5.12. Channel interference-induced power penalty for 30km upstream signal transmissions.

In addition, the results in Fig. 5.12 also indicate that, in comparison with SSB Case-I, SSB Case-II suffers higher power penalties across the entire digital filter length variation range, this is because for SSB Case-II, the introduced spectral spaces can not only reduce the channel interferences between neighbouring sub-wavelength channels but also minimize the channel interferences between the channels of the same sub-wavelength. While for SSB Case-I, the introduced ONU spectral spaces can only reduce the channel interferences between the channels within the adjacent sub-wavelengths.

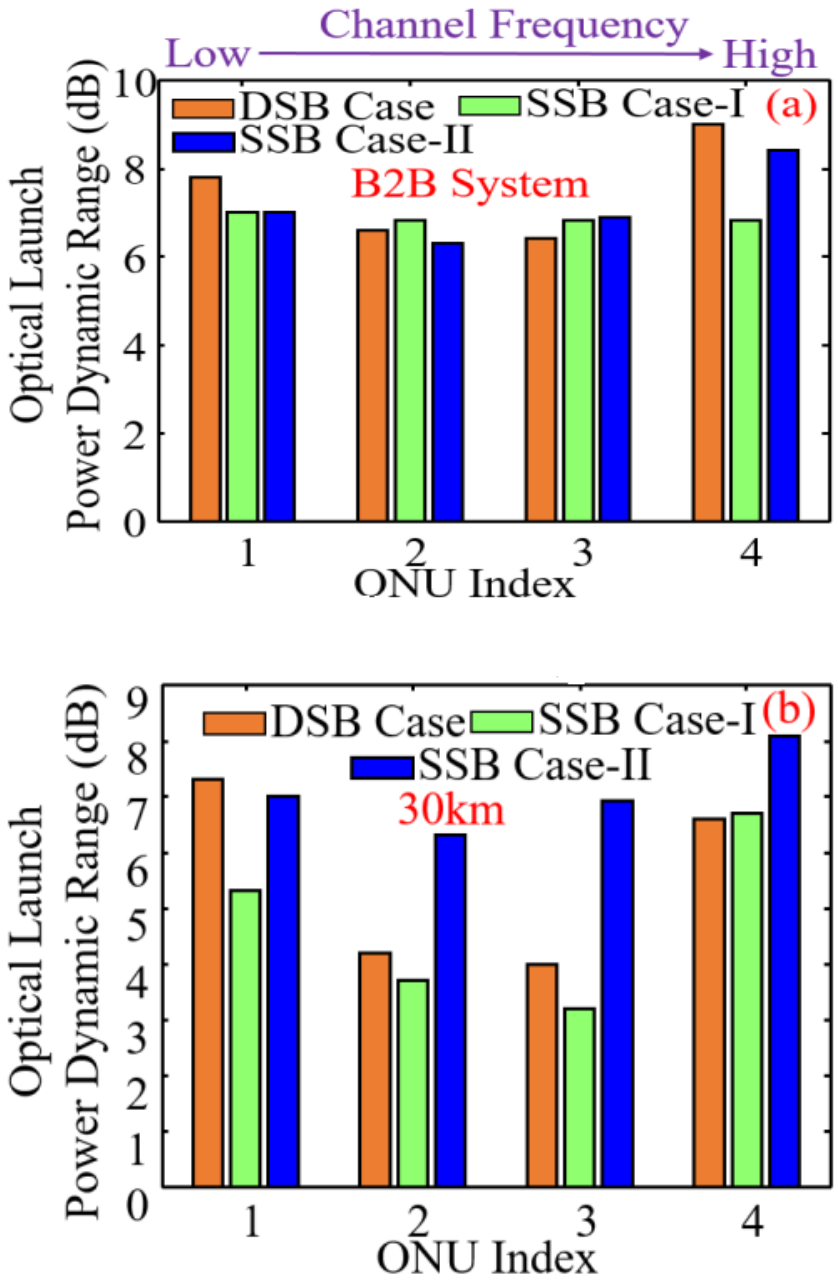

Fig. 5.13 Differential ONU optical launch power dynamic ranges for (a) optical B2B system and (b) 30km SSMF transmission.

5.5 Differential ONU Optical Launch Power Dynamic Range

For a particular ONU, the launch power dynamic variation range is defined as the maximum tolerance in its optical launch power variation for a given ROP at the OLT that maintain the BERs of all simultaneously transmitting ONUs below the adopted FEC limit. Utilizing the simulation conditions identical to those adopted in computing Fig. 5.12 and employing the identified minimum digital filter length of L=64, the system robustness against differential ONU optical launch power [7] for the considered three cases are explored in Fig. 5.13. The ROP is always fixed at -4dBm. The simulated differential optical launch power dynamic ranges for all the considered ONUs before and after 30km upstream transmissions are presented in Fig. 5.13.

As seen in Fig. 5.13(b), after transmitting through 30km SSMFs, <2dB differences in differential ONU optical launch power dynamic range between DSB Case and SSB Case-I can be achievable, indicating that the SSB Case-I-enabled improvement in upstream signal transmission capacity does not considerably affect the differential ONU optical launch power dynamic range. While for the hybrid SSB OFDM-DFMA PONs delivering upstream signal transmission capacities identical to those for the hybrid DSB OFDM-DFMA PONs, the ONUs locating at the high frequency spectral region improve their differential optical launch power dynamic ranges by >1.2dB. Such an improvement is mainly because of the SSB-induced enhancements in system robustness against the channel fading effect. This is evidenced by the fact that negligible differences in ONU differential optical launch power dynamic range are observed for SSB Case-II before and after 30km SSMF transmissions.

5.6 Conclusions

A novel IMDD-based hybrid SSB OFDM-DFMA PON has been proposed and extensively investigated, for the first time, in which multiple independent SSB OFDM channels are multiplexed utilizing the ONU-embedded software-configurable orthogonal digital filters, and simultaneously demultiplexed and demodulated by a single FFT operation in the OLT without utilizing MFs. In generating and demodulating the multiple SSB OFDM signals, the Hilbert transform DSP operations are not applied in both the ONUs and the OLT.

The upstream optimum ONU operating conditions have been identified for both the proposed hybrid SSB OFDM-DFMA PONs and the previously reported hybrid DSB OFDM-DFMA

PONs. It has been shown that compared to the DSB case, the proposed SSB PON can lead to >2dB reductions in PAPRs of digitally filtered OFDM signals. Such PAPR reductions are independent of digital filter characteristics, modulation formats and signal spectral location. As a direct result of the reduced PAPRs, >2dB reductions in optimum signal clipping ratios are also observed, which decrease the minimum DAC/ADC resolution bits by >1-bit for achieving BERs at 1×10^{-3}.

By utilizing the identified optimum ONU operating conditions, extensive upstream transmission performance comparisons have been made between the aforementioned two hybrid OFDM-DFMA PONs. Numerical simulations have indicated that the proposed hybrid SSB OFDM-DFMA PONs still maintain all the advantages associated with the hybrid DSB OFDM-DFMA PONs. More importantly, for IMDD PONs with identical overall signal transmission bandwidths, in comparison with the DSB PON, the proposed SSB PON can double the maximum aggregated upstream transmission capacity without considerably compromising their differential ONU optical launch power dynamic ranges. While for the IMDD PONs delivering similar aggregated upstream transmission capacities, in comparison with the DSB PON, the proposed SSB PON offers extra unique features including: 1) a halved overall system bandwidth, 2) >2.5dB upstream system power budget improvements, and 3) >1.2dB enhancements in differential optical launch power dynamic range for ONUs locating at high frequency spectral regions.

To rigorously verify the proposed hybrid SSB OFDM-DFMA PON architecture presented in this chapter and further evaluate the feasibility of utilizing the proposed PON to seamlessly converge optical access networks and mobile front-haul/back-haul networks, experimental investigations are currently being undertaken in our research lab, and corresponding results will be reported elsewhere in due course.

References

[1] P. T. Dat, A. Kanno, N. Yamamoto, and T. Kawanishi, “Seamless convergence of fibre and wireless systems for 5G and beyond networks,” J. Light. Technol., vol. 37, no. 2, pp. 592-605, Jan. 2019.

[2] K. Sone, G. Nakagawa, Y. Hirose, and T. Hoshida, “Demonstration of simultaneous multiple ONUs activation in WDM-PON system for 5G fronthaul,” Proc. Opt. Fibre Commun., San Diego, CA, USA, 2018, Paper M2B.6.

[3] J. Zhang , Y. Xiao, D. Song, L. Bai, and Y. Ji, “Joint wavelength, antenna, and radio resource block allocation for massive MIMO enabled beamforming in a TWDM-PON based fronthaul,” J. Light. Technol., vol. 37, no. 4, pp. 1396-1407, Feb. 2019.

[4] M. Bolea, R. P. Giddings, M. Bouich, C. Aupetit-Berthelemot, and J. M. Tang, “Digital filter multiple access PONs with DSP-enabled software reconfigurability,” J. Opt. Commun. Netw., vol. 7, no. 4, pp. 215-222, Apr. 2015.

[5] X. Duan, R. P. Giddings, S. Mansoor, and J. M. Tang, “Experimental demonstration of upstream transmission in digital filter multiple access PONs with real-time reconfigurable optical network units,” J. Opt. Commun. Netw., vol. 9, no. 1, pp. 45-52, Jan. 2017.

[6] M. L. Deng, A. Sankoh, R. P. Giddings, and J. M. Tang, “Experimental demonstrations of 30Gb/s/λ digital orthogonal filtering-multiplexed multiple channel transmissions over IMDD PON systems utilizing 10G-class optical devices,” Opt. Express, vol. 25, no. 20, pp. 24251-24261, Oct. 2017.

[7] Y. X. Dong, R. P. Giddings, and J. M. Tang, “Hybrid OFDM-digital filter multiple access PONs,” J. Light. Technol., vol. 36, no. 23, pp. 5640-5649, Dec. 2018.

[8] Y. X. Dong, W. Jin, R. P. Giddings, M. O’Sullivan, A. Tipper, T. Durrant, and J. M. Tang, “Hybrid DFT-spread OFDM-digital filter multiple access PONs for converged 5G networks,” J. Opt. Commun. Netw., vol. 11, no. 7, pp. 347-353, Jul. 2019.

[9] L. Marple, “Computing the discrete-time "analytic" signal via FFT,” IEEE Trans. Signal Processing, vol. 47, no. 9, pp. 2600-2603, Sep. 1999.

[10] Y. Zeng, Z. Dong, Y. Chen, X. Wu, H. He, J. You, and Q. Xiao, "A novel CAP-WDM-PON employing multi-band DFT-spread DMT signals based on optical Hilbert-transformed SSB modulation," IEEE Access, vol. 7, pp. 29397-29404, Mar. 2019.

[11] S. M. Jung, K. H. Mun, S. Y. Jung, and S. K. Han, "Optical-beat-induced multi-user-interference reduction in single wavelength OFDMA PON upstream multiple access systems with self-homodyne coherent detection," J. Light. Technol., vol. 34, no. 11, pp. 2804-2811, Jun. 2016.

[12] X. Q. Jin and J. M. Tang, "Experimental investigations of wavelength spacing and colorlessness of RSOA-based ONUs in real-time optical OFDMA PONs", J. Light. Technol., vol. 30, no. 16, pp. 2603-2609, Aug. 2012.

[13] E. Al-Rawachy, R. P. Giddings, and J. M. Tang, "Experimental demonstration of a real-time digital filter multiple access PON with low complexity DSP-based interference cancellation," J. Light. Technol., early access, Jun. 2019

6. Experimental Demonstrations of 30GB/S/λ Digital Orthogonal Filtering-Multiplexed Multiple Channel Transmissions Over IMDD PON Systems Utilizing 10G-Class Optical Devices

Contents

6.1 Introduction

Fuelled by a wide diversity of bandwidth-hungry applications such as high-definition TV, cloud computing, video-on-demand, the rapidly increasing number of mobile users and their various emerging services, the data bandwidth demand for broadband services continues to rise considerably. As a direct result, there is a tangible need for enhancing both the signal transmission capacities and the networking functionalities of NG-PONs whilst still maintaining their cost effectiveness due to the cost-sensitive nature of the access networks [1]. Moreover, since the quickly growing number of mobile users is the dominant driving force of the unprecedented bandwidth requirement, data traffic patterns are also becoming increasingly dynamic. This causes significant challenges for efficient bandwidth provision and network management. It is, therefore, critical to equip NG-PONs with the SDN-based network operation capability to offer highly desirable networking functionalities, including adaptability, flexibility, reconfigurability, elasticity and backwards compatibility [2,3]. Furthermore, to further improve the dynamic network operation functionalities and cost effectiveness, as well as the efficiency in both bandwidth utilization and network management, the seamless convergence of traditional optical access networks, metropolitan area networks, and 4G/5G MFH/MBH networks is also highly preferred to form integrated CANs for implementing sustainable “future-proof” optical access networks [4,5].

To meet the increasing transmission capacity demand in a cost-effective manner, extensive research has been carried out for further upgrade of the newly standardized NG-PON2 that delivers 40Gb/s downstream transmissions by stacking four 10Gb/s wavelength channels over power-split optical distribution networks to an aggregated transmission capacity of 100Gb/s with 25Gb/s per wavelength. Example experimental demonstrations of 25Gb/s single-wavelength IMDD-based transmission systems have been reported using signal modulation formats including DSB OFDM [6], four-level pulse amplitude modulation (PAM-4) [7,8], electrical/optical duobinary [9,10], and non-return-to-zero on-off-keying (NRZ-OOK) [11]. These schemes have demonstrated the feasibility of utilizing 10G-class optical devices to support 25Gb/s single-wavelength signal transmission capacity. From the cost point of view, this offers a promising technical strategy for practical implementation.

On the other hand, to improve the software-controllable network reconfigurability and network

bandwidth utilization efficiency, by making use of digital orthogonal filtering implemented with hardware-based DSP, we have recently proposed and theoretically investigated a novel channel multiplexing/demultiplexing technique [12], in which centralized SDN controller-managed, software-reconfigurable DOFs are embedded in transceivers to adaptively and dynamically combine and separate different digital signal channels according to channel spectral characteristics and network traffic status. It has been shown [12-15] that the proposed DOF-based multiplexing/demultiplexing technique not only provides the PON systems with the aforementioned online network operation functionalities, but also has the excellent potential of achieving the integrated CANs, because of its salient advantages listed below:

- Offering excellent DSP-enabled network reconfigurability, flexibility and elasticity, as well as inherent network operation transparency to underlying signal modulation/detection techniques and signal bandwidths.
- Fully supporting the conventional SDN solution and further extending the solution to the physical layer because of the implementation of software-reconfigurable DSP functions in the involved optical transceivers.
- Significantly improving the transmission spectral efficiency as the gapless aggregation of multiple signals of various characteristics can be achievable.
- Enabling DOF-based online channel aggregation in the electrical/optical domain without requiring extra analogue components, and also channel add/drop functions in network nodes when using our recently proposed flexible reconfigurable optical add/drop multiplexers [16].

From the above descriptions, it is easy to understand that, to equip 100Gb/s NG-PONs with the aforementioned advantageous network functions, it is greatly beneficial if the DOF enabled multiplexing/demultiplexing technique can be employed in 25Gb/s single wavelength IMDD PON transmission systems incorporating 10G-class optical devices.

In this chapter, by making use of off-the-shelf 10G-class optical devices, we report, for the first time, experimental demonstrations of aggregated 30.078Gb/s/λ signal transmissions over >25km SSMF multi-channel IMDD PON systems, where six independent channels are multiplexed/demultiplexed utilizing DOFs in the digital domain. The experimental results show that the achievable signal transmission capacity is mainly determined by the chromatic dispersion-induced power fading effect rather than digital filter frequency response

characteristics. As a direct result, when adaptive channel power loading is applied, the channel spectral location-independent transmission performance with a negative power penalty of >0.2dB can be obtained for all the involved channels. In addition, excellent performance robustness of the demonstrated systems is also experimentally observed for different transmission distances up to 45km.

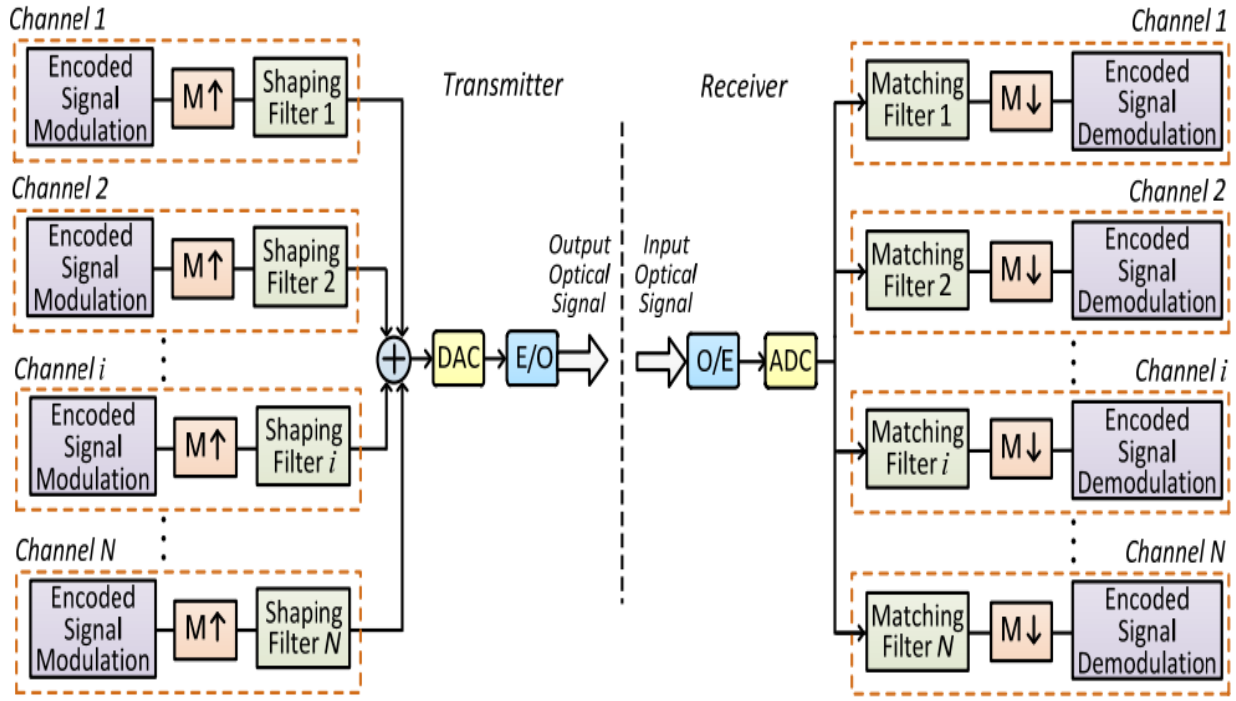

Fig. 6.1. Schematic diagram of the transceivers utilizing digital orthogonal filtering-enabled channel multiplexing/demultiplexing.

6.2 DOF-enabled Channel Multiplexing/Demultiplexing and Experimental System Setup

6.2.1 Operating Principles Of DOF-enabled Channel Multiplexing/ Demultiplexing

As a detailed theoretical analysis of the DOF-enabled channel multiplexing/demultiplexing technique has already been presented in [12], only the basic operation principles are outlined below. As shown in Fig. 6.1, *N* independent channels are multiplexed/demultiplexed utilizing DSP-based DOFs embedded in the optical transceivers. At the transmitter side, each individual channel's data is first digitally encoded by an arbitrary signal modulation format such as

OFDM, PAM and NRZ-OOK. The encoded sample sequence is then up-sampled by a factor of *M* by inserting *M*-1 zeros between two consecutive samples, and subsequently the up-sampled sequence passes through a digital orthogonal shaping filter. As a result, an orthogonal channel is generated at the output of the shaping filter. All of the generated orthogonal channels are added together in the digital domain and are input into a single DAC. The resulting analogue signal emerging from the DAC is then fed to an optical intensity modulator and the optical signal is launched into a fibre transmission link. At the receiver side, the optical signal is electrically converted and then digitalized by an ADC. After that, the digitalized electrical signal is split equally to feed *N* parallel receiver modules, where the digital signal is filtered by a corresponding MF to demultiplex the desired channel. The digitally filtered channel is down-sampled by a factor of *M* by selecting every M^{th} sample from the sample sequence. Finally, the demultiplexed channel is recovered after signal decoding.

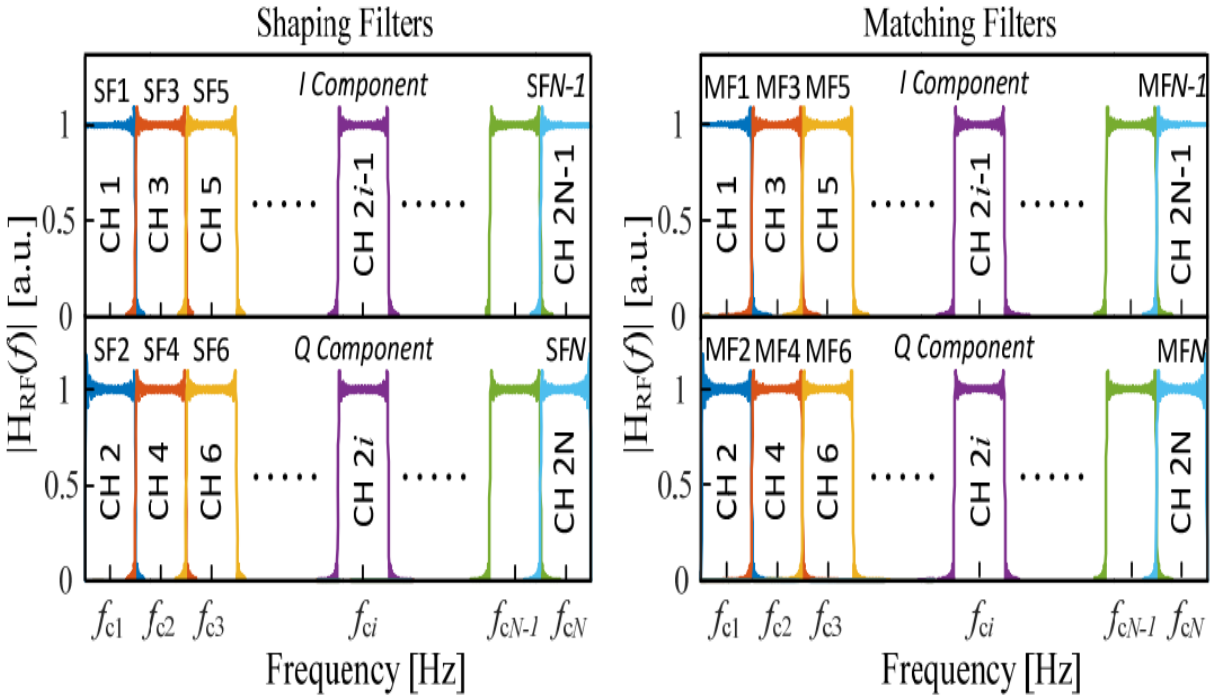

Fig. 6.2. Frequency responses of Hilbert-pair-based digital orthogonal shaping/matching filters and the gapless multiplexing/demultiplexing of N independent signal channels. The total number of channels is N, which is equal to the oversampling factor of M. SF: shaping filter; MF: matching filter; CH: channel.

To implement DOF-enabled channel multiplexing/demultiplexing, use can be made of the Hilbert-pair approach [17] to construct the required DOFs. The impulse responses of the *i*-th

Hilbert-pair, $h_i(t)$, and the baseband pulse, $p(t)$, with a square-root raised-cosine form can be given by Eq. (2.14) and Eq. (2.15).

It should be mentioned that each of individual component of the spectrally overlapped I-phase and Q-phase components can be independently used as the impulse response of an individual shaping filter. Whilst the impulse responses of the MFs can be written as the time reversals of the corresponding shaping filters, $m_i(t)$, and can be expressed as in Eq. (2.16) and Eq. (2.17) respectively. For multiplexing/demultiplexing N independent channels, the up-sampling factor, M, should satisfy $M \geq N$ [12]. In addition, the central frequency of the DOFs, f_{ci}, can be expressed as presented in Eq. (2.18).

An example of how various orthogonal shaping and MFs are dynamically assigned to individual channels is illustrated in Fig. 6.2, where the frequency responses of the orthogonal filters at different central frequencies are plotted. It is also shown in Fig. 6.2 that the channels occupying the I and Q components of a specific filter pair share the same spectral region and there are no frequency gaps between the neighbouring channels, this gives rise to an increase of spectral efficiency. From the practical network operation viewpoint, according to the end-user's demand and network traffic status which can be obtained through periodic communications between the transceiver DSP controllers and the centralized SDN network controller [13], the digital filter characteristics in each transceiver can be varied by selecting the appropriate digital filter parameters stored in the transceiver DSP controllers, this allows the dynamic allocation of optimum available filters for individual channels to be achieved online in the DOF space.

6.2.2 Experimental System Setup

The experimental setup of the considered IMDD PON transmission systems incorporating DOF-enabled channel multiplexing/demultiplexing is illustrated in Fig. 6.3, where 10G class optical devices are adopted. As already stated above, digital orthogonal filtering is inherently transparent to signal modulation format. Here OFDM is utilized to encode the user information due to its high spectral efficiency and DSP richness. Meanwhile, for simplicity but without losing any generality, six independent channels are considered in the experimental demonstrations.

As seen in Fig. 6.3, at the transmitter a MATLAB program is employed to perform the transmitter DSP procedures off-line, which consist of the following core processes: generation of six independent real-valued OFDM channels, 8× up-sampling process, shaping filter coefficient calculation, digital orthogonal filtering of each individual channel, and direct digital sample summation of the six digitally filtered channels. After carrying out the transmitter DSP procedures in MATLAB, the summed samples are first uploaded onto an arbitrary waveform generator operating at 28GS/s and then converted into an analogue waveform with a 10.5GHz bandwidth. A RF amplifier sets the voltage of the generated

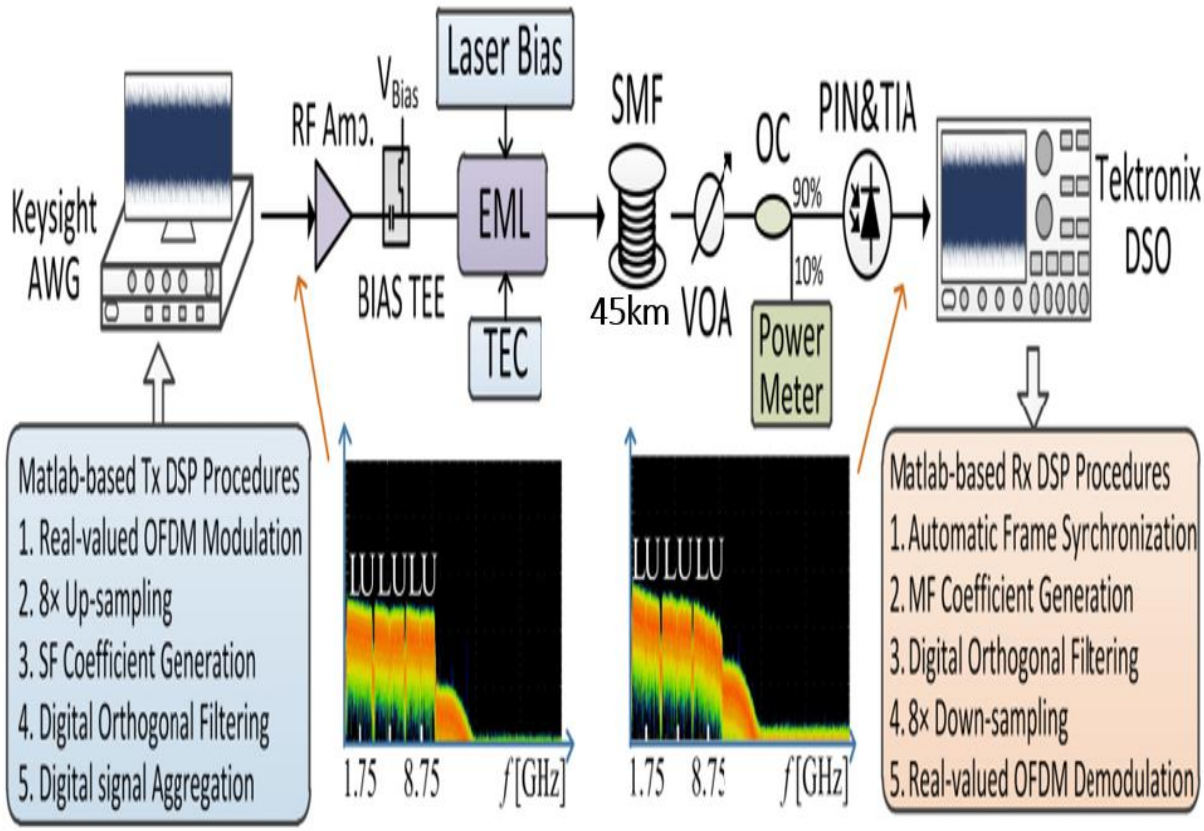

Fig. 6.3. Experimental system setup of digital orthogonal filtering-enabled 6-channel IMDD PON transmission system. AWG: arbitrary waveform generator; Amp: amplifier; EML: electro-absorption modulated laser; TEC: thermo-electric cooler; VOA: variable optical attenuator; OC: optical coupler; SSMF: standard single-mode fibre; PIN&TIA: photodetector with integrated transimpedance amplifier; DSO: digital sampling oscilloscope. The inset are measured electrical signal spectra output from the AWG and PIN. L lower sideband; U: upper sideband.

Table 6.1. Transceiver and Optical Device Parameters

Parameter	**Value**	**Parameter**	**Value**
Channel Number	6	Cyclic Prefix	1/8
Up-sampling Factor(M)	8	Clipping Ratio	13dB
Digital Filter Tap Length	64	EML Laser Operation Wavelength	~1550nm
Excess of the Bandwidth (α factor)	0	3dB Modulation Bandwidth	10GHz
Signal Bandwidth Per Channel	3.5GHz	EML Bias Current	125 mA
Information-Bearing Subcarriers Per Channel	31	EAM Bias Voltage	-0.7 V
IFFT/FFT	64	EML Laser Output Power	~2.7 dBm
Adaptive Modulated Format	QPSK, 16QAM, 32QAM	SSMF Fibre Type	MetroCor
		PIN Detector Bandwidth	10 GHz

*Corresponding to 10 Gb/s non-return-to-zero data (PRBS 2^{31}-1) at a BER of 1.0×10^{-9}.

analogue signal at $1.6V_{pp}$ for combination, via a bias-T, with an optimum DC bias of -0.7V. Afterwards, the resulting RF signal is used to drive a 10GHz electro-absorption modulator (EAM) within an electro-absorption modulated laser (EML), in which a 1550nm distributed feedback (DFB) laser is biased at a DC current of 125mA. Finally, the modulated optical signal from the EML is directly launched into a MetroCor SSMF transmission link with an input optical power of ~2.7dBm. At the receiver, the received optical signal first passes through a VOA to control its optical power level. Following a 90/10 optical coupler (OC), the received optical signal is converted to the electrical domain by a 10GHz PIN with integrated transimpedance amplifier (TIA) via direct detection. Finally, the received analogue electrical signal is captured and digitized by a real-time digital sampling oscilloscope (DSO), and then processed offline using a receiver MATLAB program. The major receiver DSP functions include signal synchronization, MF coefficient generation, DOF-based channel demultiplexing, 8× down-sampling of each individual channel, and real-valued OFDM signal recovery by employing the DSP procedures identical to those reported in [18].

In the transceiver DSP programs, all the DOFs are constructed according to the approach outlined in subsection 6.2.1 and the frequency responses of the shaping and MFs assigned to

six OFDM channels are similar to those presented in Fig. 6.2. The digital filter tap length, defined as the total number of original data samples contributing simultaneously to the filtering process, is set to 32, whilst the excess of bandwidth factor, α, is kept at 0. Moreover, in generating/recovering an OFDM signal for each individual channel, adaptively bit-loaded 31 subcarriers, with signal modulation formats selected from QPSK, 16-QAM and 32-QAM, are employed to carry a binary pseudo-random bit sequence (PRBS) with a length of 2^{15}-1. This results in a total number of 64 IFFT/FFT points for obtaining real-valued OFDM symbols via the Hermitian conjugation. A cyclic prefix ratio of 1/8 is employed and the signal clipping ratio is fixed at 13dB. A summary of the key transceiver and optical device parameters are listed in Table 6.1.

6.3 Experimental Results

To experimentally demonstrate the achievable transmission performance of the DOF multiplexed multi-channel IMDD PON systems, in subsection 6.3.1 the adaptively optimized signal characteristics of each individual channel are first presented in terms of their adaptive bit loading profiles and their relative electrical channel power levels. The optimizations of these parameters pave a solid path to the successful experimental demonstrations of aggregated 30.078Gb/s multi-channel IMDD PON transmissions over 10G-class optical device-based 25km SSMF links described in subsection 6.3.2. In addition, the transmission performances of the considered systems are also experimentally explored in subsection 6.3.3 for various transmission distances up to 45km.

6.3.1 Optimized Signal Characteristics of each individual Channel

To effectively reduce the impacts of the overall system frequency response roll-off effect on signal transmission performances, parameter optimizations of each individual channel are first conducted via adaptive bit loading for all information-bearing subcarriers. Moreover, adaptive channel power loading is also applied by redistributing the available electrical signal power among all of the channels.

For a considered 25km SSMF IMDD PON link incorporating the 10G-class optical devices subject to the operating conditions listed in Table 6.1, the resulting optimum subcarrier bit allocation profiles measured for each individual channel are presented in Fig. 6.4. It can be

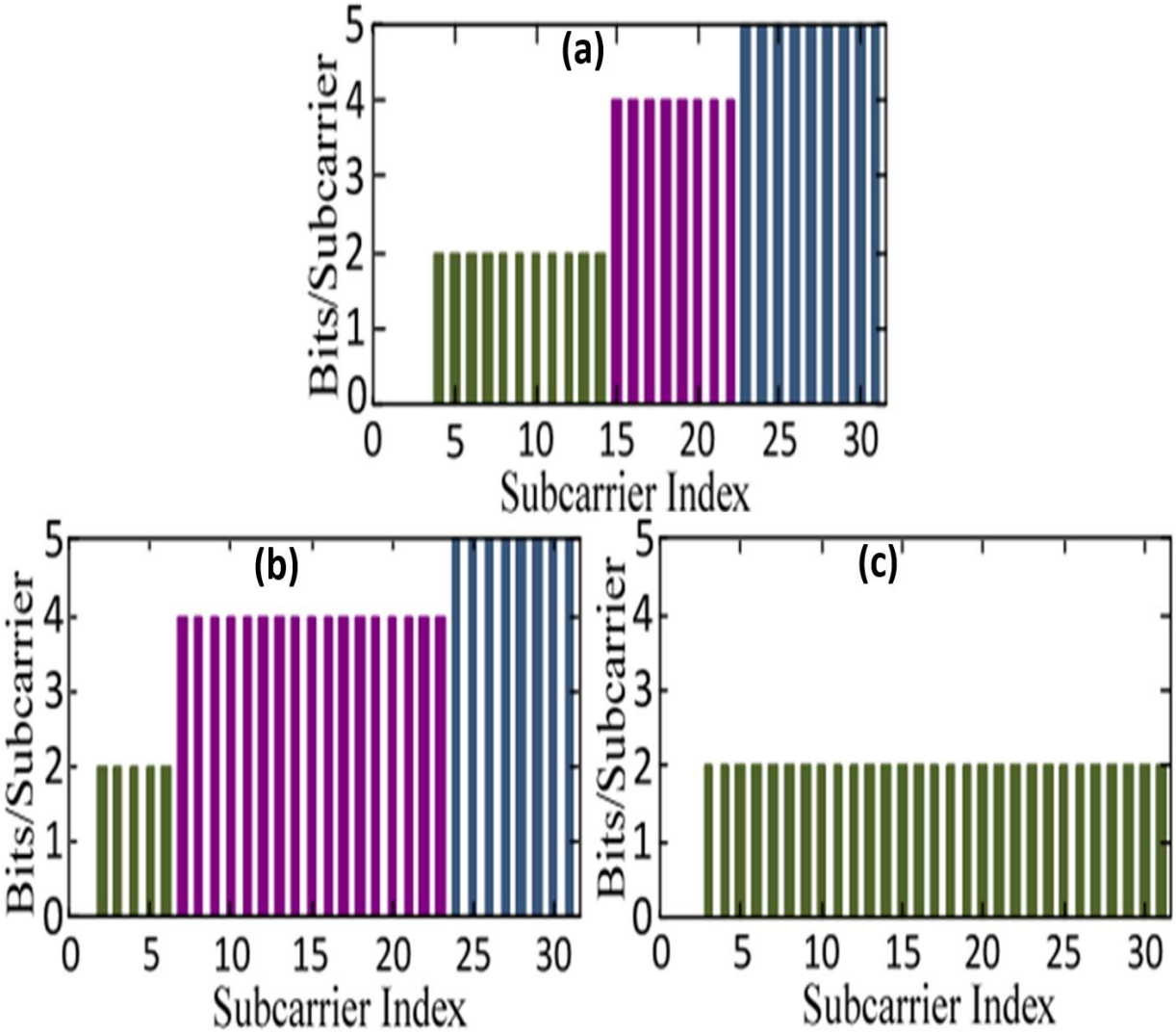

Fig. 6.4. Optimized adaptive subcarrier bit loading profiles for various channels. (a) CH1 and CH2; (b) CH3 and CH4; (c) CH5 and CH6.

seen in Fig. 6.4 that for two spectrally overlapped channels occupying the same spectral region, identical bit allocation profiles are obtained. This is because these two channels experience a similar system frequency response roll-off, which is mainly determined by the chromatic dispersion-induced power fading effect associated with the IMDD system [19]. The channels located in the high-frequency spectral region suffer from the relatively strong power fading effect, as depicted in the measured spectra inserted in Fig. 6.3, thus only the low signal modulation format (QPSK) can be assigned to the last two channels (CH5 and CH6). It can also be seen in Fig. 6.4(a) and Fig. 6.4(b) that, for a specific signal channel, higher signal modulation formats are taken on high-frequency subcarriers. This is because the DOF process produces a DSB spectrum with the original signal spectrum mapped to both the upper and

lower sidebands, as shown in the spectra inserted in Fig. 6.3. The channel roll-off effect introduces amplitude variations between the corresponding frequency components in the upper and lower sidebands, this prevents full cancellation between the sidebands of the unwanted signal when these sidebands are mapped back in the receiver. As such, the CCI effect occurs [14,15]. In particular, a larger system frequency response roll-off causes a greater amplitude variation between the two sidebands, thus lower frequency subcarriers suffer more CCI, leading to the utilization of low signal modulation formats on these subcarriers to obtain the acceptable BER performances, as observed in Fig. 6.4(a) and Fig. 6.4(b). Furthermore, because the finite tap length-induced digital filter frequency response ripples are more pronounced at the low-frequency region and as large ripples give rise to the occurrence of excessive errors on the subcarriers, for each individual channel, the first several subcarriers must be dropped. Finally, the unwanted square-law photon detection-induced intermixing frequency products also slightly increases the number of dropped subcarriers for low-frequency channels (CH1 and CH2).

Table 6.2. System Parameters for each Individual Channel

Channel Index	Central Frequency [GHz]	Total Data-Carrying Subcarriers	Relative Power Ratio[1] [dB]	Raw Signal Bit Rate [GB/s]
1	1.75	28	0	5.414
2	1.75	28	0	5.414
3	5.25	30	1.15	6.453
4	5.25	30	1.15	6.453
5	8.75	29	2.56	3.172
6	8.75	29	2.56	3.172
Total	/	/	/	30.078

[*]Normalized to the power of channel 1.

Based on Fig. 6.4 and the transceiver parameters listed in Table 6.1, it is easy to calculate the achieved signal bit rates of individual channels, which are presented in Table 6.2, thus an aggregated raw signal transmission capacity is 30.078Gb/s. In order to minimize receiver sensitivity differences between all the considered channels, it is also necessary to employ adaptive channel power allocations before multiplexing these signal channels in the digital domain. Such channel power allocation can be quantified by the power ratio between a specific channel and CH1. As listed in Table 6.2, the optimum signal power ratios for CH3/CH4 and CH5/CH6 are 1.15 dB and 2.56 dB respectively. It is interesting to note in Table 6.2 that when the optimum bit loading and channel power loading are adopted, the transmission capacities of

the signal channels located in the two low spectral bands are similar, suggesting that the achievable channel transmission capacity is mainly determined by the power fading effect of the transmission link rather than the digital filter frequency response characteristics.

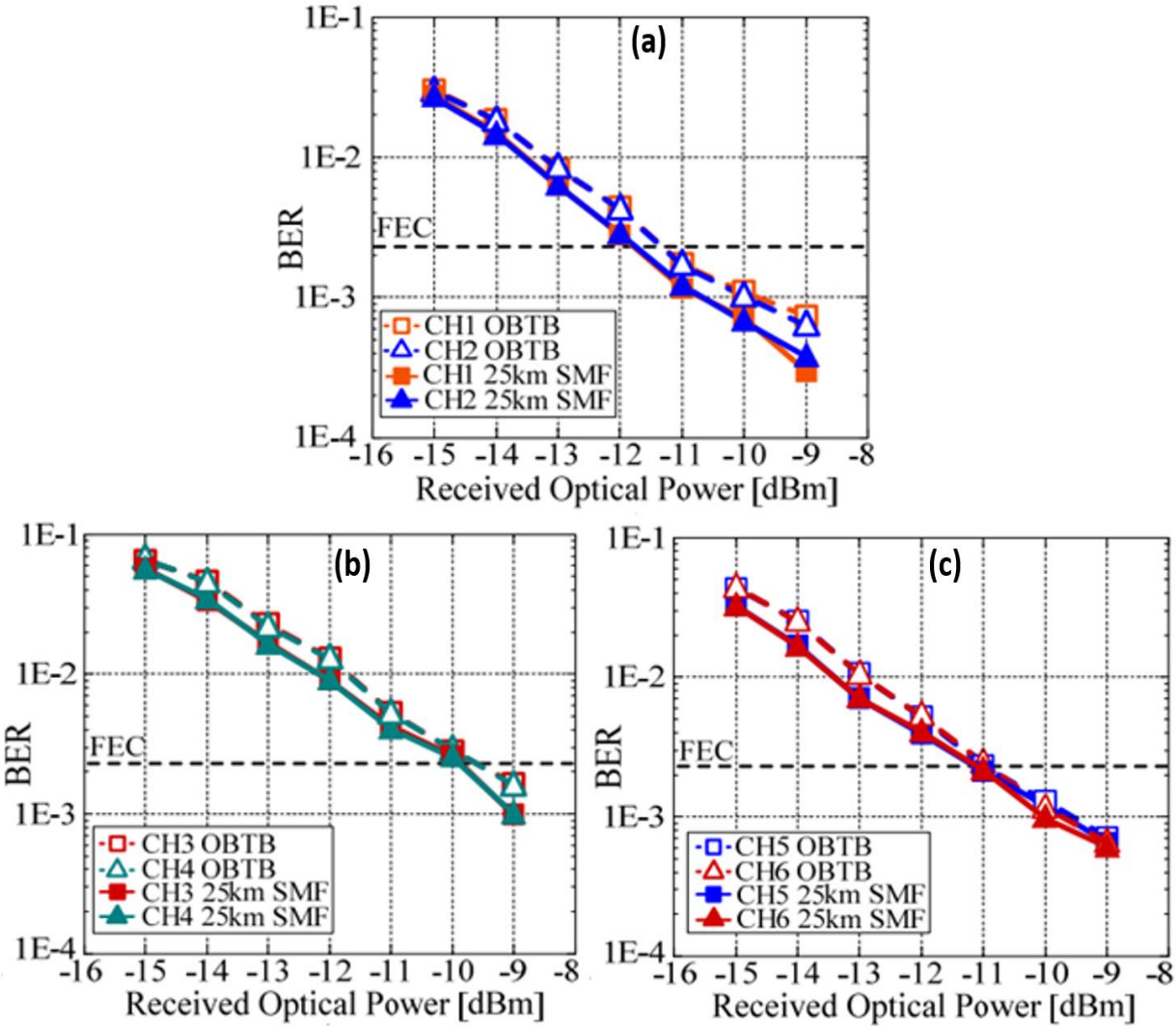

Fig. 6.5. Measured BER versus received optical power performances of each individual channel in a 25km SSMF IMDD transmission system. (a) CH1 and CH2; (b) CH3 and CH4; (c) CH5 and CH6.

6.3.2 25km SMF Transmission Performances

In this subsection, experimental measurements are undertaken of 30.078Gb/s DOF multiplexed 6-channel transmission performances over the IMDD 25km MetroCor SSMF PON link. Here the optimum bit loading profiles presented in Fig. 6.4 are employed, and the optimum device

operating conditions specified in Table 6.1 are also adopted together with the optimized channel power levels listed in Table 6.2.

For both the optical BTB and entire IMDD 25km SSMF link, Fig. 6.5 presents the measured BER performances of each individual channel as a function of ROP. As expected from the theoretical predictions [13], it is shown in Fig. 6.5 that across the entire ROP dynamic range, the BER developing trends are very similar for all the signal channels considered. This indicates that the operation performances of DOF-based channel multiplexing/demultiplexing are independent of not only the digital filter type but also the channel spectral location. As also seen in Fig. 6.5, in comparison with the other channels located in different spectral regions, for CH3 and CH4, receiver sensitivity decreases of about 1.8dB are observed at a FEC limit of 2.3×10^{-3} for the optical BTB case. Such receiver sensitivity differences are mainly contributed by the co-existence of the limited dynamic range of the channel power ratio and the high signal bit rate conveyed by CH3 and CH4. More importantly, it should also be noted in Fig. 6.5 that compared to the optical BTB case, a negative power penalty of >0.2dB at the adopted FEC limit occurs for each individual channel after a 25km MetroCor SSMF transmission. The observed performance improvements after 25km fibre transmissions imply that the MetroCor SSMF-introduced negative dispersion can compensate for the positive transient frequency chirp associated with the adopted EAM [20].

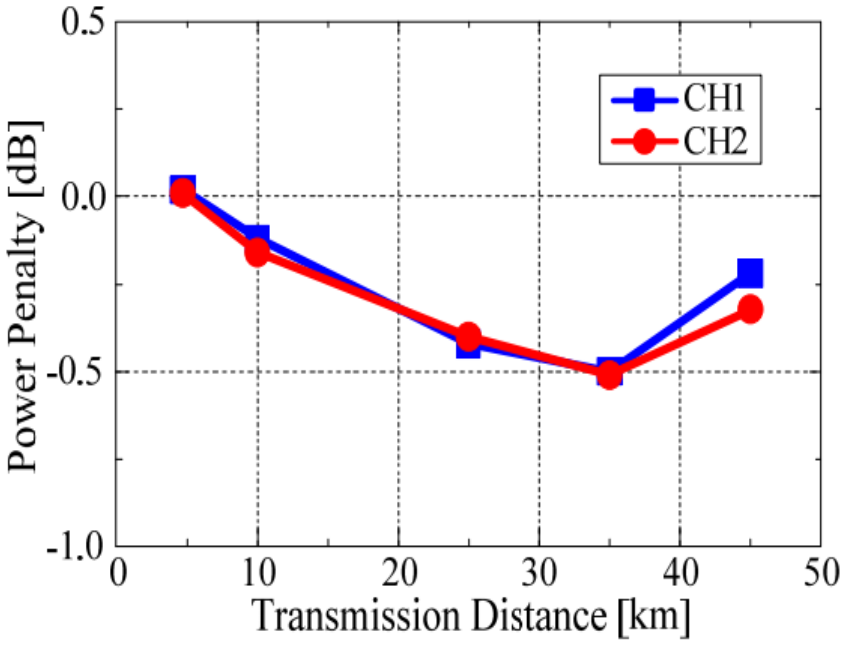

Fig. 6.6. Power penalty versus transmission distance for CH1 and CH2.

To further confirm the observed negative power penalty behaviours, the measured channel power penalty against MetroCor SSMF transmission distance is illustrated in Fig. 6.6, where only CH1 and CH2 are considered to minimize the impacts of the transmission distance dependent power fading effect and the limited optical device bandwidths on the system performance. In measuring Fig. 6.6, the adopted experimental conditions are identical to those used in Fig. 6.5, except that the transmission distance varies from 5km to 45km. It is shown in Fig. 6.6 that when the transmission distance increases from 5km to 35km, the negative power penalty rises due to the improved compensation of the EAM-associated frequency chirp effect [20]. On the other hand, for a transmission distance larger than 35km, the relatively sharp decrease of the negative power penalty occurs because the EAM-associated frequency chirp is over-compensated by the accumulated large chromatic dispersion effect. As a direct result of optimum compensation between the EML frequency chirp and the and the accumulated chromatic dispersion, a maximum negative power penalty can be obtained at a transmission distance of 35km.

After having performed channel equalization in the receiver, the subcarrier constellations corresponding to the highest signal modulation formats taken on each individual channel are exemplified in Fig. 6.7, where the constellations are recorded at s ROP of -9dBm after 25km MetroCor SSMF transmissions.

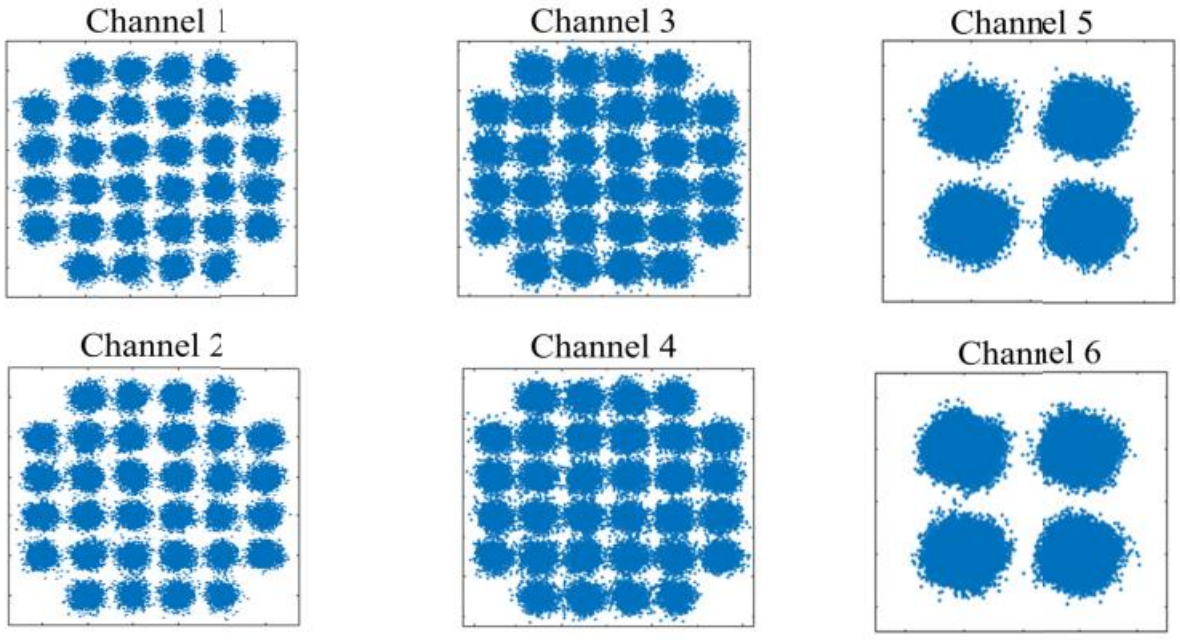

Fig. 6.7. Equalized subcarrier constellations for various channels at a ROP of -9dBm.

6.3.3 45km SMF Transmission Performances

As a direct result of the transmission distance-dependent negative power penalty shown in Fig. 6.6, it is straightforward to expect that the transmission performance of the considered system is also robust to variations in transmission distance. Such performance robustness can be greatly beneficial to the seamless convergence of various access networks with largely diversified design characteristics. To verify such an expectation, for an IMDD 45km MetroCor SSMF transmission system, the measured BER versus ROP of each individual channel are plotted in Fig. 6.8, in obtaining this figure, in comparison with Fig. 6.5, only the channel power level of each individual channel is optimized and no other alterations are made to device//transceiver/system parameters.

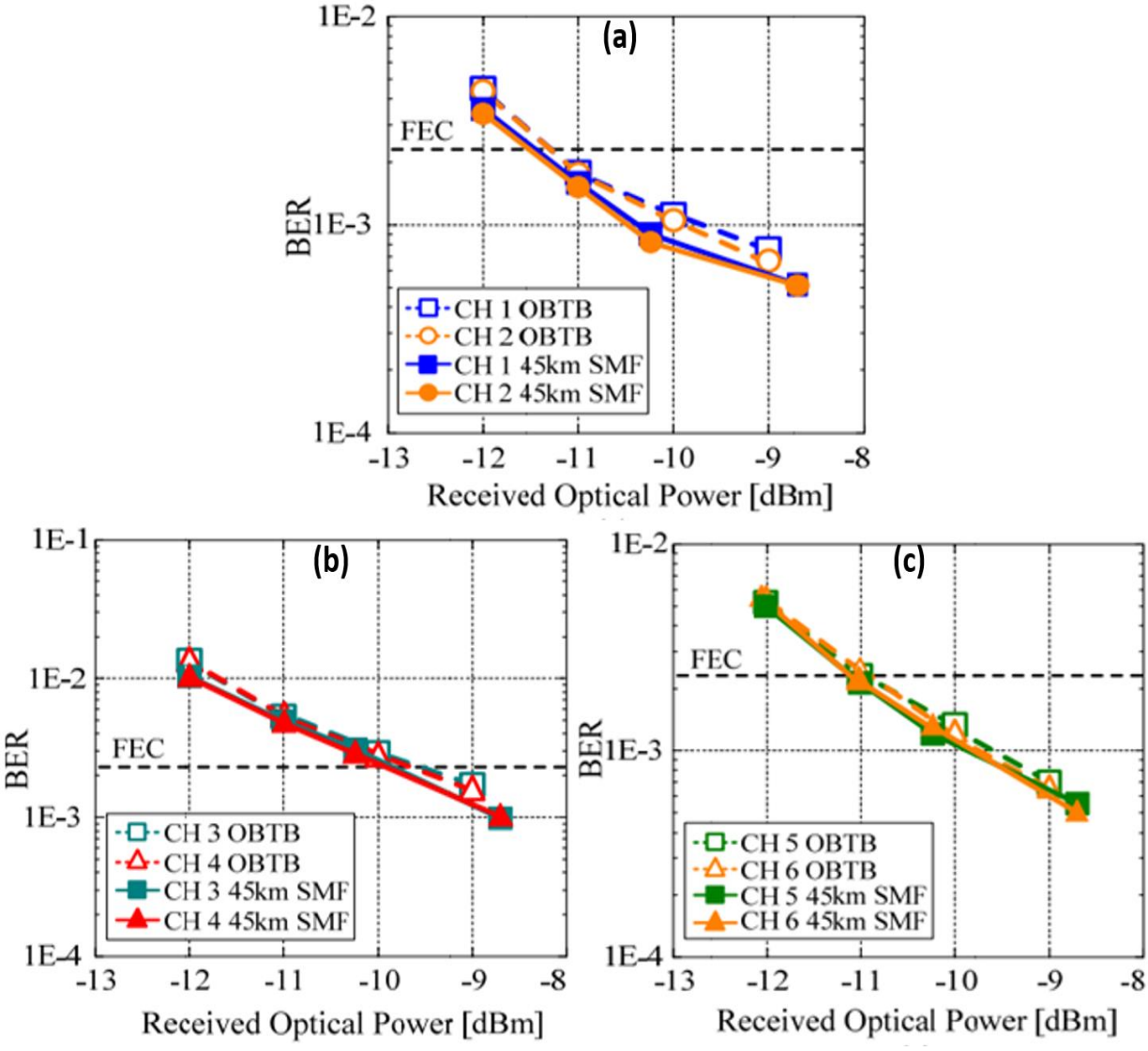

Fig. 6.8. BER versus received optical power performances after 45 km SSMF transmissions.

As seen in Fig. 6.8, compared to Fig. 6.5, just simple channel power allocation can enable similar BER developing trends for the involved channels, regardless of the long transmission distance-enhanced power fading effect. This indicates that adaptive channel power loading can provide the DOF-multiplexed multiple channel PON systems with excellent performance robustness to transmission distance. In comparison with Fig. 6.5, it is also found in Fig. 6.8 that for CH1, the negative power penalty decreases by 0.3dB. Whilst the negative power penalties of CH6 remain almost the same for both the 25km and 45km cases. The physical mechanisms underpinning the observed channel spectral location-dependent variations in power penalty is that, compared to the low-frequency channels, the high-frequency channels experience much stronger EAM-associated frequency chirp, which inevitably requires a larger accumulated chromatic dispersion for an optimum compensation. Finally, after 45km fibre transmissions, a receiver sensitivity variation of <0.5dB is obtained at the adopted FEC limit for all the six channels, this results from the co-existence of the power fading effect and the interplay between chromatic dispersion and EAM-associated frequency chirp.

6.4 Conclusions

By making use of off-the-shelf and low-cost 10G-class optical devices, aggregated 30.078Gb/s/λ over 25km SSMF multi-channel transmissions have been experimentally demonstrated, for the first time, in IMDD PON systems incorporating DOF-multiplexed six independent channels. The experimental results have shown that by employing adaptive channel power allocation, the channel spectral location-independent transmission performance with a negative power penalty of >0.2dB is obtainable for all the involved channels. Furthermore, excellent performance robustness of the demonstrated system has also been observed for various transmission distances up to 45km. This work demonstrates the great potential of the DOF-multiplexing technique for enabling integrated CANs for the seamless convergence of traditional optical access networks, metropolitan area networks and MFH/MBH networks.

References

[1] D. Nesset, "The PON roadmap," Optical Fibre Communication/National Fibre Optic Engineers Conference (OFC/NFOEC), (Anaheim, 2016), paper W4C.1.

[2] N. Cvijetic, A. Tanaka, P. Ji, K. Sethuraman, S. Murakami, and T. Wang, "SDN and OpenFlow for dynamic flex-grid optical access and aggregation networks," J. Lightwave Technol., 32(4), 864-870 (2014).

[3] G. Talli, F. Slyne, S. Porto, D. Carey, N. Brandonisio, A. Naughton, P. Ossieur, S. McGettrik, C. Blumm, M. Ruffini, D. Payne, R. Bonk, T. Pfeiffer, N. Parsons, and P. Townsend, "SDN enabled dynamically reconfigurable high capacity optical access architecture for converged services," J. Lightwave Technol., 35(3), 550-560 (2017).

[4] J. E. Mitchell, "Integrated wireless backhaul over optical access networks," J. Lightwave Technol., 32(20), 3373-3382 (2014).

[5] X. Liu and F. Effenberger, "Emerging optical access network technologies for 5G wireless," J. Opt. Commun. Netw., 8(12), B70-B79 (2016).

[6] Y. Luo, B. Lin, H. Yang, J. Li, Y. He, Z. Chen and Z. Li, "Symmetic 100-Gb/s TWDM-PON with DSB OFDM Modulation," Optical Fibre Communication/National Fibre Optic Engineers Conference (OFC/NFOEC), (San Francisco, 2014), paper W2A.61.

[7] V. Houtsma, and D. V. Veen, "Demonstration of symmetrical 25 Gbps TDM-PON with 31.5 dB optical power budget using only 10 Gbps optical components," European Conference on Optical Communication (ECOC), (Valencia, 2015), paper PDP.4.3.

[8] J. L. Wei, N. Eiselt, H. Griesser, K. Grobe, M. H. Eiselt, J. J. V. Olmos, I. T. Monroy, and J. Elbers, "Demonstration of the first real-time end-to-end 40-Gb/s PAM for next-generation access applications using 10-Gb/s transmitter," J. Lightwave Technol., 34(7), 1628-1635 (2016).

[9] Z. Li. L. Yi, X. Wang, and W. Hu, "28 Gb/s duobinary signal transmission over 40km based on 10 GHz DML and PIN for 100 Gb/s PON," Opt. Express 23(16), 20249–20256 (2015).

[10] Ye, S. Li, N. Cheng, and X. Liu, "Demonstration of high-performance cost-effective 100-Gb/s TWDM-PON using 4×25-Gb/s optical duobinary channels with 16-GHz APD and receiver-side post equalization," European Conference on Optical Communication (ECOC), (Valencia, 2015), paper Mo.3.4.4.

[11] H. Ji, L. Yi, Z. Li, L. Xue, X. Li, Q. Yang, S. Wang, Y. Yang, S. Yu, and W. Hu, "Field demonstration of a real-time 100Gb/s PON based on 10G-class optical devices," J. Lightwave Technol., 35(10), 1914-1921 (2017).

[12] M. Bolea, R. P. Giddings, and J. M. Tang, "Digital orthogonal filter enabled optical OFDM channel Multiplexing for software-reconfigurable elastic PONs," J. Lightwave Technol., 32(6), 1200-1206, (2014).

[13] M. Bolea, R. P. Giddings, M. Bouich, C. Aupeti-Berthelemot, and J. M. Tang, "Digital filter multiple access PONs with DSP-enabled software reconfigurability" J. Opt. Commun. Netw., 7(4), 215-222 (2015).

[14] Y. Dong, E. Rawachy, R. P. Giddings, W. Jin, D. Nesset, and J. M. Tang, "Multiple channel interference cancellation of digital filter multiple access PONs," J. Lightwave Technol., 35(1), 34-44 (2017).

[15] E. Rawachy, R. P. Giddings, and J. M. Tang, "Experimental demonstration of a DSP-based cross-channel interference cancellation technique for application in digital filter multiple access PONs," Opt. Express, 25(4), 3850-3862, (2017).

[16] W. Jin, X. Duan, Y. Dong, B. Cao, R. P. Giddings, C. F. Zhang, K. Qiu, and J. M. Tang, "DSP-enabled flexible ROADMs without optical filters and O-E-O conversions," J. Lightwave Technol., 33(19), 4124-4131, (2015).

[17] G. H. Im, D. D. Harman, G. Huang, A. V. Mandzik, M. H. Nguyen, and J. J. Werner, "51.84 Mb/s 16-CAP ATM LAN standard," J. Select. Areas Commun. 13(4), 620-632, (1995).

[18] M. L. Deng, Y. Ling, X. F. Chen, R. P. Giddings, Y. H. Hong, X. W. Yi, K. Qiu, and J. M. Tang, "Selfseeding-based 10Gb/s over 25km optical OFDM transmissions utilizing face-to-face dual-RSOAs at gain saturation," Opt. Express, 22(10), 11954–11965 (2014).

[19] Y. Gao, Q. Zhuge, W. Wang, X. Xu, J. M. Buset, M. Qiu, M. Morsy-Osman, M. Chagnon, F. Li, L. Wang, C. Lu, A.P. T. Lau, and D. V. Plant, "40 Gb/s CAP32 short reach transmission over 80km single mode fibre," Opt. Express, 23(9), 11412-11423, (2015).

[20] X. Zheng, X. Q. Jin, R. P. Giddings, J. L. Wei, E. Hugues-Salas, Y. H. Hong, and J. M. Tang, "Negative power penalties of optical OFDM signal transmissions in directly modulated DFB laser-based IMDD systems incorporating negative dispersion fibers," IEEE Photonics Journal, 2(4), 532-544 (2010).

7. Conclusions and Future Work

Contents

This chapter summarizes the main contributions of this thesis and highlights a few directions for future research work.

7.1 Conclusions

Optical networks form the backbones of modern communications networks. With the exponentially increasing end-user's demands for broadband services and the newly emerging 5G service requirements such as eMBB, uRLLC and mMTC, it is crucial if future optical networks provide a) high data rates to meet the growing traffic demands; b) backward compatibility for simple network migration; c) on-demand elastic bandwidth provisioning for flexible and effective bandwidth management for optimal service delivery; d) transparency to various signal modulation formats and network topologies, and e) convergence between existing optical access/metro networks and MFHs/MBHs for simplified network infrastructures and reduced operation costs. Moreover, as the data traffic demand is expected to be more dynamic in the future owing to the unpredictable user behaviour and the changing landscape of service providers supporting a wide range of different spectral bandwidths over the same optical networks, it is greatly advantageous if these networks have sufficient flexibility, elasticity and dynamic reconfigurability and must also be cost-effective to ensure commercial viability. As discussed in chapter 1, PONs are considered one of the most promising solutions for achieving these network requirements. Hence, this dissertation research has introduced the hybrid OOFDM-DFMA PONs that appropriately combines cost-effectively the conventional OOFDM-PONs and DFMA-PONs, which have undergone ever-increasing research activity in recent years for applications in cost-effective converged fixed-mobile networks.

In an attempt to deliver the key network design features that are crucial for future converged 5G networks, this thesis has presented comprehensive research into hybrid OOFDM-DFMA IMDD PONs. This has resulted in a series of demonstrations of novel PON techniques implemented by, firstly, enabling DSP in the transceiver to allow two spectrally overlapped ONU DSB OFDM signals to occupy the same spectral region for improving the spectral efficiency and signal transmission capacity. Secondly, by incorporating the DFT-spreading technique to further maximize the upstream performance and relax the hardware requirements. Subsequently, by conveying two ONUs SSB OFDM signals within the same sub-wavelength, instead of DSB, for further enhancing the spectral efficiency. Finally, by employing low-cost

narrowband 10G class electrical/optical transceiver components for achieving high transceiver cost-effectiveness. The key findings of the research work are summarized below:

In chapter 3, it has been shown that a single sub-wavelength of the hybrid OFDM-DFMA IMDD PON can be enabled by DSP to allow an ONU to share the same sub-wavelength spectral region with another ONU. As a direct result, in comparison to the previously reported conventional hybrid OFDM-DFMA PONs which halved the spectral efficiency and signal transmission capacity due to its individual sub-wavelength conveying only a single ONU sub-band, in chapter 3, the proposed PON improved the spectral efficiency and signal transmission capacity almost by a factor of 2 without significantly increasing the transceiver complexity. This was achieved by multiplexing multiple independent OFDM channels using ONU-embedded adaptive digital filters in DSP logic, whereas in the OLT without using MFs, channel demultiplexing/demodulating is performed by the single FFT operation, independent equalization of the LSB and USB subcarriers and the summing and subtraction operations of sidebands within the same sub-wavelength. Numerical results proved that compared to the conventional hybrid OFDM-DFMA PONs, the demonstrated PONs support twice as many passively multiplexed ONUs and increased the aggregate upstream signal transmission capacity by a factor >1.7 with upstream power budget degradations of <1.5dB. In contrast, supporting the same number of ONUs results in an aggregate upstream signal transmission capacity increase by a factor >2.2 with an upstream power budget increase of >0.7dB. Moreover, while the proposed PON exhibits excellent tolerance to finite digital filter tap length-induced channel interferences and nonlinearity, improved performance was observed for transmission distances of up to 50km. The results obtained indicate that the proposed PON is promising to achieve the high data rates required in future generation optical networks.

In chapter 4, since the PONs explored in chapter 3 are based on OFDM which exhibit high signal PAPRs, to relax the requirements on key transceiver components such as DACs and ADCs, a reduction in the OFDM-induced high signal PAPRs is necessary. To achieve such an objective, in chapter 4, the DFT-spread spectrally overlapped hybrid orthogonal OFDM-DFMA IMDD PON is proposed by employing the DFT-spread technique in each ONU and OLT. To demonstrate the advantages associated with the proposed PON, upstream transmission performance comparisons are made for the representative 25km SSMF IMDD PONs. It has been shown that while the proposed PON architecture retains all the salient unique features associated with the PONs in chapter 3, more importantly, a significant reduction in the

upstream signal PAPR of ≥2 dB is achieved. As a direct result, compared with the PONs in chapter 3, the proposed PONs in chapter 4 with DFT-spreading have been shown to reduce the optimal signal clipping ratio by 1 dB, achieve at least a 1-bit reduction in the minimum required DAC/ADC quantization bit, improve the upstream system power budget by ≥1.4 dB and enhanced the aggregate upstream signal transmission capacity by a factor of up to 10% without degrading nonlinearity tolerances.

In chapter 5, to explore the feasibility of further improving the upstream transmission performance of the previously reported hybrid OFDM-DFMA PONs which convey DSB signal on a single sub-wavelength, in chapter 5, without the use of the Hilbert transform operation, multiple digitally filtered SSB OFDM signals are multiplexed in the ONUs, whereas in the OLT for channel demultiplexing the single FFT operation similar to the hybrid DSB OFDM-DFMA PONs is utilized. Detailed numerical simulations have shown that the proposed SSB PON technique reduces the PAPRs by >2dB, thus leading to a >2dB decrease in optimum signal clipping ratio and >1-bit reduction in the minimum required the ADC/DAC resolution bit. By utilizing the identified optimum ONU operating conditions, more importantly, the proposed SSB PONs with the same transmission bandwidths as DSB PONs can achieve almost twice the maximum upstream signal transmission capacity and improve the upstream system power budget by >1.2dB without compromising their differential ONU optical launch power dynamic ranges. On the other hand, for delivering the same aggregated upstream transmission capacities, in comparison to the DSB PONs, the proposed SSB PONs halved the overall system bandwidth, and increases the upstream system power budget by >2.5dB and enhanced the differential optical launch power dynamic range by >1.2dB. The results obtained demonstrate that as a direct impact of the proposed PON-induced PAPR reduction which also reduces the minimum required DAC/ADC resolution bits, this PON can contribute to the crucial target of future networks for achieving high transceivers cost-effectiveness.

In chapter 6, the performance of DOF-multiplexed six independent frequency gapless channels transmission system in the offline at net bit rates of 30Gb/s over 25km SSMF has been explored and demonstrated that the proposed technique is critical for realising practical, low-complexity and highly cost-effective PONs through the utilisation of the low-cost and low-complexity IMDD transmission systems and commercially available off-the-shelf and low-cost narrowband 10G-class optical and electrical components. Experimental results have shown that using simple adaptive channel power loading the channel spectral location-independent

upstream transmission performances with a negative power penalty of >0.2dB for all channels are obtainable. In addition, the demonstrated systems are also shown to exhibit excellent performance robustness for transmission distances of up to 45 km. The results obtained give a clear indication of the proposed PON feasibility for utilizing 10G-class optical devices to support 30Gb/s single-wavelength signal transmission capacity. From the cost point of view, this offers a promising technical strategy for achieving cost-effective converged 5G networks.

In summary, this PhD dissertation research has proposed and investigated a number of essential PON features needed for constructing cost-effective converged 5G networks capable of meeting future network requirements. A proof-of-concept demonstration for the proposed PONs explores the technical feasibility of these network features, ranging from using DSP approaches for further improving the spectral efficiency and network performance robustness without increasing transceiver complexity, to the provision of dynamic on-demand elastic bandwidth allocation for efficient bandwidth utilization efficiency, to transparent network topologies with excellent backward compatibility to existing networks, to the use of low-cost and low-complexity IMDD transmission systems incorporating off-the-shelf and low-cost narrowband networking devices, as well to flexible, elastic, and dynamically reconfigurable networks for converging traditional optical access/metro networks and MFHs/MBHs to meet future requirements such as high ubiquity, simplified network infrastructures and high network cost-effectiveness. In this context, the converged fixed-mobile 5G networks incorporating the proposed technologies presented in this thesis are envisioned to not only satisfy the urgent needs associated with the emerging highly dynamic traffic demand but also offer excellent transparency to various signal modulation formats, signal bitrates and network topology. Thus, this dissertation research offers a solid foundation for the practical implementation of converging 5G networks to meet future demands.

7.2 Future Work

In this thesis, comprehensive research work has been undertaken and successfully confirms the technical feasibility of the proposed technologies for converging fixed-mobile networks. To fully explore these technologies to their maximum potential for practical implementation in future converged 5G networks, future research directions for further investigations should be undertaken and are summarised as follows:

1) Hybrid OFDM-DFMA PON Integrating Analogue Radio-over-Fibre

Although the hybrid OFDM-DFMA PON technologies presented in this thesis are promising solutions for future generation flexible 5G MFH/MBH networks, however, these technologies in terms of further improving the spectral efficiency and therefore increasing the signal transmission capacity may require further improvement to exploit the advances in ARoF technology operating at a higher frequency mmWave band to implement PONs that are capable of satisfying the future demands of MFHs/MBHs. However, ARoF is intolerant to nonlinear distortions and fibre transmission impairments and requires high-bandwidth optical/electrical devices as such they are not cost-effective for application in cost-sensitive 5G scenarios [1,4]. The unique features associated with the hybrid OFDM-DFMA PON technologies, including, for instance, robustness to fibre nonlinearity, low transceiver complexity and cost-effectiveness suggest that these technologies may be able to overcome the aforementioned challenges of ARoF. Therefore, exploring the feasibility of utilizing these technologies in ARoF MFHs/MBHs, where multiple independent ONU sub-band signals can be generated for modulation by employing electrical up-conversion with an RF carrier operating in the mmWave band will be greatly advantageous. This work should be conducted with a specific focus on demonstrating transmission data rates up to 100Gb/s/λ over 25km SSMF IMDD PON systems using low-cost 10G-class optics. The results of the PONs presented in this thesis obtained so far, and their associated unique features, including, for instance, flexible architectures and dynamic provision of elastic bandwidth allocation suggest that achieving the targeted signal transmission data rates is envisaged to be technically feasible for the proposed PON. Furthermore, to identify the best transceiver design, conducting experimentation is crucial to answering questions of prime interest such as how many ONUs can the PON support to achieve the target data rates, under what operating conditions and what factors determine the number of ONUs that can be supported by the PON.

2) Frequency-Domain Cross Channel Interference Cancellation of Hybrid OFDM-DFMA PONs

As presented in this thesis, the hybrid OFDM-DFMA PON technologies rely on maintaining a high degree of orthogonality between digital filters employed by various ONU sub-bands. However, for practical transmission systems, due to nonlinearities arising from signal generation, transmission, routing, traffic aggregation/de-aggregation and detection, the degradation of digital filtering-based ONU sub-band orthogonality is unavoidable. This may result in the hybrid OFDM-DFMA PON technologies suffering from imperfect channel

orthogonality-induced CCI and subsequent degradations in-system performance. To combat the CCI effect, novel technical approaches including CCI cancellation (CCIC) and DFMA channel interference cancellation (DCIC) techniques have recently been proposed and experimentally demonstrated for both PtP (CCIC) and PtMP (DCIC) IMDD PON transmission systems [5-7]. However, since conventional CCIC/DCIC techniques utilize digital filters for channel demultiplexing in the OLT and the interference estimation is performed in the time domain, these techniques are not practically feasible for use in the hybrid OFDM-DFMA PONs where channel demultiplexing in the OLT is performed in the frequency domain by a single FFT operation without employing MFs. Therefore, it is crucial to investigate and develop the frequency-domain cross channel interference cancellation (FD-CIC) technique, where the interference experienced by each individual ONU is estimated in the frequency domain and subsequently subtracted from the FFT output of ONUs occupying the same subwavelength spectral region. The effectiveness of using the FD-CIC DSP algorithms in further improving the PON performances should be investigated in terms of their upstream transmission performance, complexity, latency, power consumption, robustness, and transparency to the underlying network. Moreover, a comprehensive study of the use of DFT-spread and FD-CIC algorithms in further improving the PON performances should also be explored in-depth in view of the PONs presented in chapter 4. As well, it is important to conduct an experimental demonstration to verify and confirm the technical feasibility of practically implementing the transceiver designs for various application scenarios.

3) Inter-ONU STO Estimation and Compensation for Hybrid OFDM-DFMA PONs

As channel orthogonality is dependent on sample timing synchronization between spectrally overlapped orthogonal channels, sample timing offset (STO) plays an important role in maintaining orthogonality and determining the maximum achievable upstream transmission system performance. Inter-ONU STO occurs due to the propagation path delays experienced by various ONUs orthogonal sub-band signals (I-phase and Q-phase) passing through different fibre transmission distances. In particular, STO-induced synchronization error can affect channel estimation and may lead to significant system performance degradation [6,8]. For the PONs presented in this thesis, allowing two spectrally overlapped ONU sub-bands occupying the same sub-wavelength spectral region for improved spectral efficiency requires maintaining perfect timing (zero inter-ONU STO) between orthogonal ONU sub-band signals, thus, for nonideal upstream transmission conditions, further improvement may be required to implement

accurate and automatic control of the relative inter-ONU STO of various channels under different transmission system configurations. Therefore, it is highly beneficial to investigate and develop OLT-embedded DSP algorithms, using the approach adopted in wireless OFDM systems [9], where pilot symbols are transmitted to estimate the channel with STO based on power spectral density (PSD) estimation in the frequency domain and least square (LS) phase estimation, and as such compensate for the STO effect accordingly. This approach is envisaged to be applicable in the hybrid OFDM-DFMA PONs since their OLT-receiver is OFDM like and channel demultiplexing is performed in the frequency domain using the single FFT operation. For this approach, a qualitative estimation of the DSP algorithm complexity and performance should be explored in detail to verify and confirm its technical feasibility taking into account the trade-off between the receiver OLT-DSP complexity and performance. Of course, considering the limitations imposed by the precision and speed of practical DSP hardware required for realizing real-time high-speed systems, experimental investigations should be undertaken by using FPGA-based real-time DSP platforms available in Bangor.

References

[1] Rajpal, Shivika and Rakesh Goyal. “A Review on Radio-Over-Fibre Technology-Based Integrated (Optical/Wireless) Networks.” J. of Opt. Commun., pp. 19-25, 2016.

[2] M. R. N. Babir and P. K. Choudhury, "On the performance of high order QAM signals for analogue and digital radio over fibre systems," 4th Int. Conf. on Advances in Elec. Eng. (ICAEE), pp. 379-382, 2017.

[3] D. Pérez-Galacho, D. Sartiano and S. Sales, "Fronthaul links based on Analogue Radio over Fibre," Europ. Conf. on Netw. and Commun. (EuCNC), pp. 475-478, 2019.

[4] Christina Lim, Ka Lun Lee, Ampalavanapillai T. Nirmalathas, "Review of physical layer networking for optical-wireless integration," Opt. Eng. 55(3) 031113, 2015.

[5] R. P. Giddings, X. Duan, and J. M. Tang, “Experimental demonstration of cross-channel interference cancellation for digital filter multiple access PONs,” in Proc. Opt. Fibre Commun. Conf. Exhib., Anaheim, CA, USA, 2016, Paper Th3C.5.

[6] E. Al-Rawachy, R. P. Giddings, and J. M. Tang, “Experimental demonstration of a DSP-based cross-channel interference cancellation technique for application in digital filter multiple access PONs,” Opt. Exp., vol. 25, no. 4, pp. 3850–3862, 2017.

[7] Y. Dong, E. Al-Rawachy, R. P. Giddings, W. Jin, D. Nesset, and J. M. Tang, “Multiple channel interference cancellation of digital filter multiple access PONs,” J. Lightw. Technol., vol. 35, no. 1, pp. 34–44, 2017.

[8] X. Duan, R. P. Giddings, S. Mansoor and J. M. Tang, "Performance Tolerance of IMDD DFMA PONs to Channel Frequency Response Roll-Off," in IEEE Photo. Technol. Lett., vol. 29, no. 19, pp. 1655-1658, 2017.

[9] Shengping Qin, Peide Liu, Xin Zhang, Laibo Zheng and Deqiang Wang, "Channel estimation with timing offset based on PSD & LS estimation for wireless OFDM systems," Int. Sym. on Intell. Sig. Proc. and Commun. Syst., 2007, pp. 248-251, 2007.

Appendix

Publications

[1] A. Sankoh, W. Jin, Z. Q. Zhong, J. X. He, Y. H. Hong, R. P. Giddings, I. Pierce, M. O'Sullivan, J. Lee, T. Durrant, and J. M. Tang Member, "Hybrid OFDM-Digital Filter Multiple Access PONs Utilizing Spectrally Overlapped Digital Orthogonal Filtering," IEEE Photonics Journal., Vol.12, No 5, pp. 1-11, 2020.

[2] A. Sankoh, W. Jin, Z. Zhong, J. He, Y. Hong, R. Giddings, and J. Tang, "DFT-Spread Spectrally Overlapped Hybrid OFDM–Digital Filter Multiple Access IMDD PONs," Sensors, vol. 21, no. 17, p. 5903, 2021.

[3] W. Jin, A. Sankoh, Y.X. Dong, Z.Q. Zhong, R.P. Giddings, M. O'Sullivan, J. Lee, T. Durrant and J.M. Tang, "Hybrid SSB OFDM-Digital Filter Multiple Access PONs," IEEE-OSA J. Lightwave Technol., Vol. 38, No. 8, pp. 2095–2105, 2020.

[4] M. L. Deng, A. Sankoh, R. P. Giddings, and J. M. Tang, "Experimental demonstrations of 30Gb/s/λ digital orthogonal filtering-multiplexed multiple channel transmissions over IMDD PON systems utilizing 10G- class optical devices," Opt. Express, vol. 25, no. 20, pp. 24251–24261, 2017.

[5] W. Jin, Z. Q. Zhong, J. X. He, A. Sankoh, R. P. Giddings, Y. H. Hong, I. Pierce, M. O'Sullivan, C. Laperle, J. Lee, G. Mariani, T. Durrant and J. M. Tang, "Experimental Demonstrations of Hybrid OFDM-Digital Filter Multiple Access PONs," IEEE Photonics Technology Letters., Vol.32, No.13, pp.751-754, 2020.

[6] Z. Q. Zhong, W. Jin, Y. X. Dong, A. Sankoh, J. X. He, Y. H. Hong, R. P. Giddings, I. Pierce, M. O'Sullivan, J. Lee, G. Mariani, T. Durrant, J. M. Tang, "Experimental Demonstrations of Matching Filter-free Digital Filter Multiplexed SSB OFDM IMDD Transmission Systems" IEEE Photonics Journal, Vol. 13, No. 2, Art no. 7900512, 2021